# Identification of a direct interaction of protein kinase A with the L-type $Ca^{2+}$ channel and characterization of effects of *PDE3A* mutations on cardiac myocytes

Inaugural – Dissertation

to obtain the academic degree

Doctor rerum naturalium (Dr. rer. nat.)

submitted to the Department of Biology, Chemistry, Pharmacy

of Freie Universität Berlin

by

**TAMARA PALLIEN**

2022

This work was conducted from January 2019 until June 2022 at Max-Delbrück-Center for Molecular Medicine in the Helmholtz Association (MDC) under the supervision of PD Dr. Enno Klußmann.

1st Reviewer: PD Dr. Enno Klußmann

2nd Reviewer: Prof. Dr. Volker Haucke

Date of disputation: 10th of March, 2023

# Acknowledgment

First and foremost, I would like to thank PD Dr. Enno Klussmann for giving me the opportunity to work on these interesting projects. He always helped by discussing details of my work and made it possible for me to attend conferences, to work in the laboratory of collaboration partners for scientific exchange and to publish my work. In addition, I appreciate the time he took to help me with reading and correcting this thesis.

I am also thankful to Prof. Dr. Volker Haucke for being my second examiner to read and evaluate this thesis.

I would like to thank Dr. Daniela Panakova and Prof. Dr. Oliver Daumke for participating in my committee meetings thus providing feedback for my projects.

I am very grateful to the previous and present members of the Klussmann lab who always supported me mentally and in the lab. I would like to thank especially Sandrine Baltzer, Ryan Walker-Gray, Anastasiia Sholokh and Maria Ercu for always helping me regarding scientific questions but also for having such a nice time outside the lab.

I am thankful to Andrea Geelhaar and Christin Kuschke for the excellent technical assistance.

I would like to thank my collaborators in the lab of Sebastian Diecke, Norbert Hübner, Nathan Dascal and Friedrich Herberg. Thanks a lot for providing scientific feedback and giving me the opportunity to learn new methods and broaden my scientific and laboratory knowledge. Special thanks to Dr. Duncan Miller and Carolin Genehr who taught me how to culture human induced pluripotent stem cells and to establish the cardiomyocytes differentiation protocol, for always having an open ear for questions and mental support. Thanks a lot to Johannes Greiner, Philip Dierks, Isabel Florres and Judit Rosales for help with the stem cell and cardiomyocyte culture.

Many thanks also to my friends and family who were always there for me when I needed you and always supported me.

Lastly, special thanks to Michael Mücke, who I closely collaborated with for the PDE3A part of the thesis. Thanks for taking care of the hiPSC-CMs, for analyzing the $Ca^{2+}$ Imaging data and for the refreshing scientific discussions. Without you, the time at the MDC would have never been the same, for always being there for me and encouraging me to carry on despite all difficulties.

# Declaration of independence

I hereby declare that I wrote this thesis independently and have not used any sources or resources other than those specified by me and that I have not submitted the dissertation in this or any other form to any other institution.

# 1 Table of contents

# Abbreviations and Acronyms

| | |
|---|---|
| β-AR | β-adrenergic receptor |
| aa | amino acid |
| AKAP | A-kinase anchoring protein |
| C subunit | catalytic subunit of PKA |
| $Ca_v1.2$ | L-type calcium channel |
| cAMP | cyclic adenosine-3',5'-monophosphate |
| CM | Cardiac myocyte |
| DCRD | distal C-terminal regulatory domain |
| ECC | Excitation contraction coupling |
| FSK | forskolin |
| HET | heterozygous |
| hIPSC | human induced pluripotent stem cells |
| HOM | homozygous |
| HTNB | hypertension with brachydactyly |
| IBMX | 3-isobutyl-1-methylxanthine |
| Iso | isoproterenol |
| PBS | phosphate buffered saline |
| PDE3A | cGMP-inhibited cAMP phosphodiesterase 3A |
| PKA | protein kinase A |
| Rad | Ras-like G-protein |
| RT | room temperature |
| SERCA | sarco/endoplasmic reticulum $Ca^{2+}$ ATPase |
| SR | sarcoplasmic reticulum |
| WB | western blotting |
| WT | wild-type |

# Summary

In the heart, the excitation-contraction coupling (ECC) pathway links excitation at the plasma membrane to contraction of the cardiomyocytes. The L-type $Ca^{2+}$ channel (LTCC) and phosphodiesterase 3A (PDE3A) play important roles in this pathway by facilitating $Ca^{2+}$ influx into the cytosol and hydrolysis of cAMP at subcellular compartments e.g. the sarcoplasmic reticulum (SR) and in the cytosol.

Regulation of the LTCC opening is modulated by proteins found in its local environment, amongst them the catalytic subunit of PKA (PKA-CS). However, how PKA-CS is tethered to the channel is unclear. Recently, it was found that the GTP-binding protein Rad is associated with the LTCC and is blocking the pore-forming $\alpha$1c subunit in the basal state (Liu et al., 2020). PKA phosphorylation of Rad in response to $\beta$-adrenergic stimulation leads to its dissociation from the channel complex, releasing the inhibitory effect.

In the first part of this work, a novel interaction of PKA-CS with the C terminus of the $\alpha$1c subunit is described. This interaction was mapped to two regulatory regions of $\alpha$1c, the distal and the proximal regulatory domain (DCRD and PCRD). Mutating the DCRD and PCRD regions affected the interaction with PKA-CS *in vitro* but not in a cellular environment, pointing towards a complex regulatory mechanism involving several proteins or an alternative recruitment process. The two regions did not affect the enzymatic activity of PKA-CS.

The LTCC and isoform 1 of PDE3A were found in a complex in HEK293 cells, however no further functional link could be found. In the second part of this thesis, effects of mutations in *PDE3A* were characterized. These mutations cause hypertension with brachydactyly type E (HTNB). Affected individuals experience progressive hypertension and have characteristic shorter metacarpals. If untreated, patients die before the age of 50. Surprisingly, their hearts do not show hypertension-induced cardiac damage. This points to a cardioprotective effect of *PDE3A* mutations. HiPSC-CMs expressing T445N or R862C PDE3A HTNB-causing substitutions were established and differentiated to cardiac myocytes as a model system to study $Ca^{2+}$ cycling. The mutant cells showed lower PDE3A and the LTCC $\alpha$1c subunit protein levels and a longer $Ca^{2+}$ dwell time in the cytosol compared to the wild-type (WT) cells. This might be an adaptive mechanism to improve contractility of the cells that contributes to the cardioprotective effect of the mutations.

# Zusammenfassung

Der Erregungskontraktionsweg (ECC) im Herz verknüpft die Erregung an der Plasmamembran mit der Kontraktion der Kardiomyozyten. Der L-Typ $Ca^{2+}$ Kanal (LTCC) und Phosphodiesterase 3A (PDE3A) spielen eine entscheidende Rolle, indem sie den $Ca^{2+}$ Einstrom in das Zytoplasma und die Hydrolyse von cAMP in subzellulären Kompartimenten, z.B. dem sarkoplasmatischen Retikulum (SR) oder im Zytoplasma ermöglichen.

Das Öffnen des LTCCs wird durch Proteine in seiner Umgebung reguliert, unter anderem der katalytischen Untereinheit von PKA (PKA-CS). Allerdings ist es unbekannt, wie PKA-CS an den Kanal bindet. Das GTP-bindende Protein Rad ist mit dem LTCC assoziiert und blockiert die Kanal-formende Untereinheit $\alpha$1c im basalen Zustand (Liu et al., 2020). Phosphorylierung von Rad durch PKA initiiert dessen Dissoziation vom Komplex und hebt den inhibierenden Einfluss auf.

Im ersten Teil dieser Arbeit ist die direkte Interaktion von PKA-CS mit dem C Terminus der $\alpha$1c beschrieben. Diese Interaktion umfasst zwei regulatorische Regionen der $\alpha$1c, nämlich die distalen und proximalen regulatorischen Domänen (DCRD und PCRD). Mutationen in den DCRD- und PCRD-Regionen vermindern die Interaktion nicht, was darauf hindeutet, dass die regulatorischen Mechanismen deutlich komplexer sind und mehrere Proteine involviert sind oder ein alternativer Rekrutierungsprozess vorliegt. Die Regionen beeinflussen die enzymatische Aktivität der PKA-CS nicht.

Der LTCC und Isoform 1 der PDE3A befinden sich in HEK293 Zellen in einem Komplex, allerdings konnte kein funktioneller Link gefunden werden. Im zweiten Teil dieser Arbeit werden Mutationen in *PDE3A* charakterisiert. Diese Mutationen lösen Hypertonie mit Brachydaktylie vom Typ E (HTNB) aus. Betroffene Individuen haben fortschreitenden Bluthochdruck und verkürzte Mittelhandknochen. Ohne Behandlung sterben die Patienten bevor sie 50 Jahre alt werden. Trotzdem sind ihre Herzen nicht durch den Bluthochdruck geschädigt. Dies deutet auf einen herzschützenden Effekt der *PDE3A* Mutationen hin. HiPSC-CMs mit HTNB-auslösenden T445N und R862C PDE3A Aminosäuresubstitutionen werden zu Kardiomyozyten differenziert und als Modellsystem zur Untersuchung des $Ca^{2+}$-Signalweges genutzt. Die mutierten Zellen weisen ein geringeres Protein Level an PDE3A und der $\alpha$1c Untereinheit auf sowie eine längere Verweilzeit des $Ca^{2+}$ im Zytoplasma, im Vergleich zu den Wild-Typ (WT) Zellen. Dies könnte einen adaptiven Mechanismus darstellen, der die Kontraktilität der Zellen verbessert und Teil des herzschützenden Effektes der Mutationen sein.

# Preamble

This thesis consists of two parts. In the first part, the interaction between the L-type $Ca^{2+}$ channel subunit α1c with PKA catalytic subunit was studied. This project was conducted in close collaboration with the laboratory of Prof. Nathan Dascal (Tel Aviv University, Tel Aviv, Israel) who's team members conducted functional experiments, including electrophysiology measurements in *Xenopus* oocytes. This thesis describes my experimental contribution.

In the second part, the molecular mechanisms underlying the potential cardioprotective effect of *PDE3A* mutations were studied. This project was accepted for publication as: Ercu M, Mücke MB, Pallien T, Lajos M *et al.* "Mutant phosphodiesterase 3A protects from hypertension-induced cardiac damage", Circulation. Text and figures shown in this thesis might be similar to the manuscript. This project was conducted in close collaboration with Michael B. Mücke from the laboratory of Prof. Norbert Hübner (MDC Berlin, Germany). Experimental parts carried out by collaboration partners are highlighted in the corresponding text and figure legends.

# 1 Introduction

Parts of the introduction, including text and figures, were adapted from Pallien *et al*. (Pallien & Klussmann, 2020) and might show some similarities.

## 1.1 Excitation-contraction coupling (ECC) in the heart

The excitation-contraction coupling (ECC) acts as a linker of electric excitation that starts at the sarcolemma to contraction of the cardiac myocyte (Eisner et al., 2017). The ECC pathway in the heart is initiated by membrane depolarization from a resting membrane potential of – 90 mV to a positive voltage level (+ 10 mV) leading to $Ca^{2+}$ influx through the $Ca_v1.2$ L-type $Ca^{2+}$ channel (LTCC) into the cytosol (Faber et al., 2007; Pinnell et al., 2007). In the cytosol, the free $Ca^{2+}$ concentration increases about 10-fold from a resting concentration of 100 nM to 1 µM (Cruz-Garcia et al., 2021; Marks, 2013). This initiates the $Ca^{2+}$-induced $Ca^{2+}$ release (CICR) from type 2 ryanodine receptors (RyR2) located in the membrane of the sarcoplasmic reticulum (SR). The combination of $Ca^{2+}$ influx through the LTCC and $Ca^{2+}$ efflux from the SR increases the $Ca^{2+}$ concentration further. This results in the release of troponin C (TnC) from the contractile filaments, initiating myosin and actin filament sliding, shortening of the cell and contraction. The force of each contraction directly correlates with the amount of $Ca^{2+}$ in the cytosol (Eisner et al., 2017). The $Ca^{2+}$-dependent inactivation (CDI) of the LTCC and $Ca^{2+}$ removal from the cytosol into the SR by the sarcoplasmic/endoplasmic reticulum $Ca^{2+}$ ATPase 2a (SERCA2a) mediates the relaxation process (Figure 1) (W. Catterall, 2015; Moccia et al., 2019; Pallien & Klussmann, 2020). For relaxation, $Ca^{2+}$ is also transported into the extracellular space by means of sodium- $Ca^{2+}$ exchangers (NCX) (Eisner et al., 2017).

SERCA2a is inhibited by binding of phospholamban (PLN), which is released upon phosphorylation by protein kinase A (PKA) and calmodulin-dependent protein kinase δ (CaMKIIδ) (Moccia et al., 2019; Bazmi & Escobar, 2018; W. Catterall, 2015; Kumari et al., 2018; C. R. Carlson et al., 2022).

The ECC pathway is modulated by the catecholamines (epinephrine and norepinephrine) released from the sympathetic nervous system, which bind to β-adrenergic receptors (β-AR) located on the surface of cardiomyocytes. The activation of these receptors initiates exchange of GDP for GTP on the α subunits of the G protein (Gα) and dissociation of heterotrimeric G-proteins (Wang et al., 2018). The α subunits of the stimulatory G protein ($G\alpha_s$) activate adenylyl cyclases (AC), which catalyzes the synthesis of 3’-5’-cyclic adenosine monophosphate (cAMP) from adenosine triphosphate (ATP). The $G\alpha_s$ subunit hydrolyzes GTP leading to reassociation with the dimeric $G_{\beta\gamma}$ which terminates the G-protein activation (Wang et al., 2018).

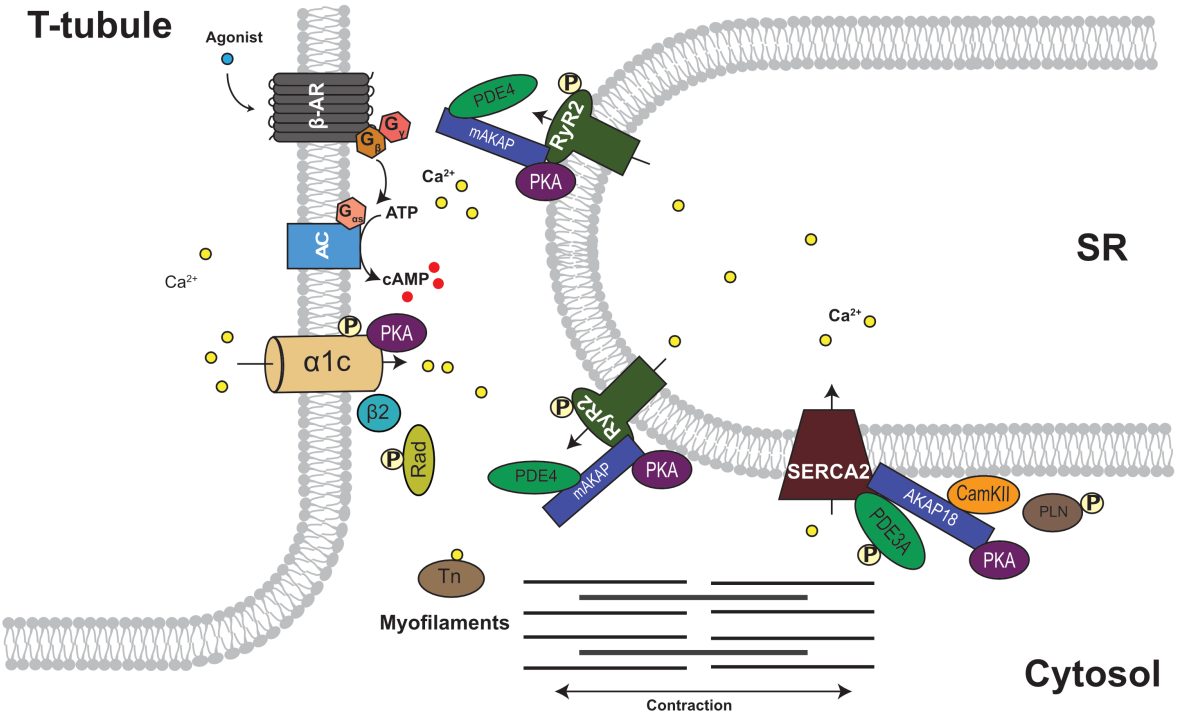


**Figure 1: Scheme of the β-adrenergic signaling in cardiomyocytes**. Upon stimulation of β-adrenergic receptors (β-AR), α-subunits of the stimulatory G-protein ($G\alpha_s$) dissociate from $G_{\beta\gamma}$ subunits and activate adenylyl cyclase (AC) at the sarcolemma. Adenylyl cyclases convert ATP to cAMP which activates protein kinase A (PKA). PKA phosphorylates phospholamban (PLN), ryanodine receptor 2 (RyR2) and Ras associated with diabetes (Rad) at the L-type $Ca^{2+}$ channel (LTCC). Influx of $Ca^{2+}$ into the cytosol via the α1c subunit of the LTCC and RyR2 leads to troponin (Tn) dissociation from the myofilaments, initiating sliding of actin and myosin and thus contraction. Relaxation is induced by phosphorylated PLN dissociating from sarcoplasmic/endoplasmic reticulum $Ca^{2+}$ ATPase (SERCA2) releasing its inhibitory effect. Local cAMP levels are regulated by phosphodiesterases (PDEs) which hydrolyze cAMP. The figure is adapted from Pallien & Klussmann, 2020.

cAMP is a second messenger involved in the regulation of cardiac contraction. PKA is an enzyme consisting of two regulatory subunits (PKA-RS) which dimerize and form holoenzymes with two catalytic subunits (PKA-CS) (Leroy et al., 2018). PKA is the major effector of cAMP (Bhogal et al., 2018; Leroy et al., 2018). cAMP binds PKA-RS resulting in the dissociation of the catalytic subunits, PKA-CS. PKA phosphorylates several proteins in the ECC pathway including PLN, RyR2 and Ras associated with diabetes (Rad). Rad interacts with the LTCC and thereby inhibits it (section 1.2.2.3)(Papa et al., 2022). The phosphorylation of PLN, RyR2 and Rad causes increased $Ca^{2+}$ entry through the LTCC, increased release by the SR and re-uptake into the SR by SERCA2. This augments inotropy, which is the contractile force of the myocardium and lusitropy, the cardiac relaxation process (Abrol et al., 2015; Hasenfuss & Teerlink, 2011; Papa et al., 2022). The cAMP level is regulated by a balanced cAMP synthesis at the AC and cAMP hydrolysis by phosphodiesterases (PDEs). The predominant PDE of the human heart is PDE3A and this protein was shown to interact with SERCA2, A-kinase anchoring protein 18 (AKAP18) and PLN to regulate local cAMP levels at the SR (Ahmad et al., 2015).

## 1.2 The L-type $Ca^{2+}$ channel (LTCC)

### 1.2.1 LTCC channel structure and isoforms

The L-type $Ca^{2+}$ channel is the transmembrane $Ca^{2+}$-specific ion channel that opens in response to membrane depolarization and is augmented by activation of the β-adrenergic signaling pathway (Dolphin, 2018; Roybal et al., 2020; Weiss et al., 2013).

The $Ca_v1$ family is classified based on the structure of the α1 subunit and consists of four members that are expressed in different tissues (W. Catterall, 2000; W. Catterall, 2011; Feng et al., 2018). The $Ca_v1.1$ channel is involved in skeletal muscle cell contraction, whereas $Ca_v1.2$ and $Ca_v1.3$ are found in cardiac cells, adrenal chromaffin cells and neuronal tissue (Bourinet et al., 2004; Feng et al., 2018). In the heart, $Ca_v1.2$ is the predominant isoform, expression of $Ca_v1.3$ is lower and not uniform (Bourinet et al., 2004). The fourth member of the family, $Ca_v1.4$, is expressed in the retina and involved in vision (Baumann et al., 2004; Pallien & Klussmann, 2020).

Structurally, the cardiac $Ca_v1.2$ consists of three subunits: the pore-forming α1c subunit (240 kDa), the regulatory, intracellular β subunit (68 kDa) and the extracellular $\alpha_2\sigma$ subunit (170 kDa), the latter two being involved in anchoring and trafficking to the membrane (W. Catterall, 2011; Hofmann et al., 1994, 2014; Katz et al., 2021). The α1c subunit consists of four transmembrane, homologous domains (I-IV), which form the $Ca^{2+}$- selective pore and cytosolic N and C termini (Figure 2). Each one of the four domains consists of six transmembrane helices (S1-S6) which are joined to each other by cytoplasmic linkers. The voltage-sensing domain is formed by helices S1-S4. The S4 helix is the voltage sensor that confers conformational changes in the pore-forming domain leading to channel opening upon to changes in membrane potential (Feng et al., 2018; Kumari et al., 2018; Tuluc et al., 2016).

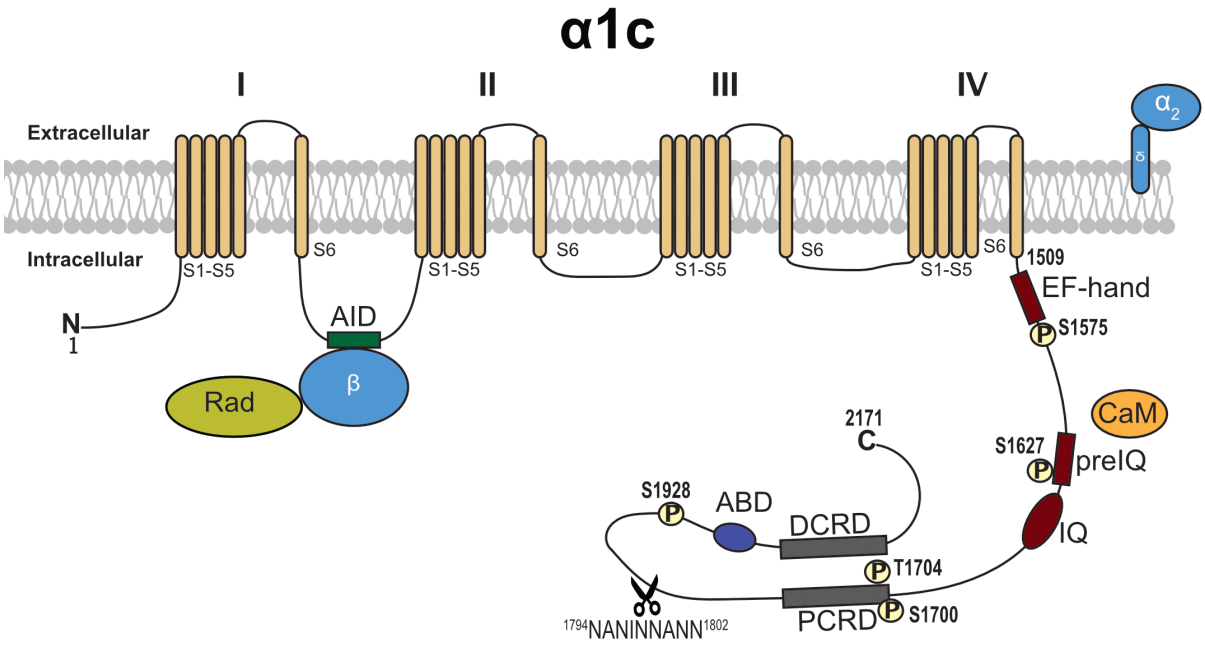


**Figure 2: Model of the α1 subunit of the cardiac L-type $Ca^{2+}$ channel.** The β-subunit (β) binds to the α-interaction domain (AID) and is associated with Rad in the basal state. The proteolytic cleavage site and main phosphorylation sites in the C terminus are shown. Calmodulin (CaM) binding involves the preIQ and IQ domains. The EF-hand motif acts as the $Ca^{2+}$ sensor (Feng et al., 2018). The $\alpha_2\sigma$ subunit is involved in membrane anchoring and trafficking. ABD – AKAP binding domain. The numbering is according to the rabbit α1c amino acid sequence (Uniprot #P15381). The figure is adapted from Pallien & Klussmann, 2020.

### 1.2.2 LTCC channel regulation

#### 1.2.2.1 PKA-mediated LTCC regulation

PKA is one of the key proteins of the β-adrenergic pathway and an important regulator of the LTCC channel. It is recruited and linked to its substrate proteins by scaffolding proteins termed A-kinase anchoring proteins (AKAPs) (Colledge & Scott, 1999; Dema et al., 2015; Gray et al., 1998; Skroblin et al., 2010; Yu et al., 2018). The cardiac $Ca_v1.2$ α1c interacts with AKAP15 (alternative names: AKAP18, AKAP7) and AKAP150 *via* a modified leucine-zipper in the distal C-terminal domain (AKAP binding domain, ABD) (W. Catterall, 2011; Hulme et al., 2003; Oliveria et al., 2007; Skroblin et al., 2010).

The AKAP-mediated recruitment of PKA to the $Ca_v1.2$ complex was intensively studied but the results are inconsistent. Blocking PKA-AKAP interactions using peptide inhibitors such as Ht31 or using a mouse model in which AKAP15 interaction with $Ca_v1.2$ α1c was ablated resulted in insensitivity to cAMP stimulation and cardiac hypertrophy (Deák & Klussmann, 2016; Fu et al., 2011; Hulme et al., 2003; Hundsrucker et al., 2006; Redden & Dodge-Kafka, 2011; Yu et al., 2018; Zhu et al., 2019).

Using a mouse model with all AKAP15 isoforms deleted, Jones *et al*. (Jones et al., 2012) analyzed if the $Ca^{2+}$ current ($I_{Ca,L}$), the intracellular $Ca^{2+}$ concentration or the re-uptake into the SR was affected in isolated cardiomyocytes. They found that the cells reacted as expected to β-adrenergic stimulation and that phosphorylation of $Ca_v1.2$ was not changed (Jones et al., 2012).

Yu *et al.* identified the AKAP Cypher/Zasp, which is localized to the z-lines (Yu et al., 2018). This AKAP co-immunoprecipitated with $Ca_v1.2$ α1c in HEK293 cells (Lin et al., 2013; Yu et al., 2018). Deletion of Cypher/Zasp in mice caused increased $Ca_v1.2$ α1c, PKA-CS and calcineurin protein levels and decreased basal $I_{Ca,L}$ (Yu et al., 2018).

When blocking PKA-AKAP interactions with Ht31, Oz *et al*. (Oz et al., 2017) could not show any impact on the cAMP-mediated $I_{Ca,L}$ increase in *Xenopus* oocytes, thereby confirming the finding of Jones *et al*. (Jones et al., 2012). In a cell-free system, the regulation of human $Ca_v1.2$ was also independent of AKAPs, as the $Ca_v1.2$ $I_{Ca,L}$ was normally upregulated upon administration of the AKAP-PKA inhibitors Ht31 and FMP-API-1 (Christian et al., 2011; Cserne Szappanos et al., 2017). Based on these findings, AKAPs are either not involved in channel regulation or the essential AKAP/s has/have not yet been found.

For many years, phosphorylation of the $Ca_v1.2$ α1c at the S1700, T1704 and S1928 residues of the α1c subunit (numbering according to the rabbit α1c sequence, Uniprot #P15381) was assumed to be the major mechanism of PKA-mediated regulation of $I_{Ca,L}$ (W. Catterall, 2015; Fu et al., 2013, 2014; Fuller et al., 2010; Hofmann et al., 2014; Hulme et al., 2003, 2006; Kumari et al., 2018; Pallien & Klussmann, 2020). In addition, PKA phosphorylation at S1574, S1626 and S1699 modulated the binding of calmodulin (CaM) at the C terminus of α1c attenuating the CDI leading to enhanced channel currents (Lei et al., 2018).

However, none of these sites was shown to be required for the regulation of the $Ca_v1.2$ in cardiac myocytes (Kumari et al., 2018; Pallien & Klussmann, 2020). Substitution of S1928 with an alanine neither attenuated the β-adrenergic receptor-mediated response in adult guinea pig myocytes nor did it affect the basal $I_{Ca,L}$ in mouse cardiomyocytes (Ganesan et al., 2006; Lemke et al., 2008). The S1928 is required for the PKA-mediated regulation of $Ca_v1.2$ in smooth muscle cells and neurons (Nystoriak et al., 2017; Qian et al., 2017). Substitutions in the S1700 and T1704 residues did not affect $I_{Ca,L}$ stimulation in adult mouse cardiomyocytes (Brandmayr et al., 2012; Katchman et al., 2017; Oz et al., 2017; L. Yang et al., 2013).

Since there is this controversy over the importance of PKA phosphorylation sites for $Ca_v1.2$ regulation and activity, Katchman *et al*, replaced all threonine and serine residues in consensus PKA phosphorylation sites (PKA consensus motif: RRXS/TY) with alanine residues and analyzed the β-adrenergic pathway in mouse cardiomyocytes (Katchman et al., 2017). They did not find differences in

the activation of the wild-type (WT) and mutant $Ca_v1.2$ channels or the current increase conferred by β-adrenergic stimulation with isoproterenol.

In conclusion, the β-adrenergic regulation of $Ca_v1.2$ is not dependent on the phosphorylation of any of the previously identified residues and potential PKA phosphorylation sites which are conserved in rabbit, human, guinea pig, mouse and rat are not involved. Thus, the major regulatory mechanism may not be dependent on phosphorylation (Pallien & Klussmann, 2020).

#### 1.2.2.2 Proteolytic cleavage of the α1c C terminus

Another mechanism playing a role in the regulation was the proteolytic cleavage of the C terminus of the α1c subunit. About 80% of the cardiac $Ca_v1.2$ α1c is proteolytically cleaved, resulting in a 240 kDa (full-length) or a truncated 210 kDa protein (Fu et al., 2011; Hulme et al., 2003, 2006; Kumari et al., 2018). Derived from the molecular weight of the truncated channel fragment and proteomics experiments with $Ca_v1.1$ channels, the cleavage site was predicted to be located at around Ala-1800 (Hulme et al., 2005; Katchman et al., 2017; L. Yang et al., 2013). When co-expressing the truncated channel with its cleaved dCT (35 kDa) in non-muscle cells, the dCT fragment remained non-covalently bound to the channel, acting as an auto-inhibitor (Brandmayr et al., 2012; Hulme et al., 2003, 2006; Katz et al., 2021; Kumari et al., 2018).

Studying the role of the proteolytic cleavage, Oz *et al*. (Oz et al., 2017) found that the cleavage at residue 1800 increased the PKA-mediated effects on $Ca_v1.2$. Although the truncation of the C terminus was essential, the existence of dCT as a separate protein was not, underpinning that the potential phospho-site S1928 is not involved in PKA-mediated regulation of $Ca_v1.2$ (Oz et al., 2017).

To study the importance of the proteolytic cleavage, Katchman *et al*. disrupted the $^{1769}$DTESP$^{1772}$ motif that functions as a substrate recognition site for calpain-like proteases. In addition, they substituted the $^{1794}$NANINNANN$^{1802}$ motif in the C terminus, which spans the suggested cleavage site (Katchman et al., 2017; Rechsteiner, 1990). They found that both motifs were essential for the proteolytic cleavage but ablation of these sites did not affect the contraction of field-stimulated cardiac myocytes or the β-adrenergic regulation pathway upon isoproterenol stimulation (Katchman et al., 2017).

### 1.2.2.3 The role of the β-subunit

The α1c subunit of $Ca_v1.2$ migrates to the sarcolemma, which is mediated by the interaction with the β-subunit, the $\beta_2$ isoform in the heart (Ahern & Satin, 2019; Arikkath & Campbell, 2003; Bichet et al., 2000; Buraei & Yang, 2010; Chien et al., 1995; Dolphin, 2003; Foell et al., 2004; Perez-Reyes et al., 1992; L. Yang et al., 2019).

In mice, β-subunit knockout by deletion of the *Cacnb2* gene resulted in a reduced $Ca^{2+}$ current (< 29%) but did not impair cardiac function. Short hairpin RNA (shRNA)-mediated $\beta_2$-subunit knockdown in adult rat cardiac myocytes significantly altered the $Ca^{2+}$ current (Cingolani et al., 2007; Meissner et al., 2011).

Similar to the α1c subunit, the β-subunit was initially assumed to be regulated by PKA phosphorylation and the phosphorylation sites on the β-subunit are residues S459, S478 and S479. Substitutions of S459, S478 and S479 with alanines did not perturb the β-adrenergic regulation (Brandmayr et al., 2012; Oz et al., 2017). Mutating all 37 serine and threonine residues of the β-subunit that represent PKA phosphorylation sites did not affect the isoproterenol- or forskolin-induced stimulation of the $I_{Ca,L}$ in transgenic mice (Liu et al., 2020; L. Yang et al., 2019). To fully reconstitute the involvement of PKA phosphorylation in channel regulation, transgenic mice have been generated expressing β- and α1c-subunits with mutated PKA phosphorylation sites and these mice have unaffected β-adrenergic stimulation (Liu et al., 2020).

The functional role of a direct β-α1c subunit interaction was studied with transgenic mice harboring alanine substitutions in the α-interaction domain (AID) of the α1c subunit (Y467, W470, I1417)(L. Yang et al., 2019). Those were proposed to form the interaction site between the two subunits (Bichet et al., 2000; Fang & Colecraft, 2011; Waithe et al., 2011; L. Yang et al., 2019). Using this model system, the authors did not find a requirement for β-subunit binding to induce α1c subunit trafficking, whereas the β-subunit was mandatory for the transduction of the β-adrenergic signals (Brandmayr et al., 2012; Miriyala et al., 2008; L. Yang et al., 2019).

Recently, the function of the β-subunit for the regulation of channel opening was unraveled by the group of Steven Marx (Liu et al., 2020; Papa et al., 2021). They used quantitative proteomics in mouse hearts to track hundreds of proteins expressed in the proximity of the $Ca_v1.2$ channel. They found the $Ca^{2+}$ - channel inhibitor Rad associated with the β-subunit and this interaction is released upon PKA phosphorylation of Rad (Liu et al., 2020) (Figure 3). Further, direct binding of the β-subunit to the AID induced the transition to a high opening channel gating mode which is even further stabilized upon Rad dissociation (Papa et al., 2022). Knock-out of Rad in mice cardiomyocytes (cRadKo) resulted in increased LTCC activity, elevated intrinsic and sleep phase heart rates (Levitan et al., 2021). Thus,

targeting the LTCC-Rad interaction could be a novel therapeutic approach for the treatment of symptomatic bradycardia and other cardiovascular diseases (Levitan et al., 2021).

Using the approach of proximity biotinylation combined with quantitative proteomics in adult rat cardiomyocytes, Cruz-Garcia *et al.* identified proteins within nanometer proximity to the $\beta_2$-subunit (Cruz-Garcia et al., 2021). They found the $\beta_2$-subunit and RyR2 in a complex. This interaction was mediated by the Src-homology 3 (SH3) domain of $\beta_2$. Functionally, the interaction upregulated the CICR at high pacing frequencies, but not at low beating rates (Cruz-Garcia et al., 2021).

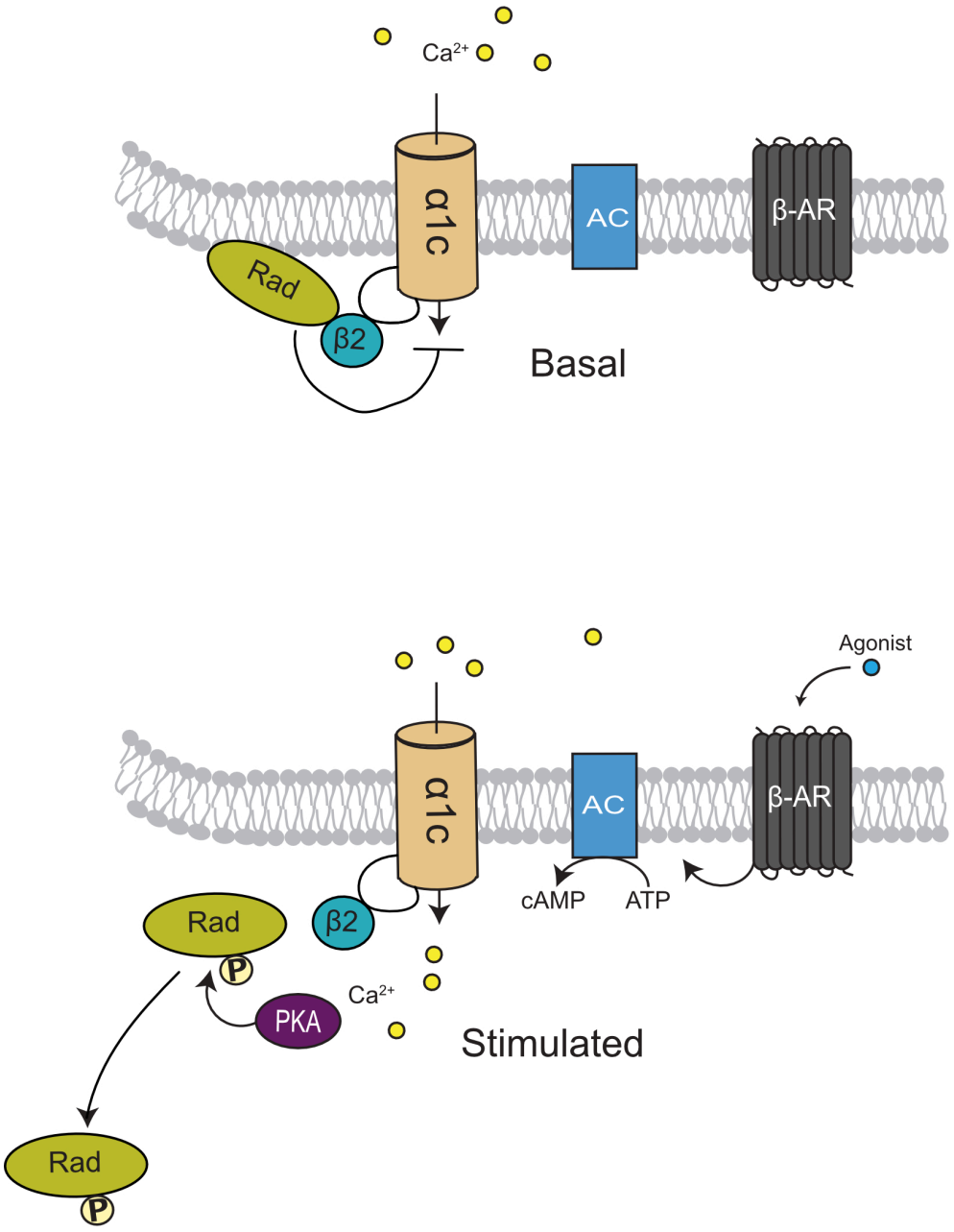


**Figure 3: Rad signaling at the LTCC.** In the basal state, the small GTPase Rad binds to the α1c subunit via the β-subunit ($\beta_2$). Upon stimulation with a β-adrenergic (β-AR) agonist, protein kinase A (PKA) phosphorylates Rad and Rad dissociates from the α1c subunit, resulting in $Ca^{2+}$ influx. The figure was adapted from Liu *et al.* (Liu et al., 2020).

#### 1.2.2.4 Autoregulatory mechanisms involving N and C termini of $\alpha$1c

The direct interaction of the N and C terminus of $Ca_v1.2$ affects channel gating and inactivation (Dick et al., 2008; Guggenheimer et al., 2016; Ivanina et al., 2000). A model for this interaction was proposed by Guggenheimer and colleagues (Guggenheimer et al., 2016). In this model, apo-CaM (= $Ca^{2+}$ free CaM) interacts with the IQ and preIQ domains (Figure 2) of the proximal C terminus of the $\alpha$1c subunit under low $Ca^{2+}$ levels. Upon depolarization, the level of $Ca^{2+}$ in the channel vicinity increased, resulting in conformational changes in the CaM $Ca^{2+}$ sensor. This remodeling of CaM led to rearrangements in the NT-CT complex and promoted channel inactivation as part of the CDI (Guggenheimer et al., 2016).

In addition to the NT-CT interaction, the proximal and distal parts of the $\alpha$1c C terminus directly interact and this interaction is inhibited by CaM (Lyu et al., 2017). In the CaM-bound state, the distal and proximal parts do not interact and the opening probability of the channel is increased. The mechanism requires the interaction between the proximal and distal C-terminal regulatory domains (PCRD and DCRD (Hulme et al., 2006)) favoring downstream complexing. At low $Ca^{2+}$ levels and CaM not being bound, the end of the distal C-terminal tail and the IQ and preIQ motifs in the proximal C terminus are interacting. The resulting conformational change reduces the open probability of the channel (Lyu et al., 2017). A dynamic model was suggested, in which the distal C terminus competes with CaM for binding at IQ and pre-IQ motifs, reducing open probability and the proximal part interaction with the distal part, blocks the inhibitory effect of the distal C terminus, enhancing channel opening (Lyu et al., 2017)

#### 1.2.2.5 The role of channel clustering

The amount of $Ca^{2+}$ influx into cardiac myocytes is directly influenced by the amount of LTCC channels clustering within sarcolemma invaginations, the so-called transverse tubules (t-tubules) where they are closely located to RyRs at the SR membrane (Bhargava et al., 2013; Bhogal et al., 2018; Kumari et al., 2018). To analyze these LTCC channel clusters, the group of Gorilek and colleagues developed a method called “super-resolution scanning patch-clamp”, which combines scanning ion conductance microscopy (SCIM) with patch-clamp (Bhargava et al., 2013; Kumari et al., 2018). They found that the channels within these clusters are connected via their C termini in a $Ca^{2+}$/CaM-dependent manner and that their opening and closing is synchronized (Dixon et al., 2015; Ito et al., 2019). In response to membrane depolarization, the individual channels within a cluster are activated resulting in a local increase in the $Ca^{2+}$ concentration. The $Ca^{2+}$ binds to CaM bound to the preIQ motif, which leads to physical interaction and activation of neighboring channels, increasing the $Ca^{2+}$ concentration even

further. Individual channel inactivation by $Ca^{2+}$-dependent inactivation (CDI) induces a local $Ca^{2+}$ decrease and channel uncoupling, terminating the $Ca^{2+}$ influx (Dixon et al., 2015).

By using a combination of fluorescence resonance energy transfer (FRET) and SCIM, it was found that t-tubules accommodate compartmentalized cAMP signaling in response to stimulation of the β-adrenergic pathway (Bhogal et al., 2018; O. et al., 2010). The above-mentioned model of channel clustering was expanded by Ito *et al.* (Ito et al., 2019) who found altered LTCC clustering in response to β-adrenoceptor agonist (isoproterenol) stimulation. The isoproterenol administration improved channel clustering at the t-tubules forming super-clusters which promoted the functional interactions. In SCIM experiments, PKA dependency of the LTCC was shown via the inhibition of PKA and the resultant effects on clustering behavior (Ito et al., 2019).

Because of the specific location of the LTCCs and other $Ca^{2+}$ handling proteins in the t-tubules, the CICR process is finely regulated by the precise positioning of these proteins (Dibb et al., 2021). LTCCs reside within caveolae and are recruited by microtubules which are controlled by bridging integrator (BIN1) (Hong et al., 2010). Anchoring of LTCC is achieved by junctophilin 2 (JPH2) (Gross et al., 2021) and caveolin-3, which is an important component of t-tubules, and was shown to recruit PKA to the LTCC complex. Recruitment of PKA mediates phosphorylation of Rad, releasing its inhibitory function on the LTCC, increasing the $I_{Ca,L}$ (Dibb et al., 2021; Kamp & Hell, 2000; Liu et al., 2020).

## 1.3 Phosphodiesterase structure and function

cAMP-hydrolyzing phosphodiesterases (PDEs) are major regulators of cAMP signaling. They hydrolyze cAMP and/or cGMP (Movsesian et al., 2018; Preedy, 2020). Eleven families of PDEs were described in mammals (PDE1-PDE11) and were classified based on their structure, substrate specificity, kinetic activity and regulatory mechanisms (Ercu & Klussmann, 2018; Maurice et al., 2014; Movsesian et al., 2018). PDE1-3, 10 and 11 are dual-specific. They hydrolyze both cAMP and cGMP; PDE4, PDE7 and PDE8 are cAMP-specific and PDE5, PDE6 and PDE9 hydrolyze cGMP (Movsesian et al., 2018).

The different PDE families share structural characteristics, i) the conserved catalytic domain, ii) the regulatory domain, N-terminal from the catalytic domain and iii) a region between the catalytic domain and the C terminus, that can be prenylated (PDE6) or phosphorylated by mitogen-activated protein kinase (MAPK) (PDE4) (Anant et al., 1992; Azevedo et al., 2014; Baillie et al., 2000; Conti & Beavo, 2007; Keravis & Lugnier, 2010). The active site of phosphodiesterases is formed by helix junctions and is highly conserved (Azevedo et al., 2014; Ke & Wang, 2007). Multiple PDE isoforms are expressed in almost all cells at different levels, with PDE1C, PDE2A, PDE3A, PDE4A and PDE7A being highly

expressed in the human heart (Azevedo et al., 2014; Bender & Beavo, 2006; Conti & Beavo, 2007; Francis et al., 2011). Of these, PDE3 and PDE4 are the predominant families degrading cAMP, with PDE3A prevailing in the human and PDE4 in rodent heart (Leroy et al., 2008, 2018; Mika et al., 2013; Richter et al., 2011).

The two isoforms of the PDE3 family are expressed in cardiomyocytes and although they are dual-specific enzymes, the turnover rates for cAMP hydrolysis are higher than for cGMP (Boyes & Loten, 1988; Degerman et al., 1997; Grant & Colman, 1984; Movsesian et al., 2018). Enzymes of the PDE3 family are derived from two genes, *PDE3A* and *PDE3B. PDE3A* encodes three isoforms that are a result of alternative transcription start and translation initiation sites, yielding two mRNAs (Meacci et al., 1992; Miki et al., 1996; Wechsler et al., 2002). The three isoforms differ only in their N-terminal region (Figure 5). PDE3A1 is the largest isoform (MW = 136 kDa), translated from the first mRNA and the protein contains two hydrophobic regions at the N-terminus (NHR) that allow the interaction with cellular membranes (Ercu & Klussmann, 2018; Kenan et al., 2000; Shakur et al., 2000). PDE3A2 (MW = 118 kDa) is translated from the second mRNA, lacks the first hydrophobic region of PDE3A1 and is localized in the cytosol or the plasma membrane (Ercu & Klussmann, 2018; Movsesian et al., 2018). The smallest isoform, PDE3A3 (MW = 94 kDa) lacks the hydrophobic regions of PDE3A1 and PDE3A2 and is therefore cytosolic.

One isoform of PDE3B has been described (MW = 124 kDa) and its catalytic domain shares 80% sequence identity with that of PDE3A (Degerman et al., 1997; Miki et al., 1996). Both, PDE3A and PDE3B, show differences in their subcellular localization and PDE3A is more abundant (Reinhardt et al., 1995). PDE3A1 and PDE3A2 localize to the SR forming a complex with SERCA2, AKAP18, PLN and CamKII (Ahmad et al., 2015; C. R. Carlson et al., 2022) PDE3A is recruited into a complex with SERCA2 upon phosphorylation and regulates cAMP levels at the SR. This affects the phosphorylation status of PLN meaning PDE3A plays an important role in the $Ca^{2+}$ re-uptake into the SR and the relaxation process (Ercu & Klussmann, 2018) (Figure 4).

PDE3B is located at the t-tubules, areas of the plasma membrane that are rich in caveolin-3. PDE3B is more involved in regulation of metabolism whereas PDE3A regulates cardiac contractility (Movsesian et al., 2018). In the mouse heart, PDE3A knock-out results in alteration of cardiac contractility, with enhanced cardiac contractility and relaxation in isolated murine hearts due to increased $Ca^{2+}$ re-uptake into the SR (Beca et al., 2013). In contrast, PDE3B knock-out protects the myocardium from ischemic damage by enrichment of antiapoptotic Bcl-2 and mitochondrial enrichment of cardioprotective proteins (Chung et al., 2015).

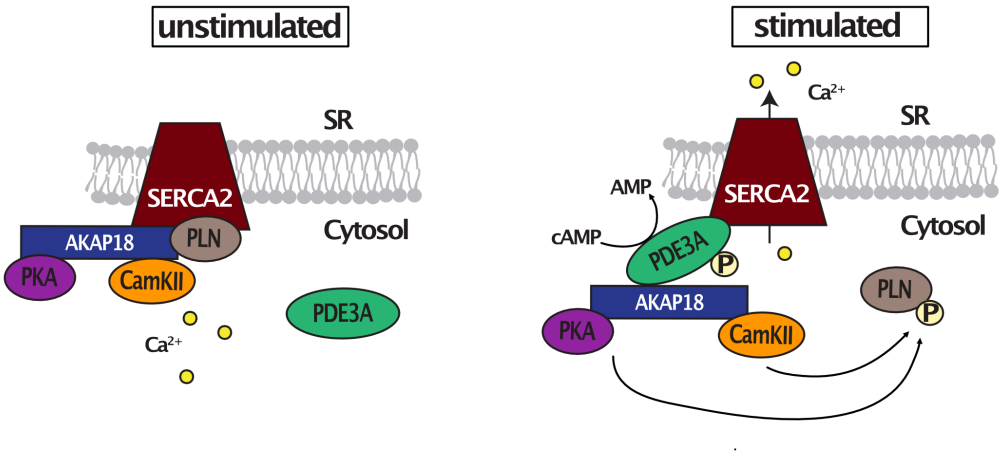


**Figure 4: PDE3A is involved in regulation of cAMP levels at the SR.** In the resting cardiac myocyte, sarcoplasmic/endoplasmic reticulum $Ca^{2+}$ ATPase (SERCA2) is inhibited by binding of phospholamban (PLN). Upon β-AR stimulation (e.g.,with isoproterenol), protein kinase A (PKA) and calmodulin-dependent protein kinase II (CamKII) phosphorylate PLN, resulting in its dissociation from the complex and $Ca^{2+}$ uptake into the SR. Phosphorylation of PDE3A incorporates it into the complex. PKA inactivation and thus termination of PLN phosphorylation is mediated by PDE3A through hydrolysis of cAMP.

### 1.3.1 Hypertension with brachydactyly type E (HTNB)

Hypertension with brachydactyly type E (HTNB) is an autosomal-dominant disease, caused by mutations in the *PDE3A* gene and was first described in a Turkish family (Bilginturan et al., 1973; Schuster et al., 1996; Toka et al., 2015). To date, ten *PDE3A* mutations were found in eleven unrelated families (Boda et al., 2016; Ercu et al., 2020; X. Li et al., 2020; Maass et al., 2015; Renkema et al., 2018; Toka et al., 2015). The disease is characterized by salt-resistant, progressive hypertension, blood vessel hyperplasia and leads to death by stroke before the age of 50, if left untreated (Bähring et al., 2008; McEniery et al., 2010; Schuster et al., 1996; Toka et al., 2015). The patients are 10-15 cm shorter than unaffected family members with no difference in the body mass index (BMI) and have characteristically shortened metacarpals (Schuster et al., 1996). Despite the life-long hypertension, the patients do not develop abnormal cardiac function or morphology (Schuster et al., 1996; Toka et al., 2015), for example their left ventricular mass and cardiac output are unaffected. They show no change of parameters associated with aortic stiffness (distensibility of the ascending aorta, aortic pulse wave velocity) and display normal platelet function (Toka et al., 2015). Blood vessel hyperplasia was associated with an increased VSMC proliferation rate (Ercu et al., 2020; Maass et al., 2015). Further, the patients do not differ from healthy individuals in terms of sodium handling or components of the renin-angiotensin-aldosterone pathway (Ercu et al., 2020; Schuster et al., 1996).

### 1.3.2 HTNB and PDE3A

HTNB-causing mutations were found to be localized in a 15 bp "hot-spot" region in the DNA encoding the N-terminal region of the PDE3A protein, affecting amino acid residues T445-G449 (Ercu et al., 2020; Maass et al., 2015; van den Born et al., 2016) (Figure 5). Since the PDE3A3 isoform has a shorter N-terminal region, starting at amino acid 484, it is not affected by the "hot-spot" mutations.

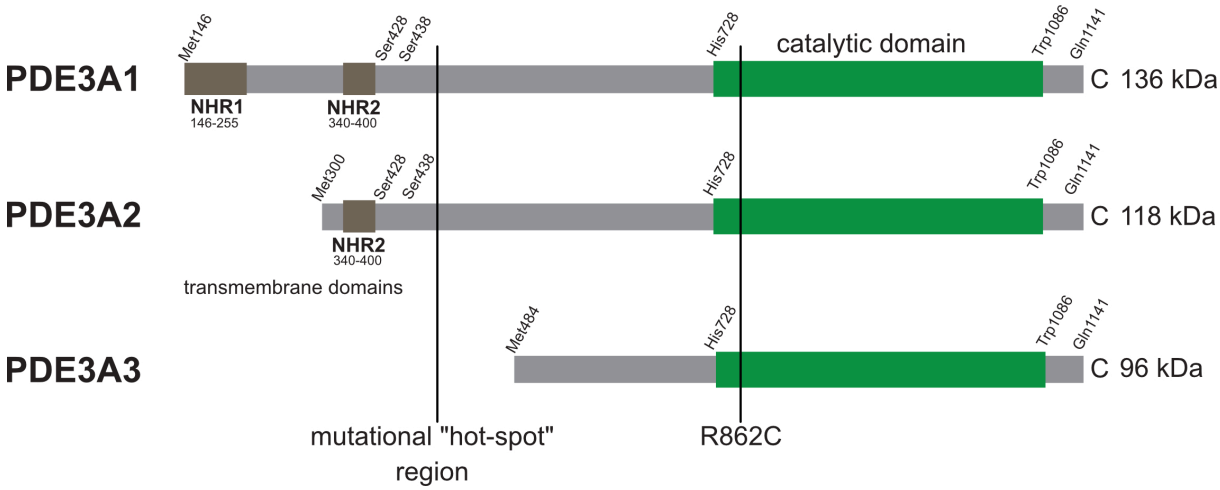


**Figure 5: Scheme of the PDE3A isoforms and location of HTNB-causing amino acid substitutions.** The three different isoforms of PDE3A are shown. The mutational hotspot region and a novel substitution affecting the catalytic domain are depicted. Amino acid numbering according to the human PDE3A protein sequence (Uniprot ID #Q14432).

Mechanistically, Maass *et al*. showed that cAMP levels in HeLa cells overexpressing the mutant PDE3A proteins are significantly reduced compared to the WT PDE3A, with cGMP levels being unaffected (Maass et al., 2015). Studying PDE3A enzyme kinetics based on the Michaelis-Menten model revealed a decreased $K_M$ of the mutant (T445N substitution) compared to the WT PDE3A1 and PDE3A2 ($K_M$ PDE3A1 - WT = 322.4 nM, $K_M$ PDE3A1 – T445N = 292.2 nM; $K_M$ PDE3A2 - WT = 111.4 nM, $K_M$ PDE3A2 – T445N = 103.9 nM) (Maass et al., 2015). This means the mutant has a higher affinity to its substrate. In line, more than 100 times higher concentrations of the PDE3A inhibitor milrinone were required to inhibit the T445N mutant protein ($IC_{50}$ PDE3A1 – WT = 0.000112 µM, $IC_{50}$ PDE3A1 – T445N = 0.234 µM, $IC_{50}$ PDE3A2 – WT = 0.0034 µM, $IC_{50}$ PDE3A2 – T445N = 1.242 µM) whereas the $IC_{50}$ values for cGMP-mediated inhibition were unchanged ($IC_{50}$ PDE3A1 – WT = 5.2 µM, $IC_{50}$ PDE3A1 – T445N = 4.8 µM) (Maass et al., 2015). PDE3A hydrolytic activity is associated with S428 and S438 phosphorylation by PKA or protein kinase C (PKC) (Hunter et al., 2009; Maass et al., 2015; M. Rubio et al., 2005; Wechsler et al., 2002). Phosphorylation of these two residues in the T445N mutant was increased in transfected

Hela cells and patient derived VSMCs. This phosphorylation was associated with increased cAMP hydrolytic activity of the mutants (Maass et al., 2015).

Ercu *et al*. established a rat model harboring a 9-bp deletion within the hotspot region of PDE3A (Δ3aa), resembling a human deletion (T445del). This rat showed the characteristic HTNB phenotype with increased blood pressure but no cardiac damage (Ercu et al., 2020). Western blot experiments revealed expression of the two isoforms of PDE3A, PDE3A1 and PDE3A2, in the heart. However, this expression was downregulated in the PDE3A-Δ3aa rats. In line with the previous study of Maass *et al*., phosphorylation of S428 was increased in the mutants leading to an increased interaction with the adaptor protein 14-3-3θ (Ercu et al., 2020).

The media to lumen ratio of second-order mesenteric arteries was increased in the PDE3A-Δ3aa rat model compared to the wildtype animals and they had lower cAMP levels in their vessels (Ercu et al., 2020). In accordance with the characteristic blood vessel hyperplasia seen in HTNB-patients, the proliferation rate of VSMCs from the mutant rats was increased compared to the wildtype (Ercu et al., 2020).

Using Hela cells transfected with PDE3A-encoding plasmids or patient-derived vascular smooth muscle cells (VSMCs) endogenously expressing the T445N substitution, it was shown that the mutations increased mitotic rates (Maass et al., 2015).

FRET measurements in HEK293 cells using a cytosolic cAMP sensor and transiently expressing PDE3A2-T445N, PDE3A2-G449V or PDE3A2-Δ3aa showed lower cAMP levels in the cells expressing mutant PDE3A2 compared to the WT. This is consistent with the increased PDE3A hydrolytic activity shown previously (Ercu et al., 2020; Maass et al., 2015).

### 1.3.3 PDE3A protein-protein interactions and non-enzymatic functions

In addition to the previously mentioned association of PDE3A in a complex with SERCA2, other protein-protein interactions (PPIs) were identified using proteomics approaches. Using PDE inhibitors such as 3-isobutyl-1-methylxantine (IBMX), cilostamide and papaverine as a bait combined with mass spectrometry, Corradini *et al*. found PDE3A associated with the phosphatase PP2A complex, consisting of , PPP2R1A scaffold subunit, PPP2CB catalytic subunit and PPP2R2A regulatory subunit (Corradini et al., 2015). Further, they found 14-3-3 bound to this complex. 14-3-3 interacts with PDE3A in its phosphorylated state and this is released upon dephosphorylation (Corradini et al., 2015; Meek et al., 2004; Pozuelo Rubio et al., 2005; M. P. Rubio et al., 2004; Vandeput et al., 2013). 14-3-3 is a scaffolding protein that is highly conserved and expressed in all eukaryotic cells. Through binding of

phosphorylated serines of a multitude of proteins, e.g. kinases, phosphatases and transmembrane receptors, they are involved in a variety of signaling pathways (Ercu et al., 2020; Muslin et al., 1996; X. Yang et al., 2006).

In cardiomyocytes, PDE3A is found in a multiprotein complex associated with PI3Kγ (Ghigo et al., 2012; Movsesian et al., 2018). How PDE3A is associated with the complex still needs to be resolved. The loss of the PI3Kγ scaffolding function leads to increases in the cAMP level und hyperphosphorylation of PLN and the LTCC (Ghigo et al., 2012; Marcantoni et al., 2006; Movsesian et al., 2018). Malfunctions of this complex are associated with contractile dysfunction, ventricular arrythmias and heart failure 10/11/22 9:44:00 AM.

In the past years, PDE3A was shown to have functions other than cAMP and cGMP hydrolysis and these functions are termed “non-canonical” and are predominantly associated with apoptotic pathways (Yan et al., 2022). The protein SLFN12 interacts with PDE3A and this interaction is induced by cytotoxic PDE3A modulators (e.g. velcrins) and is sufficient to cause cell death (Yan et al., 2022). The modulators occupy the catalytic domain of PDE3A, but do not inhibit cAMP hydrolysis most likely because of their lower affinity to the catalytic site compared to cAMP (Yan et al., 2022).

#### 1.3.3.1 PDE3A and the L-type $Ca^{2+}$ channel

PDEs control local cAMP levels and proteins in their vicinity. They are associated with the LTCC and are involved in the regulation of $Ca^{2+}$ influx through the channel. PDE2 inhibited the $I_{Ca,L}$ in frog ventricular, human atrial and rat neonatal cardiomyocytes and antagonized the β-adrenergic regulation (Fischmeister et al., 2006; Fischmeister & Hartzell, 1987; Mongillo et al., 2006; Vandecasteele et al., 2001).

In mice, the PDE4B and PDE4D isoforms are components of the LTCC complex and are thus involved in the β-adrenergic signaling pathway (Leroy et al., 2011, 2018).

To date, no direct interaction of PDE3A and the LTCC was shown, but several studies point to a role for PDE3A. Inhibition of PDE3 or PDE4 in mouse sinoatrial node cells (SANCs) increased the $Ca^{2+}$ current by around 60% and 72%, respectively. The same observation was also made in rabbit SANCs upon PDE3, but not PDE4, inhibition (Hua et al., 2012; Vinogradova, Kobrinsky, et al., 2018; Vinogradova, Sirenko, et al., 2018). The simultaneous inhibition of both, PDE3 and PDE4, in rabbit SANCs increased the $I_{Ca,L}$ by 100%, arguing for a synergistic effect of the two enzymes (Vinogradova, Kobrinsky, et al., 2018; Vinogradova, Sirenko, et al., 2018).

### 1.3.4 Compartmentalization of cardiac cAMP signaling and its implications for therapy

To ensure a high specificity in cellular responses to certain stimuli and with cAMP being an ubiquitous second messenger, its signaling pathways occur in cAMP micro- or nanodomains that are restrained to specific intracellular compartments and encompass different effector proteins (such as phosphatases, kinases and channels) and modulators (such as PDEs and AC) (Chao et al., 2019; Colombe & Pidoux, 2021; Fischmeister et al., 2006). The organization of these nanodomains is often mediated by AKAPs that anchor and target the effector and modulator proteins to the subcellular compartments (Colombe & Pidoux, 2021; Pidoux & Taskén, 2010). In these compartments, AKAPs tether PKA to their specific substrates and the activation of PKA subsets is achieved by increasing cAMP upon a certain stimulus (Chao et al., 2019; Wong & Scott, 2004). This enables rapid and selective PKA-mediated phosphorylation (Gorshkov et al., 2017; Surdo et al., 2017; Zaccolo & Pozzan, 2002). Further, these nanodomains contain ACs, which produce cAMP, PDEs for cAMP hydrolysis and phosphatases (PPs), which dephosphorylate the PKA substrates. Examples for these nanodomains include the AKAP9, AC2/9, potassium channel subunit KCNQ1 and phosphatase PP1 complex at the sarcolemma involved in the regulation of cAMP-mediated $K^+$ currents (Piggott et al., 2008) or a complex composed of mAKAP, RyR2 and PDE4D3 localized at the nucleus. The last complex regulates RyR phosphorylation and other signaling pathways (Chao et al., 2019; Passariello et al., 2015).

With the development of fluorescence resonance energy transfer (FRET)-based cAMP sensors and targeting of them to subcellular domains, novel insight into local cAMP levels and changes were provided. One of the first classes of these channels contain a cAMP sensor made of the protein Epac or only its cyclic nucleotide binding domain (CNBD) flanked by YFP and CFP (DiPilato et al., 2004; Nikolaev et al., 2004; Ponsioen et al., 2004). Upon cAMP binding this sensor changes its conformation and the FRET signal is decreased. A more novel sensor named “cAMP universal tag for imaging experiments” (CUTie) is made of the CNBD B of the PKA-RIIβ protein again flanked by YFP and CFP. In this sensor the YFP is inserted within an intra-domain loop allowing the fusion of targeting proteins to the free N terminus (Chao et al., 2019).

In cardiac diseases, cAMP nanodomains are deregulated and are thus an attractive target for therapeutics. One of the effectors in cAMP nanodomains would be PKA and inhibition of PKA with PKI in transgenic mice prevented β-AR stimulation induced cardiac hypertrophy, fibrosis and deregulation of cardiac function (Colombe & Pidoux, 2021; X. Zhang et al., 2013). Further, selective PKA inhibition was associated with an increased cardioprotective potential compared to β-blocker therapy after MI (X. Zhang et al., 2013).

In mice, overexpression of AC6 reduced mortality, decreased cardiac remodeling, retained cardiac functions and had a positive effect on contraction post-MI (Colombe & Pidoux, 2021; T. Takahashi et al., 2006). Although the exact mechanisms remained unknown, the authors associated the improved contraction with higher PLN phosphorylation increasing the SR $Ca^{2+}$ load (T. Takahashi et al., 2006).

Potential therapeutic approaches include the disruption of PPIs in subcellular signaling complexes using for example peptides or small molecules (Calejo & Taskén, 2015; Colombe & Pidoux, 2021). Peptides that disrupt PKA-AKAP interactions were designed and tested for their efficacy in the heart (Calejo & Taskén, 2015). For high specificity, the anchoring domain between AKAPs and substrates of PKA should be targeted since the AKAP-PKA interaction domain is structurally similar among different complexes. One example for a PPI-disruptor is a peptide targeting the AKAP18/PLN interaction at the SR which caused alterations in $Ca^{2+}$ re-uptake (Lygren et al., 2007). Further, a peptide disrupting mAKAP/calcineurin (CaN) decreased the hypertrophy of cardiomyocytes and a similar effect was observed by using an AKAP-Lbc/p38 disruptor peptide in a transverse aortic constriction (TAC) mouse model (J. Li et al., 2013; Pérez López et al., 2013). In the heart, a complex of Hsp20, PKA, AKAP-Lbc and PDE4D5 was described and confers cardioprotective functions *via* the Hsp20 (Blair & Baillie, 2019; Edwards et al., 2011, 2012). Hsp20 is inactivated in the presence of PDE4D5. A 25-mer cell permeable peptide (bs906) was developed to disrupt the interaction of PDE4D5 and Hsp20 (Blair & Baillie, 2019; Sin et al., 2011). Displacement of PDE4D5 resulted in attenuated ANP expression, cardiac hypertrophy, fibrosis and improved left-ventricle function in a mouse model of heart failure (Blair & Baillie, 2019; Martin et al., 2014).

### 1.3.5 PDE3 inhibitors and disruption of PDE3A subcellular localization

Pharmacological inhibition of PDE3, for example with milrinone or cilostazol, is associated with increased myocardial contractility (Anderson, 1991; Baim et al., 1983; Benotti et al., 1978; Jaski et al., 1985; Maskin et al., 1983; Monrad et al., 1984; Movsesian et al., 2018; Sinoway et al., 1983). In PDE3A or PDE3B knock-out mice the inotropic effects were only mediated by PDE3A inhibition, since PLN phosphorylation and thus SERCA2 activity, $Ca^{2+}$ cycling and the contractility are upregulated only in $PDE3A^{-/-}$ mice (Beca et al., 2013; M. Movsesian et al., 2018).

Making use of a combination of molecular modeling and site-directed mutagenesis, Zhang *et al.* identified the key residues involved in the binding of cilostazol or milrinone inhibitors to PDE3 (W. Zhang et al., 2002). They have shown that the specificity of the different inhibitors was conferred by binding to different amino acid residues in the active site (Atienza et al., 1999; W. Zhang et al., 2002). In the rabbit heart, milrinone alone had a similar effect on cAMP levels as a combination of PDE4 and

PDE3 inhibition with rolipram and cilostazol, suggesting that milrinone was also affecting PDE4 at higher doses (> 10 µM) (Shakur et al., 2002). Since PDE4 activity was lower in the failing human heart, the PDE4 effect of milrinone was less relevant (Shakur et al., 2002).

In contrast to short-term administration, chronic treatment with PDE3 inhibitors is associated with increased mortality (19% per year) (Amsallem et al., 2005; Cohn et al., 1998; DiBianco et al., 1989; Movsesian et al., 2011, 2018b; Narahara, 1991; Packer et al., 1991, 1993; Uretsky et al., 1990). One potential explanation could be the pro-hypertrophic effects of PDE3A inhibitors inducing pathological changes in the myocardium which increases the risk for arrythmias (Movsesian et al., 2018). In primary mouse cardiomyocytes chronic exposure to PDE3 inhibitors causes an upregulation of inducible cAMP early repressor (ICER). ICER reduces PDE3A protein levels by blocking its transcription and promotes apoptosis through Bcl-2 downregulation (Bork et al., 2021; Ding, Abe, Wei, Xu, et al., 2005, 2005).

As an alternative to PDE3 inhibitors, elevating cGMP levels using guanylate cyclase activators (e.g. riociguat) improved the situation of individuals affected by pulmonary hypertension (Ghofrani et al., 2013) and had a cardioprotective effect in a mouse model of ischemia/reperfusion (I/R) injury (Bork et al., 2021; Frankenreiter et al., 2017, 2018; Lukowski et al., 2021). Toka *et al.* observed that in HeLa cells transiently transfected with PDE3A wildtype or mutant constructs, elevated cGMP levels induced by the guanylyl cyclase stimulator BAY41-8543 reduced the increased cAMP hydrolytic activity of the mutants compared to that of the wildtype protein (Toka et al., 2015).

Using a mouse model with heterozygous or homozygous *Pde3a* deletion, Bork *et al*. studied how the PDE3A protein levels induced a cGMP-dependent cardioprotective effect or apoptosis *via* the cAMP pathway (Bork et al., 2021). They found a dose-dependent effect of PDE3A levels, with a moderate decrease of the PDE3A level (30 – 50%) leading to increased cGMP levels and protection against hypoxia/reperfusion (H/R)-induced death, whereas knock-out of PDE3A decreased the survival rates of the cells. Thus, the use of low dosage PDE3A inhibitors could be an attractive treatment option. In line, the use of low-doses of the PDE3 inhibitor enoximone improved the exercise capacity in patients with chronic heart failure (Bork et al., 2021; Lowes et al., 2000).

An alternative to pharmacological treatment would be to target PDE3A at subcellular sites. Since PDE3A isoforms are localized at different cellular compartments, targeting each isoform individually would affect only local cAMP levels and thus impact different cellular pathways (e.g. PDE3A1 that is membrane associated) (Movsesian et al., 2018). Targeting PDE3A isoforms by disruption of their PPIs might confer beneficial effects, for example by increasing intracellular $Ca^{2+}$ concentration and thus contractility by replacing PDE3A from the complex at the SR (Figure 4) (Movsesian et al., 2018).

# 2 Aims

The aim of this thesis was to provide insights into novel aspects of the ECC, focusing on the LTCC and PDE3A.

In the first part, together with the group of Prof. Dr. Nathan Dascal (Tel Aviv, Israel) the aim was to elucidate how PKA catalytic subunit (PKA-CS) is recruited to the LTCC complex. The recruitment was independent of AKAPs and PKA regulatory subunit (RS). Direct binding of PKA-CS to the C terminus of the $\alpha$1c subunit of the LTCC could be an alternative mechanism. For this project, biochemical methods were combined with experiments in a HEK293 cell model and the interaction sites were mapped using peptide spotting. To determine whether the interaction would influence the enzyme's catalytic activity, enzymatic assays were conducted.

A potential interaction between PDE3A and the LTCC was studied, to find out if PDE3A hydrolyzes cAMP at the LTCC, thus regulating PKA-CS activity and LTCC opening probability.

In the second part of the thesis, the aim was to contribute to elucidating the molecular mechanisms underlying the potential cardioprotective effect of *PDE3A* mutations. Human induced pluripotent stem cell-derived cardiomyocytes (hiPSC-CMs) served as the cellular model system. The hiPSC-CMs expressed PDE3A proteins harboring the HTNB-causing amino acid substitutions. To unravel the influence of mutant PDE3A enzyme on the ECC pathway and $Ca^{2+}$ signaling, $Ca^{2+}$ imaging in hiPSC-CMs was conducted and the expression of several proteins studied, amongst them the $\alpha$1c subunit of the LTCC.

One of the complexes PDE3A is associated with is a multiprotein complex with SERCA2 at the SR. PDE3A wildtype and mutant constructs were expressed in HEK293 cells together with SERCA2 and the binding of these two proteins was studied, to find out if this interaction was affected by the *PDE3A* mutations.

# 3 Material and Methods

## 3.1 Material

### 3.1.1 Equipment

**Table 1: Equipment and devices.**

| Description | Instrument | Supplier |
|---|---|---|
| Agarose gel detection system | Azure c200 Gel Imaging Workstation | Azure Biosystems, Inc. (Dublin, CA, US) |
| Agarose gel electrophoresis system | PerfectBlue™ gel system, Mini L | Peqlab Biotechnologie GmbH (Erlangen, DE) |
| Analytical balance | Secura®225D-1S SBA 52 | Sartorius AG (Göttingen, DE) |
| Bacterial shaker | Multitron standard | Infors AG (Bottmingen, CH) |
| Centrifuge | Avanti®J-E Centrifuge | Beckman Coulter GmbH (Krefeld, DE) |
| | Centrifuge 5427 R | Eppendorf AG (Hamburg, DE) |
| | Universal 320 R | Andreas Hettich GmbH & Co. KG (Tuttlingen, DE) |
| | Large Scale Centrifuge | Beckman Coulter GmbH (Krefeld, DE) |
| Cell counter | Countess™ II automated cell counter | Thermo Fisher Scientific (Waltham, MA, US) |
| Chromatography System | GE Akta Explorer<br>Unicorn® software | Amersham Pharamcia Biotech, GE Healthcare (Amersham, UK) |
| | GE AKTA Frac-950 | Amersham Pharamcia Biotech, GE Healthcare (Amersham, UK) |
| $CO_2$ incubator | CB210 | Binder GmbH (Tuttlingen, DE) |
| | MCO-18AIC | Sanyo Denki K.K. (Moriguchi, JP) |
| Flow cytometry | MACS Quant VYB | Miltenyi Biotech GmbH (Bergisch-Gladbach, DE) |
| Freezing container | Nalgene™ Freezing Container 5100-0001 | Thermo Fisher Scientific (Waltham, MA, US) |
| Magnetic stirrer | IKA®RCT standard | IKA®-Werke GmbH & Co. KG (Staufen, DE) |

| | | |
|---|---|---|
| Microscope | Axioskope | Carl Zeiss Microscopy GmbH (Jena, DE) |
| | LSM610 | Carl Zeiss Microscopy GmbH (Jena, DE) |
| | Opera Phenix High-content screening system | Perkin Elmer (Hamburg, DE) |
| Microfluidizer | M-110L Microfluidizer | Microfluidics (Westwood, US) |
| Microwave | Micromat Duo | AEG (Nürnberg, DE) |
| Myocyte Analysis System | CytoCypher MultiCell High Throughput System | Ionoptix (Amsterdam, NL) |
| Pacer | Stimulator C Type 224 | Hugo Sachs Elektronik – Harvard Apparatus (March, DE) |
| | MyoPacer MYP100 stimulator | Ionoptix (Amsterdam, NL) |
| Peptide spotter | AutoSpot-Robot ASS 222 peptide spotter | Intavis Bioanalytical Instruments AG (Köln, DE) |
| pH meter | pH-Meter 766 Calimatic | Knick Elektronische Messgeräte GmbH & Co. KG (Berlin, DE) |
| Photometer | Specord 205 | Analytic Jena (Jena, DE) |
| | Eppendorf BioPhotometer Plus | Eppendorf SE (Hamburg, DE) |
| Pipettes | Eppendorf Research pipettes | Eppendorf AG (Hamburg, DE) |
| | Eppendorf Xplorer pipette | Eppendorf AG (Hamburg, DE) |
| | Pipetboy acu | Integra Biosciences GmbH (Fernwald, DE) |
| Plate reader | EnSpire® Plate Reader | Perkin Elmer (Waltham, MA, US) |
| SDS-PAGE | Mini-Protean® Electrophoresis Cell | Bio-Rad Laboratories GmbH (Feldkirchen, DE) |
| Shaker | GFL 3017 Orbital Shaker | GFL Gesellschaft für Labortechnik GmbH (Burgwedel, DE) |
| | IKA® MS 3 basic | IKA®-Werke GmbH & Co. KG (Staufen, DE) |
| | PTR-35 Vertical Mini Rotator | Grant Instruments (Cambrigde, UK) |
| | RS-TR05 Tube Roller | Phoenix Instrument GmbH (Garbsen, DE) |

| | | |
|---|---|---|
| Sonicator | Sonoplus HD 2070 | Bandelin electronic GmbH & Co. KG (Berlin, DE) |
| Spectrophotometer | NanoDrop®ND-1000 Spectrophotometer | Peqlab Biotechnologie GmbH (Erlangen, DE) |
| Safety cabinet | Thermo Scientific™ Safe 2020 | Thermo Fisher Scientific (Waltham, MA, US) |
| Thermal cycler | TRIO Thermal Cycler | Analytic Jena GmbH (Jena, DE) |
| | ViiA™ 7 Real-time PCR System | Thermo Fisher Scientific (Waltham, MA, US) |
| Thermal mixer | Thermomixer comfort | Eppendorf AG (Hamburg, DE) |
| Ultrasound homogenizer | Sonoplus HD 2070 | Bandelin electronic GmbH & Co. KG (Berlin, DE) |
| Vacuum pump | KNF Laboport® N 86 KT.18 | KNF Neuberger GmbH (Freiburg, DE) |
| Water bath | GFL 1092 | GFL Gesellschaft für Labortechnik GmbH (Burgwedel, DE) |
| Western blot detection | Odyssey® FC | Li-Cor Biosciences (Lincoln, NE, US) |
| Western blot module | Mini Trans-Blot® Cell | Bio-Rad Laboratories GmbH (Feldkirchen, DE) |

### 3.1.2 Disposables

**Table 2: Disposable material.**

| **Description** | **Article** | **Supplier** |
|---|---|---|
| Blotting paper | Roti®-PVDF membrane, 0.45 µm | Carl Roth GmbH & Co. KG (Karlsruhe, DE) |
| Cell culture flask | Cell culture flask T75 | Sarstedt AG % Co. KG (Nümbrecht, DE) |
| Cell culture dishes | 60 mm cell culture dish | TPP (Trasadingen, CH) |
| | 35 mm glass bottom dishes | IBIDI (Gräfelfing, DE) |
| | 35 mm glass bottom dishes | Mattek (Ashlands, US) |
| Cell counting slides | Countess™ cell counting slides | Thermo Fisher Scientific (Waltham, MA, US) |

| | | |
|---|---|---|
| Columns | Pierce™ Centrifuge columns | Thermo Fisher Scientific (Waltham, MA, US) |
| Cryovials | Cryovials 2 mL | Carl Roth GmbH & Co. KG (Karlsruhe, DE) |
| FACS tubes | BD FACS tubes | BD Bioscience (Franklin Lakes, US) |
| Falcon tubes | Falcon Tubes 15 and 50 mL | Corning (Corning, NY, US) |
| Multiwell plates | Microplate, 96-well, PS, F-bottom, clear | Greiner Bio-One (Kremsmünster, DE) |
| | TopSeal®-A: 384- well Microplate | Perkin Elmer (Waltham, MA, US) |
| | 6 well plate | Greiner Bio-One (Kremsmünster, DE) |
| Parafilm | Parafilm®M sealing film | Sigma Aldrich (St. Louis, US) |
| Pipettes | Serological pipettes 5 mL, 10 mL , 25 mL, 50 mL | Sarstedt AG & Co. KG (Nümbrecht, DE) |
| Reaction tubes | Dolphin tubes, 1.5 mL | Carl Roth GmbH % Co. KG (Karlsruhe, DE) |
| | PCR tubes, 0.2 mL | Biozym Scientific GmbH (Hessisch Oldendorf, DE) |
| | Reaction tubes, 1.5 and 2 mL | Sarstedt AG & Co. KG (Nümbrecht, DE) |
| Spatula | TPP cell spatula | TPP Techno Plastic Products AG (Trasadingen, CH) |
| Syringes and needles | 100 Sterican® needle (Gr. 18) | B. Braun Melsungen AG (Melsungen, DE) |
| | Omnifix®F-syringe, 1 mL | B.Braun Melsungen AG (Melsungen, DE) |
| Tips | Filter tips | Starlab International GmbH (Hamburg, DE) |

### 3.1.3 Kits

**Table 3: Commercial kits.**

| Kit | Description | Supplier (Art. no. #) |
|---|---|---|
| Agilent Quick Change SDM XL | Site-directed mutagenesis | Agilent Technologies (Santa Clara, US), #200523 |
| Direct-zol RNA Microprep Kit | RNA purification | Zymo Research (Freiburg, DE), #R2062 |
| FoxP3 Staining buffer set | Cell permeabilization kit | Miltenyi Biotec GmbH (Auburn, US), #130-093-142 |
| NucleoSpin®Extract II kit | DNA purification from agarose gels | Macherey-Nagel (Düren, DE), #740609.50 |
| NucleoSpin® Plasmid QuickPure | Mini DNA purification | Macherey-Nagel (Düren, DE), #740615.50 |
| NucleoSpin®Plasmid Midi/Maxi | Midi DNA preparation | Macherey-Nagel (Düren, DE), #740410.50 |
| Pierce™BCA protein assay kit | Protein purification | Thermo Fisher Scientific (Bonn, DE), #23225 |
| Q5®Site-directed mutagenesis Kit | Site-directed mutagenesis | New England Biolabs (Ipswich, US), #E0554S |
| qScript®cDNA synthesis Kit | cDNA synthesis | Quanta Biosciences (Beverly, US), #95047-025 |

### 3.1.4 Software

**Table 4: Software.**

| Software | Description | Supplier/ URL |
|---|---|---|
| Affinity Designer | Graphics & Design | Serif Labs (Nottingham, UK) |
| CalTrack | $Ca^{2+}$ transient analysis | https://github.com/ToepferLab/CalTrack |
| CytoSolver Desktop | $Ca^{2+}$ transient analysis | Ionoptix (Amsterdam, NL) |
| FlowJo V. 10.8.0 | Flow cytometry analysis | www.flowjo.com |

| | | |
|---|---|---|
| GraphPad Prism 8 | Graphs and statistical analysis | GraphPad Software, Inc. (San Diego, US) |
| Image J 1.53a | Image processing | Wayne Rasband, National institutes of health (US) |
| IonWizard | $Ca^{2+}$ transient recording | Ionoptix (Amsterdam, NL) |
| Microsoft Excel 2019 | Spreadsheet | Microsoft Corporation (Redmond, US) |
| Microsoft PowerPoint 2019 | Presentation | Microsoft Corporation (Redmond, US) |
| Microsoft Word 2019 | Word processing | Microsoft Corporation (Redmond, US) |
| SnapGene Viewer | Plasmid analysis | GSL Biotech LLC (Chicago, US) |
| ViiA™ 7 V.7 | qPCR software | Thermo Fisher Scientific (Waltham, US) |
| Zotero 6.0.5 | Reference manager | https://www.zotero.org/download/ |

### 3.1.5 Antibodies

**Table 5: Primary antibodies used for western blotting, Flow cytometry and immunofluorescence.**

| Antibody | Application | Species | Supplier (Art. no. #) |
|---|---|---|---|
| AKAP150 | WB | Rabbit | Santa Cruz Biotechnology, #sc-10765 |
| Cav1.2 | WB, IP | Mouse | Alomone Labs, #ACC-003 |
| Cav1.2 | WB | Mouse | Thermo Fisher Scientific, #MA5-27717 |
| CamKII | WB | Rabbit | Thermo Fisher Scientific, #PA5-22168 |
| GAPDH | WB | Rabbit | Cell Signaling Technology, #2118 |
| GFP-Tag | WB, IP | Mouse | Thermo Fisher Scientific, #MA5-15256 |
| Hsp60 | WB | Rabbit | Cell Signaling Technology, #4870 |
| Hsp90 | WB | Mouse | Enzo Life Science, #SPA-830 |
| MLC2v | Flow cytometry | Human | Miltenyi Biotec GmbH, #130-106-184 |
| Myc-Tag | WB | Mouse | Cell Signaling Technology, #2276 |

| | | | |
|---|---|---|---|
| MyBPC3 | WB | Mouse | Santa Cruz Biotechnology, #sc-137180 |
| PDE3A | WB, IP, IF | Rabbit | Bethyl Laboratories, A302-740A |
| PKA-Cα | WB | Mouse | BD Bioscience #610980 |
| pSer/Thr PKA substrate | WB | Rabbit | Cell Signaling Technology, #9621 |
| PKA RIIα | WB | Mouse | BD Bioscience, #612243 |
| PLN | WB | Mouse | Thermo Fisher Scientific, #MA3-922 |
| pPLN (S16) | WB | Rabbit | Sigmal Aldrich, #07-052 |
| REA control antibody (I)-APC | Flow cytometry | Human | Miltenyi Biotec GmbH, #130-120-709 |
| REA control antibody (I)-FITC | Flow cytometry | Human | Miltenyi Biotec GmbH, #130-120-354 |
| TNNT2-FITC | Flow cytometry | Human | Miltenyi Biotec GmbH, #130-119-575 |
| Troponin I | WB | Rabbit | Cell Signaling Technology, #4002 |
| pTpn I (S23/24) | WB | Rabbit | Cell Signaling Technology, #4004 |
| SERCA2 | WB | Mouse | Thermo Fisher Scientific, #MA3-919 |

**Table 6: Secondary antibodies used for western blotting and immunofluorescence.**

| Antibody | Application | Species | Supplier (Art. no. #) |
|---|---|---|---|
| Peroxidase (POD)-anti-mouse IgG | WB | Donkey | Jackson ImmunoResearch Laboratories, #705-035-151 |
| POD-anti-rabbit IgG | WB | Donkey | Jackson ImmunoResearch Laboratories, #705-035-152 |

### 3.1.6 Buffers and chemicals

**Table 7: Composition of buffers and solutions.**

| Buffer | Application | Composition |
|---|---|---|
| Blocking buffer | WB | 5 % bovine serum albumine (BSA) or 5 % skim milk in 1 x TBS-T |
| $Ca^{2+}$ Imaging buffer | $Ca^{2+}$ Imaging | 135 mM NaCl, 4 mM KCl, 10 mM Hepes, 5 mM Glucose, 1.8 mM $CaCl_2$, 1 mM $MgCl_2$, pH 7.3 |
| Cook Assay buffer | PKA activity assay | 100 mM MOPS, 10 mM $MgCl_2$, 1 mM phosphoenolpyruvate (PEP), 1 mM ATP, 15 U/mL Lactate dehydrogenase (LDH), 8.4 U/mL Pyruvatekinase, 0.2 mM nicotinamidadenindinucleotide (NADH), 5 mM β-mercaptoethanol (β-ME), pH 7 |
| Coomassie de-stain solution | Coomassie | 40 % acetic acid, 10 % ethanol |
| Coomassie staining solution | Coomasssie | 0.025 % Coomassie brilliant blue, 10 % acetic acid |
| FACS buffer | Flow Cytometry | 0.5 % BSA, 2 mM EDTA, DPBS |
| Lämmli sample buffer (3x) | WB | 40 % glycerol, 8 % SDS, 0.4 bromophenol blue, 312.5 mM Tris-HCl, 200 mM DTT, pH 6.8 |
| Lysogeny broth (LB) medium | Bacteria culture | 10 g/L peptone, 5 g/L yeast extract, 5 g/L NaCl, pH 7.5 |
| LB agar medium | Bacteria culture | 10 g/L peptone, 5 g/L yeast extract, 5 g/L NaCl, 15 g/L agar |
| Phosphate-buffered saline (PBS) | Cell lysis | 137 mM NaCl, 2.7 mM KCL, 1.5 mM $KH_2PO_4$, 8.1 mM $Na_2HPO_4$, pH 7.4 |
| PKA Kinase buffer | PKA activity assay | 40 mM Tris-HCl, 20 mM $MgCl_2$, 0.1 mg/mL BSA, 50 µM DTT |
| PKA storage buffer | Protein purification | 20 mM MOPS, 150 mM NaCl, 0.1 mg/mL BSA, 1.5 mM β-ME, pH 7 |
| SDS-PAGE running buffer | WB | 25 mM Tris-HCl, 192 mM glycine, 0.1 % SDS |
| Separating gel buffer | WB | 625 mM Tris-HCl, pH 6.8 |

| | | |
|---|---|---|
| Standard lysis buffer (SLB) | Cell lysis | 10 mM $K_2HPO_4$, 150 mM NaCl, 5 mM EDTA, 5 mM EGTA, 0.5 % Triton-X-100, pH 7.4, 0.2 % sodium deoxycholate |
| Stacking gel buffer | WB | 750 mM Tris-HCl, pH 8.8 |
| TALON Buffer A | Protein purification | 30 mM Hepes, 500 mM NaCl, 10 mM Imidazole, 1 mM Benzamidine, pH 8.0 |
| TALON Buffer B | Protein purification | 30 mM Hepes, 500 mM NaCl, 300 mM Imidazole, 1 mM Benzamidine, pH 8.0 |
| Tank blot transfer buffer | WB | 20 mM Tris, 150 mM glycine, 10 % methanol, 0.02 % SDS |
| TBS + Tween (TBS-T) | WB | 1 x TBS, 0.05 % Tween-20 |
| Tris-acetate-EDTA (TAE) buffer | Agarose gels | 40 mM Tris, 1 mM EDTA, 1.14 % (v/v) glacial acetic acid |
| Tris-buffered saline (TBS) | WB | 10 mM Tris-HCl, pH 7.4, 150 mM NaCl |

**Table 8: Media, chemicals and fluorescent dyes.**

| **Substance** | **Application** | **Supplier (Art. no. #)** |
|---|---|---|
| 30 % Acrylamide/Bis solution | SDS-PAGE | Bio-Rad Laboratories GmbH (München, DE), #1610156 |
| 6 x DNA loading buffer blue | Agarose gels | New England BioLabs (Ipswich, US), #B7025S |
| Anti-FLAG®M2 Magnetic beads | IP | Sigma-Aldrich, (St.Louis, US), #M8823 |
| B-27™ supplement, 50 x | Cell culture | Thermo Fisher Scientific (Bonn, DE), #17504044 |
| B-27™ Minus Insulin, 50 x | Cell culture | Thermo Fisher Scientific (Bonn, DE), #A18956-01B27 |
| Bovine Serum Albumin (BSA) | WB | SERVA Electrophoresis GmbH (Heidelberg, DE), #11926.04 |
| CHIR-99021 | Cell culture | SelleckChem (München, DE), #S2924 |
| Cilostamide | Cell treatment | Sigma-Aldrich (St.Louis, US), #C7971 |

| | | |
|---|---|---|
| Coomassie Plus™ Protein Assay Reagent | Bradford Assay | Thermo Fisher Scientific (Bonn, DE), #1856210 |
| Cultrex UltiMatrix RGF | Cell culture | R&D Systems (Minneapolis, US), #BME-001-01 |
| DMEM, GlutaMAX™ | Cell culture | Life Technologies GmbH (Darmstadt, DE), #21885108 |
| DPBS (10 x) | Cell culture | Life Technologies GmbH (Darmstadt, DE), #14200067 |
| DRAQ5™ | FRET | Thermo Fisher Scientific (Bonn, DE), #62251 |
| Essential 8 (E8) medium | Cell culture | Thermo Fisher Scientific (Bonn, DE), #A15171-01 |
| Fetal calf serum (FCS) | Cell culture | Biochrom AG (Berlin, DE), #S0613 |
| Fibronectin, human plasma | Cell culture | Sigma-Aldrich (St. Louis, US), #F0895 |
| Fluo-8®-AM | $Ca^{2+}$ Imaging | AAT Bioquest (Sunnydale, US), #1345980-40-6 |
| Forskolin | Cell treatment | Biaffin GmbH & Co KG Life Sciences Institute (Kassel, DE), #PKE-FORS-050 |
| Fura-2/AM | $Ca^{2+}$ Imaging | Life Technologies (California, US), #F1221 |
| Geltrex™ | Cell culture | Thermo Fisher Scientific (Bonn, DE), #A1413302 |
| HyperLadder™ 1kbp | Agarose gels | BioLine GmbH (Luckenwalde, DE), #BIO33053 |
| IBMX | Cell treatment | Santa Cruz Biotechnology (Dallas, US), #28822-58-4 |
| Immobilon™ Western Chemiluminescent HRP substrate | WB | Merck Millipore (Schwalbach, DE), #WBKLS0500 |
| Immu-Mount™ | IF | Thermo Fisher Scientific (Bonn, DE), # 99-904-12 |
| (+)-Isoproterenol hydrochloride | Cell treatment | Sigma-Aldrich (St. Louis, US), #I5627 |
| Isopropyl-β-D-thiogalactopyranosid (IPTG) | Protein purification | Carl Roth GmbH & Co. KG (Karlsruhe, DE), #2316.4 |

| | | |
|---|---|---|
| IWR-1-endo | Cell culture | SelleckChem (München, DE), #S7086 |
| KnockOut™ serum replacement | Cell culture | Thermo Fisher Scientific (Bonn, DE), #10828028 |
| Lipofectamine™ 2000 | Transfection | Thermo Fisher Scientific (Bonn, DE) #11669-019 |
| Lipofectamine™ 3000 | Transfection | Thermo Fisher Scientific (Bonn, DE), #L3000-008 |
| Lipofectamine™ Stem | Transfection | Thermo Fisher Scientific (Bonn, DE), #15793407 |
| Corning® Matrigel® | Cell culture | Corning, Inc. (New York, US), #CLS354234-1EA |
| Milrinone | Cell treatment | Sigma-Aldrich (St. Louis, US), #M4659 |
| OptiMEM | Transfection | Life Technologies GmbH (Darmstadt, DE), #31985 |
| Penicillin/Streptomycin (P/S) | Cell culture | Merck Millipore (Schwalbach, DE), #A2213 |
| Pluronic®F-127 | Cell culture | AAT Bioquest (Sunnydale, US), #ABD-20050 |
| Precision Plus Protein Standard Dual color | SDS-PAGE | Bio-Rad Laboratories GmbH (München, DE), #1610374 |
| Protein-A-sepharose | IP | Sigma-Aldrich (St.Louis, US), #P3391 |
| RedSafe™ | Agarose gels | Intron Biotechnology (Seongnam, KR), #21141 |
| RevitaCell™ Supplement, 100 x | Cell culture | Thermo Fisher Scientific (Bonn, DE), #A2644501 |
| Gibco™ RPMI-1640 | Cell culture | Thermo Fisher Scientific (Bonn, DE), #11875-093 |
| RPMI-1640 w/o glucose | Cell culture | Thermo Fisher Scientific (Bonn, DE), #11879-020 |
| RPMI-1640, no phenol red | FRET | Thermo Fisher Scientific (Bonn, DE), #11835030 |
| Skim milk powder | WB | Fluka Analytical/Sigma (Taufkirchen, DE), #70166 |

| | | |
|---|---|---|
| TRIzol™ Reagent | RNA isolation | Thermo Fisher Scientific (Bonn, DE), #15596026 |
| Trypsin-EDTA 10 x | Cell culture | Biochrom AG (Berlin, DE), #L2153 |
| TrypLE Select 10 x | Cell culture | Thermo Fisher Scientific (Bonn, DE) #A1217701 |
| VioBility 405/452 dye | Cell culture | Miltenyi Biotec GmbH (Bergisch-Gladbach, DE), #130-120-354 |
| Y-27632 Rock Inhibitor | Cell culture | SelleckChem (München, DE), #S1049 |

### 3.1.7 Beads

**Table 9: Beads used for protein purification, pull-down and immunoprecipitation.**

| Name | Application | Supplier (Art. no. #) |
|---|---|---|
| Glutathione Sepharose™ 4B | Pull down | Cytiva (Marlborough, US), #17-0756-01 |
| Ni-NTA Agarose | Pull down, protein purification | Qiagen (Düsseldorf, DE), #30250 |
| Talon® Metal Affinity Resin | Protein purification | Takara Biotech (Kusatsu, JPN), #635503 |

### 3.1.8 Plasmids

Plasmid maps for non-commercial plasmids can be found in the appendix.

**Table 10: DNA plasmids.**

| Name | Vector | Resistance | Supplier (Art. no. #) |
|---|---|---|---|
| CFP-rCav1.2 | CFP-N1 | Kanamycin | Prof. Dr. Mark DelAcqua (University of Colorado, US) |
| CFP-rCav1.2-DCRD EE/AA | CFP-N1 | Kanamycin | custom-made |
| CFP-rCav1.2-PCRD RR/KK | CFP-N1 | Kanamycin | custom-made |

| | | | |
|---|---|---|---|
| CFP-rCav1.2-PCRD AAAA/ DCRD AA | CFP-N1 | Kanamycin | custom-made |
| CFP-rCav1.2-PCRD AAAAKK | CFP-N1 | Kanamycin | custom-made |
| CFP-rCav1.2-PCRD KK/ DCRD AA | CFP-N1 | Kanamycin | custom-made |
| Cerulean-N1 | Cerulean-N1 | Kanamycin | Addgene, (Cambridge, US), #54742 |
| DCRD-Cerulean | Cerulean-N1 | Kanamycin | selfmade |
| His-DCRD-Myc | petDUET1 | Ampicillin | Prof. Dr. Nathan Dascal (Tel Aviv University, ISR) |
| His-SUMO-PCRD | petDUET1 | Ampicillin | Prof. Dr. Nathan Dascal (Tel Aviv University, ISR) |
| PCRD-Cerulean | Cerulean-N1 | Kanamycin | custom-made |
| PDE3A1-Δ3aa-HA | pcDNA3.1 | Ampicillin | generated by Dr. Carolin Schächterle |
| PDE3A1-R862C-HA | pcDNA3.1 | Ampicillin | generated by Dr. Carolin Schächterle |
| PDE3A1-T445N-HA | pcDNA3.1 | Ampicillin | generated by Dr. Carolin Schächterle |
| PDE3A1-WT-HA | pcDNA3.1 | Ampicillin | generated by Dr. Carolin Schächterle |
| PLN-epac | pcDNA3 | Ampicillin | Prof. Dr. Viacheslav Nikolaev (Universitätsklinikum Hamburg, DE) |
| PKA-Venus | Venus-N1 | Kanamycin | custom-made |
| pET15b PKA-Cα | pET15b | Ampicillin | Prof. Dr. Friedrich Herberg (Universität Kassel, DE) |
| SERCA2-WT-Flag | pcDNA3.1 | Ampicillin | generated by Dr. Carolin Schächterle |

### 3.1.9 Oligonucleotides

Oligonucleotides were produced by BioTeZ Berlin-Buch GmbH (Berlin, DE) in 10 nmol scale. Primers were dissolved in dd$H_2O$ according to the manufacturer guidelines to get 50 µM stocks. If not otherwise stated, the working concentrations for the primers were 5 µM.

**Table 11: DNA oligonucleotides used for sequencing, PCR, qPCR and cloning.**

*designed by Dr. Carolin Schächterle

| Name | Application | DNA sequence 5'-3' |
|---|---|---|
| ACTC1_Fwd | qPCR | GACCTTCAATGTCCCTGCCA* |
| ACTC1_Rev | qPCR | ACCATCCCCAGAGTCCAGAA* |
| Cav1.2_CFP | Sequencing | AGCTCAAGCTTCGAATTCTGC |
| Cav1.2_1 | Sequencing | CAACCTGGAACGAGTGGAAT |
| Cav1.2_2 | Sequencing | AGAAGCAGCAGCTGGAAGAG |
| Cav1.2_3 | Sequencing | CGACAATTTCCCGCAGTC |
| Cav1.2_4 | Sequencing | CCTGCACAAGGGCTCTTTCT |
| Cav1.2_5 | Sequencing | ATGTTCGTCCTCATCCTGCT |
| Cav1.2_6 | Sequencing | CCCACCATCTGGATGAATTT |
| Cav1.2_7 | Sequencing | CAGCAGCTACTCGTCCACC |
| Cav1.2_8 | Sequencing | CCAGGGGAGACAGTTCCAT |
| Cav1.2_segment_fwd | Sub-cloning | AATGAAGCTTCCTTCCTGATCATCAATCTCT |
| Cav1.2_segment_rev | Sub-cloning | CATTCTCGAGGCTGTTCCGGTTAACTCCAGG |
| CMV-F | Sequencing | CGCAAATGGGCGGTAGGCGTG |
| DCRD_foward | Sub-cloning | AATGGCTAGCATGAGACAGTTCCATGGCAGCGCCAG |
| DCRD_reverse | Sub-cloning | TGCTTACTCGAGTTAGCTCTGCCGGGCGCC |
| DCRD_AA_fwd | SDM | GCGATCTGACCATAGCGGCGATGGAGAACGCGGC |
| DCRD_AA_rev | SDM | GCCGCGTTCTCCATCGCCGCTATGGTCAGATCGC |
| DuetDOWN1 | Sequencing | GATTATGCGGCCGTGTACAA |
| EXFP_rev | PCR, Sequencing | GTCTTGTAGTTGCCGTCGTC |
| GAPDH_Fwd | qPCR | AGCCACATCGCTCAGACAC* |
| GAPDH_Rev | qPCR | GCCCAATACGACCAAATCC* |
| hPKA-fwd | Sub-cloning | AATGGCTAGCATGGGCAACGCCGCCGCCGCCAA |
| hPKA-rev | Sub-cloning | CATTAAGCTTAAACTCAGAAAACTCCTTGCCAC |

| | | |
|---|---|---|
| MYBP3_fwd | qPCR | CCTTCATGCCTATCGGTCCC |
| MYBPC3_rev | qPCR | GTACTCCACGCTGTAGCCAT |
| MYH7_Fwd | qPCR | CGCCATCATGCACTTTGGAAA* |
| MYH7_Rev | qPCR | CCCATGAGGTAGGCAGACTTG* |
| NPPA_Fwd | qPCR | GTCAGACCAGAGCTAATCCCA* |
| NPPA_Rev | qPCR | GCTTCTTCATTCGGCTCACTG* |
| NPPB_Fwd | qPCR | TTCAGCCTCGGACTTGGAAAC* |
| NPPB_Rev | qPCR | AGGGATGTCTGCTCCACCT* |
| PCRD_forward | Sub-cloning | TAAGCAGCTAGCATGGGCAAGCCCTCCCAGAGGA |
| PCRD_reverse | Sub-cloning | TGCTTACTCGAGTTAGGTCTGGGGGAAGGCGCT |
| PCRD_AAAA_fwd | SDM | ACTCTGCACGACATCGCGGCTGCGGCCCGACGGGCC ATCTCC |
| PCRD_AAAA_rev | SDM | GGAGATGGCCCGTCGGGCCGCAGCCGCGATGTCGTG CAGAGT |
| PCRD_KK_fwd | SDM | GACATCGGGCCTGAGATCAAAAAGGCCATCTCCGGA GACCT |
| PCRD_KK_rev | SDM | AGGTCTCCGGAGATGGCCTTTTTGATCTCAGGCCCGA TGTC |
| PCRD_AAAAKK_fwd | SDM | GACATCGCGGCTGCGGCCAAAAAGGCCATCTCCGGA GACCT |
| PCRD_AAAAKK_rev | SDM | AGGTCTCCGGAGATGGCCTTTTTGGCCGCAGCCGCGA TGTC |
| PDE3A catalytic domain Fwd | Sequencing | ATCCCTGCCTTGGAGTTGATG* |
| PDE3A end Fw | Sequencing | AGTCGCACTCTTCAGAACAGA* |
| PDE3A exon 4 Fw | Sequencing | CTCCTGGCAGACCCTTCTCTT* |
| PDE3A start Fw | Sequencing | CAAGGGAATCCTGCTGATGAG* |
| pET upstream | Sequencing | ATGCGTCCGGCGTAGA |
| SERCA2_254 | Sequencing | AGATGAATTTGGGGAACAGC* |
| SERCA2_596 | Sequencing | AGACCAATCTGACCTTCGTTGG* |

| | | |
|---|---|---|
| SERCA2_907 | Sequencing | GAAATGTGTAACGCCCTCAACA* |
| T7 Promoter | Sequencing | TAATACGACTCACTATAGG |
| T7 Terminator | Sequencing | GCTAGTTATTGCTCAGCGG |
| qPCR_LTCC_Fwd | qPCR | AGCTGCCTGTTCAAAATCGC |
| qPCR_LTCC_Rev | qPCR | GGGATCACTAAAGTAACCCTTGG |
| qPCR_PDE3A_Fwd | qPCR | ATTCCAGGCCTCTCAACTGT* |
| qPCR_PDE3A_Rev | qPCR | CATACAGCGCCATCAACTCC* |
| qPCR_SERCA2_Fwd | qPCR | CTGCAACTCAGTCATTAAACAGC |
| qPCR_SERCA2_Rev | qPCR | CACCTTCAGGAGCACCCTTC |
| qPCR_TpnI_Fwd | qPCR | CGTGTGGACAAGGTGGATGAAG |
| qPCR_TpnI_Rev | qPCR | GCCGCTTAAACTTGCCTCGAAG |
| XL39 | Sequencing | TAGGACAAGGCTGGTGG |

### 3.1.10 Enzymes and Cloning reagents

**Table 12: Enzymes, PCR and qPCR reagents.**

| Reagent | Concentration | Supplier (Art. no. #) |
|---|---|---|
| Bcl I | 10,000 U/mL | New England Biolabs (Ipswich, US), #R0160S |
| CutSmart Buffer | 10 x | New England Biolabs (Ipswich, US), #B7204S |
| dNTP mix | 5 mM | Roboklon GmbH (Berlin, DE), #E2800-04 |
| Dpn I | 20.000 U/mL | New England Biolabs (Ipswich, US), #R0176S |
| Hind III | 20.000 U/mL | New England Biolabs (Ipswich, US), #R0104S |
| Hpa I | 5.000 U/mL | New England Biolabs (Ipswich, US), #R0105S |
| Nhe I-HF® | 20.000 U/mL | New England Biolabs (Ipswich, US), #R3131S |
| Taq DNA Polymerase | 400 units | New England Biolabs (Ipswich, US), #M0267S |
| T4 ligase | 400.000 U/mL | New England Biolabs (Ipswich, US), #R0176S |
| T4 ligase reaction buffer | 10 x | New England Biolabs (Ipswich, US), #R0176S |

| | | |
|---|---|---|
| PowerSYBR™Green Master Mix | 2 x | Thermo Fisher Scientific (Waltham, US), #4367659 |
| Xho I | 20.000 U/mL | New England Biolabs (Ipswich, US), #R0176S |

### 3.1.11 Bacterial strains

**Table 13: Bacterial strains used for molecular cloning and protein purification.**

| Strain | Genotype | Supplier (Art. no. #) |
|---|---|---|
| *E.Coli* DH5-α | fhuA2 Δ(argF-lacZ)U169 phoA glnV44 Φ80 Δ(lacZ)M15 gyrA96 recA1 relA1 endA1 thi-1 hsdR17 | New England Biolabs (Ipswich, US), #C2987H |
| Rosetta™2(DE3) Singles™ | F- ompT hsdSB(rB- mB-) gal dcm (DE3) pRARE2 (CamR) | Sigma-Aldrich (St. Louis, US), #71400 |

### 3.1.12 Eukaryotic cell lines

**Table 14: Eukaryotic cell lines.**

| Cell line | Description | Culture medium | Supplier (Art. no. #) |
|---|---|---|---|
| HEK293 | Human embryonic kidney cell line | DMEM-GlutaMAX™, 10 % FCS, 1 % P/S | Deutsche Sammlung von Mikroorganismen und Zellkulturen GmbH (DSMZ, Braunschweig, DE) #ACC305 |

### 3.1.13 Peptides

**Table 15: Peptides.**

| Name | Sequence | Supplier (Art. no. #) |
|---|---|---|
| Kemptide | LRRASLG-NH2 | #BS590 |

### 3.1.14 Proteins

**Table 16: Recombinant proteins.**

| Name | Species | Size (kDa) | Concentration | Supplier (Art. no. #) |
|---|---|---|---|---|
| PKA-Cα | Bovine | 40 | | Promega Corporation, #V5161 |
| PKA-Cα | Human | 40 | 30 U/mg | Prof. Dr. Fitz Herberg (Kassel, DE) |
| PKA- RIα | Human | 43 | 130 mg/mL | Prof. Dr. Fitz Herberg (Kassel, DE) |
| GST-PKA-$RII_{\beta}$ Fraction A7 | Human | 43 | | Dr. Ryan Walker Gray (Klussmann lab) |
| His-DCRC-Myc | Rabbit | 11.5 | 0.5-1.4 mg/mL | Prof. Dr. Nathan Dascal (Tel Aviv) |
| His-DCRD-Myc Fraction C1 | Rabbit | 11.5 | 1.4 mg/mL | custom-made |
| His-SUMO-PCRD | Rabbit | 18 | 0.1-0.5 mg/mL | custom-made |

## 3.2 Methods

### 3.2.1 Peptide spot array

In collaboration with Dr. Kerstin Zühlke (Klussmann lab), mouse PKA-CSα (Genbank #NM_008854) was spot-synthesized as 25-mer peptides on a membrane using an AutoSpot Robot ASS 222 device (Intavis Bioanalytical Instruments, Cologne, Germany) and the membrane was incubated with 0.1 µM recombinant His-DCRD-Myc or His-SUMO-PCRD at 4°C overnight in 50 mM Tris pH 7.4, 5 mM $MgCl_2$. Binding of DCRD or PCRD to PKA-CS was analyzed using anti-His Tag antibody (PCRD) or anti-Myc Tag (DCRD).

### 3.2.2 Generation of mammalian expression plasmids

For overexpression of DCRD and PCRD in HEK293 cells, both DNA segments were cloned from pET-DUET1 vector into Cerulean-N1 using the restriction enzymes Nhe I-HF and Xho I (both 20 U) in 1 x CutSmart buffer (NEB). DCRD and PCRD inserts were amplified from pET-DUET1 vector and Nhe I and Xho I restriction sites inserted using primers with a non-homologous overhang (DCRD_forward, DCRD_reverse, PCRD_forward and PCRD_reverse) (Table 11).

For expression of PKA-CS, Nhe I-HF and Hind III restriction sites were added to the human PKA-CS sequence via PCR. The amplified sequence was inserted into Venus-N1 vector using the Nhe I and Hind III restriction enzymes (both 20 U).

The cut DNA sequence was ligated with T4 DNA ligase (400,000 cohesive end U/mL) and transformed into chemically competent *E.Coli* DH5α by heat shock. The plasmid DNA was isolated from bacteria using the NuceloBond® Xtra Midi Kit (Macherey-Nagel) according to the manufacturer protocol. The correct orientation of the insert was verified by Sanger sequencing (LGC Genomics, Berlin, Germany).

### 3.2.3 Cell culture and transfection

The cell line HEK293 was grown in DMEM-GlutaMAX™ (Thermo Fisher Scientific, Waltham, USA) supplemented with 10% fetal calf serum (FCS) and 1% penicillin/streptomycin (100 U/mL) and maintained at 37°C in 5% $CO_2$ atmosphere.

For transfection with DCRD-Cerulean, PCRD-Cerulean and PKA-CSα-Venus, HEK293 cells were seeded in 60 mm cell culture dishes at a density of $1.5*10^6$ cells in 5 mL DMEM without antibiotics. After 24 h,

HEK293 cells were transfected with 2 µg plasmid DNA using polyethylenimine (PEI) cationic polymer. Immunoprecipitation experiments were conducted 48 h after transfection.

For transfection with CFP-rCav1.2 and PKA-CSα-Venus, the cells were seeded in 60 mm dishes aiming for 50% confluence on day 1. After 24h, HEK293 cells were transfected with 2.2 µg DNA using equimolar ratios of CFP-rCav1.2 α1c and PKA-CSα-Venus constructs and Lipofectamine 2000 reagent. After 24 h, cells were lysed and used for immunoprecipitation as described in section 3.2.4.

### 3.2.4 Cell lysis, immunoprecipitation and Western blotting

Transfected HEK293 cells were washed with ice-cold PBS and lysed in 500 µL standard lysis buffer (SLB) supplemented with protease and phosphatase inhibitors (0.5 mM Benzamidine, 0.5 mM phenylmethansulfonyl fluoride, 3.2 µg/mL trypsin-inhibitor, 2 µg/mL aprotinin, 50 mM NaF, 0,1 mM $Na_3VO_4$,). For removal of cell debris, the suspension was centrifuged at 14,000 rpm for 15 min at 4°C and protein concentration of the supernatant was determined using Bradford assay. For the input sample, 30 µg of total protein was diluted in 3 x Lämmli sample buffer (40% glycerol, 8% SDS, 0.4 bromophenol blue, 312.5 mM Tris-HCl, 200 mM DTT, pH 6.8) and stored at -20°C.

For immunoprecipitation of YFP-tagged PKA-CS protein from HEK293 cells, 1 mg of protein was incubated with 50 µL Protein A-conjugated Sepharose beads (Sigma) and 2 µg of the appropriate antibody (anti-PKA-CSα, BD Bioscience) for 2 h at RT. The beads were washed three times in lysis buffer, proteins eluted using 3 x Lämmli sample buffer and analyzed by Western blotting.

For immunoprecipitation of CFP-rCav1.2 α1c, 1 mg of total protein was incubated with 1 µg anti-Cav1.2 α1c antibody (ACC-003, Alomone labs) and rotated at 4°C overnight. The next day, the beads were washed three times with 500 µL SLB and proteins eluted with 30 µL 3 x Lämmli sample buffer.

For Western blotting, input and eluted proteins were denatured for 10 min at 95°C and separated by SDS-polyacrylamide gel electrophoresis (SDS-PAGE). Transfer of the proteins onto a polyvinylidene fluoride (PVDF) membrane was conducted using the wet tank blot method at 100 V for 90 min. Blocking of nonspecific protein binding was performed in either 3% BSA, 5% BSA or 5% milk in TBS (10 mM Tris-HCl pH 7.4, 150 mM NaCl) for 1 h at RT. The following primary antibodies were used: mouse anti-PKA-CSα (1:1000) and mouse anti-GFP Tag (1:1000). Membranes were incubated with the primary antibody diluted in blocking solution for either 2 h at RT or overnight at 4°C. Afterwards, membranes were washed three times in TBS-T (TBS + 0.05% Tween-20) and incubated with mouse specific horseradish peroxidase (POD)-coupled antibody (1:5000) for 1 h at RT. For detection, membranes were again washed for three times in TBS-T, incubated with Immobilon Western chemiluminescent HRP substrate

(Thermo Fisher Scientific) and detected at an Odyssey Fc Imaging System (LI-COR Biotechnology, Lincoln, USA).

### 3.2.5 Recombinant protein purification of channel fragments

pDu-8His-SUMO-Tev-PCRD and pDu-8His-Tev-DCRD-Myc vectors for the expression of His-SUMO-PCRD and His-DCRD-Myc were kindly provided by the laboratory of Prof. Dr. Nathan Dascal (Tel Aviv, Israel).

Plasmid DNA was transformed into chemically competent *Rosetta™* (DE3) bacteria using heat shock method. The transformed bacteria were inoculated in LB medium and grown overnight in a shaking incubator at 37°C, 220 rpm. The next day, a glycerol stock was prepared for each construct, by diluting the liquid culture 1:1 with 100 % glycerol. Glycerol stocks were stored at -80°C until usage.

For recombinant protein purification, 50 µL of the glycerol stock was spread on an agar plate containing ampicillin (100 µg/mL). Plates were incubated overnight at 37°C, 5% $CO_2$ and bacteria detached from the plates the next day, using 10 mL LB medium per plate. Bacteria suspensions were inoculated in 800 mL LB-medium containing 100 µg/mL ampicillin. Cultures were incubated at 37°C, 220 rpm until they reached an $OD_{600}$ of 0.6-0.8. Cultures were inoculated with 0.375 mM isopropyl β-D-1-thiogalactopyranoside (IPTG) and incubated overnight at 16°C, 220 rpm. The next day, bacteria cultures were centrifuged at 4,500 x *g* for 10 min at 4°C and bacteria pellet resuspended in 35 mL Talon A buffer (with protease inhibitor, Thermo Scientific). The pellet was homogenized with a Sonicator (30 sec at 20 kHz) and disrupted using microfluidizer. The sample was centrifuged at 25,000 x *g* for 35 min at 4°C and the supernatant added to a TALON Metal affinity resin (Takara Bio Europe). The supernatant and beads were incubated on a rolling device for 3 h at 4°C, followed by centrifugation of the beads at 1,000 x *g* for 15 min at 4°C, washing for 3 times with Talon A buffer and application of the bead suspension to Pierce™ centrifuge columns (Thermo Scientific). The proteins were eluted with Talon B buffer and the columns incubated on a rolling device for 30 min at 4°C. The sample was eluted from the column and applied to the AKTA FPLC device (Amersham Bioscience). The fractions containing the desired protein were collected and snap frozen in liquid nitrogen. Proteins were stored at -80°C.

### 3.2.6 Coomassie staining and BCA assay

To analyze protein integrity and estimate the protein concentration for each purification, the protein suspension was diluted 1:5 in $H_2O$ and 5 µL 3 x Lämmli buffer added. Samples were denatured for 10

min at 90°C before loading. Proteins were separated on a 15% SDS-PAGE gel and stained for 1 h with Coomassie reagent. To remove the staining solution, the gel was incubated for 3 h with de-stain solution, slowly rotating.

To determine the protein concentration, the Pierce™ BCA protein assay kit was used according to the manufacturer instructions (Thermo Fisher).

### 3.2.7 Pull down

To analyze if His-DCRD-Myc or His-SUMO-PCRD interfere with PKA-RIIβ binding to PKA-CSα, 2 µg of GST-PKA-RIIβ was pulled down with 25 µL of gluthadione-beads in pull down buffer (20 mM HEPES pH 7.5, 200 mM NaCl, 1 mM Benzamidine, 1 mM EDTA, 2 mM DTT, 0.05% Tween-20) for 2 h at RT in the presence of 1 µg PKA-CSα and various concentrations of DCRD or PCRD. After 2 h, the beads were washed two times with pull down buffer and spun down at 1000 x *g* for 1 min. For elution, 30 µL of 3 x Lämmli buffer was added to the beads and incubated for 10 min at 95°C. Samples were run on an SDS-PAGE for protein separation and stained using Coomassie solution.

### 3.2.8 Cook Assay

In this assay, the human PKA-CSα activity in the presence of the two channel fragments was derived from a three-step reaction as described previously (Cook et al., 1982). This enzymatic assay is based on a reaction chain where ADP accumulates during kemptide (sequence: LRRASLG) phosphorylation and is used by Pyruvate kinase to transform phosphoenolpyruvate into pyruvate and ATP. In a third reaction, the pyruvate is used to transform pyruvate + NADH + $H^+$ into lactate + $NAD^+$. The decrease of NADH + $H^+$ is measured at 340 nm and can directly be correlated to PKA-CS activity (Cook et al., 1982). The assay buffer contained 100 mM MOPS pH 7, 10 mM $MgCl_2$, 1 mM phosphoenolpyruvate, 1 mM ATP, 2.5 mM β-Mercaptoethanol, 113 U/mL lactate dehydrogenase, 63 U/mL pyruvate kinase, 0.1 mg/mL BSA and NADH. For the measurement, 1 µM or 10 µM of His-DCRD-Myc or His-SUMO-PCRD were added to 100 µL assay mix. 30 nM of human PKA-CSα was added, and the reaction started by addition of 260 µM kemptide. NADH depletion was measured using spectrophotometer (Specord 205, Analytic Jena) at a wavelength of 340 nm for a time period of 30 sec. The slope of each measurement was calculated in the WinAspect software and the values exported to Prism V for statistical analysis.

### 3.2.9 ADP-Glo Assay

The ADP-Glo™ Assay (Promega, Germany) is a luminescence-based kinase assay in which the amount of produced ADP is proportional to the luminescence signal. The ADP is a product of the PKA-mediated phosphorylation reaction, in which one phosphor from ATP is used. Here, 20 nM bovine PKA-CS was incubated with kemptide as substrate in PKA kinase buffer (40 mM Tris-HCl, pH 7.4, 20 mM $MgCl_2$, 0.1 mg/mL BSA, 50 µM DTT). 10 µM of His-DCRD-Myc or His-SUMO-PCRD were added to the reaction mix. To inhibit kinase activity, 30 µM of H89 were added. Samples were diluted in PKA kinase buffer and reactions set up in a 384 well plate. Kinase reaction was conducted for 5 min at RT. The reaction was stopped by addition of 5 µL ADP Glo reagent and the plate incubated for 40 min at RT. 10 µL of kinase detection reagent was added and the plate incubated for 30 min at RT. The luminescence was recorded using a Tecan plate reader with an integration time of 0.5 sec.

### 3.2.10 Molecular cloning

#### 3.2.10.1 Site-directed mutagenesis

As a template, rabbit $Ca_v1.2$ $\alpha$1c in pcDNA3 was used. Because of the size of the template vector (~12,000 bp), in a first approach the part of the vector covering the DCRD and PCRD sites was cut out using Hind III and Xho I (20 units each) restriction sites and ligated into pCMV6-Entry vector using T4 DNA ligase (New England Biolabs).

For site-directed mutagenesis the Agilent Quick Change II XL Kit (Agilent Technologies) was used according to the manufacturer's instructions (Table 18, 19).

Primer pairs DCRD_AA_fwd, DCRD_AA_rev, PCRD_AAAA_fwd, PCRD_AAAA_rev, PCRD_KK_fwd, PDRD_KK_rev and PCRD_AAAAKK_fwd, PDRD_AAAAKK_rev (Table 11) were used to introduce the different point mutations. The PCR product was then Dpn I digested and transformed into DH5$\alpha$ competent cells. The next day, single colonies were picked from the plate and analyzed via Colony PCR (Table 19, 20).

**Table 17: Quick Change II XL reaction mix.**

| Reagent | Stock Concentration | Final concentration/volume |
|---|---|---|
| Reaction buffer | 10 x | 1 x |
| DNA template | - | 10 ng |

| | | |
|---|---|---|
| Forward primer | 5 µM | 125 ng |
| Reverse primer | 5 µM | 125 ng |
| dNTP mix | - | 1 µL |
| Quick Solution Reagent | - | 3 µL |
| $H_2O$ | - | Up to 50 µL final |

**Table 18: Thermo cycler parameters.**

| Segment | Cycles | Temperature | Time |
|---|---|---|---|
| 1 | 1 | 95 °C | 1 minute |
| 2 | 18 | 95 °C | 50 seconds |
| | | 60 °C | 50 seconds |
| | | 68 °C | 1 min/kb of plasmid length |
| 3 | 1 | 68 °C | 7 minutes |

**Table 19: Colony PCR reaction mix.**

| Reagent | Stock Concentration | Final concentration/volume |
|---|---|---|
| Reaction buffer | 10 x | 1 x |
| DNA template | - | In 10 µL $H_2O$ |
| Forward primer | 5 µM | 200 nM |
| Reverse primer | 5 µM | 200 nM |
| dNTP mix | 5 mM | 200 µM |
| Taq DNA Polymerase | - | 0.625 units |
| $H_2O$ | - | Up to 25 µL final |

**Table 20: Thermo cycler parameters for Colony PCR.**

| Segment | Cycles | Temperature | Time |
|---|---|---|---|
| 1 | 1 | 95 °C | 30 seconds |
| 2 | 18 | 95 °C | 20 seconds |
| | | 60 °C | 30 seconds |
| | | 68 °C | 1 min/kb of plasmid length |
| 3 | 1 | 68 °C | 5 minutes |

10 µL of the PCR product was run on a 1% agarose gel at 120 V for 1 h. Bacteria containing the desired plasmid construct were grown in LB medium overnight and the DNA isolated the next day using NucleoSpin Plasmid Mini Kit according to the manufacturer instructions (Macherey-Nagel). Successful mutation of the target site was confirmed by Sanger sequencing (LGC Genomics, Berlin). In the last step, mutated regions were put back into the original construct using Bcl I and Hpa I (20 units each) restriction sites. After restriction digest, samples were run on a 1% agarose gel at 100 V for 1 h and DNA purified from the gel using NucleoSpin gel and PCR clean-up kit as described in the manufacturer's protocol (Macherey-Nagel). The digested DNA sequence was added to the digested vector backbone and ligated using T4 DNA ligase (New England Biolabs). Correct insertion of the mutated sequence was confirmed by sequencing using primers listed in table 11 (LGC Genomics, Berlin).

### 3.2.10.2 Sub-cloning into CFP-rCav1.2 vector

To express $rCa_v1.2$ $\alpha$1c in HEK293 cells, the mutated DCRD and PCRD segments in pCMV6-Entry, created as described in section 3.2.10.1, were sub-cloned into CFP-rCav1.2 $\alpha$1c vector (kindly provided by Prof. Dr. Mark DelAcqua, Colorado, US). For this approach, mutated segments were cut from pCMV6-constructs using Bcl I and Hpa I (20 units each) restriction sites. The mutated segments were separated from the vector backbone on a 1% DNA agarose gel, purified from the gel and ligated into CFP-rCav1.2 $\alpha$1c using T4 DNA ligase (New England Biolabs) and transformed into DH5$\alpha$. Clones were analyzed the next day using Colony PCR with CMV-F and pBABE3' primers. Positive clones were inoculated in LB medium, the DNA isolated the next day and confirmed via sequencing (LGC Genomics).

### 3.2.11 Analysis of the potential interaction between the LTCC and PDE3A

To study the interaction of PDE3A and the LTCC $\alpha$1c subunit, PDE3A1- and PDE3A2-HA constructs were overexpressed with the LTCC $\alpha$1c subunit and AKAP150 in HEK293 cells as described in section 3.2.3. After 24 h, the cells were lysed as described in section 3.2.4. PDE3A1- or PDE3A2-HA constructs were precipitated from the HEK293 cells using anti-HA magnetic beads and the potential co-immunoprecipitation (Co-IP) of the LTCC $\alpha$1c subunit and AKAP150 studied performing Western blot method. For detection the following antibodies were used: anti-Cav1.2 (Alomone labs, 1:1000), anti-PDE3A (1:1000), anti-AKAP150 (1:1000), anti-GAPDH (1:1000) and anti-PKA-CS (1:1000).

For the overlay experiments, the C terminus of the $\alpha$1c subunit was spotted on a membrane as described in section 3.2.1. PDE3A1-Flag was transiently expressed in HEK293 cells and isolated from the cells after 24 h using anti-Flag magnetic beads (this experiment was carried out by Dr. Ryan Walker-Gray, Klussmann lab). The protein was eluted from the magnetic beads via competitive binding of Flag peptide (200 µg/mL) for 15 min at RT. The protein concentration was determined using Bradford protein assay. For the detection of PDE3A, the membrane was stained with anti-PDE3A (1:1000) antibody.

### 3.2.12 hiPSC culture and differentiation to cardiomyocytes

hiPSCs were mutated and characterized by Michael Mücke (Hübner lab, MDC) using TALEN's and CRISPR/Cas9 approach to express T445N or R862C substitutions. Single clones were analyzed for successful insertion of the mutation using Sanger sequencing. Since the R862C substitutions is less penetrant in humans but also in our animal model (Ercu *et al*., 2022, accepted for publication) the homozygous mutation was introduced into the iPSCs (Figure S1).

For differentiation, hiPSCs were seeded at 1:12 ratio on Matrigel-coated (1:100) 6-well plates on day -3 and cultured in Essential (E8) medium under normoxia conditions (37°C, 5 % $CO_2$). The medium was changed every day. The iPSCs were differentiated to cardiac myocytes using a protocol comprising Wnt-pathway activation and inhibition with small molecules. The activation of the Wnt-signaling pathway (with CHIR-99021) induced stem cell differentiation into the endo- and mesodermal state (Hödar et al., 2010; Laco et al., 2018; McCubrey et al., 2014). To induce cardiac differentiation *via* inhibition of the Wnt-pathway the small molecule, IWR-1-endo, was added to the cell culture medium (Lian et al., 2013). Enrichment for cardiac myocytes was achieved by metabolic selection using culture medium without glucose. The cardiomyocytes in contrast to non-differentiated cells were able to survive under glucose depletion

As soon as hiPSCs reached 90-95 % confluence, differentiation was initiated by replacing the medium with cardiac priming medium (RPMI-1640, B-27 minus Insulin (1 x), 10 µM CHIR). On day one, 4 mL of basal medium (RPMI-1640, B-27 minus insulin (1 x)) was added to each well. On day three, the medium was replaced with 4 mL cardiac induction medium (RPMI-1640, B27 minus Insulin (1 x), 5 µM IWR-1) and on day 5, without removing the previous medium, 4 mL basal medium was added. On day 7, the medium was replaced with 2 mL cardiac maintenance medium (RPMI-1640, B27 (1 x)). In between days 9 and 11, cardiomyocytes were metabolically selected using cardiac selection medium (RPMI-1630 without glucose, B27 (1 x)), on day 11 medium was replaced by cardiac maintenance medium. On day 15, cells were replated on Matrigel-coated (1:60) 6-well plates at a density of $1.5*10^6$ cells/well (Figure 6, differentiation scheme).

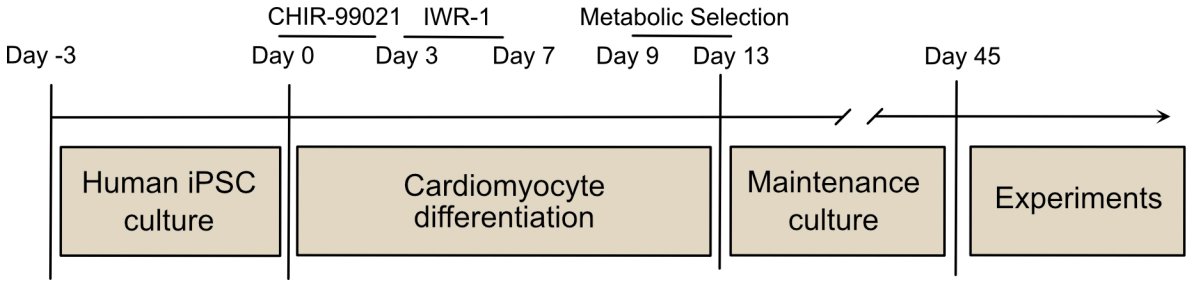


**Figure 6: hiPSC to cardiomyocyte differentiation scheme.** CHIR-99021 was used at 10 µM concentration and IWR-1 at 5 µM.

### 3.2.13 Flow cytometry

hiPSC-CMs were dissociated on day 45 using 10 x TrypLE reagent for 12 min. The viability of the cells was determined by staining the cells with VioBility 405/452 (Miltenyi Biotech) dye for 20 min at RT, followed by fixation using the FoxP3 Kit (Miltenyi Biotech) and cardiac marker proteins stained with anti-TNNT2-FITC (1:10) (Miltenyi Biontech) and anti-MLC2v-APC (1:10) (Miltenyi Biontech) according to the manufacturer's instructions. For the isotype control, cells were stained with REA-APC antibody (1:50) and REA-FITC antibody (1:50). Cells were analyzed on a MACSQuant VYB (Miltenyi Biontech) device and data analyzed using FlowJo V.10 software. The gating strategy that is based on the isotype control sample is shown in Figure S3.

### 3.2.14 $Ca^{2+}$ Imaging using Fluo-8

On day 45, cells were seeded on fibronectin-coated glass bottom dishes (35 mm, IBIDI) at a density of 60,000 cells/dish and medium was changed every second day for another 7-10 days. On the day of the

experiment, cells were loaded with 2 µM Fluo-8-AM $Ca^{2+}$ binding dye in the presence of 0.01% Pluronic F-127 acid for 10 min at 37°C, 5% $CO_2$. Cells were washed two times with imaging buffer and kept at 37°C, 5% $CO_2$ for 20 min to recover. To synchronize the contraction of the cells for imaging, the cells were paced at 10 V, 0.5 Hz with a 2 ms biphasic pulse at RT using Stimulator C pacer. The measurements were conducted on a Zeiss NLO with the following microscope settings: 40 x objective, laser = 488 nm, pinhole = open. Images were acquired in line scan mode with 20,000 lines and 1.92 ms per line. For the treatment with 0.2% DMSO, 1 µM isoproterenol, 20 µM cilostamide or the combination of both, the imaging buffer was replaced with 1 mL fresh buffer containing the compound and the dish incubated for 10 min at RT before conducting another round of line-scan measurements. The data analysis was conducted by Michael Mücke converting the lsm-images to a Matlab format used as an input for CalTrack (Psaras et al., 2021) (Figure 7). The derived $Ca^{2+}$ transient parameters are summarized in table 21.

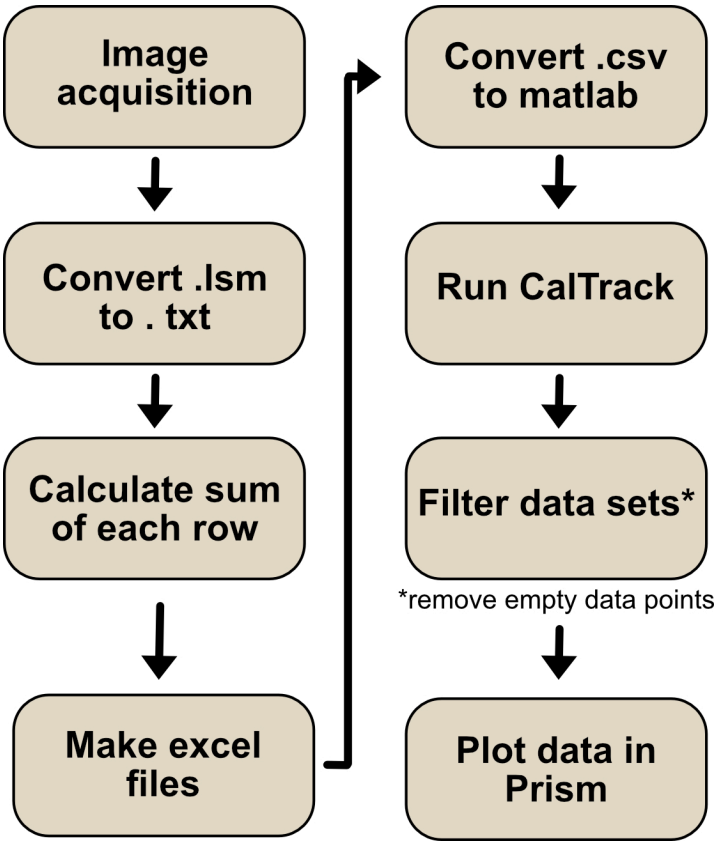


**Figure 7: Flow chart depicting the major steps of the $Ca^{2+}$ imaging data analysis.** The line-scan images were converted to a Matlab format and this used as an input to run the CalTrack analysis pipeline. The resulting data sets were further filtered and plotted in Prism. Each step except for the plotting of the data was done by Michael Mücke (Hübner lab, MDC Berlin).

**Table 21: $Ca^{2+}$ transient parameters derived for hiPSC-CMs with CalTrack.**

| Parameter | Unit | Description |
|---|---|---|
| CD | ms | Duration of the $Ca^{2+}$ transient |
| CD90 | ms | Time $Ca^{2+}$ is above 90 % of the signal |
| CD50 | ms | Time $Ca^{2+}$ is above 50 % of the signal |
| CD10 | ms | Time $Ca^{2+}$ is above 10 % of the signal |
| Ton | ms | Time at which $Ca^{2+}$ is maximal |
| Ton90 | ms | Time to 90 % contraction (from $T_0$) |
| Ton50 | ms | Time to 50 % contraction (from $T_0$) |
| Ton10 | ms | Time to 10 % contraction (from $T_0$) |
| Toff | ms | Time from peak to $T_{end}$ |
| Toff90 | ms | Time to 90 % relaxation from peak |
| Toff50 | ms | Time to 50 % relaxation from peak |
| Toff10 | ms | Time to 10 % relaxation from peak |
| $T_0$ | ms | intersection between signal (before peak) and baseline |
| $T_{end}$ | ms | intersection between signal (after peak) and baseline |

### 3.2.15 $Ca^{2+}$ Imaging using Fura-2 dye

On day 45, cells were seeded on fibronectin-coated glass bottom dishes (35 mm, MatTek) at a density of 60,000 cells/dish and medium changed every second day for 7-10 days. The $Ca^{2+}$ measurement with the Ionoptix device was performed by Dr. Rene Jüttner (Gotthardt lab, MDC Berlin). On the day of the experiment, cells were loaded with 1 µM Fura-2-AM $Ca^{2+}$ binding dye for 30 min at 37 °C. The cells were washed with $Ca^{2+}$ imaging buffer. After 30 min of recovery, the cardiomyocytes were field stimulated with a supra-threshold voltage of 10 V at a frequency of 20 Hz (bipolar pulse, 5ms) for 10 s using a pair of platinum wires on opposite sides of the chamber. $Ca^{2+}$ transients were recorded at 250 Hz using IonWizard data acquisition software and the transients calculated by CytoSolver Desktop. The transients were analyzed by Michael Mücke (Hübner lab, MDC Berlin) using the CalTrack algorithm.

### 3.2.16 hiPSC-CMs RNA isolation, cDNA synthesis and qPCR

To induce hypertrophy in hiPSC-CMs, the cells were seeded in 12-well plates on day 45 of differentiation and left to recover for 5-7 days. At day 50-52, cells were treated with endothelin-1 (ET-1) for 72 h, with the medium being changed every 24 h containing fresh ET-1. For cell lysis, each well was washed with PBS (-/-), 300 µL Trizol reagent was added and cell membranes destroyed using syringes. For RNA isolation, the Directzol RNA Microprep Kit (Zymo Research) was used and RNA eluted in 15 µL water. RNA quality and integrity was analyzed on a BioAnalyzer (Figure S2) and the RNA concentration determined using NanoDrop.

For cDNA synthesis, 500 ng RNA was transcribed using qScript cDNA synthesis kit according to the manufacturer's instructions (Quantabio, USA). 14 ng cDNA have been used for the qPCR reaction mix using Power SYBR$^{TM}$ Green PCR master mix (Thermo Fisher Scientific) (Table 22) and the primers listed in Table 11. The plate was centrifuged at 1,200 x *g* for 5 min and the measurement conducted in a ViiA7 qPCR device with the following settings: 40 cycles, 95°C/15 sec and 1 min of 60°C. Relative gene expression levels were calculated using $\Delta\Delta$Ct method. In the first step the relative expression of the target gene to the housekeeping gene (here: *GAPDH*) was calculated ($\Delta$Ct). Next, the values of the treated cells were corrected for the values of control cells ($\Delta\Delta$Ct = treated – untreated). In the last step the $2^{-\Delta\Delta Ct}$ value was calculated and plotted.

**Table 22: qPCR reaction mix per well**

| Reagent | Stock Concentration | Final concentration/volume |
|---|---|---|
| SYBRGreen Master Mix | - | 10 µL |
| cDNA template | 25 ng/µL | 14 ng |
| Forward primer | 5 µM | 350 µM |
| Reverse primer | 5 µM | 350 µM |

### 3.2.17 Protein and gene expression in hiPSC-CMs

hiPSC-CMs at day 45 were sedimented by centrifugation at 300 x *g* for 3 min and cell pellets lysed in 300 µL standard lysis buffer (SLB) containing protease and phosphatase inhibitors as described in section 3.2.4. Cells were passed through a syringe and spun down at 14,000 rpm for 15 min at 4°C. The supernatant was transferred into a new tube and protein concentration determined using Bradford

assay. Before loading on an SDS-gel, 3 x Lämmli buffer was added and samples were denatured at 95°C for 10 min. 40 µg of whole protein lysate was run on a 10% polyacrylamide gel and transferred on PVDF membranes using Tank blot method at 110 V for 140 minutes. Blocking was performed in either 5% BSA or 5% milk in TBS for 1 h at RT. Membranes were incubated with the following primary antibodies in blocking solution overnight at 4°C: anti-Cav1.2 (Thermo Scientific, 1:250), anti-PDE3A (1:1000), anti-PKA-CS (1:1000), anti-PLN (1:1000), anti-Tpn I (1:1000), anti-Hsp60 (1:1000), anti-SERCA2 (1:500), anti-MyBPC3 (1:100), anti-pTpn I (1:1000), anti-pPLN (1:500) and anti-CamKII (1:1000). The next day the membranes were washed 3 times with TBS-T and incubated with secondary antibody (1:5000) for 1 h at RT. For detection of similar sized proteins, the membranes were stripped in Restore™ PLUS western blot stripping buffer (Thermo Scientific) for 5 min at RT.

To analyze the expression of the *CACNA1C*, *ATP2A2*, *MYBPC3*, *TNNI3* and *PDE3A* genes, the RNA was isolated as described above (section 3.2.16). RNA was transcribed using the qScript cDNA synthesis kit and qPCR reaction mix set-up using Power SYBR™ Green PCR master mix. The used primer pairs are listed in Table 11. To calculate the gene expression levels of the mutants compared to the WT, in the first step the relative expression of the target gene to the housekeeping gene (here: *GAPDH*) was calculated ($\Delta$Ct). Next, the gene expression values for the mutants were corrected for the average value of the WT ($\Delta\Delta$Ct = mutant – mean WT; for WT: $\Delta\Delta$Ct = WT – mean WT). In the last step the $2^{-\Delta\Delta Ct}$ value was calculated and plotted as ratio of gene expression in comparison to the WT.

### 3.2.18 Transfection of hiPSC-CMs and fluorescence resonance energy transfer (FRET)

To analyze local cAMP signaling, an Epac-based cAMP-binding FRET sensor that is targeted to the SR was kindly provided by Viacheslav Nikolaev (Universitätsklinikum Hamburg-Eppendorf (UKE), Hamburg, DE).

For FRET measurement, the cells were dissociated on Day 45 using 10 x TrypLE for 12 min at 37°C, 5 % $CO_2$ and seeded at a density of 60,000 cells/well in a CellCarrier 96-well microplate (Perkin Elmer). After 5-7 days, the cells were transfected with 150 ng plasmid DNA and 0.75 µL LipoStem reagent (Thermo Fisher) in 25 µL OptiMEM. After 48 h, cells were washed with PBS and nuclei stained using 5 µM Drq5 dye (Thermo Scientifc). Cells were incubated for 30 min at RT and FRET signal measured using Opera Phenix High-content screening system (Perkin Elmer). For treatment with DMSO, 1 µM isoproterenol, 20 µM forskolin, 20 µM milrinone, 100 µM IBMX and the combination of agonist and inhibitor, medium was removed and 100 µL fresh medium with either compound added to the corresponding wells. The plate was incubated for 30 min at 37°C with the inhibitors (milrinone and IBMX) and 5 min for agonist and control (DMSO, forskolin, isoproterenol). For the analysis, cells were

selected based on their nuclei and cytoplasm staining using CellProfiler. The FRET efficacy was calculated using a custom-made R-pipeline (Janani Gayathri Nadar, FMP Berlin). The results were plotted using Prism software.

### 3.2.19 Co-IP SERCA2-Flag and PDE3A1-HA constructs

This experiment was conducted in collaboration with Dr. Maria Ercu (Klussmann lab, MDC Berlin).

HEK293 cells were cultured as described earlier. 24 h before transfection, cells were seeded on 10 cm cell culture dishes. On day 1, cells were transfected with 6 µg DNA per construct and 12 µL Lipofectamine 2000. The following constructs were used: SERCA2-Flag, PDE3A1-WT-HA, PDE3A1-Δ3-HA, PDE3A1-T445N-HA and PDE3A1-R862C-HA. The cells were lysed 24 h after transfection in 800 µL SLB and cell debris removed by centrifugation at 14,000 rpm for 15 min at 4°C. SERCA2 was precipitated using anti-Flag magnetic beads and co-precipitation of the PDE3A1 constructs as well as SERCA2 expression was analyzed using Western blotting with the following antibodies: anti-SERCA2 (1:1000), anti-PDE3A (1:1000) and anti-Hsp60 (1:1000).

### 3.2.20 Statistical analysis

Statistical analyses were performed in GraphPad Prism Version 8 (GraphPad, La Jolla, Ca, US). Nonparametric, One-way ANOVA (Kruskal Wallis test) with post hoc Dunn´s test was applied. Significant differences were denoted as *$p \leq 0.05$, ** $p \leq 0.01$, *** $p \leq 0.001$ and **** $p \leq 0.0001$. If not otherwise indicated the mean ± standard deviation (SD) was plotted.

# 4 Results

## 4.1 Identification of a direct interaction of PKA-CS with the LTCC α1c subunit

### 4.1.1 PKA-CS binds α1c at the C terminus

The Rad protein was recently shown to be one of the major regulators of LTCC open probability and Rad is a substrate for PKA-mediated phosphorylation. PKA phosphorylated Rad increases the open probability of the LTCC. However, how PKA-CS is recruited is still unknown.

As the C terminus of α1c is cytoplasmatic, this part might act as a potential docking site for PKA-CS. In an initial experiment conducted by members of the Dascal lab, recombinant PKA-CS protein was incubated with spot-synthesized Cav1.2 α1c C terminus. Three major interaction sites with PKA-CS were found, with two of them representing the regulatory regions, PCRD and DCRD (Figure S4). To verify this result, PKA-CS peptides were overlaid with recombinant His-DCRC-Myc or His-SUMO-PCRD proteins (kindly provided by Prof. Dr. Nathan Dascal). This experiment revealed two interaction sites of DCRD with PKA-CS and two interaction sites with PCRD, with one site being shared between the two proteins (Figure 8B, C). The binding sites on PKA-CS span functional regions associated with the catalytic assembly of the C-spine and overlap with PKA regulatory subunit (PKA-RS) and substrate binding sites (Figure 8C, E). The involved residues are highly conserved in human and mice (Figure 8D).

As the potential PCRD binding site on PKA-CS partially overlaps with binding sites of the PKA-RS, His-DCRD-Myc and His-SUMO-PCRD were purified from Rosetta™ bacteria to determine if binding of PKA-RS to the CS was altered in the presence of DCRD or PCRD channel fragments. For this, recombinant GST-PKA-RIIβ was pulled down with glutathione-beads and the binding of His-PKA-CSα was analyzed in the presence of the channel fragments. GST-PKA-RIIβ was purified by Dr. Ryan Walker-Gray (Klussman lab). His-PKA-CSα was kindly provided by the laboratory of Prof. Dr. Friedrich Herberg (Universität Kassel, Germany). No effect of either His-DCRC-Myc or His-SUMO-PCRD on the interaction of CS with RS of PKA could be detected (34 ± 0.144% for 12.5 µM DCRD, 29 ± 0.18% for 12.5 µM PCRD compared to 28 ± 6% for buffer only) (Figure 9). As a control, the PKA complex was dissociated with 100 µM cAMP and PKA-CS was no longer detectable on the Coomassie gel. To preclude non-specific binding effects, 30 µg BSA was added to the reaction mixture, and this had no effect on the interaction between the two subunits (Figure 9B).

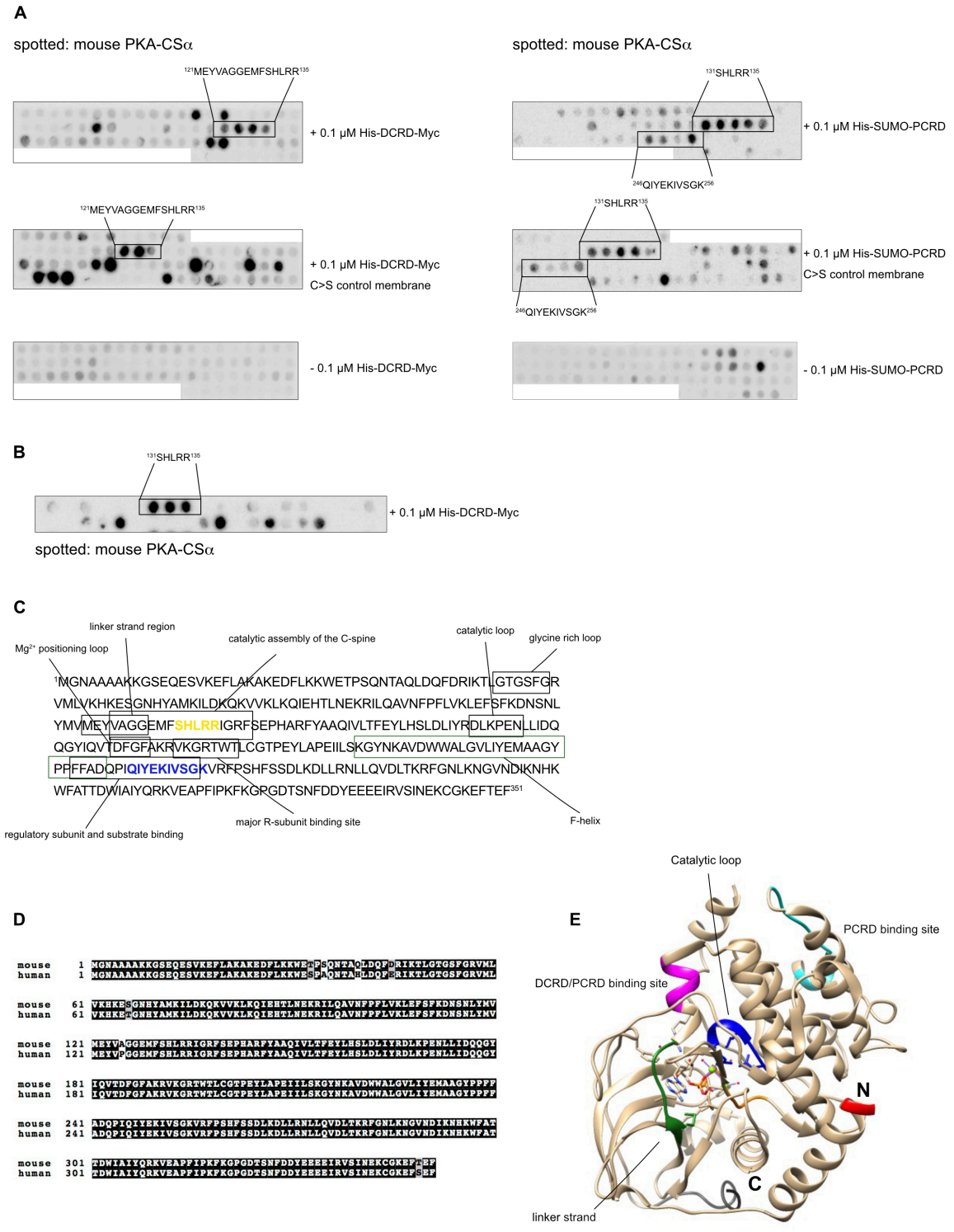


**Figure 8: Mapping the interaction sites of PCRD and DCRD with PKA-CS.** A) An array of 25-mer overlapping peptides of mouse PKA-CS spotted on a membrane was overlaid with purified His-DCRD-Myc or His-SUMO-PCRD to reveal common and unique binding sites on PKA-CS. The binding regions and the corresponding amino acid sequences are shown. B) An array of 25-mer peptides with a 10 amino acid sequence offset of PKA-CS was overlaid with His-DCRD-Myc. C) His-DCRD-Myc and His-SUMO-PCRD binding sites on PKA-CS are shown together with structural features of the enzyme (modified from McClendon et al., 2014). Yellow = DCRD and PCRD binding site, blue = PCRD binding site. D) Alignment of human and mouse PKA-CS protein sequences shows conservation of the residues involved in DCRD and PCRD binding. E) Shown is the PKA-CS crystal structure

with DCRD and PCRD binding sites highlighted (magenta and turquoise), catalytic loop (blue) and linker strand (green). Protein data bank (PDB) code: 4WB5.

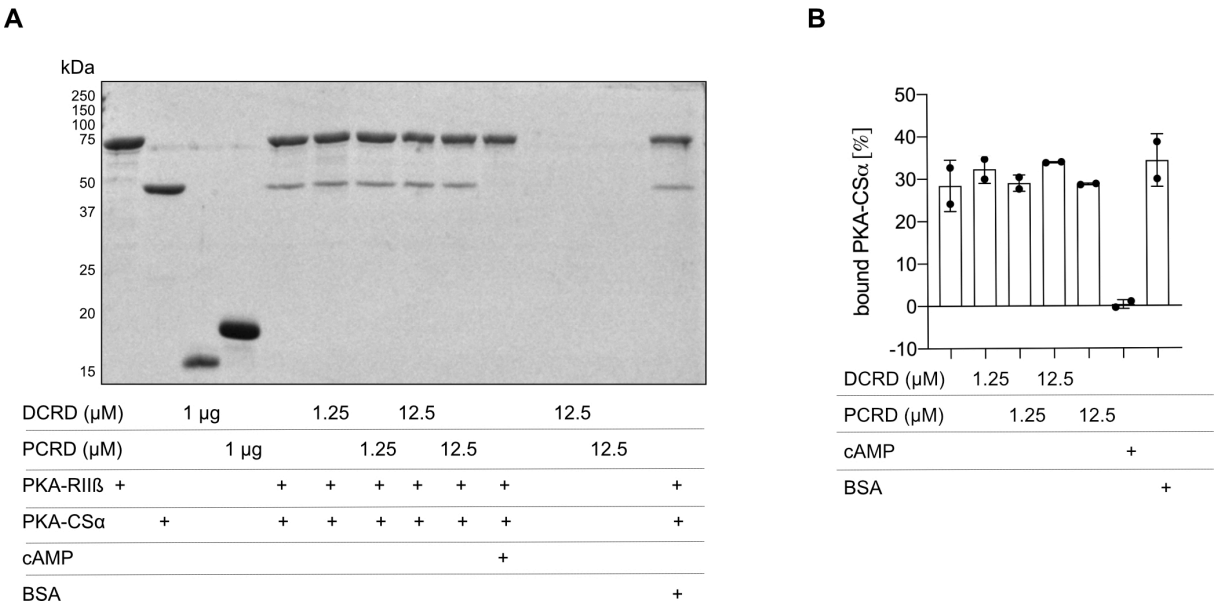


**Figure 9: His-DCRD-Myc or His-SUMO-PCRD do not affect the PKA CS-RS interaction.** A) Representative Coomassie gel of the pull-down experiment. 150 nM GST-PKA-RIIβ protein was pulled-down using glutathione agarose beads. 125 nM PKA-CS was used per reaction. The indicated concentrations of DCRD and PCRD were added. B) Semiquantitative analysis of PKA-CS binding to the RS. The graph shows the mean ± SD of two independent experiments.

To analyze the interaction of PKA-CS with the two channel fragments in a cellular model, DCRD and PCRD were transiently expressed in HEK293 cells. Both were tagged with Cerulean and anti-GFP antibody used for detection in Western blots. The PKA-CS protein was precipitated from the cells using anti-PKA-CS antibody. Figure 10 shows that both, DCRD-Cerulean and PCRD-Cerulean co-immunoprecipitated (Co-IP) with PKA-CS and this interaction was neither affected by treatment with the cAMP elevating agent forskolin (Fsk, 30 µM) nor the DMSO control treatment (DCRD DMSO: 1.1 ± 0.3, DCRD forskolin 1.2 ± 0.4 to DCRD untreated 1.4 ± 0.8; PCRD DMSO 0.75 ± 0.2, PCRD forskolin 0.77 ± 0.1 to PCRD untreated 0.95 ± 0.44) (Figure 10B).

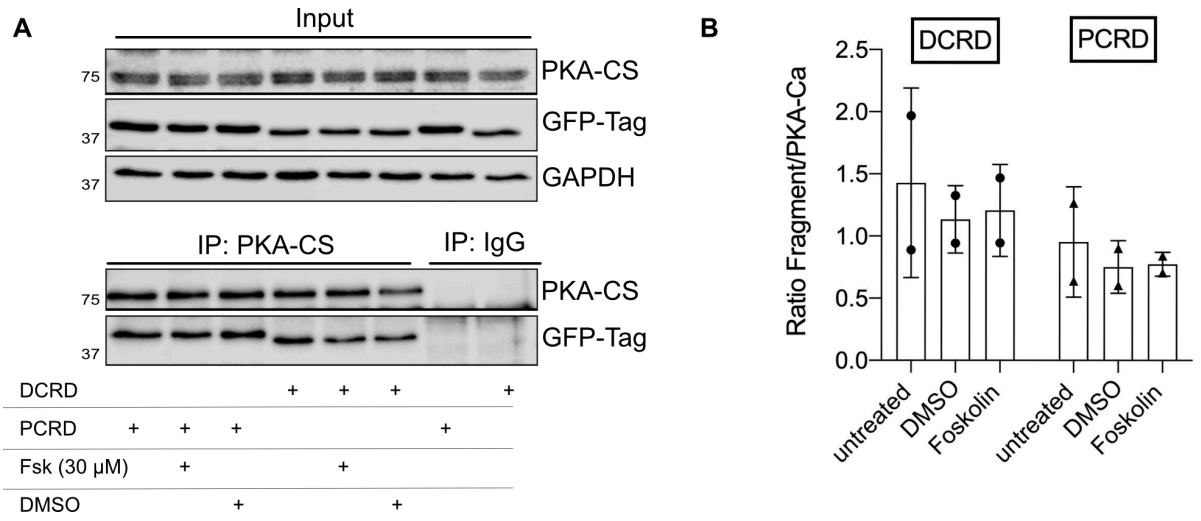


**Figure 10: DCRD- and PCRD-Cerulean are found in a complex with PKA-CS in HEK293 cells.** A) DCRD-Cerulean, PCRD-Cerulean and PKA-CS-YFP were overexpressed at equimolar ratios in HEK293 cells. After 48 h, cells were either left untreated or treated with the indicated agent and PKA-CS immunoprecipitated from protein lysates using anti-PKA-CS antibody. Representative Western blot image. B) Quantitative analysis of the ratio of DCRD-Cerulean and PCRD-Cerulean signal to PKA-CS in the IP samples. The graph shows the mean ± SD of two independent experiments.

### 4.1.2 DCRD and PCRD mutations do not affect the interaction with PKA-CS

Based on the overlay results shown in Figure 8, different mutations causing amino acid substitutions were inserted into the *CACNA1C* DNA sequence and the interaction of the mutant proteins with PKA-CS analyzed. To express and detect the α1c subunit in HEK293 cells, the protein coding DNA sequence was fused with an N-terminal CFP-tag and cells transfected with this construct. The mutations in *CACNA1C* caused amino acid substitutions to alanines (DCRD EE/AA, PCRD GPEI/AAAA) and substitution of two arginines to lysines in the PCRD sequence (PCRD RR/KK, PCRD GPEIRR/AAAAKK). These substitutions reduced the binding of PKA-CS to PCRD/DCRD (data not shown, Dascal lab). Here, no differences were detected regarding the pull down of PKA-CS with α1c constructs (Figure 11).

This implies that in a cellular environment the recruitment of PKA-CS is more complex, potentially involving other proteins as well.

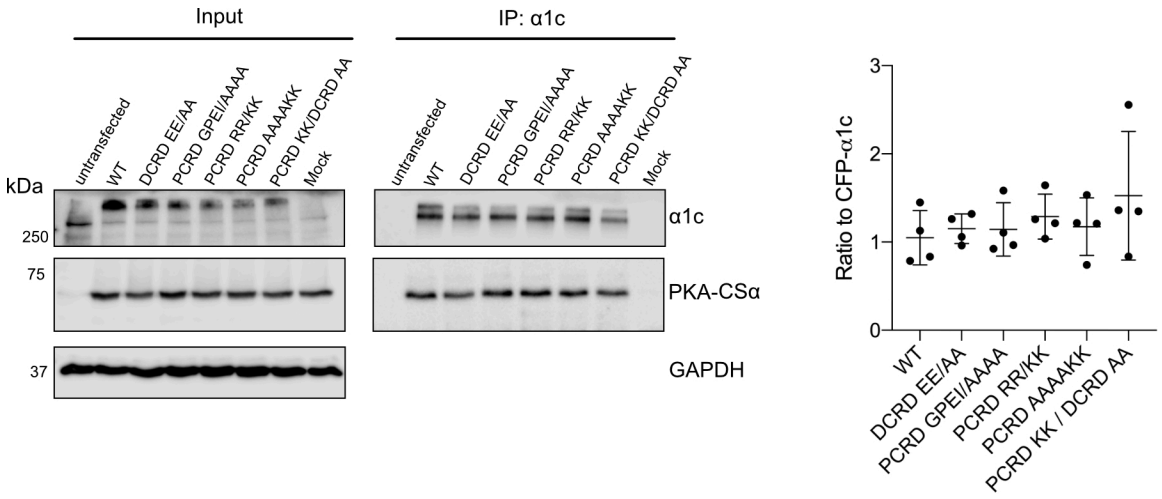


**Figure 11: Mutations in DCRD and PCRD do not affect the interaction with PKA-CS**. A) CFP- α1c wildtype (WT) or mutants were overexpressed in HEK293 cells together with PKA-CS-Venus. The image shows a representative blot of four independent experiments. B) Semiquantitative analysis of the co-immunoprecipitation of PKA-CS with the CFP-α1c constructs. The mean values ± SD are shown. For statistical analysis, Kruskal-Wallis non-parametric test was used with post-hoc Dunn's test. No significant differences were detected.

### 4.1.3 The DCRD or PCRD channel fragments do not affect PKA-CS catalytic activity

The main function of PKA-CS is the phosphorylation of substrate proteins in its close vicinity. Interaction of PKA-CS with the C terminus of the α1c might allow phosphorylation of target proteins at the channel complex. Since the channel fragments themselves are not phosphorylated by PKA-CS (see section 1.2.2.1), it was hypothesized that they might affect the catalytic activity of the enzyme through conformational mechanisms. Based on the structural model of McClendon *et al.* the amino acids mediating the interaction are involved in catalytic functions by assembly of the C-spine (sequence: HLRR) and stabilization of an active conformation of the activation loop (sequence: GKVRF) (McClendon et al., 2014). HEK293 cells were transfected with varying amounts of DCRD- and PCRD-Cerulean plasmids and the amount of phosphorylated PKA substrate proteins was analyzed by Western blot using anti-phosphorylated PKA substrate (anti-pPKA substrate) antibody (Figure 12A). The cells were treated with 1 µM forskolin to dissociate the PKA holoenzyme and to release PKA-CS. Even at the highest concentration of plasmid DNA (1 µg), the pPKA substrate signal was only moderately increased by 16% for DCRD and 28% for PCRD. For a more sensitive detection, the Cook Assay was employed in a second *in vitro* approach. This experiment was conducted in the laboratory of Prof. Dr. Friedrich Herberg. The Herberg lab kindly provided two different recombinant PKA-CS proteins (His-PKA-CSα and untagged PKA-CSα). No effect of the channel proteins on the catalytic activity of PKA-CS was detected (ratio to PKA-CS only control: 1 µM DCRD = 0.99 ± 0.04, 10 µM DCRD = 1.1 ± 0.05, 1 µM PCRD = 0.97 ± 0.03, 10 µM PCRD = 1.02 ± 0.04) (Figure 12B). To investigate if the channel fragments

interfered with PKA-CS/PKA-RS or PKA-CS/PKI interaction, the measurements were repeated in the presence of these two proteins/peptides (Figure 12B, lower part). As expected, PKA-RIα and PKI both inhibited PKA-CS (60% for PKA-RIα and 74% for PKI). Addition of DCRD did not ablate the inhibitory effect of the two proteins/peptides, though PCRD increased the activity of PKA-CS in the presence of PKI by around 40%. Further, no additive effect of PCRD and DCRD in the same reaction mix was detected (Figure 12B). In a final experimental approach, the ADP-Glo$^{TM}$ Kinase Assay (Promega, Germany) was conducted using recombinant proteins and the kemptide substrate peptide. 10 µM of His-DCRD-Myc or His-SUMO-PCRD were added to the reaction mix and 30 µM H89 was included as a control, to confirm that the inhibitor decreased the measured luminescence signal. Addition of neither DCRD nor PCRD significantly affected the PKA activity in this assay format and they also did not interfere with the H89 binding to PKA (Figure 12C). Since both *in vitro* assays used kemptide as a substrate, both experiments were plotted together in one final graph (Figure 12D) and this showed only a slight decrease in the PKA activity compared to the control sample with PKA-CS and kemptide only (1.6 ± 0.1% decrease for 10 µM DCRD, 4.8 ± 0.09% decrease for 10 µM PCRD).

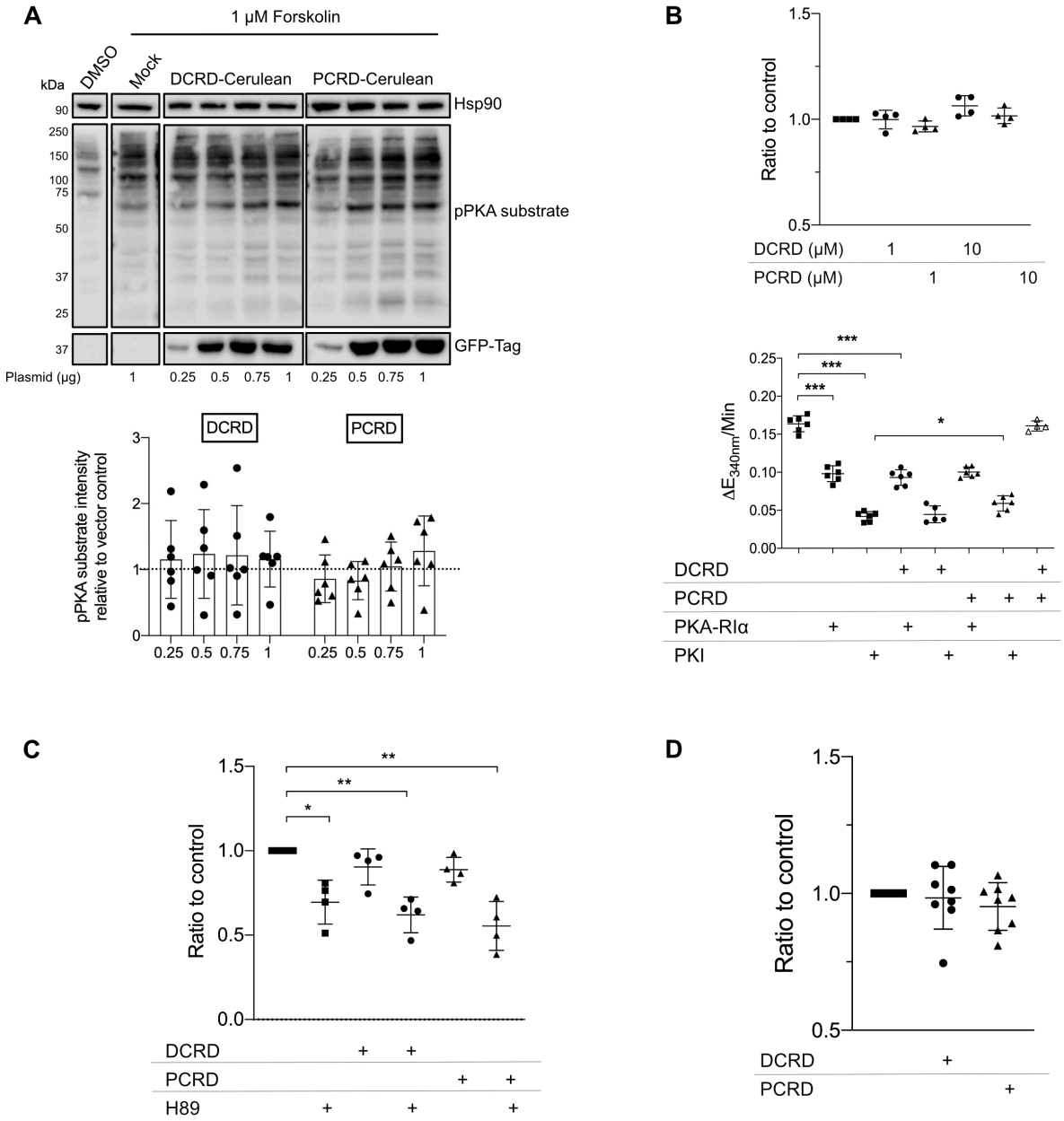


**Figure 12: DCRD and PCRD fragments do not affect PKA-CS catalytic activity** A) Varying amounts of DCRD- and PCRD-Cerulean plasmids were expressed in HEK293 cells and the amount of phosphorylated PKA substrate protein detected using anti-pPKA substrate antibody. The empty vector control (Mock) shows, that the Forskolin stimulation worked and induced phosphorylation of PKA substrates. The graph shows the mean of the pPKA substrate signal ± SD to the Mock control sample (n=6). B) In the Cook assay, 40 nM of human PKA-CS was incubated with the indicated concentrations of His-DCRD-Myc or His-SUMO-PCRD with 250 nM kemptide. The upper graph shows the ratio to the PKA-CS and kemptide only control measurements ± SD (n=4). For the lower graph, 30 nM PKA-RIα or 30 nM PKI were added in the presence and absence of the channel fragments (10 µM) (n = 6 independent measurements, n = 4 for DCRD/PCRD combination). C) 10 µM of His-DCRD-Myc, His-SUMO-PCRD or 30 µM H89 were incubated with 20 nM bovine PKA-CS and the resulting luminescence signal measured. The graph shows the ratio to the control sample (PKA-CS + kemptide) ± SD (n=4). D) Cumulative graph of the Cook Assay (B) and ADP Glo Assay (C). For statistics, Kruskal-Wallis test with Dunn's correction was applied. *$p \leq 0.05$, ** $p \leq 0.01$, *** $p \leq 0.001$.

## 4.2 PDE3A1 but not PDE3A2 interacts with the α1c subunit of the LTCC

Another potential interaction partner and thus regulator of the LTCC complex could be PDE3A. It would control local cAMP levels and thus PKA-CS activity and Rad phosphorylation in the vicinity of LTCC.

To study a potential interaction between the α1c subunit and PDE3A, PDE3A1 and PDE3A2 isoforms were transiently expressed in HEK293 cells together with the α1c subunit. Since in future experiments this interaction will be analyzed in context of the HTNB-causing *PDE3A* mutations, the PDE3A3 isoform was not included here, as it lacks the N-terminal mutational hotspot region.

Both isoforms were successfully precipitated from the cell lysate and detected in a Western blot. The PDE3A1 isoform but not PDE3A2 co-precipitated the LTCC α1c subunit (Figure 13A). This complex formation was independent of AKAP150, since PDE3A1 also pulled down the α1c subunit in the absence of AKAP150. AKAP150 was included as it interacts with the Cav1.2 α1c and could thus anchor various proteins to the channel (W. Catterall, 2011; Hulme et al., 2003; Oliveria et al., 2007).

PDE3A1 was then overlaid on peptides derived from the α1c subunit C terminus. Antibody binding was detected at two spots of the membrane, indicating that this region at the end of the C terminus could act as the binding site (Figure 13B).

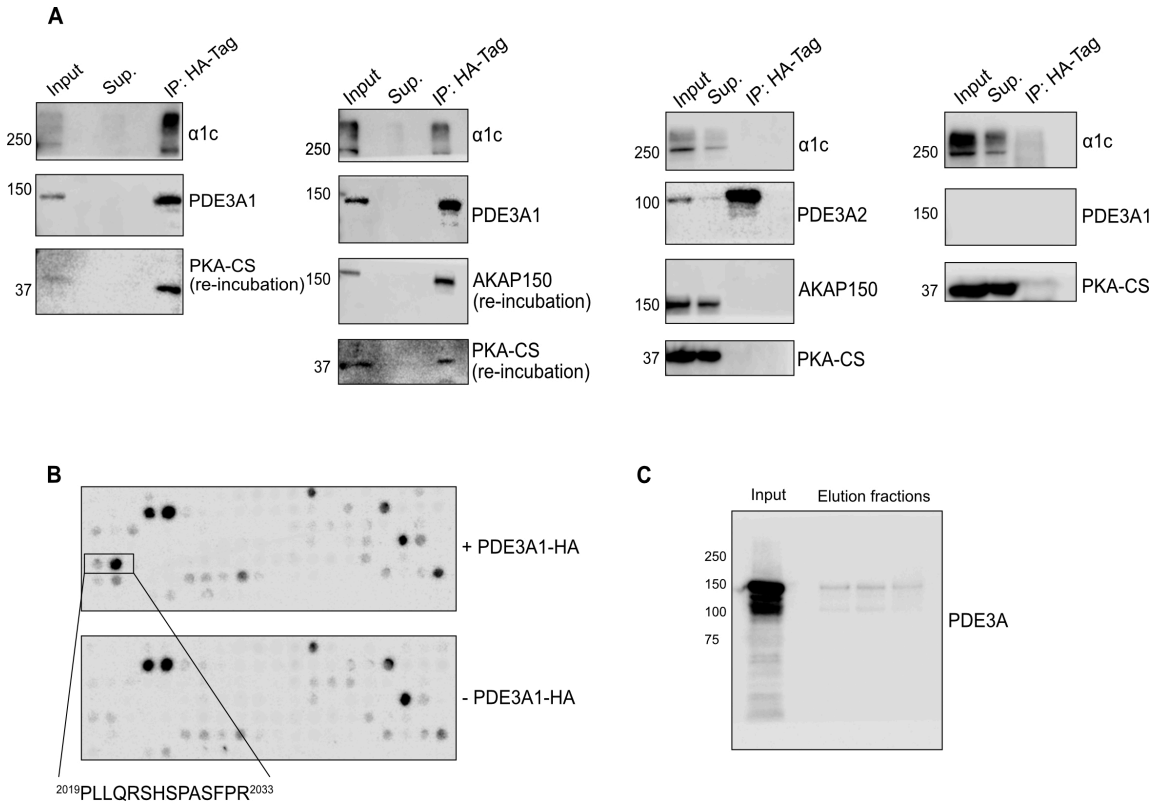


**Figure 13: PDE3A1 but not PDE3A2 co-immunoprecipitates with the LTCC α1c subunit, PKA-CS and AKAP150.** A) PDE3A1-HA or PDE3A2-HA, the α1c subunit and AKAP150 were co-expressed in HEK293 cells and precipitated using anti-HA magnetic beads. AKAP150 and PKA-CS were detected upon stripping of the membrane with Restore™ stripping buffer. The supernatant

which contains the unbound proteins is shown as well. The empty vector control does not show unspecific binding of α1c (upper right blot). Shown are representative blots of n=2 experiments. B) PDE3A1-Flag was overlaid on spotted α1c C terminus. The box shows a potential interaction site with the corresponding amino acid sequence of the α1c C terminus. The negative control is shown as well. The membrane is a representative of n=2 experiments. C) Western blotting confirms the presence of PDE3A1-HA in the elution fractions. These ones were used for the overlay experiment.

## 4.3 HTNB-causing *PDE3A* mutations affect the $Ca^{2+}$ signaling in cardiomyocytes

### 4.3.1 hiPSC-CMs with *PDE3A* mutations show differences in protein expression

Amino acid substitutions localized in the N-terminal region of PDE3A cause hypertension in the affected individuals, but the patients are protected from cardiac damage. The mutant PDE3A enzyme is hyperactive and aberrantly phosphorylated potentially causing changes in the interaction with other proteins (see section 1.4.1). The underlying molecular mechanism protecting the heart from damage is unclear. Here, hiPSC-CMs were used as a model system to study these mechanisms.

Human iPSCs were obtained from the Max-Delbrück-Center Stem Cell Core facility (Cell line: BIHi-049-A). The HTNB causing amino acid substitutions, T445N and R862C, were introduced by Michael Mücke using TALENs and CRISPR/Cas 9 methods (Richardson et al., 2016; Yusa, 2013), respectively. The hiPSCs were differentiated to cardiomyocytes as described in section 3.2.12. At day 45 of differentiation, the WT and mutant cells were analyzed for the expression of cardiac troponin T (TNNT2) and myosin light chain 2 ventricular-type (MLC2v) using a flow cytometry approach.

The WT and mutant cells showed similarly high expression of TNNT2 at day 45 ($TNNT2^+$ (WT) = 99 ± 0.53%, $TNNT2^+$ (T445N) = 98 ± 2.8%, $TNNT2^+$ (R862C) = 99.7 ± 0.3%, Figure S5A). The expression of MLC2v protein was lower as the TNNT2 expression, which could be explained by the immature phenotype of the differentiated cells. The expression of MLC2v ($MLC2v^+$) for the WT was 15.1 ± 5.9%, for T445N $MLC2v^+$ = 15.9 ± 6% and for R862C $MLC2v^+$ = 11.3 ± 6.8% (Figure S5B). The relative amount of double positive cells ($TNNT^+$, $MLC2v^+$) was not significantly different between the three genotypes ($TNNT2^+$, $MLC2v^+$ (WT) = 13.7 ± 2.5%, $TNNT2^+$, $MLC2v^+$ (T445N) = 14.3 ± 1.5%, $TNNT2^+$, $MLC2v^+$ (R862C) = 10.5 ± 4.3%) (Figure 14D). In summary, all genotypes expressed cardiac marker proteins to a similar extent and did not show *PDE3A* mutation-induced differences in TNNT2 and MLC2v expression.

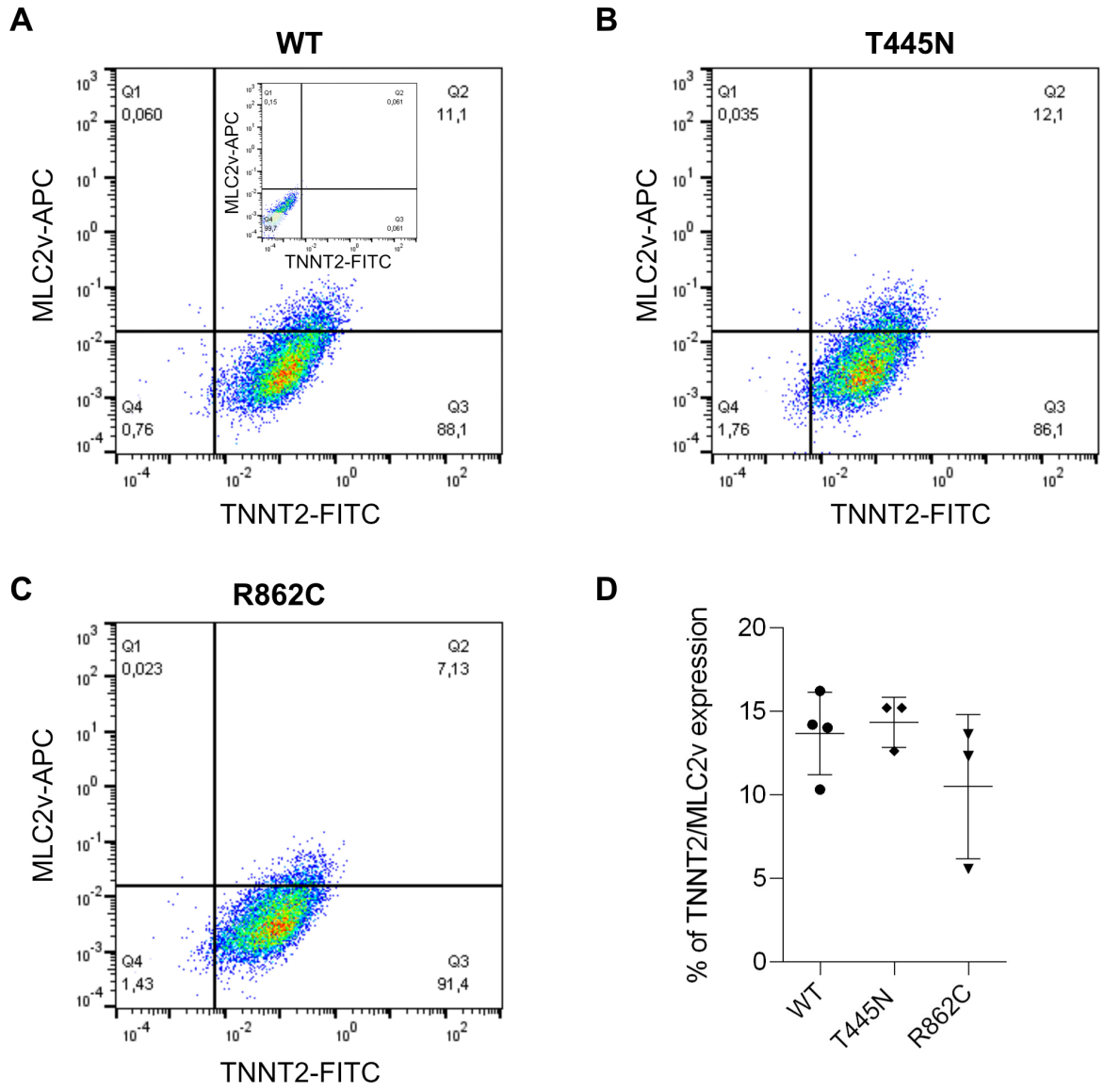


**Figure 14: hiPSC-CMs express cardiac troponin T (TNNT2) and myosin light chain 2v (MLC2v).** Depicted are representative flow cytometry images showing the expression of TNNT2 and MLC2v for the WT (A) and mutant cell lines (B, C) at day 45. The inlet in the left panel shows the IgG control sample. D) The graph depicts the percentage of positive cells for both, $TNNT2^{+}$ and $MLC2v^{+}$ for 4 (WT) and 3 differentiation experiments (T445N, R862C). Using Kruskal-Wallis non-parametric test with Dunn's multiple testing correction did not show any significant differences.

The expression of proteins involved in the $Ca^{2+}$ signaling pathway was analyzed. The Western blot experiment revealed no significant differences in the expression of PKA-CS, PLN and SERCA2 (Figure 15B). The expression of PDE3A1, but not PDE3A2, was significantly downregulated in the R862C mutant (PDE3A1 = 0.26 ± 0.253) and in the T445N mutant (PDE3A1 = 0.25 ± 0.23) compared to the WT (PDE3A1 = 0.83 ± 0.3). Further, the expression of the LTCC $\alpha$1c subunit was significantly lower in both mutants compared to the WT (WT = 0.993 ± 0.22, T445N = 0.56 ± 0.23, R862C = 0.47 ± 0.22). For the T445N, but not the R862C mutant, the myosin binding protein C3 (MyBPC3) was significantly

downregulated (MyBPC3 = 0.725 ± 0.7 to 1.5 ± 0.4 for WT). In the basal state, the phosphorylation of Troponin I was decreased (T445N = 0.63 ± 0.38, WT = 1.95 ± 1.3). For PKA-mediated phosphorylation of Serine 16 of PLN (pPLN), a trend toward lower signal intensity in the mutants compared to the WT was observed.

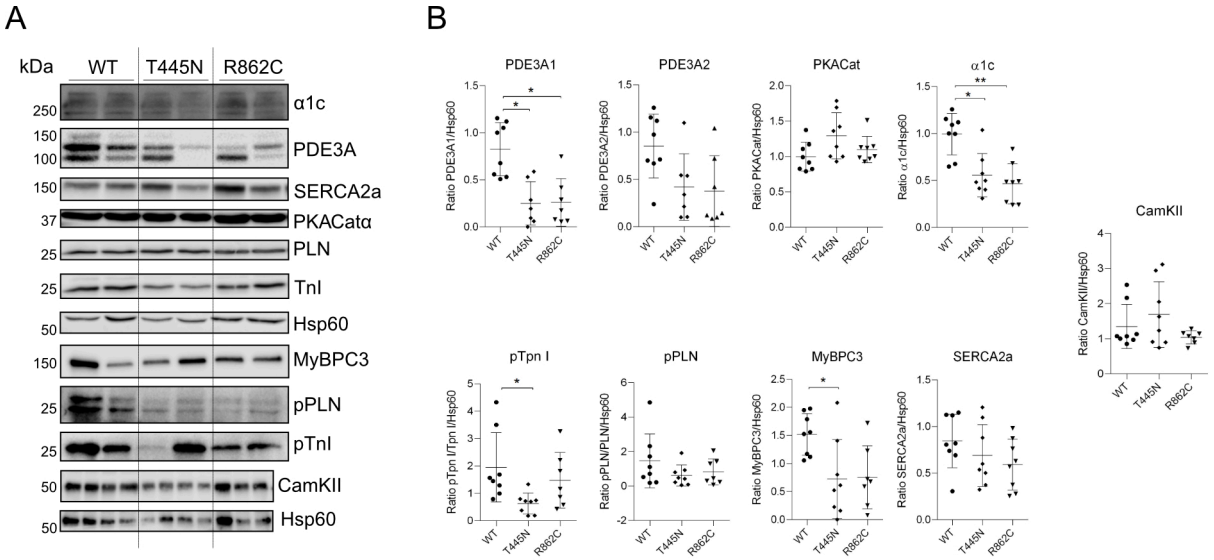


**Figure 15: Mutant hiPSC-CMs show decreased expression of PDE3A, α1c, pTpn I and MyBPC3.** A) Shown are representative Western blots. The corresponding protein sizes in kDa are depicted on the left. Representative loading controls (Hsp60) are shown as well. B) The graphs highlight the mean ± SD for 8 individual samples per genotype. The ratio of the protein signal intensity normalized to the corresponding loading control is plotted. For the pPLN and pTpn I quantifications, the membrane signals were normalized to the corresponding loading control and to the amount of PLN or Tpn I signal. Statistical analysis was carried out using Kruskal-Wallis Test and post-hoc Dunn's test. *$p \leq 0.05$, ** $p \leq 0.01$.

To elucidate if the differences seen in protein levels were a result of a decreased mRNA level, cDNA expression was studied. For this, the expression of genes encoding the LTCC α1c (*CACNA1C*), SERCA2 (*ATP2A2*), MyBPC3 (*MYBPC3*), Troponin I (*TNNI3*) and PDE3A (*PDE3A*) was compared between the three different genotypes. There were no significant differences between the WT and the mutant cells detectable (Figure 16).

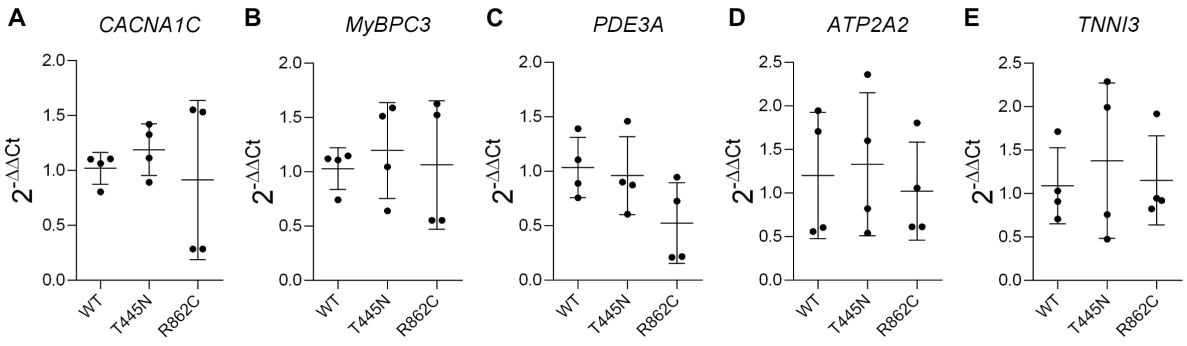


**Figure 16: The mRNA expression is not affected in the mutant cells.** For quantification, the fold change normalized to the mean value of the WT samples was calculated. Shown is the expression of *CACNA1C* (A), *MyBPC3* (B), *PDE3A* (C), *ATP2A2* (D) and *TNNI3* (E). The graphs show the mean ± SD of two independent experiments with altogether four samples.

## 4.4 The *NPPB* gene expression is higher in the T445N mutant than in the WT upon endothelin stimulation

One characteristic hallmark of cardiac damage is the increase in left ventricular mass, caused by cellular hypertrophy. The hiPSC-CMs were treated for 48 h with 10 nM endothelin-1 (ET-1). As expected, in the WT the ET-1 treatment induced a more than 5-fold increase in the *NPPA* and *NPPB* expression.

ET-1 is a commonly used substance to cause cardiac hypertrophy and induces increased cell size and expression of hypertrophic genes in different *in vitro* models (Aggarwal et al., 2014; C. Carlson et al., 2013; Deisl et al., 2019; Földes et al., 2011; Johansson et al., 2020; Ovchinnikova et al., 2018; A. Tanaka et al., 2014). Johansson *et al.* detected an increase in *NPPA*, *NPPB* and *ACTA1* genes already after 24 h of treatment with ET-1 (Johansson et al., 2020).

The treatment with ET-1 resulted in a 6-8-fold increase in the expression of *NPPA* and *NPPB* genes also for the mutant cells, but only moderately affected the expression of *MYH7* and *ACTC* genes (Figure 17). ET-1 induced expression of *NPPA* to a similar extent in all three genotypes (fold change WT = 6.8 ± 1.4, T445N = 7.1 ± 1.4 and R862C = 6.2 ± 2.7). The expression of *NPPB* was almost doubled in the T445N mutant compared to the WT and R862C (fold change WT = 7.7 ± 1.6, T445N = 12.7 ± 3.8, R862C = 6.6 ± 1.7) (Figure 17).

In addition to ET-1, the cells were also treated with isoproterenol. Either the concentration of isoproterenol or the duration of the treatment was not sufficient to induce an upregulation of the hypertrophy associated genes in any of the genotypes (Figure S6).

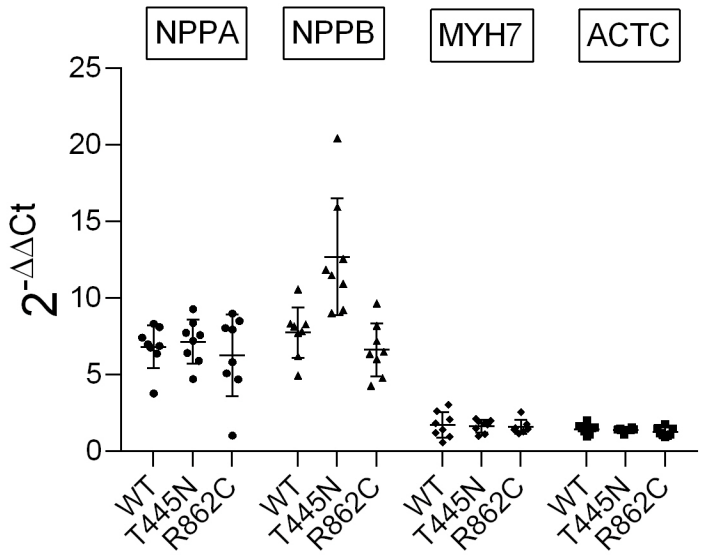


**Figure 17: The expression of the *NPPA* and *NPPB* genes is increased in WT and mutants.** hiPSC-CMs were treated with 10 nM endothelin-1 for 48 h and the expression of hypertrophy marker genes analyzed using qPCR approach. The graph shows the mean ± SD fold change ($2^{-\Delta\Delta Ct}$ method) of two independent experiments.

## 4.5 Mutant hiPSC-CMs have longer $Ca^{2+}$ transients

PDE3A is found in a complex with SERCA2, AKAP18, PKA, CamKII$\delta$, PLN and involved in controlling $Ca^{2+}$ re-uptake into the SR by regulating local cAMP levels. *PDE3A* mutations affecting the N-terminal region, like the T445N mutation, lead to increased cAMP affinity and thus enzymatic activity (Ercu et al., 2020; Maass et al., 2015). For this reason, the hiPSC-CM model was used to analyze if the mutations in *PDE3A* affect the $Ca^{2+}$ re-uptake into the SR. The $Ca^{2+}$ binding dye Fluo-8-AM was used and the $Ca^{2+}$ transients visualized using fluorescence microscopy and line-scan mode. To synchronize the contraction of the individual cells, they were paced at 0.5 Hz, 10 V using a biphasic cycle.

In the first experiment, the $Ca^{2+}$ transients were analyzed in imaging buffer only. Because a non-ratiometric dye was used which might be affected by photobleaching effects, the absolute $Ca^{2+}$ concentration could not be determined.

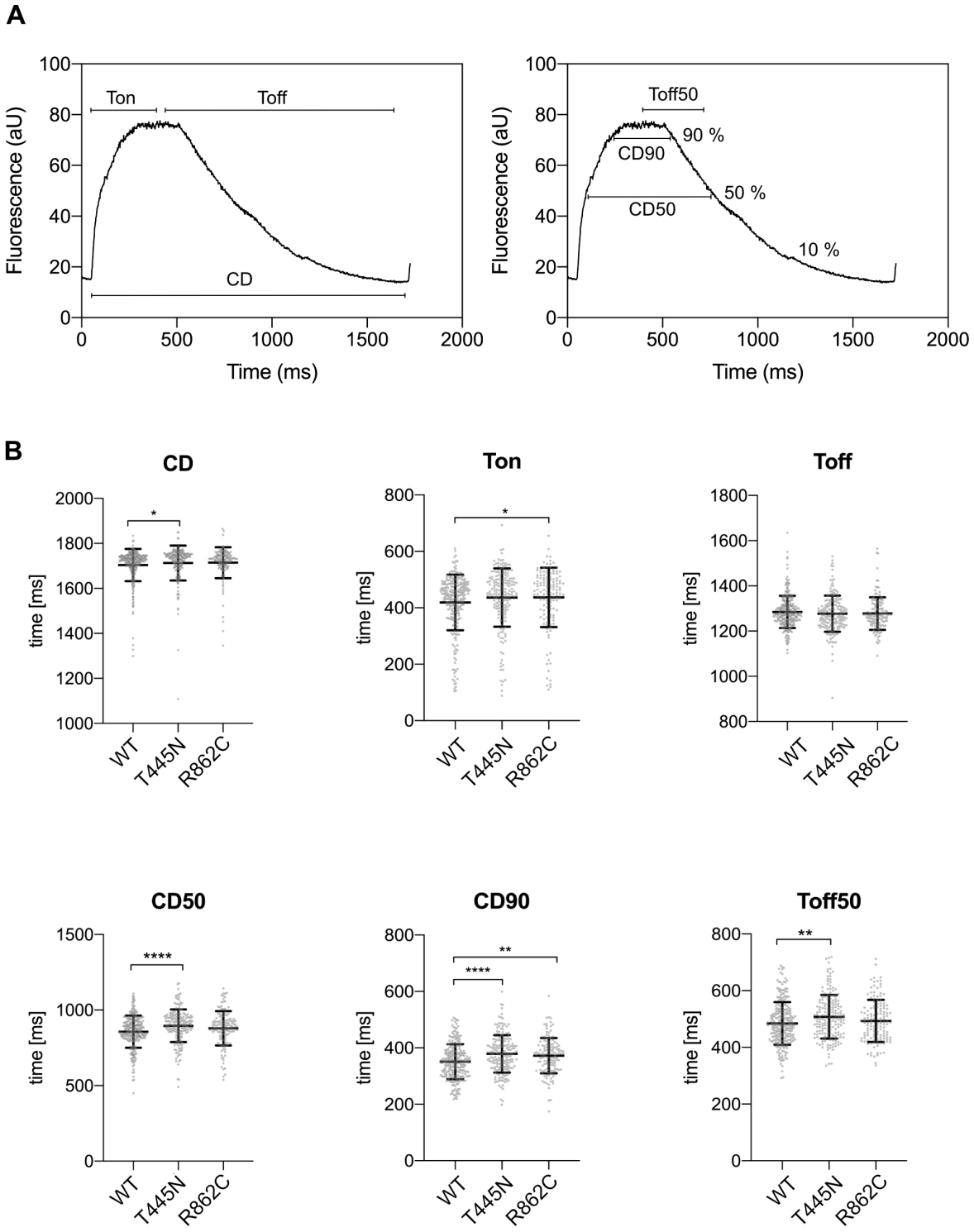


**Figure 18: hiPSC-CMs with *PDE3A* mutations have longer $Ca^{2+}$ transients.** A) Schematic representation of a $Ca^{2+}$ transient with the calculated parameters indicated. B) The T445N mutant has longer $Ca^{2+}$ transient duration (CD) and longer transients at 50% and 90% above the baseline signal (CD50 and CD90, respectively) compared to the WT. The $Ca^{2+}$ re-uptake to 50% of the signal is slower (Toff50). The R862C mutant has slower $Ca^{2+}$ accumulation (Ton) and longer transients at 90% above the baseline signal (CD90). The graphs show the mean ± SD of 260 cells for WT, 192 cells for T445N and 141 cells for R862C. Statistical test: Kruskal-Wallis test with Dunn's correction. *$p \leq 0.05$, ** $p \leq 0.01$, ****$p \leq 0.0001$.

The T445N mutant cells had significantly longer $Ca^{2+}$ transient duration at 50% amplitude (CD50) compared to the WT and R862C (WT = 857 ± 106 ms, T445N = 896 ± 109 ms, R862C = 879 ± 113 ms) and this effect was also seen for the R862C mutant at 90% of the signal above baseline (CD90) (WT = 351 ± 62 ms, T445N = 379 ± 67 ms, R862C = 372 ± 63 ms) (Figure 18). For the time to the maximal $Ca^{2+}$ concentration (Ton) for both mutants this range was longer compared to the WT (WT = 419 ± 99 ms, T445N = 436 ± 103 ms, R862C = 437 ± 106). This effect could not be seen when the time to 90%, 50% or 10% of signal was analyzed (Ton90, 50, 10) (Figure S7A). For the time from peak to the end of the transient (Toff), the mutants did not differ significantly from the WT cells. If analyzing only the part of the transient from peak to 50% of the declining transient (Toff50) the T445N mutant was significantly slower than the WT (WT = 484 ± 75 ms, T445N = 508 ± 77 ms, R862C = 493 ± 74 ms). This effect was no longer seen for the two other Toff parameters (Toff10 and Toff90) (Figure S7A).

The $Ca^{2+}$ signaling was further analyzed in the presence of the β-adrenergic receptor agonist, isoproterenol (Iso, 1 μM), the PDE3-specific inhibitor cilostamide (Cilo, 20 μM) or both reagents together. Since both compounds were dissolved in DMSO, as a control the cells were treated with 0.2% DMSO dissolved in Imaging buffer. As shown in Figure 19, the hiPSC-CMs were sensitive to DMSO (here: 0.2% DMSO), because the differences in the $Ca^{2+}$ transients mentioned before were no longer seen in the presence of DMSO.

The stimulations with Iso or Cilo had different effects on the two mutants (Figure 19). For the duration of the $Ca^{2+}$ transient, the T445N mutant had a significantly longer transient than the WT upon stimulation with Iso and the combination of Iso and Cilo, whereas the R862C mutant did not differ from the WT (Iso condition: WT = 1582 ± 184 ms, T445N = 1662 ± 117 ms, R862C = 1581 ± 226 ms, Iso + Cilo condition: WT = 1574 ± 171 ms, T445N = 1650 ± 115 ms, R862C = 1593 ± 183 ms). This trend also persisted for the $Ca^{2+}$ duration at 50% and 90% above baseline (CD50 and CD90). For the CD50 values, the R862C mutant had significantly longer transient durations compared to the WT upon Iso + Cilo treatment (WT = 692 ± 98 ms, T445N = 764 ± 103 ms, R862C = 722 ± 117 ms) and this trend was observed for the CD90 value as well.

The combination of Iso + Cilo had a significantly different effect on the mutants, with both reaching the maximum $Ca^{2+}$ concentration (Ton) later than the WT (WT = 313 ± 106 ms, T445N = 351 ± 120 ns, R862C = 353 ± 116 ms). No difference in any of the conditions was seen for the time to 50% and 90% amplitude (Ton50, Ton90) (Figure S7B).

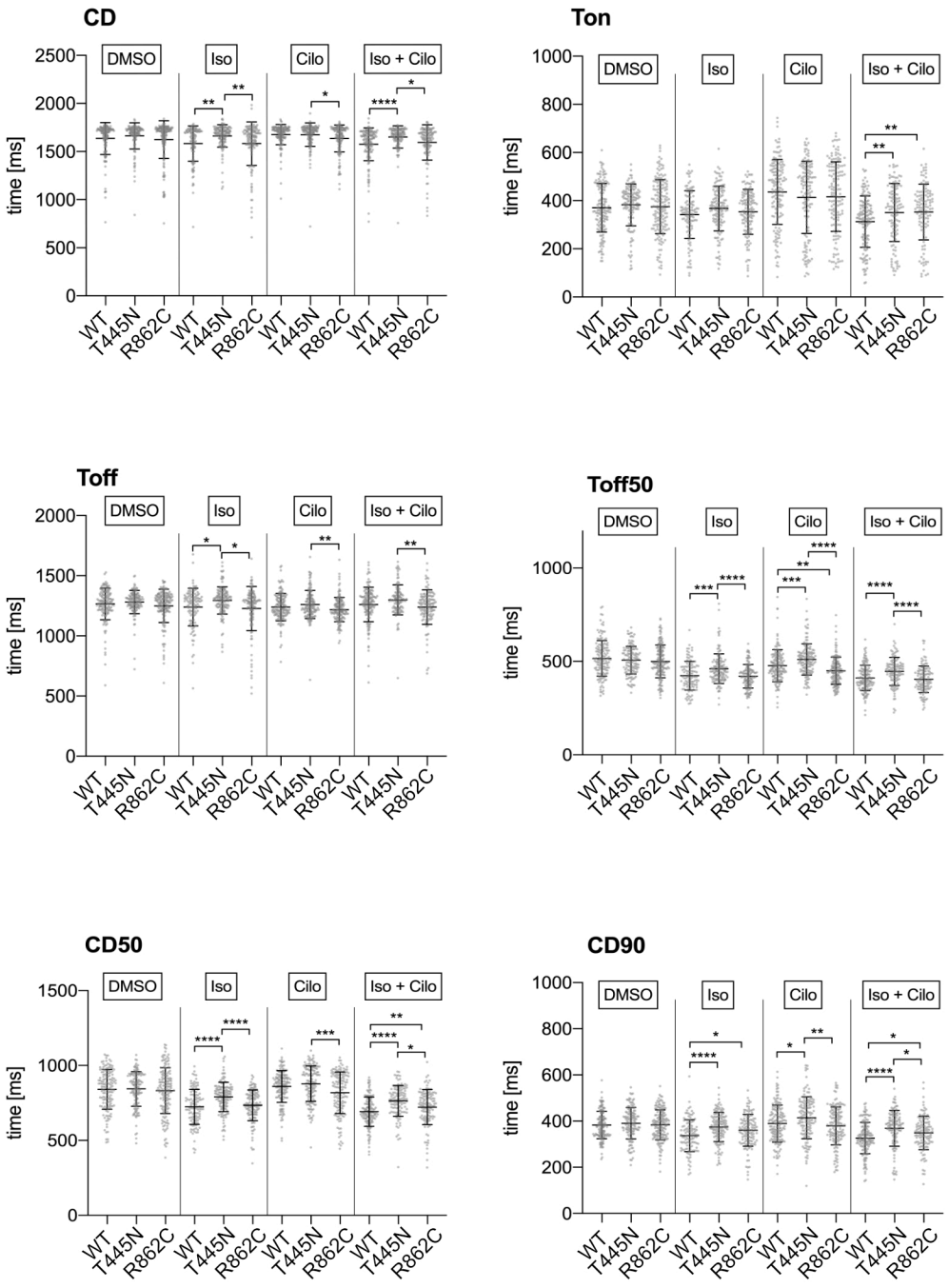


**Figure 19: hiPSC-CMs with *PDE3A* mutations show differences in $Ca^{2+}$ transient duration upon stimulation with isoproterenol, cilostamide or the combination of both.** Cells were treated with DMSO (0.2%) as solvent and 1 µM isoproterenol, 20 µM cilostamide or both for 10 min at room temperature. The treatments induced differences between wildtype (WT) and mutant cells (T445N, R862C) for the different parameters. The graphs show the mean ± SD for WT = 149 cells for DMSO, 113 cells for Iso, 151 cells for Cilo, 145 cells for Cilo + Iso, T445N = 133 cells for DMSO, 136 cells for Iso, 139 cells for Cilo, 117 cells for Cilo + Iso and R862C = 162 cells for DMSO, 129 cells for Iso, 146 cells for Cilo, 119 cells for Cilo + Iso. For statistics, a Kruskal-Wallis test with Dunn's multiple testing correction was applied. *$p \leq 0.05$, ** $p \leq 0.01$, ***$p \leq 0.001$, ****$p \leq 0.0001$.

For the time from peak to 50% of the transient (Toff50) both the T445N and the R862C showed significant differences upon Cilo stimulation. The inhibition of PDE3 resulted in slower $Ca^{2+}$ re-uptake in the T445N mutant but faster uptake in the R862C mutant compared to the WT (WT = 477 ± 85 ms, T445N = 511 ± 84 ms, R862C = 450 ± 72 ms). Further, the T445N mutant had slower re-uptake also upon Iso and Iso + Cilo treatment, whereas the R862C did not differ from the WT (Iso condition: WT = 423 ± 77 ms, T445N = 461 ± 79 ms, R862C = 420 ± 63 ms, Iso + Cilo condition: WT = 411 ± 68 ms, T445N = 446 ± 75 ms, R862C = 405 ± 70 ms). This pattern persisted also for the decline to 10% and 90% of the amplitude (Toff10, Toff90) (Figure S7B).

Generally, the two mutants responded different from each other to the treatments, the R862C mutant behaved more like the wildtype than like the T445N mutant.

## 4.6 Analysis of the $Ca^{2+}$ amplitude in the WT and mutant cells using Fura-2

Since photobleaching effects cannot be precluded using Fluo-8 non-ratiometric $Ca^{2+}$ dye, together with Rene Jüttner (Gotthardt lab, MDC Berlin), $Ca^{2+}$ imaging experiments were conducted using Fura-2 ratiometric dye and Ionoptix device.

In contrast to the initial measurements, these experiments were performed at 37°C and the pacing frequency was adjusted to 2 Hz. Since no $Ca^{2+}$ standard curve was measured, the absolute $Ca^{2+}$ concentration in the cytosol could not be determined.

Due to the low number of experiments (n=2) no statistical test was conducted for the Fura-2 measurements. However, in the basal state, the T445N mutant had a trend towards a higher baseline signal (F0) (WT = 0.92 ± 0.14, T445N = 0.99 ± 0.14, R862C = 0.88 ± 0.16), measured as the ratio of excitation at 340 and 380 nm ($Ca^{2+}$ bound to $Ca^{2+}$ unbound signal of Fura-2 $Ca^{2+}$-binding dye) (Figure 20). Further, the T445N mutant showed a trend towards a higher $Ca^{2+}$ amplitude (Fmax) compared to the WT and R862C mutant (WT = 0.37 ± 0.17, T445N = 0.422 ± 0.13, R862C = 0.28 ± 0.17). For the duration of the $Ca^{2+}$ transient at 50% amplitude (CD50), both mutants had a trend towards longer duration compared to the WT (WT = 191 ± 15.5 ms, T445N = 205 ± 35 ms, R862C = 218 ± 26 ms), which is in the line with the previous experiment.

To analyze the effect of β-adrenergic stimulation or PDE3 inhibition on the $Ca^{2+}$ amplitude and transients, cells were treated with 0.02% DMSO as control, 1 µM Iso, 20 µM milrinone (Mil) and the combination of Iso and milrinone. Other than in the previous experiment (Figure 19), PDE3 was inhibited with milrinone, as this compound is soluble at higher concentrations in DMSO (here: 200 mM) to minimize the DMSO effects. Upon stimulation with Iso, the T445N mutant had a slight increase

in the $Ca^{2+}$ amplitude, whereas the WT showed a slight decrease compared to the DMSO control (WT (DMSO) = 0.44 ± 0.16, WT (Iso) = 0.39 ± 0.11, T445N (DMSO) = 0.38 ± 0.11, T445N (Iso) = 0.47 ± 0.12). The amplitude of the R862C remained unchanged (R862C (DMSO) = 0.37 ± 0.1, R862C (Iso) = 0.38 ± 0.1). When PDE3 was inhibited with 20 µM Mil, both mutants had smaller amplitudes compared to the WT (WT (Mil) = 0.55 ± 0.15, T445N (Mil) = 0.36 ± 0.12, R862C (Mil) = 0.25 ± 0.1). Again, there was an effect of DMSO, since both mutants had lower $Ca^{2+}$ amplitudes in the DMSO condition (Figure 21).

For the baseline signal, Mil had a slight effect on the WT and R862C, but none of the other stimulations caused a change in the signal intensity compared to the control measurement.

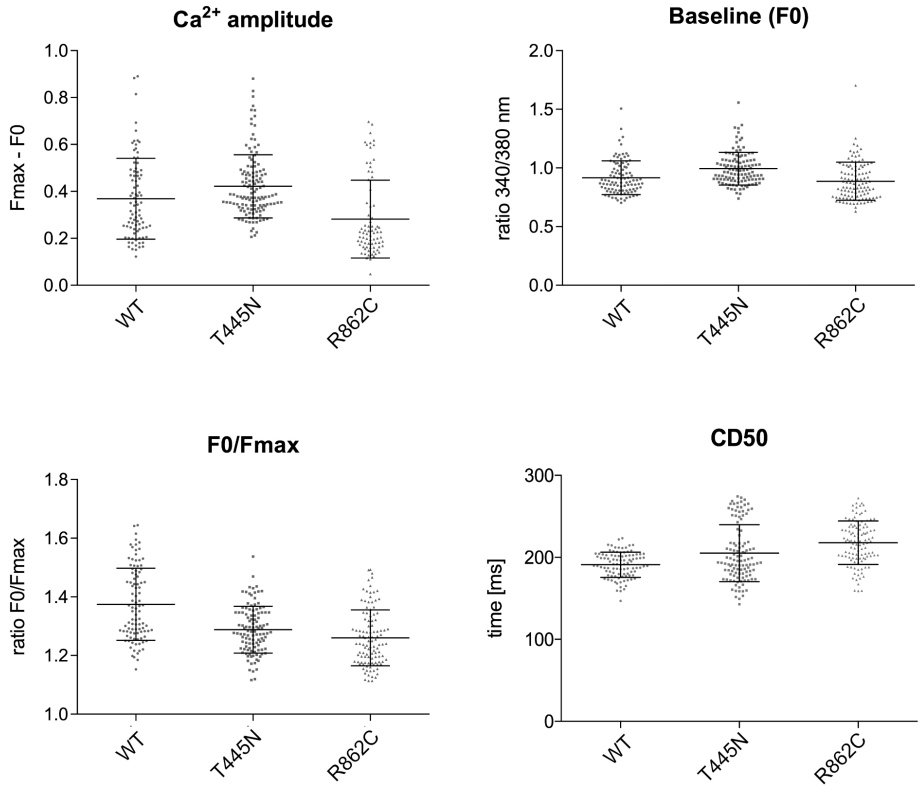


**Figure 20: Trends in $Ca^{2+}$ duration and amplitude for measurements with Fura-2 in mutant and WT cells.** In the basal state, the T445N mutant has a trend towards higher $Ca^{2+}$ amplitude (Fmax – F0) but also a higher baseline (F0). The ratio of maximum amplitude to the baseline seems to be lower in both mutants. The $Ca^{2+}$ transient duration at 50% amplitude is longer in both mutants compared to the WT. The graphs show the mean ± SD for WT = 98 cells, T445N = 113 cells, R862C = 109 cells of two independent experiments.

In line with the effects on baseline and amplitude, only the PDE3-inhibitor Mil slightly affected the ratio of Fmax to F0 in both mutants compared to the WT (WT (Mil) = 1.44 ± 0.11, T445N (Mil) = 1.28 ± 0.08, R862C (Mil) = 1.2 ± 0.05) (Figure 21). The CD50 was longer in the T445N mutant upon Mil administration and only slightly increased upon Iso administration and the combination of Iso and Mil

(WT (Mil) = 188.3 ± 15.9 ms, T445N (Mil) = 206 ± 19.8 ms, R862C (Mil) = 183 ± 20.7 ms, WT (Iso + Mil) = 173 ± 14.2 ms, T445N (Iso + Mil) = 192 ± 18.8 ms, R862C (Iso + Mil) = 203 ± 14.6 ms).

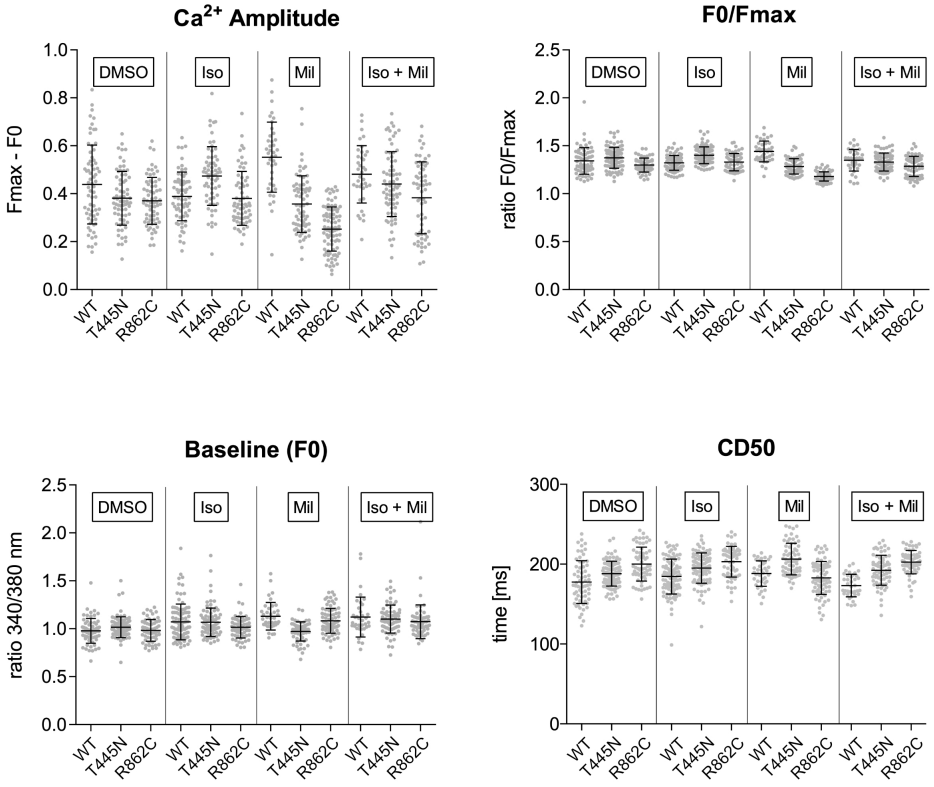


**Figure 21: Effects of DMSO, isoproterenol and milrinone on $Ca^{2+}$ amplitude, the ratio F0/Fmax and the duration of the transient.** Upon milrinone (Mil) administration both mutants show a decrease in the $Ca^{2+}$ amplitude and a decrease in the ratio Fmax/F0. The baseline is slightly affected in the T445N mutant in the Mil condition. The transient duration at 50% amplitude (CD50) is increased in the T445N mutant upon PDE3 inhibition. The graphs show the mean ± SD for WT (DMSO) = 65 cells, T445N (DMSO) = 90 cells, R862C (DMSO) = 61 cells, WT (isoproterenol, Iso) = 95 cells, T445N (Iso) = 89 cells, R862C (Iso) = 63 cells, WT (Mil) = 39 cells, T445N (Mil) = 64 cells, R862C (Mil) = 78 cells, WT (Iso + Mil) = 37 cells, T445N (Iso + Mil) = 70 cells, R862C (Iso + Mil) = 62 cells. The measurements (n=2) were conducted in collaboration with Dr. Rene Jüttner (MDC Berlin).

## 4.7 An approach to study local cAMP levels in cells expressing HTNB-causing *PDE3A* mutations

Local cAMP levels were analyzed using a compartment-specific cAMP FRET sensor. The senor was fused to PLN to study the cAMP level at the SR. More specifically, it consists of an Epac-based cAMP binding domain flanked by a YFP and CFP fluorophore pair. In a low cAMP environment, the sensor is in a closed conformation, resulting in a high FRET signal. Upon elevation of the cAMP level, cAMP binds and induces an opening of the sensor, resulting in decrease of the FRET signal (Figure 22A).

The sensor was expressed in the WT and *PDE3A*-mutant hiPSC-CMs. The cAMP level at the SR was measured in the basal state and upon treatment with cAMP elevating agents (1 µM isoproterenol or 20 µM forskolin), PDE3 inhibitor (20 µM milrinone) or PDE1 – 5 inhibition (100 µM IBMX).

In the basal state, there was no difference in the FRET signals of the mutants compared to the WT (WT = 2.8 ± 0.5, T445N = 2.5 ± 0.5, R862C = 2.7 ± 0.5) (Figure 22B). Unfortunately, the administration of IBMX or the combination of Iso and IBMX did not affect the FRET signal relative to the DMSO control (0.1% DMSO) (Figure 22C). This indicates that either the sensor sensitivity was not ideal or that the cells did not respond to the treatments in this experimental set-up.

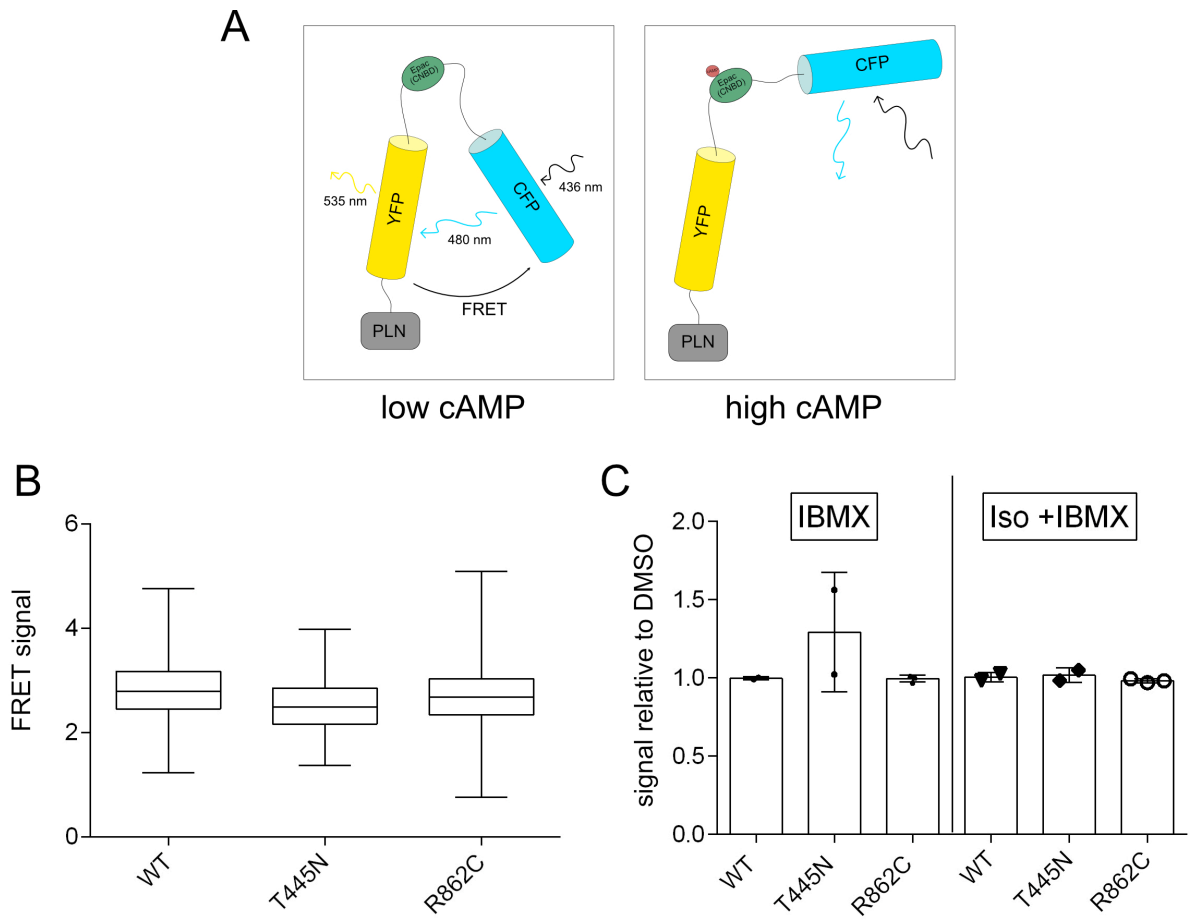


**Figure 22: hiPSC-CMs do not respond to cAMP elevating agents.** A) The cAMP FRET sensor consists of a YFP-CFP fluorophore pair and Epac as the cAMP binding domain. CFP is excited at 436 nm and emits at 480 nm which excites YFP in low cAMP environments. Upon cAMP elevation, the sensor changes its conformation, resulting in a lower signal. The sensor is fused to PLN to be targeted to the SR. B) In the basal state, the T445N and R862C mutants do not differ from the WT in cAMP levels at the SR. The graph shows the mean ± SD of WT = 3 experiments (3,096 cells), T445N = 2 experiments (1,019 cells), R862C = 5 experiments (4,054 cells). C) Upon PDE inhibition with 100 µM IBMX or stimulation with 1 µM Iso + 100 µM IBMX, no change in the FRET signal compared to the DMSO control (0.1%) was detected. The graph shows the mean ± SD for WT = 2 experiments, T445N = 2 experiments and R862C = 3 experiments. The measurements were performed in collaboration with Dr. Katina Lazarow and the analysis pipeline written by Janani Gayathri Nadar (both FMP Berlin).

## 4.8 Mutations in *PDE3A* decrease the interaction with SERCA2 in a HEK293 model

The $Ca^{2+}$ re-uptake into the SR is regulated by the proteins of the complex comprising of SERCA2, PLN, PDE3A, CamKII$\delta$ and AKAP18. The slower $Ca^{2+}$ uptake that was detected in the T445N mutant (Figures 18 + 19) could be associated with lower local cAMP and thus activity of PKA-CS. A reduced cAMP level could be a result of either increased PDE3A enzymatic activity as shown in previous work or decreased abundance in the multiprotein complex with SERCA2. Thus, SERCA2 and PDE3A1 WT and mutants were transiently expressed in HEK293 cells and their interaction studied using Co-IP.

The three constructs harboring *PDE3A* mutations interacted less with SERCA2 compared to the WT (Figure 23B). The ratio of PDE3A1-WT being associated with SERCA2 was 3.75 ± 1.95. The binding of PDE3A1-$\Delta$3aa was more than half times lower, 1.41 ± 0.52. The binding of the PDE3A1-T445N and PDE3A1-R862C mutants was reduced to a similar level with a PDE3A1/SERCA2 ratio of 1.077 ± 0.37 and 1.045 ± 0.15, respectively.

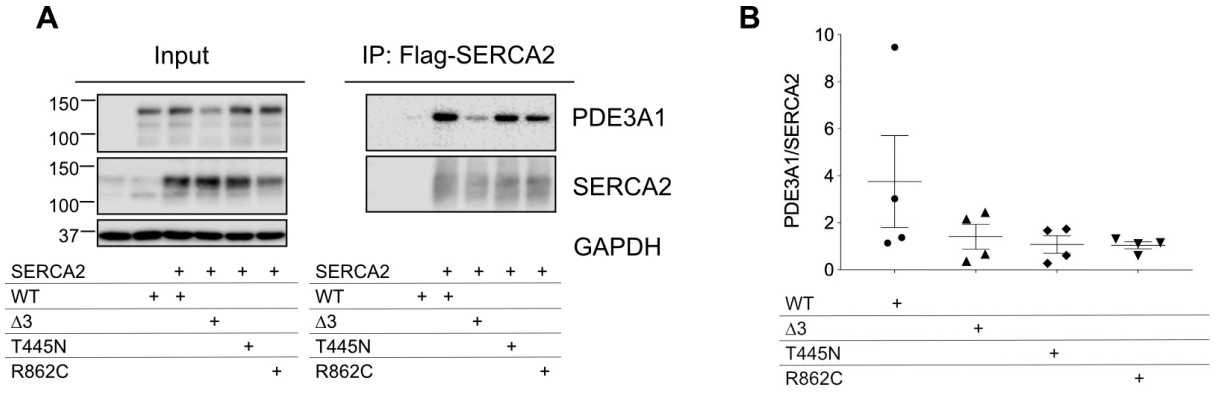


**Figure 23: Effects of *PDE3A* mutations on the interaction of SERCA2 with PDE3A**. A) Representative Western blot confirming SERCA2-Flag and PDE3A1-HA expression. As a loading control, GAPDH was used. B) The amount of PDE3A1 co-immunoprecipitated with SERCA2 is plotted. Shown is the mean ± SEM of four independent experiments. This experiment was conducted in collaboration with Dr. Maria Ercu, Klussmann lab.

# 5 Discussion

## 5.1 PKA-CS interacts with DCRD and PCRD at the LTCC α1c subunit

### 5.1.1 The complex formation involves common interaction sites of all three proteins

In this thesis, PKA-CS was found to be directly associated with the C terminus of the LTCC α1c subunit in *in vitro* assays and in a HEK293 cell model.

The PKA-CS interaction sites on the α1c subunit encompass the DCRD and PCRD regulatory regions, that interact with each other and inhibit the channel α1c subunit (Hulme et al., 2006; Lyu et al., 2017). Structurally, the interaction of DCRD with PCRD is mediated *via* electrostatic interactions of positively charged residues in PCRD (R1696 and R1697) with negatively charged amino acids in DCRD (E2103, E2106 and D2111) (Hulme et al., 2006). These amino acid residues are localized in α-helical structures and exposed to the cytoplasm, making them an accessible docking site for other proteins. Thus, amino acid substitutions to polar, neutral charged residues in PCRD and DCRD disrupt the electrostatic interactions and prevent the formation of the inhibitory complex (Hulme et al., 2006). Recently, the interaction was shown to be modulated by CaM in a $Ca^{2+}$-dependent manner. CaM binding to the IQ and pre-IQ motifs is prevented by the presence of the region containing DCRD (Lyu et al., 2017). The deduced model required DCRD interaction with PCRD as the initial step. The resulting conformational change leads to CaM-competitive domain (CCD) binding to IQ and pre-IQ, preventing CaM binding which leads to decreased channel activity. In this model, the phosphorylation of S1700 in PCRD by PKA was suggested to release the interaction, but since this site is not involved in channel regulation, an alternative mechanism would be plausible (Lyu et al., 2017).

The main residues of DCRD and PCRD involved in the interaction with PKA-CS, match with the ones that are required for DCRD and PCRD complex formation. Both, DCRD and PCRD, interact with the $^{131}$SHLRR$^{135}$ sequence in PKA-CS which lies in α-helical structures at the surface of the protein (section 4.1.1, Figure 8A, B, E). The binding sequence consists of positively charged amino acids with the ability to form salt bridges with negatively charged residues, as, for example, the two glutamic acid residues E2103 and E2104 in DCRD. The binding site of PCRD comprises the sequence $^{246}$QIYEKIVSGK$^{256}$, which contains E249 with a negative charge and K250, K256 residues being positively charged. Thus, some of the residues might be involved in salt-bridges with the PCRD residues, or the polar residues form hydrogen bonds to facilitate the interaction. The Y247 residue in PKA-CS involved in PCRD binding was shown to form hydrogen bonds with the Y205 residue of the regulatory subunit of PKA (PKA-RI) (C. Kim et al., 2007). Another example of how PKA-CS is structurally complexed with another protein is the interaction of PKA-CS with PLN. PLN is phosphorylated by PKA-CS and thus interacts with the kinase *via* its PKA-CS consensus sequence ($^{13}$RRAST$^{17}$). The R14 residue interacts with E203, Y204 and E230 in

the large lobe of PKA-CS while the R13 interacts with S51 and the hydroxyl group of Y330 (J. Kim et al., 2015).

### 5.1.2 Potential regulatory mechanisms at the LTCC complex

Amino acid substitutions of the key residues in DCRD and PCRD involved in the interaction were expected to either diminish or prevent the association with PKA-CS. To study this in a cellular context, alanine and lysine substitutions in DCRD and PCRD were introduced into the $\alpha$1c subunit. Constructs harboring DCRD EE/AA, PCRD GPEI/AAAA, PCRD RR/KK, PCRD GPEIRR/AAAAKK or DCRD EE/AA in combination with PCRD RR/KK substitutions were overexpressed in HEK293 cells and the co-precipitation of PKA-CS analyzed.

In this thesis, there was no decrease in the interaction of PKA-CS with the different DCRD and PCRD mutant constructs detectable using Western blot method (section 4.1.3, Figure 11). Due to conformational changes or folding mechanisms in the whole $\alpha$1c subunit upon introduction of the substitutions, alternative binding sites might be involved and mediate the PKA-CS-$\alpha$1c complex formation. Another explanation would be, that in a cellular context there is another protein acting as a linker to scaffold the PKA-CS and LTCC $\alpha$1c subunit and this linker is not affected by the mutations in DCRD or PCRD.

Even though the exact mechanism of how PKA-CS is recruited and bound to the LTCC still remains part of further research, the potential target protein at the LTCC would be Rad. Rad was identified as the crucial regulator of the LTCC complex and $\alpha$1c opening mechanism (Liu et al., 2020). Rad binding to the complex is regulated by PKA-mediated phosphorylation. Rad can bind both the $\alpha$1c and $\beta$ subunit of the LTCC. Phosphorylation of Rad by PKA reduced the interaction with the $\beta$- subunit (Papa et al., 2022; T. Yang et al., 2012). The complex of Rad and $\beta$-subunit interacts with the $\alpha$1c at the I – II loop and dissociation of Rad leads to stabilization of a high opening gating mode, mediated by stable $\alpha$1c and $\beta$ subunit complex formation (Papa et al., 2022).

Two separate regulatory mechanisms at the LTCC were identified in a *Xenopus* oocyte model, Rad-dependent and Rad-independent effects (Figure 24) (Katz et al., 2021). The “Rad-independent” mechanism was referred to as a 20 – 30% increase in channel currents ($I_{BA}$) upon cAMP injection and this effect is not dependent on $\beta$-subunit or Rad expression. Further, the Rad-independent regulation involved the truncated $\alpha$1c C-terminal segment and the presence of an inhibitory module at the $\alpha$1c N terminus (Katz et al., 2021). The larger increase in $I_{BA}$ requires expression of Rad and is termed the “Rad-dependent” effect (Katz et al., 2021).

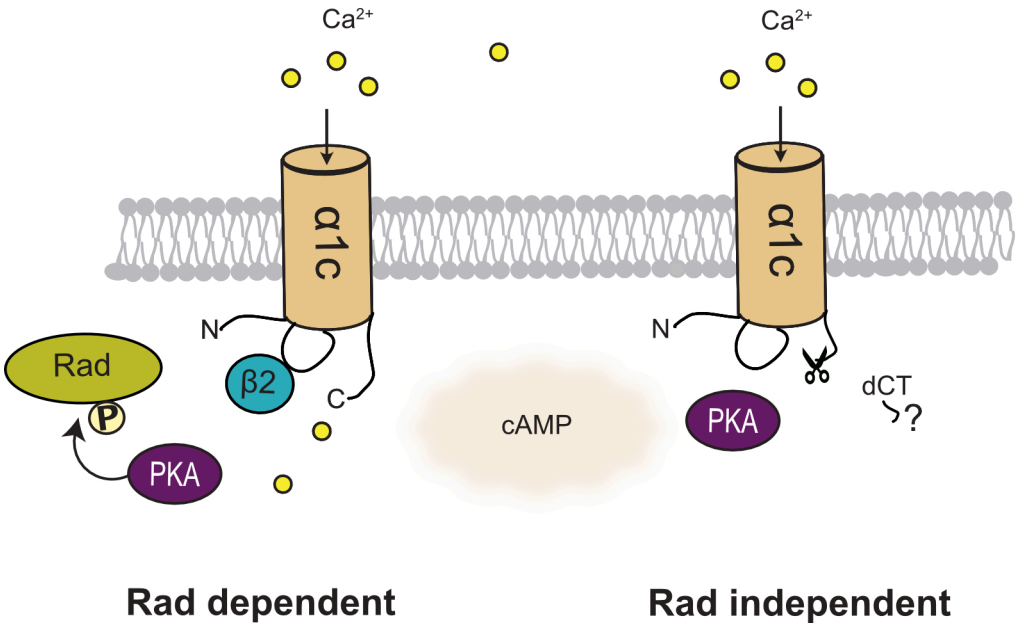


**Figure 24: Rad-dependent and independent mechanisms at the LTCC.** Two potentially independent or complementary pathways for the Rad regulation at the LTCC were described (Katz et al., 2021). The Rad-dependent mechanism requires the β2-subunit and Rad. For the Rad-independent effect, the N terminus and truncated C terminus of the α1c are required. If the clipped distal C terminus (dCT) is involved is still not fully understood. Both models require activation of PKA by increased cAMP levels.

In addition to the mechanism of Rad regulation, the role of the α1c proteolytic cleavage and NT-CT interaction was studied. Deletion of the N-terminal region of the truncated α1c (α1cΔ20Δ1821) abrogated the PKA-dependent regulation but had no effect on Rad-dependent regulatory mechanisms. Titration of Rad-expressing mRNA with a truncated Cav1.2 α1c Δ1821 or full-length Cav1.2 α1c both showed Rad-dependent decrease in the current ($I_{BA}$) and current increase upon stimulation with the cAMP-elevating agent forskolin, meaning the Rad-dependent effects do not require the presence of a cleaved C-terminal segment (Katz et al., 2021).

In the frame of a whole $\beta_1$-AR pathway reconstitution in *Xenopus* oocytes it was found that Iso increased $I_{BA}$ in the presence of Rad and this effect was blocked upon administration of the PKI peptide, that inhibits PKA (Katz et al., 2021). Interestingly, Iso did not have any effect in the absence of Rad and the effect of the agonist was higher for truncated α1c Δ1821 compared to the full-length channel (147% to 87%) (Katz et al., 2021).

Combining the observations of this thesis with the study of Katz *et al.,* the full reconstitution of the PKA-CS interaction with the LTCC might be difficult, because there are two regulatory mechanisms involved. The presence of Rad and the truncation of the α1c subunit might be required to further

analyze the interaction of PKA-CS and the α1c. Also, since in the HEK293 only the α1c and PKA-CS were overexpressed without any other proteins from the β-AR signaling pathway, the required signal for the recruitment of PKA-CS might be lacking in the HEK293 cell model.

### 5.1.3 DCRD and PCRD do not affect the PKA-CS catalytic activity

Proteins that interact with PKA-CS and anchor the protein to various subcellular sites include PKA-RS, the small GTPase Rab13, Caveolin-1 or PDE7A1. These proteins affect the PKA-CS enzymatic activity. Caveolin-1 is associated with PKA-CS through a scaffolding domain at its C terminus and the binding decreases PKA-CS enzymatic activity, explaining PKA-CS hyperactivity in Caveolin-1 KO mice (Cohen et al., 2004; Razani & Lisanti, 2001; Søberg & Skålhegg, 2018). The PDE7A1 isoform interacts with PKA-CS *via* its N terminus that contains two PKA pseudo substrate sequences and inhibits the kinase activity *in vitro* (Han et al., 2006; Søberg & Skålhegg, 2018).

In cardiomyocytes, PKA-CS is associated with ryanodine receptors and this interaction mediates the phosphorylation of RyR2 but also affects the catalytic activity of PKA-CS (Haji-Ghassemi et al., 2019). Similar to the LTCC, PKA-CS recruitment to the RyR2 was initially described as being AKAP-dependent and to require the interaction with leucine zipper motifs (Haji-Ghassemi et al., 2019; Marx et al., 2001). However, quantitative measurements are not available and cryogenic electron microscopy (cryo-EM) of RyR2 did not show the existence of leucine zippers, challenging this hypothesis (Haji-Ghassemi et al., 2019). The interaction that was shown by Haji-Ghassemi *et al*. comprises the entire periphery of the large lobe (= C-lobe) of PKA-CS, and some of the residues (S130, L132, R133, R256, S259) were also involved in PKA-CS interaction with DRCD and PCRD (Haji-Ghassemi et al., 2019). As these residues are highly conserved among the 150 homologous cAMP-dependent kinase families, this interaction could provide a unique mechanism of PKA-CS-substrate and interaction partner binding.

Phosphomimic of the S2813 residue in RyR2 (S2813D) induced a new alpha helix which resulted in increased affinity and higher catalytic activity of the PKA-CS (Haji-Ghassemi et al., 2019). Since the DCRD and PCRD interaction sites on PKA-CS are located in the C-lobe, which is associated with catalytic activity, the effect of DCRD and PCRD on the enzyme function was studied. The presence of DCRD or PCRD did not affect the catalytic activity in different enzymatic assays (see section 4.1.2, Figure 12). This might be explained by (i) a low binding affinity of DCRD and PCRD to PKA-CS and instability of the complex, (ii) a missing linker protein that is further stabilizing the interaction or (iii) that the only function of the interaction is recruitment of PKA-CS. Further experiments are needed to clarify the functional role of the PKA-CS and α1c interaction.

### 5.1.4 PDE3A1 as a potential regulator at the LTCC complex

With PKA-CS being required for Rad-dependent regulation of the LTCC, local control of cAMP levels by PDEs could represent another regulatory mechanism.

In the work presented here, the PDE3A1 but not PDE3A2 isoform was shown to form a complex with the $\alpha$1c subunit and this complex formation was independent of AKAP150 (section 4.1.4, Figure 13). The overlay of PDE3A1 on peptides derived from the C terminus of the $\alpha$1c only revealed one potential interaction site, spanning the $^{2019}$PLLQRSHSPASFRR$^{2033}$. The sequence is located upstream of the DCRD region in the C terminus of the $\alpha$1c which is cytosolic, making it an accessible docking site for interaction partners. It would be interesting to find out if the HTNB-causing mutations in *PDE3A* might affect the interaction with the LTCC $\alpha$1c and to confirm the interaction with endogenously expressed proteins.

Several PDEs, including various PDE4 isoforms, PDE3A and PDE1C were shown to be closely located to the LTCC $\alpha$1c (Liu et al., 2020; Muller et al., 2021).

In mouse cardiomyocytes, PDE4D and PDE4B are tethered to the LTCC and knock-out models of these two proteins are associated with longer $Ca^{2+}$ transients, cell contraction and spontaneous $Ca^{2+}$ release events (Leroy et al., 2011). PDE4D is associated with the $\alpha$1c subunit but is not involved in channel regulation under basal conditions, since *Pde4d* knock-out did not affect the channel current or the $\beta$-AR mediated regulation. In addition, the PDE4B isoform was shown to also Co-IP with the $\alpha$1c and *Pde4b*$^{-/-}$ mice have aberrations in $\beta$-AR mediated current regulation, $Ca^{2+}$ transients and contraction, exhibiting altered relaxation and $Ca^{2+}$ transient decay (Leroy et al., 2011). Since PDE4B is targeted to the LTCC, the phosphorylation levels of RyR2 and PLN were unaffected in the knock-out mouse model (Leroy et al., 2011).

PDE1C, which is predominantly expressed in the hearts of larger animals, is associated with $\alpha$1c conductance and but inhibition of PDE1C neither affect PLN, Tn I or MyBP-C phosphorylation, nor the SR $Ca^{2+}$ load (Muller et al., 2021). Interestingly, the inhibition of both, PDE1 and PDE3 enhanced the LTCC $Ca^{2+}$ current, while only PDE3 inhibition also augmented the SR $Ca^{2+}$ release (Muller et al., 2021).

## 5.2 *PDE3A* mutations induce aberrant $Ca^{2+}$ cycling in cardiomyocytes

### 5.2.1 The R862C and T445N substitutions affect ECC protein expression in hiPSC-CMs

In this thesis, hiPSC-CMs harboring HTNB-causing T445N and R862C amino acid substitutions were used as a model system to study $Ca^{2+}$ cycling and local cAMP levels. The amino acid substitutions were

localized at the N terminus and the catalytic domain of PDE3A. The N-terminal sequence is not present in PDE3A3, thus the T445N substitution affects only PDE3A1 and PDE3A2. Both substitutions cause HTNB and are associated with a potential cardioprotective effect, since affected individuals do not show cardiac damage (Ercu et al., 2020; Maass et al., 2015; Toka et al., 2015).

The hiPSC-CMs differing in their PDE3A proteins (WT, T445N, R862C) express cardiac Troponin T and ventricular MLC2 to a similar extent at day 45 of differentiation (section 4.3.1, Figure 14), ruling out an effect of the substitutions on cardiac differentiation efficiency. However, the expression of PDE3A1 and PDE3A2 isoforms was downregulated in both mutants compared to the WT, though PDE3A1 to a larger extent. This is in line with previous observations made in a HTNB rat model, where the protein expression of both isoforms was reduced in the hearts of the animals (Ercu et al., 2020). In the hiPSC-CMs model used in this thesis, *PDE3A* gene expression was reduced in the R862C mutant and slightly affected in the T445N cells, though not to a significantly different level from the WT.

Since PDE3A with HTNB-causing substitutions is hyperactive, a potential mechanism would be a feedback loop in which *PDE3A* mRNA and protein expression are downregulated to compensate for the hyperactivity. However, how this is achieved on the molecular basis still needs to be resolved.

The splicing and degradation of *PDE* transcripts was reported to be regulated by the $p54^{nrb}$/NONO nuclear protein and splicing factor proline and glutamine rich (SFPQ) (Chung et al., 2015; Lu & Sewer, 2015). SFPQ depletion resulted in decreased *PDE3A* mRNA expression levels in RNA-seq and RT-qPCR experiments. SFPQ binds to the *PDE3A* promoter and the binding process is regulated by serum concentration, although the specific serum factors have not been identified, yet (Rhee et al., 2017). In the human failing heart, *PDE3A* expression is downregulated while inducible cAMP early repressor (ICER) expression is upregulated (Ding, Abe, Wei, Huang, et al., 2005; Omori & Kotera, 2007). This results in activation of the cAMP/PKA pathway which further contributes to ICER expression causing cardiomyocyte apoptosis. This represents an autoregulatory mechanism which is called the PDE3A-ICER feedback loop (Ding, Abe, Wei, Xu, et al., 2005; Omori & Kotera, 2007).

In addition to PDE3A, the abundance of certain other proteins involved in the ECC pathway was also decreased in the T445N mutant (section 4.3.2, Figure 15), including the $\alpha$1c subunit of the LTCC in both mutants, MyBPC3, and phosphorylated Tpn I. In a mouse model with hypertension, the global level of LTCC channels and thus the $I_{Ca}$ was reduced (30 – 40% less protein). This was compensated by local, hyperactive LTCCs mediating larger $Ca^{2+}$ uptake but reduced sensitivity of $Ca^{2+}$-activated $K^+$ (BK) channels causing vascular dysfunction (Tajada et al., 2013). Electrophysiological measurements would be needed to study the LTCC activity in the hiPSC-CMs model.

Cardiac myosin binding protein C (MyBPC3) is one of the key elements of the sarcomere-binding myosin filaments, myosin heads and actin filaments, which represent the contractile unit in

cardiomyocytes (Helms et al., 2020; Previs et al., 2012, 2015). Phosphorylation of MyBPC is associated with decreased myosin interactions, increased ATPase activity and actin interactions promoting cross bridging (Kensler et al., 2011; Toepfer et al., 2019). The loss of MyBPC protein in cardiomyocytes leads to hypercontractility and slows down the relaxation process (Fraysse et al., 2012; Harris et al., 2002; Pohlmann et al., 2007; Toepfer et al., 2019; van Dijk et al., 2018).

Cardiac Troponin I (Tpn I) is involved in the regulation of sarcomere contraction and relaxation. It acts as an inhibitor within the troponin complex and resides on actin filaments to maintain tropomyosin at the actin. This blocks myosin-specific sites on the thin filament and prevents force development (Wijnker et al., 2014). Upon $Ca^{2+}$ binding to troponin C (Tpn C), the complex undergoes a conformational change resulting in Tpn I release from the actin filaments enabling actin-myosin interaction (Lehman & Craig, 2008; Wijnker et al., 2014). Tpn I is phosphorylated by PKA at residues S23/24 and this reduces the sensitivity of myofilaments to $Ca^{2+}$ and increases the speed of relaxation (Takimoto et al., 2004; Wijnker et al., 2014). Dephosphorylation is achieved by protein phosphatases PP1 and PP2A (Deshmukh et al., 2007; Jideama et al., 2006; Wijnker et al., 2011, 2014). Decreased phosphorylation of Tpn I is associated with heart failure, (van der Velden, 2011) and increased myofilament $Ca^{2+}$ sensitivity impairing the relaxation process (Vandervelden et al., 2003; Wijnker et al., 2011). Further, the reduced Tpn I phosphorylation is also detectable in patients with hypertrophic cardiomyopathy (HCM) or in post-mortem hearts with a mild hypertrophic phenotype (Messer et al., 2009; van Dijk et al., 2009, 2012; Wijnker et al., 2014; J. Zhang et al., 2011).

Since none of the ECC proteins was significantly downregulated on the mRNA level in the hiPSC-CMs model, the lower protein expression would be the result of regulatory mechanisms on the protein level such as the ubiquitin-proteasome system. The downregulation of Tpn I phosphorylation could either be associated with decreased PKA catalytic activity, potentially due to low cAMP levels, or increased activity of phosphatases. However, the exact molecular mechanisms for the lower protein expression levels still need to be resolved.

### 5.2.2 *NPPB* and *NPPA* hypertrophy marker genes and their role in cardiac hypertrophy

Sustained increase in the blood pressure resulted in cardiac hypertrophy as the heart adopts to the high pressure (Bernardo et al., 2010; Linzbach, 1976; Modesti et al., 2000; Oldfield et al., 2020; Weeks & McMullen, 2011). Since cardiomyocytes are unable to divide (or only very limited), the increase in the muscle is the result of an increased growth of the individual cardiomyocytes (Bergmann et al., 2009; Oldfield et al., 2020; Steinhauser & Lee, 2011). Physiological hypertrophy defines an adaptation of the heart to growth of the body, increased exercise or pregnancy and is associated with 10-20%

increase in heart weight to body weight ratio (Hill & Olson, 2008; Maillet et al., 2013; Oldfield et al., 2020; Shimizu & Minamino, 2016; Weeks & McMullen, 2011). Pathological hypertrophy is often associated with cardiovascular diseases and results in cardiac dysfunction and heart failure (Oldfield et al., 2020; Shimizu & Minamino, 2016; Tham et al., 2015; Weeks & McMullen, 2011).

The family of natriuretic peptides (NPs) consists of three members, the atrial natriuretic peptide (ANP), brain natriuretic peptide (BNP) and C-type natriuretic peptide (CNP) (Forte et al., 2019; Levin & Samson, 1998). ANP is mainly synthesized in the atria of the heart, whereas BNP is synthesized in the ventricles. Both peptides are secreted in response to stretching of the myocardial walls in pressure overload and regulate the water-salt balance and the volume of the body fluid (Forte et al., 2019; Rubattu et al., 2008, 2019; Volpe et al., 2014). Their secretion is induced by endothelin-1 or β-adrenoceptor activation (Forte et al., 2019; Thibault et al., 1999). Circulating NPs are used as diagnostic and prognostic markers in heart failure, MI or stroke (Daniels, 2010; Paget et al., 2011; Rubattu et al., 2019; Sabatine et al., 2012; Seronde et al., 2013; Volpe et al., 2014).

In this thesis, upon endothelin-1 stimulation the expression of *NPPA* and *NPPB* increased by around 7-fold for the WT and R862C mutant (section 4.4, Figure 17). For the T445N mutant, the fold increase of *NPPB* expression was 13, indicating that the cells respond stronger to the stimulant. The expression of *MYH7* and *ACTC* was not increased upon treatment, indicating that there were no cellular remodeling processes in either WT or mutants. In a rat model with hypertension, the expression of *NPPA* and *NPPB* is positively correlated with ventricular hypertrophy (Cerrudo et al., 2021).

Despite the use of ANP and BNP as diagnostic markers, their overexpression confer a protection from hypertension (Kerkelä et al., 2015; Newton-Cheh et al., 2009). They reduce cardiac pre- and afterload in response to stress and confer anti-inflammatory and anti-fibrotic effects (Cerrudo et al., 2021; Goetze et al., 2020; Nakagawa et al., 2019). This could indicate that the increased *NPPB* expression in the T445N mutant could represent a cardioprotective effect. However, some more replications of the experiment would be needed to confirm the pattern described in this thesis. Since the protective effects are mediated by the secreted peptides, their cellular level would need to be analyzed. Further, the qPCR experiment in this thesis could be complemented with IF staining and analysis of the hiPSC-CM size to draw a conclusion on whether the cells show a hypertrophic phenotype or not.

### 5.2.3 The cardioprotective effect of *PDE3A* mutations could be associated with adaptations of the $Ca^{2+}$ signaling

Adaptations in the $Ca^{2+}$ signaling pathway might be beneficial in an initial phase of the ECC, but chronic changes are often associated with heart failure (Fearnley et al., 2011; Roderick et al., 2007). These

changes could be caused by increased SERCA2 activity, either due to an increased protein expression, decreased PLN expression or elevated PLN phosphorylation (Fearnley et al., 2011). The opposite situation, with decreased SERCA2 activity due to changes in PLN expression or phosphorylation slowing down the relaxation process is also critical (Fearnley et al., 2011; Roderick et al., 2007).

The T445N substitution causes increased PDE3A enzymatic activity and alterations in the PDE3A phosphorylation pattern, which might lead to changes in localization and protein-protein interactions (Ercu et al., 2020; Maass et al., 2015). In the hiPSC-CMs, these effects together with the observed changes in ECC protein expression, would be expected to cause changes in the $Ca^{2+}$ transients.

The experiments in hiPSC-CMs using the $Ca^{2+}$ binding dye Fluo-8 showed that in the basal state the $Ca^{2+}$ transient duration and re-uptake into the SR was longer/slower in the T445N cells (section 4.5, Figure 18). This could be explained by either local hyperactivity of PDE3A or with the reduced phosphorylation of Tpn I and MyBPC3 protein level. Since both proteins are more involved in the contraction mechanism, it would be assumed that there is an effect on the sarcomere shortening hence cardiomyocyte contraction. It would be of interest to follow this up with high resolution immunofluorescence analysis. The R862C mutant only showed a significant difference in the $Ca^{2+}$ accumulation process and the duration of the transient at 90% amplitude. This mutant did not exhibit significant downregulation of MyBPC3 and pTpn I which might explain why the relaxation process is less affected.

Upon treatment with Iso, the differences between WT and the T445N mutant or T445N compared to the R862C mutant were getting more distinct. The T445N mutant had significantly longer $Ca^{2+}$ transient duration and slower re-uptake compared to the WT cells. The R862C mutant behaved more like the WT, being significantly different from the T445N in terms of transient duration and re-uptake. Upon inhibition of PDE3 with the specific inhibitor Cilo, the differences between T445N and WT were getting smaller, indicating that differences in the enzymatic activity might account for the $Ca^{2+}$ transient aberrations. For the R862C mutant, inhibiting PDE3 resulted in a significantly faster $Ca^{2+}$ re-uptake compared to the T445N and WT at 50% amplitude. Given the overall lower protein level compared to the WT, the inhibition had increased relative cAMP to a higher level than the WT. To clarify the molecular mechanisms underlying the $Ca^{2+}$ imaging results, cAMP FRET measurements at subcellular sites would be needed to measure local cAMP levels.

When combining Iso with Cilo, the $Ca^{2+}$ re-uptake and transient duration at 50% amplitude were slower for all three different genotypes. Further, this condition elucidated even more prominent differences between the mutants and WT.

The measurements using the Fura-2 $Ca^{2+}$- binding dye and alternative measurement set-up partially confirmed the results of the initial experiment (section 4.6, Figures 20, 21). Both mutants had a longer

$Ca^{2+}$ transient duration at 50% compared to the WT. For the T445N mutant, the $Ca^{2+}$ amplitude was higher than the one of the R862C and WT in the basal state. However, for the distance of the baseline to maximum amplitude, the mutants were not different from the WT. Only upon Mil stimulation the mutants showed a trend towards lower F0 – Fmax signal, in line with the reduced $Ca^{2+}$ amplitude. PDE3 inhibition would increase cAMP levels, leading to an increase in $Ca^{2+}$ influx from the extracellular space and SR. PDE3A hyperactivity and reduced accessibility to the inhibitor would be an explanation for the reduced $Ca^{2+}$ amplitude compared to the WT. Further, the reduced $\alpha$1c protein level could have led to decreased $Ca^{2+}$ influx which would have also caused lower $Ca^{2+}$ amplitudes. Overall, the results of the experiment with the Fura-2 should be interpreted with caution, since the n-number for the WT and T445N mutant is only two and the inter-batch variability of the hiPSC-CMs can be quite high. However, given that the experiments suggest a clear trend and corroborate previous observation with Fluo-8, a future aim would be to perform additional experiments allowing statistical analysis to be conducted.

### 5.2.4 Reduced interaction of mutant PDE3A with SERCA2 and the potential effect on the $Ca^{2+}$ transients

PDE3A is recruited to a multiprotein complex at the SR upon PKA phosphorylation of S292 and S293 residues (Ahmad et al., 2015; Ercu et al., 2020). Thus, changes in the phosphorylation of these two residues might be associated with increased or reduced interaction with this complex, which would affect local cAMP levels.

In this thesis, PDE3A1 constructs harboring T445N, R862C and $\Delta$3 substitutions/deletions were overexpressed in HEK293 cells together with SERCA2 (section 4.8, Figure 23). The interaction of the different constructs with SERCA2 was analyzed using Co-IP approach. The three different mutations in *PDE3A* reduced the interaction with SERCA2 compared to the WT construct. With less PDE3A being associated with SERCA2, the cAMP level would be high and thus phosphorylated PLN dissociated from the complex. The $Ca^{2+}$ imaging experiments showed a slower $Ca^{2+}$ re-uptake into the SR, pointing towards less phosphorylation of PLN, inhibiting SERCA2. This finding contradicts the reduced interaction of PDE3A mutants with SERCA. A potential explanation would be that mutant PDE3A, which is hyperactive, is less present at the SR but the cAMP is still at a very low level, since the remaining PDE3A proteins have increased cAMP hydrolytic activity.

### 5.2.5 Advantages and disadvantages of the hiPSC-CMs model

IPSC-derived cardiomyocytes are an attractive model to study patient-specific mutations causing certain cardiovascular diseases and for drug screening assays. However, their immature phenotypic and functional status remains a common problem of this cell model. In addition, hiPSC-CMs display a high variability and this is in accordance with the results shown in this thesis (Kane et al., 2015).

HPSCs were first induced from human fibroblasts in 2007 by the group of Shinya Yamanaka, and have the advantages of being derived from humans, easily accessible, and can be maintained in culture for several months (K. Takahashi et al., 2007; Tani & Tohyama, 2022). HiPSC-CMs resemble prenatal cells in terms of structure, expression of genes, energy, the density of ion channels and $Ca^{2+}$ kinetics (Tani & Tohyama, 2022).

In several studies, the $Ca^{2+}$ signaling pathway in hiPSC-CMs was compared to adult cardiomyocytes. The hiPSC-CMs show quantitative differences to the adult cardiomyocytes, which should be considered when interpreting $Ca^{2+}$ data from hiPSC-CMs (X. Zhang & Morad, 2020). Phenotypically, hiPSC-CMs differ from adult cardiomyocytes in terms of their cellular shape, disorganization of z-lines and sarcomeres (Gherghiceanu et al., 2011; Hwang et al., 2015; Rao et al., 2013), lack of t-tubules (S. Li et al., 2013; Lundy et al., 2013; Parikh et al., 2017) and their spontaneous beating behavior in culture (Kane et al., 2015; X. Zhang & Morad, 2020; X.-H. Zhang et al., 2015). Generally, the rise and decay time of $Ca^{2+}$ transients as well as fractional $Ca^{2+}$ is lower in hiPSC-CMs (J. J. Kim et al., 2015; Lee et al., 2011; X.-H. Zhang et al., 2013). The expression of the major $Ca^{2+}$ signaling proteins, including RyR2, SERCA2, PLN, Junctin (Jun) or calsequestrin (CSQ2) is maintained in hiPSC-CMs and this is in line with the results of this thesis (Fong et al., 2016; Germanguz et al., 2011; Hwang et al., 2015; Itzhaki et al., 2011; C. B. Jung et al., 2012; X. Zhang & Morad, 2020).

In response to β-AR agonists, hiPSC-CMs display positive chronotropic and inotropic effects similar to the response seen in adult or neonatal CMs (Germanguz et al., 2011; Ivashchenko et al., 2013; Kane et al., 2015; T. Tanaka et al., 2009; Yokoo et al., 2009; X. Zhang & Morad, 2020; Zwi et al., 2009). The expression of β-AR is maturation-dependent, with $\beta_2$-AR being the predominant isoform in cells younger than 30 days and $\beta_1$-AR being higher expressed in cell cultures aged 30 – 60 days (G. Jung et al., 2016). PKA signaling works more efficiently in older cultures (G. Jung et al., 2016; X. Zhang & Morad, 2020).

Methods to improve the maturity of hiPSC-CMs include prolonged culture time, alteration of cellular energy sources (mainly with the medium), electrical stimulation, peroxisome proliferator-activated receptors (PPARs) and complex cultures such as human engineered heart tissue (EHT) (Chan et al., 2013, p. 20; Feyen et al., 2020; Hu et al., 2018; J. J. Kim et al., 2015; Kroll et al., 2017; Murphy et al.,

2021; Tani & Tohyama, 2022; X. Yang et al., 2019). Feyen *et al*. used a medium containing physiologically relevant levels of glucose and $Ca^{2+}$ supplemented with albumin-bound fatty acids (AlbuMAX), creatine, L-carnitine and taurine which supports fatty acid oxidation (FAO). A 3 – to 5 – weeks administration of this medium improved the maturity of electrophysiological, structural, SR and mechanical properties of the hiPSC-CM suggesting a potential linkage between metabolism and maturation pathways (Feyen et al., 2020).

An alternative method to improve the morphological maturity of hiPSC-CMs is the use of three-dimensional (3D) cardiac models which are generated by a combination of relevant sensors and external mechanical or electrical stimulation (Tani & Tohyama, 2022). Superior to standard 2D cell culture models, the 3D models can be used to study physiological hypertrophy, which is widely prevalent and cause of heart diseases (Tani & Tohyama, 2022). The first 3D cardiac model was developed by Zimmermann *et al*. They generally consist of hydrogels combined with cardiomyocytes cast in a mold with two elastomeric pillars (Tani & Tohyama, 2022; Zimmermann et al., 2002). Nowadays, a variety of 3D cardiac tissue models are available, including scaffold-free microtissues such as cardiac spheroid microtissue (CMT) or spheroids on a micro-needle array and scaffold-based microtissues including EHT, engineered heart muscle (EHM) or cardiac biowire (Arai et al., 2020; Garzoni et al., 2009; Hansen et al., 2010; Tani & Tohyama, 2022; Tiburcy et al., 2017; Zhao et al., 2019).

Despite all the improvements that have been made in the recent years, the issue of immaturity is still not solved. Therefore, hiPSC-CM models should ideally be complemented with animal models or cell lines (Tani & Tohyama, 2022). Although not included as part of this thesis, this was also the case for these hiPSC-CMs harboring the *PDE3A* mutation, which were complemented by rat models that were previously established in the laboratory of Enno Klussmann (Ercu et al., 2020). Both, the T445N and R862C rat models, resemble the human phenotype and, upon catecholamine administration, do not exceed the cardiac hypertrophy level of the WT (Ercu et al., 2020, Ercu et al., 2022, accepted). This points towards a cardioprotective effect of the *PDE3A* mutations also in the rat models. In complementation to this thesis, $Ca^{2+}$ imaging in isolated primary rat cardiomyocytes harboring the HTNB-causing mutations could be done.

# 6 Conclusions and outlook

In this thesis, different biochemical and cell models were used to analyze two of the key proteins in the ECC, the LTCC and PDE3A. The LTCC α1c was shown to interact with PKA-CS and the interaction sites were mapped revealing involvement of the DCRD and PCRD regions of the LTCC. The DCRD and PCRD proteins did not affect the catalytic activity of PKA-CS, implying that this interaction mediates the recruitment of PKA-CS rather than regulating its activity. Rad is a feasible target for PKA-CS at the LTCC. It would be interesting to see if DCRD and PCRD recruit PKA-CS to the LTCC to mediate the Rad phosphorylation and channel activation. For this, local signaling and mechanisms at the LTCC complex need to be studied

However, the experimental approaches, cell models and the time frame of this thesis were not sufficient to resolve the underlying molecular mechanisms of this interaction and to clarify its functionality.

Alternative model systems could involve hiPSC-CMs or animal models with different mutations in the interaction sites. Those models could be used to analyze the interaction with endogenously expressed proteins. To specifically discriminate functions of the transgenic, mutant LTCC from the endogenous WT channel, a dihydropyridine (DHP) – resistant channel could be used (Liu et al., 2020; L. Yang et al., 2013). Using this approach, the functionality of the transgenic channel could be analyzed upon application of a LTCC antagonist, such as nisoldipine. To define if the amino acid substitutions in DCRD or PCRD affect the channel opening, electrophysiological experiments could be conducted. Further, the $Ca^{2+}$ influx through the LTCC could be analyzed with $Ca^{2+}$ binding dyes such as Fura-2. Upon inhibition of ryanodine with a specific antagonist, the amount of $Ca^{2+}$ influx by the LTCC can be measured.

Single-molecule tracking (SMT) techniques would be an elegant tool to study the kinetics of PKA-CS in the cell and identify how and upon which signal PKA-CS is recruited to the LTCC. For a SMT experiment, PKA-CS needs to be fluorescently labelled. Then, the protein is imaged with a high signal – to – noise ratio at an appropriate resolution to measure the kinetics. The different localizations of the protein are combined to model trajectories (Boka et al., 2021). The labeling of PKA-CS could be achieved by either fusing it to a fluorophore or tagging with a peptide which binds small molecule fluorophores (Boka et al., 2021). However, this approach requires sufficient fluorescence intensity, protein expression and specialized microscopy equipment.

PDE3 is the predominant PDE family in human cardiomyocytes and mutations in PDE3A cause HTNB. Surprisingly the associated hypertension does not cause cardiac damage. In the ECC pathway, PDE3A is localized to a complex at the SR and is involved in the relaxation process. HTNB-causing *PDE3A*

mutations cause alterations in the expression of ECC proteins, the $Ca^{2+}$ transient duration and the relaxation process (Figure 25). These alterations might affect the cytosolic $Ca^{2+}$ concentration and contractility of the cells.

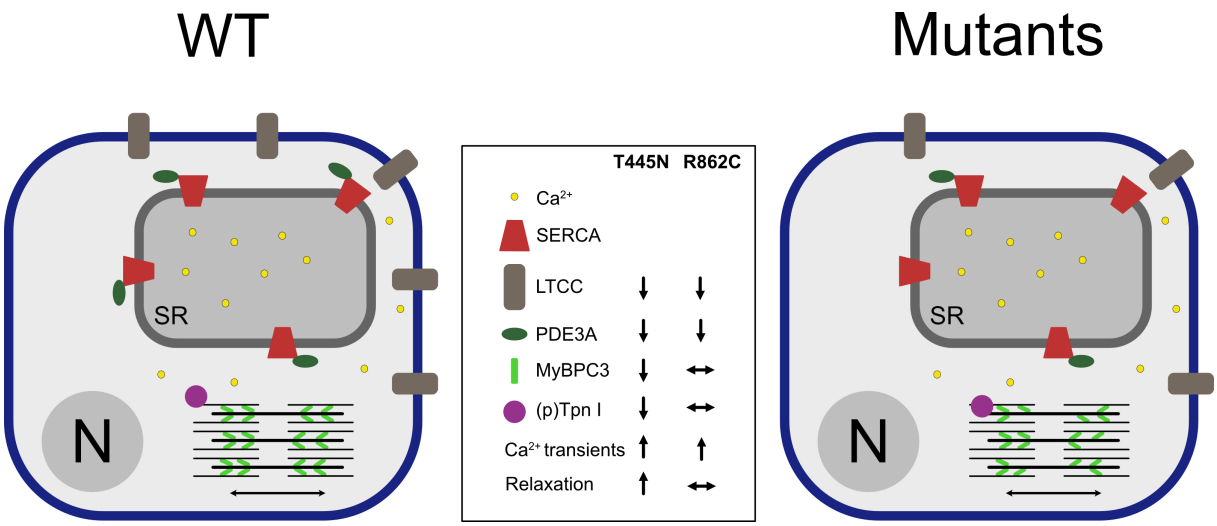


**Figure 25: Alterations in the PDE3A mutant cells in comparison to the WT.** The hiPSC-CMs harboring mutations in *PDE3A* have decreased protein expression of the L-type $Ca^{2+}$channel (LTCC) and phosphodiesterase 3A (PDE3A). The T445N mutant has reduced expression of Myosin binding protein C (MyBPC3) and less phosphorylation of Troponin I (Tpn I). For both mutants the $Ca^{2+}$ transient duration is increased, with the T445N mutant showing slower relaxation. The legend shows the corresponding shapes for each protein. Downward arrow indicates downregulation, upwards shows increased duration and the other arrows indicates that there is no change. N – nucleus, SR – sarcoplasmic reticulum.

The preliminary data shown in this thesis, would need to be complemented with more measurements with the Fura-2 $Ca^{2+}$ dye, ideally combined with a $Ca^{2+}$ standard curve to determine the absolute $Ca^{2+}$ concentration in the cytosol of mutant and WT cells. The concentration could then be analyzed in context of the decreased LTCC α1c protein level and alterations in the $Ca^{2+}$ transient in T445N and R862C. Due to the variable shape and immaturity of the hiPSC-CMs, the change in sarcomere length which correlates with contractility could not be measured with the Ionoptix system. To measure the contractile behavior of the hiPSC-CMs, the cells could be grown as an engineered heart tissue, as described in the previous section, which is arranged between micropillars and a force-sensing probe. In this experimental set-up the force of contraction generated by the tissues is directly correlated to the movement of the micropillars which is sensed by the probe (Dostanic et al., 2020).

The mutant PDE3A protein is hyperactive in *in vitro* enzymatic assays and a HEK293 model (Ercu et al., 2020; Maass et al., 2015), but measurements in a more physiological environment are still missing. Here, a SR-targeted cAMP FRET sensor was used to analyze cAMP levels at this subcellular compartment. Upon treatment with the PDE inhibitor IBMX or AC – activating agent forskolin, the

cAMP level would increase resulting in a change in the FRET signal. In the hiPSC-CM model, the stimulation with IBMX and the combination of Iso + IBMX did not change the FRET signal, implying that either the sensitivity of the cAMP sensor or the change in the local cAMP level was too low to be detected with the microscopy system used. To solve this problem, sensors with a brighter fluorophore pair, such as turquoise and venus might be used or the resolution of the microscopes improved. Further, the cells could be transfected with sensors targeted to other subcellular sites (cytosol, sarcolemma, contractile filaments) and the FRET signal at these compartments upon cAMP elevation studied. This would provide information if either the cAMP change at the SR was indeed too low to be detectable or if the sensor itself was causing the problem.

The initial experiment in HEK293 cells, analyzing the SERCA2 interaction with PDE3A1 should be complemented with endogenous proteins either precipitated from the hiPSC-CMs or isolated rat cardiomyocytes. This would then allow to combine the $Ca^{2+}$ imaging results with the PDE3A1 abundance at the SR and could clarify the molecular mechanisms in a more physiologically relevant environment.

# 7 References

Abrol, N., de Tombe, P. P., & Robia, S. L. (2015). Acute Inotropic and Lusitropic Effects of Cardiomyopathic R9C Mutation of Phospholamban. *Journal of Biological Chemistry*, *290*(11), 7130–7140. https://doi.org/10.1074/jbc.M114.630319

Aggarwal, P., Turner, A., Matter, A., Kattman, S. J., Stoddard, A., Lorier, R., Swanson, B. J., Arnett, D. K., & Broeckel, U. (2014). RNA expression profiling of human iPSC-derived cardiomyocytes in a cardiac hypertrophy model. *PloS One*, *9*(9), e108051. https://doi.org/10.1371/journal.pone.0108051

Ahern, B. M., & Satin, J. (2019). The L-type calcium channel current modulation mechanism: The plot thickens and fogs. *Journal of Clinical Investigation*, *129*(2), 496–498. https://doi.org/10.1172/JCI12595

Ahmad, F., Shen, W., Vandeput, F., Szabo-Fresnais, N., Krall, J., Degerman, E., Goetz, F., Klussmann, E., Movsesian, M., & Manganiello, V. (2015). Regulation of sarcoplasmic reticulum Ca2+ ATPase 2 (SERCA2) activity by phosphodiesterase 3A (PDE3A) in human myocardium: Phosphorylation-dependent interaction of PDE3A1 with SERCA2. *Journal of Biological Chemistry*, *290*(11), 6763–6776. https://doi.org/10.1074/jbc.M115.638585

Amsallem, E., Kasparian, C., Haddour, G., Boissel, J. P., & Nony, P. (2005). Phosphodiesterase III inhibitors for heart failure. *Cochrane Database of Systematic Reviews*, *1*. https://doi.org/10.1002/14651858.CD002230.pub2

Anant, J. S., Ong, O. C., Xie, H. Y., Clarke, S., O'Brien, P. J., & Fung, B. K. (1992). In vivo differential prenylation of retinal cyclic GMP phosphodiesterase catalytic subunits. *Journal of Biological Chemistry*, *267*(2), 687–690. https://doi.org/10.1016/S0021-9258(18)48336-6

Anderson, J. L. (1991). Hemodynamic and clinical benefits with intravenous milrinone in severe chronic heart failure: Results of a multicenter study in the United States. *American Heart Journal*, *121*(6, Part 2), 1956–1964. https://doi.org/10.1016/0002-8703(91)90832-3

Arai, K., Murata, D., Takao, S., Nakamura, A., Itoh, M., Kitsuka, T., & Nakayama, K. (2020). Drug response analysis for scaffold-free cardiac constructs fabricated using bio-3D printer. *Scientific Reports*, *10*(1), 8972. https://doi.org/10.1038/s41598-020-65681-y

Arikkath, J., & Campbell, K. P. (2003). Auxiliary subunits: Essential components of the voltage-gated calcium channel complex. *Current Opinion in Neurobiology*, *13*(3), 298–307. https://doi.org/10.1016/S0959-4388(03)00066-7

Atienza, J. M., Susanto, D., Huang, C., McCarty, A. S., & Colicelli, J. (1999). Identification of Inhibitor Specificity Determinants in a Mammalian Phosphodiesterase. *Journal of Biological Chemistry*, *274*(8), 4839–4847. https://doi.org/10.1074/jbc.274.8.4839

Azevedo, M. F., Faucz, F. R., Bimpaki, E., Horvath, A., Levy, I., de Alexandre, R. B., Ahmad, F., Manganiello, V., & Stratakis, C. A. (2014). Clinical and Molecular Genetics of the Phosphodiesterases (PDEs). *Endocrine Reviews*, *35*(2), 195–233. https://doi.org/10.1210/er.2013-1053

Bähring, S., Kann, M., Neuenfeld, Y., Gong, M., Chitayat, D., Toka, H. R., Toka, O., Plessis, G., Maass, P., Rauch, A., Aydin, A., & Luft, F. C. (2008). Inversion Region for Hypertension and Brachydactyly on Chromosome 12p Features Multiple Splicing and Noncoding RNA. *Hypertension*, *51*(2), 426–431. https://doi.org/10.1161/HYPERTENSIONAHA.107.101774

Baillie, G. S., MacKenzie, S. J., McPhee, I., & Houslay, M. D. (2000). *Sub-family selective actions in the ability of Erk2 MAP kinase to phosphorylate and regulate the activity of PDE4 cyclic AMP-speci®c phosphodiesterases*. *131*, 9.

Baim, D. S., McDowell, A. V, Cherniles, J., Monrad, E. S., Parker, J. A., Edelson, J., Braunwald, E., & Grossman, W. (1983). Evaluation of a new bipyridine inotropic agent—Milrinone—In patients with severe congestive heart failure. *The New England Journal of Medicine*, *309*(13), 748–756. https://doi.org/10.1056/NEJM198309293091302

Baumann, L., Gerstner, A., Zong, X., Biel, M., & Wahl-Schott, C. (2004). Functional Characterization of the L-type $Ca^{2+}$ Channel $Ca_v$ 1.4α1 from Mouse Retina. *Investigative Opthalmology & Visual Science*, *45*(2), 708. https://doi.org/10.1167/iovs.03-0937

Bazmi, M., & Escobar, A. L. (2018). How Ca2+ influx is attenuated in the heart during a “fight or flight” response. *Journal of General Physiology*, *151*(6), 722–726. https://doi.org/10.1085/JGP.201912338

Beca, S., Ahmad, F., Shen, W., Liu, J., Makary, S., Polidovitch, N., Sun, J., Hockman, S., Chung, Y. W., Movsesian, M., Murphy, E., Manganiello, V., & Backx, P. H. (2013). Phosphodiesterase type 3A regulates basal myocardial contractility through interacting with sarcoplasmic reticulum calcium ATPase type 2a signaling complexes in mouse heart. *Circulation Research*, *112*(2), 289–297. https://doi.org/10.1161/CIRCRESAHA.111.300003

Bender, A. T., & Beavo, J. A. (2006). Cyclic Nucleotide Phosphodiesterases: Molecular Regulation to Clinical Use. *Pharmacological Reviews*, *58*(3), 488–520. https://doi.org/10.1124/pr.58.3.5

Benotti, J. R., Grossman, W., Braunwald, E., Davolos, D. D., & Alousi, A. A. (1978). Hemodynamic assessment of amrinone. A new inotropic agent. *The New England Journal of Medicine*, *299*(25), 1373–1377. https://doi.org/10.1056/NEJM197812212992501

Bergmann, O., Bhardwaj, R. D., Bernard, S., Zdunek, S., Barnabé-Heider, F., Walsh, S., Zupicich, J., Alkass, K., Buchholz, B. A., Druid, H., Jovinge, S., & Frisén, J. (2009). Evidence for Cardiomyocyte Renewal in Humans. *Science*, *324*(5923), 98–102. https://doi.org/10.1126/science.1164680

Bernardo, B. C., Weeks, K. L., Pretorius, L., & McMullen, J. R. (2010). Molecular distinction between physiological and pathological cardiac hypertrophy: Experimental findings and therapeutic strategies. *Pharmacology & Therapeutics*, *128*(1), 191–227. https://doi.org/10.1016/j.pharmthera.2010.04.005

Bhargava, A., Lin, X., Novak, P., Mehta, K., Korchev, Y., Delmar, M., & Gorelik, J. (2013). Super-resolution Scanning Patch Clamp Reveals Clustering of Functional Ion Channels in Adult Ventricular Myocyte. *Circulation Research*, *112*(8), 1112–1120. https://doi.org/10.1161/CIRCRESAHA.111.300445

Bhogal, N. K., Hasan, A., & Gorelik, J. (2018a). The development of compartmentation of cAMP signaling in cardiomyocytes: The role of T-tubules and caveolae microdomains. *Journal of Cardiovascular Development and Disease*, *5*(2). https://doi.org/10.3390/jcdd5020025

Bhogal, N. K., Hasan, A., & Gorelik, J. (2018b). The development of compartmentation of cAMP signaling in cardiomyocytes: The role of T-tubules and caveolae microdomains. *Journal of Cardiovascular Development and Disease*, *5*(2). https://doi.org/10.3390/jcdd5020025

Bichet, D., Cornet, V., Geib, S., Carlier, E., Volsen, S., Hoshi, T., Mori, Y., & De Waard, M. (2000). The I-II Loop of the Ca2+ Channel α1 Subunit Contains an Endoplasmic Reticulum Retention Signal Antagonized by the β Subunit. *Neuron*, *25*(1), 177–190. https://doi.org/10.1016/S0896-6273(00)80881-8

Bilginturan, N., Zileli, S., Karacadag, S., & Pirnar, T. (1973). Hereditary brachydactyly associated with hypertension. *Journal of Medical Genetics*, *10*(3), 253–259. https://doi.org/10.1136/jmg.10.3.253

Blair, C. M., & Baillie, G. S. (2019). Reshaping cAMP nanodomains through targeted disruption of compartmentalised phosphodiesterase signalosomes. *Biochemical Society Transactions*, *47*(5), 1405–1414. https://doi.org/10.1042/BST20190252

Boda, H., Uchida, H., Takaiso, N., Ouchi, Y., Fujita, N., Kuno, A., Hata, T., Nagatani, A., Funamoto, Y., Miyata, M., Yoshikawa, T., Kurahashi, H., & Inagaki, H. (2016). A PDE3A mutation in familial hypertension and brachydactyly syndrome. *Journal of Human Genetics*, *61*(8), 701–703. https://doi.org/10.1038/jhg.2016.32

Boka, A. P., Mukherjee, A., & Mir, M. (2021). Single-molecule tracking technologies for quantifying the dynamics of gene regulation in cells, tissue and embryos. *Development*, *148*(18), dev199744. https://doi.org/10.1242/dev.199744

Bork, N. I., Kuret, A., Cruz Santos, M., Molina, C. E., Reiter, B., Reichenspurner, H., Friebe, A., Skryabin, B. V., Rozhdestvensky, T. S., Kuhn, M., Lukowski, R., & Nikolaev, V. O. (2021). Rise of cGMP by partial phosphodiesterase-3A degradation enhances cardioprotection during hypoxia. *Redox Biology*, *48*, 102179. https://doi.org/10.1016/j.redox.2021.102179

Bourinet, E., Mangoni, M. E., & Nargeot, J. (2004). Dissecting the functional role of different isoforms of the L-type Ca2+ channel. *The Journal of Clinical Investigation*, *113*(10), 1382–1384. https://doi.org/10.1172/JCI21815

Boyes, S., & Loten, E. G. (1988). Purification of an insulin-sensitive cyclic AMP phosphodiesterase from rat liver. *European Journal of Biochemistry*, *174*(2), 303–309. https://doi.org/10.1111/j.1432-1033.1988.tb14098.x

Brandmayr, J., Poomvanicha, M., Domes, K., Ding, J., Blaich, A., Wegener, J. W., Moosmang, S., & Hofmann, F. (2012). Deletion of the C-terminal Phosphorylation Sites in the Cardiac β-Subunit Does Not Affect the Basic β-Adrenergic Response of the Heart and the Cav1.2 Channel*. *Journal of Biological Chemistry*, *287*(27), 22584–22592. https://doi.org/10.1074/jbc.M112.366484

Buraei, Z., & Yang, J. (2010). The β Subunit of Voltage-Gated Ca2+ Channels. *Physiological Reviews*, *90*(4), 1461–1506. https://doi.org/10.1152/physrev.00057.2009

Calejo, A. I., & Taskén, K. (2015). Targeting protein–protein interactions in complexes organized by A kinase anchoring proteins. *Frontiers in Pharmacology*, *6*. https://doi.org/10.3389/fphar.2015.00192

Carlson, C., Koonce, C., Aoyama, N., Einhorn, S., Fiene, S., Thompson, A., Swanson, B., Anson, B., & Kattman, S. (2013). Phenotypic screening with human iPS cell-derived cardiomyocytes: HTS-compatible assays for interrogating cardiac hypertrophy. *Journal of Biomolecular Screening*, *18*(10), 1203–1211. https://doi.org/10.1177/1087057113500812

Carlson, C. R., Aronsen, J. M., Bergan-Dahl, A., Moutty, M. C., Lunde, M., Lunde, P. K., Jarstadmarken, H., Wanichawan, P., Pereira, L., Kolstad, T. R. S., Dalhus, B., Subramanian, H., Hille, S., Christensen, G., Müller, O. J., Nikolaev, V., Bers, D. M., Sjaastad, I., Shen, X., … Sejersted, O. M. (2022). AKAP18δ Anchors and Regulates CaMKII Activity at Phospholamban-SERCA2 and RYR. *Circulation Research*, *130*(1), 27–44. https://doi.org/10.1161/CIRCRESAHA.120.317976

Catterall, W. (2015). Regulation of Cardiac Calcium Channels in the Fight-or-Flight Response. *Current Molecular Pharmacology*, *8*(1), 12–21. https://doi.org/10.2174/1874467208666150507103417

Catterall, W. a. (2000). S Tructure and R Egulation of. *Annual Reviews of Cell and Developmental Biology*, *16*(521), 555.

Catterall, W. A. (2011). Voltage-gated calcium channels. *Cold Spring Harbor Perspectives in Biology*, *3*(8), a003947. https://doi.org/10.1101/cshperspect.a003947

Cerrudo, C. S., Cavallero, S., Rodríguez Fermepín, M., González, G. E., Donato, M., Kouyoumdzian, N. M., Gelpi, R. J., Hertig, C. M., Choi, M. R., & Fernández, B. E. (2021). Cardiac Natriuretic Peptide Profiles in Chronic Hypertension by Single or Sequentially Combined Renovascular and DOCA-Salt Treatments. *Frontiers in Physiology*, *12*, 651246. https://doi.org/10.3389/fphys.2021.651246

Chan, Y.-C., Ting, S., Lee, Y.-K., Ng, K.-M., Zhang, J., Chen, Z., Siu, C.-W., Oh, S. K. W., & Tse, H.-F. (2013). Electrical Stimulation Promotes Maturation of Cardiomyocytes Derived from Human Embryonic Stem Cells. *Journal of Cardiovascular Translational Research*, *6*(6), 989–999. https://doi.org/10.1007/s12265-013-9510-z

Chao, Y.-C., Surdo, N. C., Pantano, S., & Zaccolo, M. (2019). Imaging cAMP nanodomains in the heart. *Biochemical Society Transactions*, *47*(5), 1383–1392. https://doi.org/10.1042/BST20190245

Chien, A. J., Zhao, X., Shirokov, R. E., Puri, T. S., Chang, C. F., Sun, D., Rios, E., & Hosey, M. M. (1995). Roles of a Membrane-localized βSubunit in the Formation and Targeting of Functional L-type Ca2+ Channels(∗). *Journal of Biological Chemistry*, *270*(50), 30036–30044. https://doi.org/10.1074/jbc.270.50.30036

Christian, F., Szaszák, M., Friedl, S., Drewianka, S., Lorenz, D., Goncalves, A., Furkert, J., Vargas, C., Schmieder, P., Götz, F., Zühlke, K., Moutty, M., Göttert, H., Joshi, M., Reif, B., Haase, H., Morano, I., Grossmann, S., Klukovits, A., … Klussmann, E. (2011). Small Molecule AKAP-Protein Kinase A (PKA) Interaction Disruptors That Activate PKA Interfere with Compartmentalized cAMP Signaling in Cardiac Myocytes*. *Journal of Biological Chemistry*, *286*(11), 9079–9096. https://doi.org/10.1074/jbc.M110.160614

Chung, Y. W., Lagranha, C., Chen, Y., Sun, J., Tong, G., Hockman, S. C., Ahmad, F., Esfahani, S. G., Bae, D. H., Polidovitch, N., Wu, J., Rhee, D. K., Lee, B. S., Gucek, M., Daniels, M. P., Brantner, C. A., Backx, P. H., Murphy, E., & Manganiello, V. C. (2015). Targeted disruption of PDE3B, but not PDE3A, protects murine heart from ischemia/reperfusion injury. *Proceedings of the National Academy of Sciences of the United States of America*, *112*(17), E2253-62. https://doi.org/10.1073/pnas.1416230112

Cingolani, E., Ramirez Correa, G. A., Kizana, E., Murata, M., Cho, H. C., & Marbán, E. (2007). Gene Therapy to Inhibit the Calcium Channel β Subunit. *Circulation Research*, *101*(2), 166–175. https://doi.org/10.1161/CIRCRESAHA.107.155721

Cohen, A. W., Razani, B., Schubert, W., Williams, T. M., Wang, X. B., Iyengar, P., Brasaemle, D. L., Scherer, P. E., & Lisanti, M. P. (2004). Role of Caveolin-1 in the Modulation of Lipolysis and Lipid Droplet Formation. *Diabetes*, *53*(5), 1261–1270. https://doi.org/10.2337/diabetes.53.5.1261

Cohn, J. N., Goldstein, S. O., Greenberg, B. H., Lorell, B. H., Bourge, R. C., Jaski, B. E., Gottlieb, S. O., McGrew, F. 3rd, DeMets, D. L., & White, B. G. (1998). A dose-dependent increase in mortality with vesnarinone among patients with severe heart failure. Vesnarinone Trial Investigators. *The New England Journal of Medicine*, *339*(25), 1810–1816. https://doi.org/10.1056/NEJM199812173392503

Colledge, M., & Scott, J. D. (1999). AKAPs: From structure to function. *Trends in Cell Biology*, *9*(6), 216–221. https://doi.org/10.1016/S0962-8924(99)01558-5

Colombe, A.-S., & Pidoux, G. (2021). Cardiac cAMP-PKA Signaling Compartmentalization in Myocardial Infarction. *Cells*, *10*(4), 922. https://doi.org/10.3390/cells10040922

Conti, M., & Beavo, J. (2007). Biochemistry and Physiology of Cyclic Nucleotide Phosphodiesterases: Essential Components in Cyclic Nucleotide Signaling. *Annual Review of Biochemistry*, *76*(1), 481–511. https://doi.org/10.1146/annurev.biochem.76.060305.150444

Cook, P. F., Neville, M. E. J., Vrana, K. E., Hartl, F. T., & Roskoski, R. J. (1982). Adenosine cyclic 3',5'-monophosphate dependent protein kinase: Kinetic mechanism for the bovine skeletal muscle catalytic subunit. *Biochemistry*, *21*(23), 5794–5799. https://doi.org/10.1021/bi00266a011

Corradini, E., Klaasse, G., Leurs, U., Heck, A. J. R., Martin, N. I., & Scholten, A. (2015). Charting the interactome of PDE3A in human cells using an IBMX based chemical proteomics approach. *Molecular BioSystems*, *11*(10), 2786–2797. https://doi.org/10.1039/C5MB00142K

Cruz-Garcia, Y., Barkovits, K., Kohlhaas, M., Pickel, S., Gulentz, M., Heindl, C., Pfeiffer, K., Eder-Negrin, P., Maack, C., Marcus, K., Kuhn, M., & Miranda-Laferte, E. (2021). Nanoenviroments of the β-Subunit of L-Type Voltage-Gated Calcium Channels in Adult Cardiomyocytes. *Frontiers in Cell and Developmental Biology*, *9*, 724778. https://doi.org/10.3389/fcell.2021.724778

Cserne Szappanos, H., Muralidharan, P., Ingley, E., Petereit, J., Millar, H. A., & Hool, L. C. (2017). Identification of a novel cAMP dependent protein kinase A phosphorylation site on the human cardiac calcium channel. *Scientific Reports*, *7*(1), 1–16. https://doi.org/10.1038/s41598-017-15087-0

Daniels, L. B. (2010). Natriuretic Peptides and Assessment of Cardiovascular Disease Risk in Asymptomatic Persons. *Current Cardiovascular Risk Reports*, *4*(2), 120–127. https://doi.org/10.1007/s12170-010-0078-8

Deák, A. V., & Klussmann, E. (2016). Pharmacological Interference With Protein-protein Interactions of Akinase Anchoring Proteins as a Strategy for the Treatment of Disease. In *Current Drug Targets* (Vol. 17, Issue 10, pp. 1147–1171). http://dx.doi.org/10.2174/1389450116666150416114247

Degerman, E., Belfrage, P., & Manganiello, V. C. (1997). Structure, localization, and regulation of cGMP-inhibited phosphodiesterase (PDE3). *The Journal of Biological Chemistry*, *272*(11), 6823–6826. https://doi.org/10.1074/jbc.272.11.6823

Deisl, C., Fine, M., Moe, O. W., & Hilgemann, D. W. (2019). Hypertrophy of human embryonic stem cell-derived cardiomyocytes supported by positive feedback between Ca(2+) and diacylglycerol signals. *Pflugers Archiv : European Journal of Physiology*, *471*(8), 1143–1157. https://doi.org/10.1007/s00424-019-02293-0

Dema, A., Perets, E., Schulz, M. S., Deák, V. A., & Klussmann, E. (2015). Pharmacological targeting of AKAP-directed compartmentalized cAMP signalling. *Cellular Signalling*, *27*(12), 2474–2487. https://doi.org/10.1016/j.cellsig.2015.09.008

Deshmukh, P. A., Blunt, B. C., & Hofmann, P. A. (2007). Acute modulation of PP2a and troponin I phosphorylation in ventricular myocytes: Studies with a novel PP2a peptide inhibitor. *American Journal of Physiology-Heart and Circulatory Physiology*, *292*(2), H792–H799. https://doi.org/10.1152/ajpheart.00225.2006

Dibb, K. M., Louch, W. E., & Trafford, A. W. (2021). Cardiac Transverse Tubules in Physiology and Heart Failure. *Annual Review of Physiology*. https://doi.org/10.1146/annurev-physiol-061121-040148

DiBianco, R., Shabetai, R., Kostuk, W., Moran, J., Schlant, R. C., & Wright, R. (1989). A comparison of

oral milrinone, digoxin, and their combination in the treatment of patients with chronic heart failure. *The New England Journal of Medicine*, *320*(11), 677–683. https://doi.org/10.1056/NEJM198903163201101

Dick, I. E., Tadross, M. R., Liang, H., Tay, L. H., Yang, W., & Yue, D. T. (2008). A modular switch for spatial Ca2+ selectivity in the calmodulin regulation of CaV channels. *Nature*, *451*(7180), 830–834. https://doi.org/10.1038/nature06529

Ding, B., Abe, J., Wei, H., Huang, Q., Walsh, R. A., Molina, C. A., Zhao, A., Sadoshima, J., Blaxall, B. C., Berk, B. C., & Yan, C. (2005). Functional Role of Phosphodiesterase 3 in Cardiomyocyte Apoptosis: Implication in Heart Failure. *Circulation*, *111*(19), 2469–2476. https://doi.org/10.1161/01.CIR.0000165128.39715.87

Ding, B., Abe, J., Wei, H., Xu, H., Che, W., Aizawa, T., Liu, W., Molina, C. A., Sadoshima, J., Blaxall, B. C., Berk, B. C., & Yan, C. (2005). A positive feedback loop of phosphodiesterase 3 (PDE3) and inducible cAMP early repressor (ICER) leads to cardiomyocyte apoptosis. *Proceedings of the National Academy of Sciences*, *102*(41), 14771–14776. https://doi.org/10.1073/pnas.0506489102

DiPilato, L. M., Cheng, X., & Zhang, J. (2004). Fluorescent indicators of cAMP and Epac activation reveal differential dynamics of cAMP signaling within discrete subcellular compartments. *Proceedings of the National Academy of Sciences*, *101*(47), 16513–16518. https://doi.org/10.1073/pnas.0405973101

Dixon, R. E., Moreno, C. M., Yuan, C., Opitz-Araya, X., Binder, M. D., Navedo, M. F., & Santana, L. F. (2015). Graded Ca\textsuperscript{2+}/calmodulin-dependent coupling of voltage-gated Ca\textsubscript{V}1.2 channels. *ELife*, *4*, e05608. https://doi.org/10.7554/eLife.05608

Dolphin, A. C. (2003). β Subunits of Voltage-Gated Calcium Channels. *Journal of Bioenergetics and Biomembranes*, *35*(6), 599–620. https://doi.org/10.1023/B:JOBB.0000008026.37790.5a

Dolphin, A. C. (2018). Voltage-gated calcium channels: Their discovery, function and importance as drug targets. *Brain and Neuroscience Advances*, *2*, 239821281879480. https://doi.org/10.1177/2398212818794805

Dostanic, M., Windt, L. M., Stein, J. M., van Meer, B. J., Bellin, M., Orlova, V., Mastrangeli, M., Mummery, C. L., & Sarro, P. M. (2020). A Miniaturized EHT Platform for Accurate Measurements of Tissue Contractile Properties. *Journal of Microelectromechanical Systems*, *29*(5), 881–887. https://doi.org/10.1109/JMEMS.2020.3011196

Edwards, H. V., Cameron, R. T., & Baillie, G. S. (2011). The emerging role of HSP20 as a multifunctional protective agent. *Cellular Signalling*, *23*(9), 1447–1454. https://doi.org/10.1016/j.cellsig.2011.05.009

Edwards, H. V., Scott, J. D., & Baillie, G. S. (2012). The A-kinase-anchoring protein AKAP-Lbc facilitates cardioprotective PKA phosphorylation of Hsp20 on Ser16. *Biochemical Journal*, *446*(3), 437–443. https://doi.org/10.1042/BJ20120570

Eisner, D. A., Caldwell, J. L., Kistamás, K., & Trafford, A. W. (2017). Calcium and Excitation-Contraction Coupling in the Heart. *Circulation Research*, *121*(2), 181–195. https://doi.org/10.1161/CIRCRESAHA.117.310230

Ercu, M., & Klussmann, E. (2018). Roles of A-Kinase Anchoring Proteins and Phosphodiesterases in the Cardiovascular System. *Journal of Cardiovascular Development and Disease*, *5*(1), 14. https://doi.org/10.3390/jcdd5010014

Ercu, M., Markó, L., Schächterle, C., Tsvetkov, D., Cui, Y., Maghsodi, S., Bartolomaeus, T. U. P., Maass,

P. G., Zühlke, K., Gregersen, N., Hübner, N., Hodge, R., Mühl, A., Pohl, B., Illas, R. M., Geelhaar, A., Walter, S., Napieczynska, H., Schelenz, S., … Klussmann, E. (2020). Phosphodiesterase 3A and Arterial Hypertension. *Circulation*, *142*(2), 133–149. https://doi.org/10.1161/CIRCULATIONAHA.119.043061

Faber, G. M., Silva, J., Livshitz, L., & Rudy, Y. (2007). Kinetic properties of the cardiac L-type Ca2+ channel and its role in myocyte electrophysiology: A theoretical investigation. *Biophysical Journal*, *92*(5), 1522–1543. https://doi.org/10.1529/biophysj.106.088807

Fang, K., & Colecraft, H. M. (2011). Mechanism of auxiliary β-subunit-mediated membrane targeting of L-type (CaV1.2) channels. *Journal of Physiology*, *589*(18), 4437–4455. https://doi.org/10.1113/jphysiol.2011.214247

Fearnley, C. J., Roderick, H. L., & Bootman, M. D. (2011). Calcium Signaling in Cardiac Myocytes. *Cold Spring Harbor Perspectives in Biology*, *3*(11), a004242–a004242. https://doi.org/10.1101/cshperspect.a004242

Feng, T., Kalyaanamoorthy, S., & Barakat, K. (2018). *L-Type Calcium Channels: Structure and Functions*. https://doi.org/10.5772/intechopen.77305

Feyen, D. A. M., McKeithan, W. L., Bruyneel, A. A. N., Spiering, S., Hörmann, L., Ulmer, B., Zhang, H., Briganti, F., Schweizer, M., Hegyi, B., Liao, Z., Pölönen, R.-P., Ginsburg, K. S., Lam, C. K., Serrano, R., Wahlquist, C., Kreymerman, A., Vu, M., Amatya, P. L., … Mercola, M. (2020). Metabolic Maturation Media Improve Physiological Function of Human iPSC-Derived Cardiomyocytes. *Cell Reports*, *32*(3), 107925. https://doi.org/10.1016/j.celrep.2020.107925

Fischmeister, R., Castro, L. R. V., Abi-Gerges, A., Rochais, F., Jurevičius, J., Leroy, J., & Vandecasteele, G. (2006). Compartmentation of Cyclic Nucleotide Signaling in the Heart: The Role of Cyclic Nucleotide Phosphodiesterases. *Circulation Research*, *99*(8), 816–828. https://doi.org/10.1161/01.RES.0000246118.98832.04

Fischmeister, R., & Hartzell, H. C. (1987). Cyclic guanosine 3',5'-monophosphate regulates the calcium current in single cells from frog ventricle. *The Journal of Physiology*, *387*(1), 453–472. https://doi.org/10.1113/jphysiol.1987.sp016584

Foell, J. D., Balijepalli, R. C., Delisle, B. P., Yunker, A. M. R., Robia, S. L., Walker, J. W., McEnery, M. W., January, C. T., & Kamp, T. J. (2004). Molecular heterogeneity of calcium channel β-subunits in canine and human heart: Evidence for differential subcellular localization. *Physiological Genomics*, *17*(2), 183–200. https://doi.org/10.1152/physiolgenomics.00207.2003

Földes, G., Mioulane, M., Wright, J. S., Liu, A. Q., Novak, P., Merkely, B., Gorelik, J., Schneider, M. D., Ali, N. N., & Harding, S. E. (2011). Modulation of human embryonic stem cell-derived cardiomyocyte growth: A testbed for studying human cardiac hypertrophy? *Journal of Molecular and Cellular Cardiology*, *50*(2), 367–376. https://doi.org/10.1016/j.yjmcc.2010.10.029

Fong, A. H., Romero-López, M., Heylman, C. M., Keating, M., Tran, D., Sobrino, A., Tran, A. Q., Pham, H. H., Fimbres, C., Gershon, P. D., Botvinick, E. L., George, S. C., & Hughes, C. C. W. (2016). Three-Dimensional Adult Cardiac Extracellular Matrix Promotes Maturation of Human Induced Pluripotent Stem Cell-Derived Cardiomyocytes. *Tissue Engineering Part A*, *22*(15–16), 1016–1025. https://doi.org/10.1089/ten.tea.2016.0027

Forte, Madonna, Schiavon, Valenti, Versaci, Zoccai, Frati, & Sciarretta. (2019). Cardiovascular Pleiotropic Effects of Natriuretic Peptides. *International Journal of Molecular Sciences*, *20*(16), 3874. https://doi.org/10.3390/ijms20163874

Francis, S. H., Blount, M. A., & Corbin, J. D. (2011). Mammalian Cyclic Nucleotide Phosphodiesterases: Molecular Mechanisms and Physiological Functions. *Physiological Reviews*, *91*(2), 651–690. https://doi.org/10.1152/physrev.00030.2010

Frankenreiter, S., Bednarczyk, P., Kniess, A., Bork, N. I., Straubinger, J., Koprowski, P., Wrzosek, A., Mohr, E., Logan, A., Murphy, M. P., Gawaz, M., Krieg, T., Szewczyk, A., Nikolaev, V. O., Ruth, P., & Lukowski, R. (2017). CGMP-Elevating Compounds and Ischemic Conditioning Provide Cardioprotection Against Ischemia and Reperfusion Injury via Cardiomyocyte-Specific BK Channels. *Circulation*, *136*(24), 2337–2355. https://doi.org/10.1161/CIRCULATIONAHA.117.028723

Frankenreiter, S., Groneberg, D., Kuret, A., Krieg, T., Ruth, P., Friebe, A., & Lukowski, R. (2018). Cardioprotection by ischemic postconditioning and cyclic guanosine monophosphate-elevating agents involves cardiomyocyte nitric oxide-sensitive guanylyl cyclase. *Cardiovascular Research*, *114*(6), 822–829. https://doi.org/10.1093/cvr/cvy039

Fraysse, B., Weinberger, F., Bardswell, S. C., Cuello, F., Vignier, N., Geertz, B., Starbatty, J., Krämer, E., Coirault, C., Eschenhagen, T., Kentish, J. C., Avkiran, M., & Carrier, L. (2012). Increased myofilament Ca2+ sensitivity and diastolic dysfunction as early consequences of Mybpc3 mutation in heterozygous knock-in mice. *Journal of Molecular and Cellular Cardiology*, *52*(6), 1299–1307. https://doi.org/10.1016/j.yjmcc.2012.03.009

Fu, Y., Westenbroek, R. E., Scheuer, T., & Catterall, W. A. (2013). Phosphorylation sites required for regulation of cardiac calcium channels in the fight-or-flight response. *Proceedings of the National Academy of Sciences*, *110*(48), 19621–19626. https://doi.org/10.1073/pnas.1319421110

Fu, Y., Westenbroek, R. E., Scheuer, T., & Catterall, W. A. (2014). Basal and β-adrenergic regulation of the cardiac calcium channel CaV1.2 requires phosphorylation of serine 1700. *Proceedings of the National Academy of Sciences*, *111*(46), 16598–16603. https://doi.org/10.1073/pnas.1419129111

Fu, Y., Westenbroek, R. E., Yu, F. H., Clark, J. P., Marshall, M. R., Scheuer, T., & Catterall, W. A. (2011). Deletion of the Distal C Terminus of CaV1.2 Channels Leads to Loss of β-Adrenergic Regulation and Heart Failure in Vivo*. *Journal of Biological Chemistry*, *286*(14), 12617–12626. https://doi.org/10.1074/jbc.M110.175307

Fuller, M. D., Emrick, M. A., Sadilek, M., Scheuer, T., & Catterall, W. A. (2010). Molecular Mechanism of Calcium Channel Regulation in the Fight-or-Flight Response. *Science Signaling*, *3*(141), ra70–ra70. https://doi.org/10.1126/scisignal.2001152

Ganesan, A. N., Maack, C., Johns, D. C., Sidor, A., & O'Rourke, B. (2006). \&\#x3b2;-Adrenergic Stimulation of L-type $Ca^{2+}$ Channels in Cardiac Myocytes Requires the Distal Carboxyl Terminus of \&\#x3b1;$_{1C}$ but Not Serine 1928. *Circulation Research*, *98*(2), e11–e18. https://doi.org/10.1161/01.RES.0000202692.23001.e2

Garzoni, L. R., Rossi, M. I. D., de Barros, A. P. D. N., Guarani, V., Keramidas, M., Balottin, L. B. L., Adesse, D., Takiya, C. M., Manso, P. P., Otazú, I. B., Meirelles, M. de N., & Borojevic, R. (2009). Dissecting coronary angiogenesis: 3D co-culture of cardiomyocytes with endothelial or mesenchymal cells. *Experimental Cell Research*, *315*(19), 3406–3418. https://doi.org/10.1016/j.yexcr.2009.09.016

Germanguz, I., Sedan, O., Zeevi-Levin, N., Shtrichman, R., Barak, E., Ziskind, A., Eliyahu, S., Meiry, G., Amit, M., Itskovitz-Eldor, J., & Binah, O. (2011). Molecular characterization and functional properties of cardiomyocytes derived from human inducible pluripotent stem cells. *Journal of Cellular and Molecular Medicine*, *15*(1), 38–51. https://doi.org/10.1111/j.1582-4934.2009.00996.x

Gherghiceanu, M., Barad, L., Novak, A., Reiter, I., Itskovitz-Eldor, J., Binah, O., & Popescu, L. M. (2011). Cardiomyocytes derived from human embryonic and induced pluripotent stem cells: Comparative ultrastructure. *Journal of Cellular and Molecular Medicine*, *15*(11), 13.

Ghigo, A., Perino, A., Mehel, H., Zahradníková, A. J., Morello, F., Leroy, J., Nikolaev, V. O., Damilano, F., Cimino, J., De Luca, E., Richter, W., Westenbroek, R., Catterall, W. A., Zhang, J., Yan, C., Conti, M., Gomez, A. M., Vandecasteele, G., Hirsch, E., & Fischmeister, R. (2012). Phosphoinositide 3-kinase γ protects against catecholamine-induced ventricular arrhythmia through protein kinase A-mediated regulation of distinct phosphodiesterases. *Circulation*, *126*(17), 2073–2083. https://doi.org/10.1161/CIRCULATIONAHA.112.114074

Ghofrani, H.-A., D'Armini, A. M., Grimminger, F., Hoeper, M. M., Jansa, P., Kim, N. H., Mayer, E., Simonneau, G., Wilkins, M. R., Fritsch, A., Neuser, D., Weimann, G., & Wang, C. (2013). Riociguat for the treatment of chronic thromboembolic pulmonary hypertension. *The New England Journal of Medicine*, *369*(4), 319–329. https://doi.org/10.1056/NEJMoa1209657

Goetze, J. P., Bruneau, B. G., Ramos, H. R., Ogawa, T., de Bold, M. K., & de Bold, A. J. (2020). Cardiac natriuretic peptides. *Nature Reviews Cardiology*, *17*(11), 698–717. https://doi.org/10.1038/s41569-020-0381-0

Gorshkov, K., Mehta, S., Ramamurthy, S., Ronnett, G. V., Zhou, F.-Q., & Zhang, J. (2017). AKAP-mediated feedback control of cAMP gradients in developing hippocampal neurons. *Nature Chemical Biology*, *13*(4), 425–431. https://doi.org/10.1038/nchembio.2298

Grant, P. G., & Colman, R. W. (1984). Purification and characterization of a human platelet cyclic nucleotide phosphodiesterase. *Biochemistry*, *23*(8), 1801–1807. https://doi.org/10.1021/bi00303a034

Gray, P. C., Johnson, B. D., Westenbroek, R. E., Hays, L. G., Yates, J. R., Scheuer, T., Catterall, W. A., & Murphy, B. J. (1998). Primary Structure and Function of an A Kinase Anchoring Protein Associated with Calcium Channels. *Neuron*, *20*(5), 1017–1026. https://doi.org/10.1016/S0896-6273(00)80482-1

Gross, P., Johnson, J., Romero, C. M., Eaton, D. M., Poulet, C., Sanchez-Alonso, J., Lucarelli, C., Ross, J., Gibb, A. A., Garbincius, J. F., Lambert, J., Varol, E., Yang, Y., Wallner, M., Feldsott, E. A., Kubo, H., Berretta, R. M., Yu, D., Rizzo, V., … Houser, S. R. (2021). Interaction of the Joining Region in Junctophilin-2 With the L-Type Ca2+ Channel Is Pivotal for Cardiac Dyad Assembly and Intracellular Ca2+ Dynamics. *Circulation Research*, *128*(1), 92–114. https://doi.org/10.1161/CIRCRESAHA.119.315715

Guggenheimer, A. B., Almagor, L., Tsemakhovich, V., Tripathy, D. R., Hirsch, J. A., & Dascal, N. (2016). Interactions between N and C termini of α1C subunit regulate inactivation of CaV1.2 L-type Ca2+ channel. *Channels*, *10*(1), 55–68. https://doi.org/10.1080/19336950.2015.1108499

Haji-Ghassemi, O., Yuchi, Z., & Van Petegem, F. (2019). The Cardiac Ryanodine Receptor Phosphorylation Hotspot Embraces PKA in a Phosphorylation-Dependent Manner. *Molecular Cell*, *75*(1), 39-52.e4. https://doi.org/10.1016/j.molcel.2019.04.019

Han, P., Sonati, P., Rubin, C., & Michaeli, T. (2006). PDE7A1, a cAMP-specific Phosphodiesterase, Inhibits cAMP-dependent Protein Kinase by a Direct Interaction with C. *Journal of Biological Chemistry*, *281*(22), 15050–15057. https://doi.org/10.1074/jbc.M601333200

Hansen, A., Eder, A., Bönstrup, M., Flato, M., Mewe, M., Schaaf, S., Aksehirlioglu, B., Schwörer, A., Uebeler, J., & Eschenhagen, T. (2010). Development of a Drug Screening Platform Based on Engineered Heart Tissue. *Circulation Research*, *107*(1), 35–44. https://doi.org/10.1161/CIRCRESAHA.109.211458

Harris, S. P., Bartley, C. R., Hacker, T. A., McDonald, K. S., Douglas, P. S., Greaser, M. L., Powers, P. A., & Moss, R. L. (2002). Hypertrophic Cardiomyopathy in Cardiac Myosin Binding Protein-C Knockout Mice. *Circulation Research*, *90*(5), 594–601. https://doi.org/10.1161/01.RES.0000012222.70819.64

Hasenfuss, G., & Teerlink, J. R. (2011). Cardiac inotropes: Current agents and future directions. *European Heart Journal*, *32*(15), 1838–1845. https://doi.org/10.1093/eurheartj/ehr026

Helms, A. S., Tang, V. T., O'Leary, T. S., Friedline, S., Wauchope, M., Arora, A., Wasserman, A. H., Smith, E. D., Lee, L. M., Wen, X. W., Shavit, J. A., Liu, A. P., Previs, M. J., & Day, S. M. (2020). Effects of MYBPC3 loss-of-function mutations preceding hypertrophic cardiomyopathy. *JCI Insight*, *5*(2), e133782. https://doi.org/10.1172/jci.insight.133782

Hill, J. A., & Olson, E. N. (2008). Cardiac Plasticity. *New England Journal of Medicine*, *358*(13), 1370–1380. https://doi.org/10.1056/NEJMra072139

Hödar, C., Assar, R., Colombres, M., Aravena, A., Pavez, L., González, M., Martínez, S., Inestrosa, N. C., & Maass, A. (2010). Genome-wide identification of new Wnt/beta-catenin target genes in the human genome using CART method. *BMC Genomics*, *11*, 348. https://doi.org/10.1186/1471-2164-11-348

Hofmann, F., Biel, M., & Flockerzi, V. (1994). Molecular Basis for CA2+ Channel Diversity. *Annual Review of Neuroscience*, *17*(1), 399–418. https://doi.org/10.1146/annurev.ne.17.030194.002151

Hofmann, F., Flockerzi, V., Kahl, S., & Wegener, J. W. (2014). L-type CaV1.2 calcium channels: From in vitro findings to in vivo function. *Physiological Reviews*, *94*(1), 303–326. https://doi.org/10.1152/physrev.00016.2013

Hong, T.-T., Smyth, J. W., Gao, D., Chu, K. Y., Vogan, J. M., Fong, T. S., Jensen, B. C., Colecraft, H. M., & Shaw, R. M. (2010). BIN1 localizes the L-type calcium channel to cardiac T-tubules. *PLoS Biology*, *8*(2), e1000312. https://doi.org/10.1371/journal.pbio.1000312

Hu, D., Linders, A., Yamak, A., Correia, C., Kijlstra, J. D., Garakani, A., Xiao, L., Milan, D. J., van der Meer, P., Serra, M., Alves, P. M., & Domian, I. J. (2018). Metabolic Maturation of Human Pluripotent Stem Cell-Derived Cardiomyocytes by Inhibition of HIF1α and LDHA. *Circulation Research*, *123*(9), 1066–1079. https://doi.org/10.1161/CIRCRESAHA.118.313249

Hua, R., Adamczyk, A., Robbins, C., Ray, G., & Rose, R. A. (2012). Distinct Patterns of Constitutive Phosphodiesterase Activity in Mouse Sinoatrial Node and Atrial Myocardium. *PLoS ONE*, *7*(10), e47652. https://doi.org/10.1371/journal.pone.0047652

Hulme, J. T., Konoki, K., Lin, T. W.-C., Gritsenko, M. A., Camp, D. G., Bigelow, D. J., & Catterall, W. A. (2005). Sites of proteolytic processing and noncovalent association of the distal C-terminal domain of CaV1.1 channels in skeletal muscle. *Proceedings of the National Academy of Sciences*, *102*(14), 5274–5279. https://doi.org/10.1073/pnas.0409885102

Hulme, J. T., Lin, T. W. C., Westenbroek, R. E., Scheuer, T., & Catterall, W. A. (2003). β-Adrenergic regulation requires direct anchoring of PKA to cardiac CaV1.2 channels via a leucine zipper interaction with A kinase-anchoring protein 15. *Proceedings of the National Academy of Sciences of the United States of America*, *100*(22), 13093–13098. https://doi.org/10.1073/pnas.2135335100

Hulme, J. T., Yarov-Yarovoy, V., Lin, T. W. C., Scheuer, T., & Catterall, W. A. (2006). Autoinhibitory control of the CaV1.2 channel by its proteolytically processed distal C-terminal domain. *Journal of Physiology*, *576*(1), 87–102. https://doi.org/10.1113/jphysiol.2006.111799

Hundsrucker, C., Rosenthal, W., & Klussmann, E. (2006). Peptides for disruption of PKA anchoring.

*Biochemical Society Transactions*, *34*(4), 472–473. https://doi.org/10.1042/BST0340472

Hunter, R. W., Mackintosh, C., & Hers, I. (2009). Protein kinase C-mediated phosphorylation and activation of PDE3A regulate cAMP levels in human platelets. *The Journal of Biological Chemistry*, *284*(18), 12339–12348. https://doi.org/10.1074/jbc.M807536200

Hwang, H. S., Kryshtal, D. O., Feaster, T. K., Sánchez-Freire, V., Zhang, J., Kamp, T. J., Hong, C. C., Wu, J. C., & Knollmann, B. C. (2015). Comparable calcium handling of human iPSC-derived cardiomyocytes generated by multiple laboratories. *Journal of Molecular and Cellular Cardiology*, *85*, 79–88. https://doi.org/10.1016/j.yjmcc.2015.05.003

Ito, D. W., Hannigan, K. I., Ghosh, D., Xu, B., del Villar, S. G., Xiang, Y. K., Dickson, E. J., Navedo, M. F., & Dixon, R. E. (2019). β-adrenergic-mediated dynamic augmentation of sarcolemmal Ca V 1.2 clustering and co-operativity in ventricular myocytes. *Journal of Physiology*, *597*(8), 2139–2162. https://doi.org/10.1113/JP277283

Itzhaki, I., Rapoport, S., Huber, I., Mizrahi, I., Zwi-Dantsis, L., Arbel, G., & Gepstein, L. (2011). Calcium Handling in Human Induced Pluripotent Stem Cell Derived Cardiomyocytes. *PLoS ONE*, *6*(4), 12.

Ivanina, T., Blumenstein, Y., Shistik, E., Barzilai, R., & Dascal, N. (2000). Modulation of L-type Ca2+ Channels by Gβγ and Calmodulin via Interactions with N and C Termini of α1C*. *Journal of Biological Chemistry*, *275*(51), 39846–39854. https://doi.org/10.1074/jbc.M005881200

Ivashchenko, C. Y., Pipes, G. C., Lozinskaya, I. M., Lin, Z., Xiaoping, X., Needle, S., Grygielko, E. T., Hu, E., Toomey, J. R., Lepore, J. J., & Willette, R. N. (2013). Human-induced pluripotent stem cell-derived cardiomyocytes exhibit temporal changes in phenotype. *American Journal of Physiology-Heart and Circulatory Physiology*, *305*(6), H913–H922. https://doi.org/10.1152/ajpheart.00819.2012

Jaski, B. E., Fifer, M. A., Wright, R. F., Braunwald, E., & Colucci, W. S. (1985). Positive inotropic and vasodilator actions of milrinone in patients with severe congestive heart failure. Dose-response relationships and comparison to nitroprusside. *The Journal of Clinical Investigation*, *75*(2), 643–649. https://doi.org/10.1172/JCI111742

Jideama, N. M., Crawford, B. H., Hussain, A. A., & Raynor, R. L. (2006). Dephosphorylation specificities of protein phosphatase for cardiac troponin I, troponin T, and sites within troponin T. *International Journal of Biological Sciences*, 1–9. https://doi.org/10.7150/ijbs.2.1

Johansson, M., Ulfenborg, B., Andersson, C. X., Heydarkhan-Hagvall, S., Jeppsson, A., Sartipy, P., & Synnergren, J. (2020). Cardiac hypertrophy in a dish: A human stem cell based model. *Biology Open*, *9*(9), bio052381. https://doi.org/10.1242/bio.052381

Jones, B. W., Brunet, S., Gilbert, M. L., Nichols, C. B., Su, T., Westenbroek, R. E., Scott, J. D., Catterall, W. A., & McKnight, G. S. (2012). Cardiomyocytes from AKAP7 knockout mice respond normally to adrenergic stimulation. *Proceedings of the National Academy of Sciences*, *109*(42), 17099–17104. https://doi.org/10.1073/pnas.1215219109

Jung, C. B., Moretti, A., Mederos y Schnitzler, M., Iop, L., Storch, U., Bellin, M., Dorn, T., Ruppenthal, S., Pfeiffer, S., Goedel, A., Dirschinger, R. J., Seyfarth, M., Lam, J. T., Sinnecker, D., Gudermann, T., Lipp, P., & Laugwitz, K. (2012). Dantrolene rescues arrhythmogenic RYR2 defect in a patient-specific stem cell model of catecholaminergic polymorphic ventricular tachycardia. *EMBO Molecular Medicine*, *4*(3), 180–191. https://doi.org/10.1002/emmm.201100194

Jung, G., Fajardo, G., Ribeiro, A. J. S., Kooiker, K. B., Coronado, M., Zhao, M., Hu, D., Reddy, S., Kodo,

K., Sriram, K., Insel, P. A., Wu, J. C., Pruitt, B. L., & Bernstein, D. (2016). Time-dependent evolution of functional *vs.* remodeling signaling in induced pluripotent stem cell-derived cardiomyocytes and induced maturation with biomechanical stimulation. *The FASEB Journal*, *30*(4), 1464–1479. https://doi.org/10.1096/fj.15-280982

Kamp, T. J., & Hell, J. W. (2000). Regulation of Cardiac L-Type Calcium Channels by Protein Kinase A and Protein Kinase C. *Circulation Research*, *87*(12), 1095–1102. https://doi.org/10.1161/01.RES.87.12.1095

Kane, C., Couch, L., & Terracciano, C. M. N. (2015). Excitation–contraction coupling of human induced pluripotent stem cell-derived cardiomyocytes. *Frontiers in Cell and Developmental Biology*, *3*. https://doi.org/10.3389/fcell.2015.00059

Katchman, A., Yang, L., Zakharov, S. I., Kushner, J., Abrams, J., Chen, B. X., Liu, G., Pitt, G. S., Colecraft, H. M., & Marx, S. O. (2017). Proteolytic cleavage and PKA phosphorylation of α1C subunit are not required for adrenergic regulation of CaV1.2 in the heart. *Proceedings of the National Academy of Sciences of the United States of America*, *114*(34), 9194–9199. https://doi.org/10.1073/pnas.1706054114

Katz, M., Subramaniam, S., Chomsky-Hecht, O., Tsemakhovich, V., Flockerzi, V., Klussmann, E., Hirsch, J. A., Weiss, S., & Dascal, N. (2021). Reconstitution of β-adrenergic regulation of CaV1.2: Rad-dependent and Rad-independent protein kinase A mechanisms. *Proceedings of the National Academy of Sciences of the United States of America*, *118*(21). https://doi.org/10.1073/pnas.2100021118

Ke, H., & Wang, H. (2007). Crystal Structures of Phosphodiesterases and Implications on Substrate Specificity and Inhibitor Selectivity. *Current Topics in Medicinal Chemistry*, *7*(4), 391–403. https://doi.org/10.2174/156802607779941242

Kenan, Y., Murata, T., Shakur, Y., Degerman, E., & Manganiello, V. C. (2000). Functions of the N-terminal region of cyclic nucleotide phosphodiesterase 3 (PDE 3) isoforms. *The Journal of Biological Chemistry*, *275*(16), 12331–12338. https://doi.org/10.1074/jbc.275.16.12331

Kensler, R. W., Shaffer, J. F., & Harris, S. P. (2011). Binding of the N-terminal fragment C0–C2 of cardiac MyBP-C to cardiac F-actin. *Journal of Structural Biology*, *174*(1), 44–51. https://doi.org/10.1016/j.jsb.2010.12.003

Keravis, T., & Lugnier, C. (2010). Cyclic Nucleotide Phosphodiesterases (PDE) and Peptide Motifs. *Current Pharmaceutical Design*, *16*(9), 1114–1125. https://doi.org/10.2174/138161210790963760

Kerkelä, R., Ulvila, J., & Magga, J. (2015). Natriuretic Peptides in the Regulation of Cardiovascular Physiology and Metabolic Events. *Journal of the American Heart Association*, *4*(10), e002423. https://doi.org/10.1161/JAHA.115.002423

Kim, C., Cheng, C. Y., Saldanha, S. A., & Taylor, S. S. (2007). PKA-I Holoenzyme Structure Reveals a Mechanism for cAMP-Dependent Activation. *Cell*, *130*(6), 1032–1043. https://doi.org/10.1016/j.cell.2007.07.018

Kim, J. J., Yang, L., Lin, B., Zhu, X., Sun, B., Kaplan, A. D., Bett, G. C. L., Rasmusson, R. L., London, B., & Salama, G. (2015). Mechanism of automaticity in cardiomyocytes derived from human induced pluripotent stem cells. *Journal of Molecular and Cellular Cardiology*, *81*, 81–93. https://doi.org/10.1016/j.yjmcc.2015.01.013

Kim, J., Masterson, L. R., Cembran, A., Verardi, R., Shi, L., Gao, J., Taylor, S. S., & Veglia, G. (2015).

Dysfunctional conformational dynamics of protein kinase A induced by a lethal mutant of phospholamban hinder phosphorylation. *Proceedings of the National Academy of Sciences*, *112*(12), 3716–3721. https://doi.org/10.1073/pnas.1502299112

Kroll, K., Chabria, M., Wang, K., Häusermann, F., Schuler, F., & Polonchuk, L. (2017). Electro-mechanical conditioning of human iPSC-derived cardiomyocytes for translational research. *Progress in Biophysics and Molecular Biology*, *130*, 212–222. https://doi.org/10.1016/j.pbiomolbio.2017.07.003

Kumari, N., Gaur, H., & Bhargava, A. (2018a). Cardiac voltage gated calcium channels and their regulation by β-adrenergic signaling. *Life Sciences*, *194*(December 2017), 139–149. https://doi.org/10.1016/j.lfs.2017.12.033

Kumari, N., Gaur, H., & Bhargava, A. (2018b). Cardiac voltage gated calcium channels and their regulation by β-adrenergic signaling. *Life Sciences*, *194*(January), 139–149. https://doi.org/10.1016/j.lfs.2017.12.033

Kumari, N., Gaur, H., & Bhargava, A. (2018c). Cardiac voltage gated calcium channels and their regulation by β-adrenergic signaling. *Life Sciences*, *194*(December 2017), 139–149. https://doi.org/10.1016/j.lfs.2017.12.033

Laco, F., Woo, T. L., Zhong, Q., Szmyd, R., Ting, S., Khan, F. J., Chai, C. L. L., Reuveny, S., Chen, A., & Oh, S. (2018). Unraveling the Inconsistencies of Cardiac Differentiation Efficiency Induced by the GSK3β Inhibitor CHIR99021 in Human Pluripotent Stem Cells. *Stem Cell Reports*, *10*(6), 1851–1866. https://doi.org/10.1016/j.stemcr.2018.03.023

Lee, Y.-K., Ng, K.-M., Lai, W.-H., Chan, Y.-C., Lau, Y.-M., Lian, Q., Tse, H.-F., & Siu, C.-W. (2011). Calcium Homeostasis in Human Induced Pluripotent Stem Cell-Derived Cardiomyocytes. *Stem Cell Reviews and Reports*, *7*(4), 976–986. https://doi.org/10.1007/s12015-011-9273-3

Lehman, W., & Craig, R. (2008). Tropomyosin and the Steric Mechanism of Muscle Regulation. In P. Gunning (Ed.), *Tropomyosin* (Vol. 644, pp. 95–109). Springer New York. https://doi.org/10.1007/978-0-387-85766-4_8

Lei, M., Xu, J., Gao, Q., Minobe, E., Kameyama, M., & Hao, L. (2018). PKA phosphorylation of Cav1.2 channel modulates the interaction of calmodulin with the C terminal tail of the channel. *Journal of Pharmacological Sciences*, *137*(2), 187–194. https://doi.org/10.1016/j.jphs.2018.05.010

Lemke, T., Welling, A., Christel, C. J., Blaich, A., Bernhard, D., Lenhardt, P., Hofmann, F., & Moosmang, S. (2008). Unchanged β-Adrenergic Stimulation of Cardiac L-type Calcium Channels in Cav1.2 Phosphorylation Site S1928A Mutant Mice*. *Journal of Biological Chemistry*, *283*(50), 34738–34744. https://doi.org/10.1074/jbc.M804981200

Leroy, J., Abi-Gerges, A., Nikolaev, V. O., Richter, W., Lechêne, P., Mazet, J.-L., Conti, M., Fischmeister, R., & Vandecasteele, G. (2008). Spatiotemporal Dynamics of β-Adrenergic cAMP Signals and L-Type Ca $^{2+}$ Channel Regulation in Adult Rat Ventricular Myocytes: Role of Phosphodiesterases. *Circulation Research*, *102*(9), 1091–1100. https://doi.org/10.1161/CIRCRESAHA.107.167817

Leroy, J., Richter, W., Mika, D., Castro, L. R. V., Abi-Gerges, A., Xie, M., Scheitrum, C., Lefebvre, F., Schittl, J., Mateo, P., Westenbroek, R., Catterall, W. A., Charpentier, F., Conti, M., Fischmeister, R., & Vandecasteele, G. (2011). Phosphodiesterase 4B in the cardiac L-type Ca2+ channel complex regulates Ca2+ current and protects against ventricular arrhythmias in mice. *Journal of Clinical Investigation*, *121*(7), 2651–2661. https://doi.org/10.1172/JCI44747

Leroy, J., Vandecasteele, G., & Fischmeister, R. (2018). Cyclic AMP signaling in cardiac myocytes. *Current Opinion in Physiology*, *1*, 161–171. https://doi.org/10.1016/j.cophys.2017.11.004

Levin, E. R., & Samson, W. K. (1998). Natriuretic Peptides. *The New England Journal of Medicine*, 8.

Levitan, B. M., Ahern, B. M., Aloysius, A., Brown, L., Wen, Y., Andres, D. A., & Satin, J. (2021). Rad-GTPase contributes to heart rate via L-type calcium channel regulation. *Journal of Molecular and Cellular Cardiology*, *154*, 60–69. https://doi.org/10.1016/j.yjmcc.2021.01.005

Li, J., Vargas, M. A. X., Kapiloff, M. S., & Dodge-Kafka, K. L. (2013). Regulation of MEF2 transcriptional activity by calcineurin/mAKAP complexes. *Experimental Cell Research*, *319*(4), 447–454. https://doi.org/10.1016/j.yexcr.2012.12.016

Li, S., Chen, G., & Li, R. A. (2013). Calcium signalling of human pluripotent stem cell-derived cardiomyocytes: Ca $^{2+}$ signalling of hPSC-derived cardiomyocytes. *The Journal of Physiology*, *591*(21), 5279–5290. https://doi.org/10.1113/jphysiol.2013.256495

Li, X., Li, Z., Chen, P., Wang, Y., Wang, D. W., & Wang, D. W. (2020). Whole-exome sequencing identifies a de novo PDE3A variant causing autosomal dominant hypertension with brachydactyly type E syndrome: A case report. *BMC Medical Genetics*, *21*(1), 144. https://doi.org/10.1186/s12881-020-01077-z

Lian, X., Zhang, J., Azarin, S. M., Zhu, K., Hazeltine, L. B., Bao, X., Hsiao, C., Kamp, T. J., & Palecek, S. P. (2013). Directed cardiomyocyte differentiation from human pluripotent stem cells by modulating Wnt/β-catenin signaling under fully defined conditions. *Nature Protocols*, *8*(1), 162–175. https://doi.org/10.1038/nprot.2012.150

Lin, C., Guo, X., Lange, S., Liu, J., Ouyang, K., Yin, X., Jiang, L., Cai, Y., Mu, Y., Sheikh, F., Ye, S., Chen, J., Ke, Y., & Cheng, H. (2013). Cypher/ZASP Is a Novel A-kinase Anchoring Protein*. *Journal of Biological Chemistry*, *288*(41), 29403–29413. https://doi.org/10.1074/jbc.M113.470708

Linzbach, A. J. (1976). Hypertrophy, Hyperplasia and Structural Dilatation of the Human Heart. In V. Manninen & P. I. Halonen (Eds.), *Advances in Cardiology* (Vol. 18, pp. 1–14). S. Karger AG. https://doi.org/10.1159/000399507

Liu, G., Papa, A., Katchman, A. N., Zakharov, S. I., Roybal, D., Hennessey, J. A., Kushner, J., Yang, L., Chen, B. X., Kushnir, A., Dangas, K., Gygi, S. P., Pitt, G. S., Colecraft, H. M., Ben-Johny, M., Kalocsay, M., & Marx, S. O. (2020). Mechanism of adrenergic CaV1.2 stimulation revealed by proximity proteomics. *Nature*, *577*(7792), 695–700. https://doi.org/10.1038/s41586-020-1947-z

Lowes, B. D., Higginbotham, M., Petrovich, L., DeWood, M. A., Greenberg, M. A., Rahko, P. S., Dec, G. W., LeJemtel, T. H., Roden, R. L., Schleman, M. M., Robertson, A. D., Gorczynski, R. J., & Bristow, M. R. (2000). *Low-Dose Enoximone Improves Exercise Capacity in Chronic Heart Failure*. *36*(2), 8.

Lu, J. Y., & Sewer, M. B. (2015). P54 $^{nrb}$ /NONO Regulates Cyclic AMP-Dependent Glucocorticoid Production by Modulating Phosphodiesterase mRNA Splicing and Degradation. *Molecular and Cellular Biology*, *35*(7), 1223–1237. https://doi.org/10.1128/MCB.00993-14

Lukowski, R., Cruz Santos, M., Kuret, A., & Ruth, P. (2021). cGMP and mitochondrial K $^{+}$ channels—Compartmentalized but closely connected in cardioprotection. *British Journal of Pharmacology*, bph.15536. https://doi.org/10.1111/bph.15536

Lundy, S. D., Zhu, W.-Z., Regnier, M., & Laflamme, M. A. (2013). Structural and Functional Maturation of Cardiomyocytes Derived from Human Pluripotent Stem Cells. *Stem Cells and Development*, *22*(14),

1991–2002. https://doi.org/10.1089/scd.2012.0490

Lygren, B., Carlson, C. R., Santamaria, K., Lissandron, V., McSorley, T., Litzenberg, J., Lorenz, D., Wiesner, B., Rosenthal, W., Zaccolo, M., Taskén, K., & Klussmann, E. (2007). AKAP complex regulates $Ca^{2+}$ re-uptake into heart sarcoplasmic reticulum. *EMBO Reports*, *8*(11), 1061–1067. https://doi.org/10.1038/sj.embor.7401081

Lyu, L., Gao, Q., Xu, J., Minobe, E., Zhu, T., & Kameyama, M. (2017). A new interaction between proximal and distal C-terminus of Cav1.2 channels. *Journal of Pharmacological Sciences*, *133*(4), 240–246. https://doi.org/10.1016/j.jphs.2017.03.002

Maass, P. G., Aydin, A., Luft, F. C., Schächterle, C., Weise, A., Stricker, S., Lindschau, C., Vaegler, M., Qadri, F., Toka, H. R., Schulz, H., Krawitz, P. M., Parkhomchuk, D., Hecht, J., Hollfinger, I., Wefeld-Neuenfeld, Y., Bartels-Klein, E., Mühl, A., Kann, M., … Bähring, S. (2015). PDE3A mutations cause autosomal dominant hypertension with brachydactyly. *Nature Genetics*, *47*(6), 647–653. https://doi.org/10.1038/ng.3302

Maillet, M., van Berlo, J. H., & Molkentin, J. D. (2013). Molecular basis of physiological heart growth: Fundamental concepts and new players. *Nature Reviews Molecular Cell Biology*, *14*(1), 38–48. https://doi.org/10.1038/nrm3495

Marcantoni, A., Levi, R. C., Gallo, M. P., Hirsch, E., & Alloatti, G. (2006). Phosphoinositide 3-kinaseγ (PI3Kγ) controls L-type calcium current (ICa,L) through its positive modulation of type-3 phosphodiesterase (PDE3). *Journal of Cellular Physiology*, *206*(2), 329–336. https://doi.org/10.1002/jcp.20467

Marks, A. R. (2013). Calcium cycling proteins and heart failure: Mechanisms and therapeutics. *The Journal of Clinical Investigation*, *123*(1), 46–52. https://doi.org/10.1172/JCI62834

Martin, T. P., Hortigon-Vinagre, M. P., Findlay, J. E., Elliott, C., Currie, S., & Baillie, G. S. (2014). Targeted disruption of the heat shock protein 20-phosphodiesterase 4D (PDE4D) interaction protects against pathological cardiac remodelling in a mouse model of hypertrophy. *FEBS Open Bio*, *4*(1), 923–927. https://doi.org/10.1016/j.fob.2014.10.011

Marx, S. O., Reiken, S., Hisamatsu, Y., Gaburjakova, M., Gaburjakova, J., Yang, Y.-M., Rosemblit, N., & Marks, A. R. (2001). Phosphorylation-dependent Regulation of Ryanodine Receptors: A Novel Role for Leucine/Isoleucine Zippers. *The Journal of Cell Biology*, *153*, 10.

Maskin, C. S., Sinoway, L., Chadwick, B., Sonnenblick, E. H., & Le Jemtel, T. H. (1983). Sustained hemodynamic and clinical effects of a new cardiotonic agent, WIN 47203, in patients with severe congestive heart failure. *Circulation*, *67*(5), 1065–1070. https://doi.org/10.1161/01.CIR.67.5.1065

Maurice, D. H., Ke, H., Ahmad, F., Wang, Y., Chung, J., & Manganiello, V. C. (2014). Advances in targeting cyclic nucleotide phosphodiesterases. *Nature Reviews. Drug Discovery*, *13*(4), 290–314. https://doi.org/10.1038/nrd4228

McClendon, C. L., Kornev, A. P., Gilson, M. K., & Taylor, S. S. (2014). Dynamic architecture of a protein kinase. *Proceedings of the National Academy of Sciences*, *111*(43), E4623 LP-E4631. https://doi.org/10.1073/pnas.1418402111

McCubrey, J. A., Steelman, L. S., Bertrand, F. E., Davis, N. M., Sokolosky, M., Abrams, S. L., Montalto, G., D'Assoro, A. B., Libra, M., Nicoletti, F., Maestro, R., Basecke, J., Rakus, D., Gizak, A., Demidenko, Z., Cocco, L., Martelli, A. M., & Cervello, M. (2014). GSK-3 as potential target for therapeutic intervention

in cancer. *Oncotarget; Vol 5, No 10*.

McEniery, C. M., Yasmin, null, Maki-Petaja, K. M., McDonnell, B. J., Munnery, M., Hickson, S. S., Franklin, S. S., Cockcroft, J. R., & Wilkinson, I. B. (2010). The Impact of Cardiovascular Risk Factors on Aortic Stiffness and Wave Reflections Depends on Age. *Hypertension*, *56*(4), 591–597. https://doi.org/10.1161/HYPERTENSIONAHA.110.156950

Meacci, E., Taira, M., Moos, M. J., Smith, C. J., Movsesian, M. A., Degerman, E., Belfrage, P., & Manganiello, V. (1992). Molecular cloning and expression of human myocardial cGMP-inhibited cAMP phosphodiesterase. *Proceedings of the National Academy of Sciences of the United States of America*, *89*(9), 3721–3725. https://doi.org/10.1073/pnas.89.9.3721

Meek, S. E. M., Lane, W. S., & Piwnica-Worms, H. (2004). Comprehensive Proteomic Analysis of Interphase and Mitotic 14-3-3-binding Proteins. *Journal of Biological Chemistry*, *279*(31), 32046–32054. https://doi.org/10.1074/jbc.M403044200

Meissner, M., Weissgerber, P., Londoño, J. E. C., Prenen, J., Link, S., Ruppenthal, S., Molkentin, J. D., Lipp, P., Nilius, B., Freichel, M., & Flockerzi, V. (2011). Moderate Calcium Channel Dysfunction in Adult Mice with Inducible Cardiomyocyte-specific Excision of the cacnb2 Gene*. *Journal of Biological Chemistry*, *286*(18), 15875–15882. https://doi.org/10.1074/jbc.M111.227819

Messer, A. E., Gallon, C. E., McKenna, W. J., Dos Remedios, C. G., & Marston, S. B. (2009). The use of phosphate-affinity SDS-PAGE to measure the cardiac troponin I phosphorylation site distribution in human heart muscle. *PROTEOMICS - Clinical Applications*, *3*(12), 1371–1382. https://doi.org/10.1002/prca.200900071

Mika, D., Bobin, P., Pomérance, M., Lechêne, P., Westenbroek, R. E., Catterall, W. A., Vandecasteele, G., Leroy, J., & Fischmeister, R. (2013). Differential regulation of cardiac excitation–contraction coupling by cAMP phosphodiesterase subtypes. *Cardiovascular Research*, *100*(2), 336–346. https://doi.org/10.1093/cvr/cvt193

Miki, T., Taira, M., Hockman, S., Shimada, F., Lieman, J., Napolitano, M., Ward, D., Taira, M., Makino, H., & Manganiello, V. C. (1996). Characterization of the cDNA and gene encoding human PDE3B, the cGIP1 isoform of the human cyclic GMP-inhibited cyclic nucleotide phosphodiesterase family. *Genomics*, *36*(3), 476–485. https://doi.org/10.1006/geno.1996.0493

Miriyala, J., Nguyen, T., Yue, D. T., & Colecraft, H. M. (2008). Role of CaVβ Subunits, and Lack of Functional Reserve, in Protein Kinase A Modulation of Cardiac CaV1.2 Channels. *Circulation Research*, *102*(7), e54–e64. https://doi.org/10.1161/CIRCRESAHA.108.171736

Moccia, F., Lodola, F., Stadiotti, I., Pilato, C. A., Bellin, M., Carugo, S., Pompilio, G., Sommariva, E., & Maione, A. S. (2019). Calcium as a key player in arrhythmogenic cardiomyopathy: Adhesion disorder or intracellular alteration? *International Journal of Molecular Sciences*, *20*(16). https://doi.org/10.3390/ijms20163986

Modesti, P. A., Vanni, S., Bertolozzi, I., Cecioni, I., Polidori, G., Paniccia, R., Bandinelli, B., Perna, A., Liguori, P., Boddi, M., Galanti, G., & Serneri, G. G. N. (2000). Early sequence of cardiac adaptations and growth factor formation in pressure- and volume-overload hypertrophy. *American Journal of Physiology-Heart and Circulatory Physiology*, *279*(3), H976–H985. https://doi.org/10.1152/ajpheart.2000.279.3.H976

Mongillo, M., Tocchetti, C. G., Terrin, A., Lissandron, V., Cheung, Y.-F., Dostmann, W. R., Pozzan, T., Kass, D. A., Paolocci, N., Houslay, M. D., & Zaccolo, M. (2006). Compartmentalized Phosphodiesterase-

2 Activity Blunts β-Adrenergic Cardiac Inotropy via an NO/cGMP-Dependent Pathway. *Circulation Research*, *98*(2), 226–234. https://doi.org/10.1161/01.RES.0000200178.34179.93

Monrad, E. S., McKay, R. G., Baim, D. S., Colucci, W. S., Fifer, M. A., Heller, G. V, Royal, H. D., & Grossman, W. (1984). Improvement in indexes of diastolic performance in patients with congestive heart failure treated with milrinone. *Circulation*, *70*(6), 1030–1037. https://doi.org/10.1161/01.CIR.70.6.1030

Movsesian, M., Ahmad, F., & Hirsch, E. (2018a). Functions of PDE3 isoforms in cardiac muscle. *Journal of Cardiovascular Development and Disease*, *5*(1). https://doi.org/10.3390/jcdd5010010

Movsesian, M., Ahmad, F., & Hirsch, E. (2018b). Functions of PDE3 isoforms in cardiac muscle. *Journal of Cardiovascular Development and Disease*, *5*(1). https://doi.org/10.3390/jcdd5010010

Movsesian, M., Ahmad, F., & Hirsch, E. (2018c). Functions of PDE3 Isoforms in Cardiac Muscle. *Journal of Cardiovascular Development and Disease*, *5*(1), 10. https://doi.org/10.3390/jcdd5010010

Movsesian, M., Wever-Pinzon, O., & Vandeput, F. (2011). PDE3 inhibition in dilated cardiomyopathy. *Current Opinion in Pharmacology*, *11*(6), 707–713. https://doi.org/10.1016/j.coph.2011.09.001

Muller, G. K., Song, J., Jani, V., Wu, Y., Liu, T., Jeffreys, W. P. D., O'Rourke, B., Anderson, M. E., & Kass, D. A. (2021). PDE1 Inhibition Modulates Ca $_{v}$ 1.2 Channel to Stimulate Cardiomyocyte Contraction. *Circulation Research*, *129*(9), 872–886. https://doi.org/10.1161/CIRCRESAHA.121.319828

Murphy, S. A., Miyamoto, M., Kervadec, A., Kannan, S., Tampakakis, E., Kambhampati, S., Lin, B. L., Paek, S., Andersen, P., Lee, D.-I., Zhu, R., An, S. S., Kass, D. A., Uosaki, H., Colas, A. R., & Kwon, C. (2021). PGC1/PPAR drive cardiomyocyte maturation at single cell level via YAP1 and SF3B2. *Nature Communications*, *12*(1), 1648. https://doi.org/10.1038/s41467-021-21957-z

Muslin, A. J., Tanner, J. W., Allen, P. M., & Shaw, A. S. (1996). Interaction of 14-3-3 with Signaling Proteins Is Mediated by the Recognition of Phosphoserine. *Cell*, *84*(6), 889–897. https://doi.org/10.1016/S0092-8674(00)81067-3

Nakagawa, Y., Nishikimi, T., & Kuwahara, K. (2019). Atrial and brain natriuretic peptides: Hormones secreted from the heart. *Peptides*, *111*, 18–25. https://doi.org/10.1016/j.peptides.2018.05.012

Narahara, K. A. (1991). Oral enoximone therapy in chronic heart failure: A placebo-controlled randomized trial. *American Heart Journal*, *121*(5), 1471–1479. https://doi.org/10.1016/0002-8703(91)90154-A

Newton-Cheh, C., Larson, M. G., Vasan, R. S., Levy, D., Bloch, K. D., Surti, A., Guiducci, C., Kathiresan, S., Benjamin, E. J., Struck, J., Morgenthaler, N. G., Bergmann, A., Blankenberg, S., Kee, F., Nilsson, P., Yin, X., Peltonen, L., Vartiainen, E., Salomaa, V., … Wang, T. J. (2009). Association of common variants in NPPA and NPPB with circulating natriuretic peptides and blood pressure. *Nature Genetics*, *41*(3), 348–353. https://doi.org/10.1038/ng.328

Nikolaev, V. O., Bünemann, M., Hein, L., Hannawacker, A., & Lohse, M. J. (2004). Novel Single Chain cAMP Sensors for Receptor-induced Signal Propagation. *Journal of Biological Chemistry*, *279*(36), 37215–37218. https://doi.org/10.1074/jbc.C400302200

Nystoriak, M. A., Nieves-Cintrón, M., Patriarchi, T., Buonarati, O. R., Prada, M. P., Morotti, S., Grandi, E., Fernandes, J. D. S., Forbush, K., Hofmann, F., Sasse, K. C., Scott, J. D., Ward, S. M., Hell, J. W., & Navedo, M. F. (2017). Ser1928 phosphorylation by PKA stimulates the L-type Ca2+ channel Cav1.2 and vasoconstriction during acute hyperglycemia and diabetes. *Science Signaling*, *10*(463).

https://doi.org/10.1126/scisignal.aaf9647

O., N. V., Alexey, M., R., L. A., Michele, M., Pavel, N., Helen, P., J., L. M., E., K. Y., E., H. S., & Julia, G. (2010). B2-Adrenergic Receptor Redistribution in Heart Failure Changes cAMP Compartmentation. *Science*, *327*(5973), 1653–1657. https://doi.org/10.1126/science.1185988

Oldfield, C. J., Duhamel, T. A., & Dhalla, N. S. (2020). Mechanisms for the transition from physiological to pathological cardiac hypertrophy. *Canadian Journal of Physiology and Pharmacology*, *98*(2), 74–84. https://doi.org/10.1139/cjpp-2019-0566

Oliveria, S. F., Dell'Acqua, M. L., & Sather, W. A. (2007). AKAP79/150 Anchoring of Calcineurin Controls Neuronal L-Type Ca2+ Channel Activity and Nuclear Signaling. *Neuron*, *55*(2), 261–275. https://doi.org/10.1016/j.neuron.2007.06.032

Omori, K., & Kotera, J. (2007). Overview of PDEs and Their Regulation. *Circulation Research*, *100*(3), 309–327. https://doi.org/10.1161/01.RES.0000256354.95791.f1

Ovchinnikova, E., Hoes, M., Ustyantsev, K., Bomer, N., de Jong, T. V, van der Mei, H., Berezikov, E., & van der Meer, P. (2018). Modeling Human Cardiac Hypertrophy in Stem Cell-Derived Cardiomyocytes. *Stem Cell Reports*, *10*(3), 794–807. https://doi.org/10.1016/j.stemcr.2018.01.016

Oz, S., Pankonien, I., Belkacemi, A., Flockerzi, V., Klussmann, E., Haase, H., & Dascal, N. (2017). Protein kinase A regulates C-terminally truncated CaV1.2 in Xenopus oocytes: Roles of N- and C-termini of the α1C subunit. *Journal of Physiology*, *595*(10), 3181–3202. https://doi.org/10.1113/JP274015

Packer, M., Carver, J. R., Rodeheffer, R. J., Ivanhoe, R. J., DiBianco, R., Zeldis, S. M., Hendrix, G. H., Bommer, W. J., Elkayam, U., & Kukin, M. L. (1991). Effect of oral milrinone on mortality in severe chronic heart failure. The PROMISE Study Research Group. *The New England Journal of Medicine*, *325*(21), 1468–1475. https://doi.org/10.1056/NEJM199111213252103

Packer, M., Narahara, K. A., Elkayam, U., Sullivan, J. M., Pearle, D. L., Massie, B. M., Creager, M. A., & The Principal Investigators of the Reflect Study. (1993). Double-blind, placebo-controlled study of the efficacy of flosequinan in patients with chronic heart failure. *Journal of the American College of Cardiology*, *22*(1), 65–72. https://doi.org/10.1016/0735-1097(93)90816-J

Paget, V., Legedz, L., Gaudebout, N., Girerd, N., Bricca, G., Milon, H., Vincent, M., & Lantelme, P. (2011). N-Terminal Pro-Brain Natriuretic Peptide: A Powerful Predictor of Mortality in Hypertension. *Hypertension*, *57*(4), 702–709. https://doi.org/10.1161/HYPERTENSIONAHA.110.163550

Pallien, T., & Klussmann, E. (2020a). New aspects in cardiac L-type Ca2+ channel regulation. *Biochemical Society Transactions*, *48*(1), 38–49. https://doi.org/10.1042/BST20190229

Pallien, T., & Klussmann, E. (2020b). New aspects in cardiac L-type Ca2+ channel regulation. *Biochemical Society Transactions*, *48*(1), 38–49. https://doi.org/10.1042/BST20190229

Papa, A., Kushner, J., Hennessey, J. A., Katchman, A. N., Zakharov, S. I., Chen, B. X., Yang, L., Lu, R., Leong, S., Diaz, J., Liu, G., Roybal, D., Liao, X., Del Rivero Morfin, P. J., Colecraft, H. M., Pitt, G. S., Clarke, O., Topkara, V., Ben-Johny, M., & Marx, S. O. (2021). Adrenergic CaV1.2 Activation via Rad Phosphorylation Converges at α1CI-II Loop. *Circulation Research*, 76–88. https://doi.org/10.1161/CIRCRESAHA.120.317839

Papa, A., Kushner, J., & Marx, S. O. (2022). Adrenergic Regulation of Calcium Channels in the Heart. *Annual Review of Physiology*, *84*(1), 285–306. https://doi.org/10.1146/annurev-physiol-060121-041653

Parikh, S. S., Blackwell, D. J., Gomez-Hurtado, N., Frisk, M., Wang, L., Kim, K., Dahl, C. P., Fiane, A., Tønnessen, T., Kryshtal, D. O., Louch, W. E., & Knollmann, B. C. (2017). Thyroid and Glucocorticoid Hormones Promote Functional T-Tubule Development in Human-Induced Pluripotent Stem Cell–Derived Cardiomyocytes. *Circulation Research*, *121*(12), 1323–1330. https://doi.org/10.1161/CIRCRESAHA.117.311920

Passariello, C. L., Li, J., Dodge-Kafka, K., & Kapiloff, M. S. (2015). MAKAP—A Master Scaffold for Cardiac Remodeling: *Journal of Cardiovascular Pharmacology*, *65*(3), 218–225. https://doi.org/10.1097/FJC.0000000000000206

Pérez López, I., Cariolato, L., Maric, D., Gillet, L., Abriel, H., & Diviani, D. (2013). A-Kinase Anchoring Protein Lbc Coordinates a p38 Activating Signaling Complex Controlling Compensatory Cardiac Hypertrophy. *Molecular and Cellular Biology*, *33*(15), 2903–2917. https://doi.org/10.1128/MCB.00031-13

Perez-Reyes, E., Castellano, A., Kim, H. S., Bertrand, P., Baggstrom, E., Lacerda, A. E., Wei, X. Y., & Birnbaumer, L. (1992). Cloning and expression of a cardiac/brain beta subunit of the L-type calcium channel. *The Journal of Biological Chemistry*, *267*(3), 1792–1797.

Pidoux, G., & Taskén, K. (2010). Specificity and spatial dynamics of protein kinase A signaling organized by A-kinase-anchoring proteins. *Journal of Molecular Endocrinology*, *44*(5), 271–284. https://doi.org/10.1677/JME-10-0010

Piggott, L. A., Bauman, A. L., Scott, J. D., & Dessauer, C. W. (2008). *The A-kinase anchoring protein Yotiao binds and regulates adenylyl cyclase in brain*. 6.

Pinnell, J., Turner, S., & Howell, S. (2007). Cardiac muscle physiology. *Continuing Education in Anaesthesia Critical Care & Pain*, *7*(3), 85–88. https://doi.org/10.1093/bjaceaccp/mkm013

Pohlmann, L., Kröger, I., Vignier, N., Schlossarek, S., Krämer, E., Coirault, C., Sultan, K. R., El-Armouche, A., Winegrad, S., Eschenhagen, T., & Carrier, L. (2007). Cardiac Myosin-Binding Protein C Is Required for Complete Relaxation in Intact Myocytes. *Circulation Research*, *101*(9), 928–938. https://doi.org/10.1161/CIRCRESAHA.107.158774

Ponsioen, B., Zhao, J., Riedl, J., Zwartkruis, F., van der Krogt, G., Zaccolo, M., Moolenaar, W. H., Bos, J. L., & Jalink, K. (2004). Detecting cAMP-induced Epac activation by fluorescence resonance energy transfer: Epac as a novel cAMP indicator. *EMBO Reports*, *5*(12), 1176–1180. https://doi.org/10.1038/sj.embor.7400290

Pozuelo Rubio, M., Campbell, D. G., Morrice, N. A., & Mackintosh, C. (2005). Phosphodiesterase 3A binds to 14-3-3 proteins in response to PMA-induced phosphorylation of Ser428. *Biochemical Journal*, *392*(1), 163–172. https://doi.org/10.1042/BJ20051103

Preedy, M. E. J. (2020). Cardiac Cyclic Nucleotide Phosphodiesterases: Roles and Therapeutic Potential in Heart Failure. *Cardiovascular Drugs and Therapy*, *34*(3), 401–417. https://doi.org/10.1007/s10557-020-06959-1

Previs, M. J., Previs, S. B., Gulick, J., Robbins, J., & Warshaw, D. M. (2012). Molecular Mechanics of Cardiac Myosin-Binding Protein C in Native Thick Filaments. *Science*, *337*(6099), 1215–1218. https://doi.org/10.1126/science.1223602

Previs, M. J., Prosser, B. L., Mun, J. Y., Previs, S. B., Gulick, J., Lee, K., Robbins, J., Craig, R., Lederer, W. J., & Warshaw, D. M. (2015). Myosin-binding protein C corrects an intrinsic inhomogeneity in cardiac

excitation-contraction coupling. *Science Advances*, *1*(1), e1400205. https://doi.org/10.1126/sciadv.1400205

Psaras, Y., Margara, F., Cicconet, M., Sparrow, A. J., Repetti, G. G., Schmid, M., Steeples, V., Wilcox, J. A. L., Bueno-Orovio, A., Redwood, C. S., Watkins, H. C., Robinson, P., Rodriguez, B., Seidman, J. G., Seidman, C. E., & Toepfer, C. N. (2021). CalTrack: High-Throughput Automated Calcium Transient Analysis in Cardiomyocytes. *Circulation Research*, *129*(2), 326–341. https://doi.org/10.1161/CIRCRESAHA.121.318868

Qian, H., Patriarchi, T., Price, J. L., Matt, L., Lee, B., Nieves-Cintrón, M., Buonarati, O. R., Chowdhury, D., Nanou, E., Nystoriak, M. A., Catterall, W. A., Poomvanicha, M., Hofmann, F., Navedo, M. F., & Hell, J. W. (2017). Phosphorylation of Ser1928 mediates the enhanced activity of the L-type Ca2+ channel Cav1.2 by the β2-adrenergic receptor in neurons. *Science Signaling*, *10*(463). https://doi.org/10.1126/scisignal.aaf9659

Rao, C., Prodromakis, T., Kolker, L., Chaudhry, U. A. R., Trantidou, T., Sridhar, A., Weekes, C., Camelliti, P., Harding, S. E., Darzi, A., Yacoub, M. H., Athanasiou, T., & Terracciano, C. M. (2013). The effect of microgrooved culture substrates on calcium cycling of cardiac myocytes derived from human induced pluripotent stem cells. *Biomaterials*, *34*(10), 2399–2411. https://doi.org/10.1016/j.biomaterials.2012.11.055

Razani, B., & Lisanti, M. P. (2001). Two distinct caveolin-1 domains mediate the functional interaction of caveolin-1 with protein kinase A. *American Journal of Physiology-Cell Physiology*, *281*(4), C1241–C1250. https://doi.org/10.1152/ajpcell.2001.281.4.C1241

Rechsteiner, M. (1990). PEST sequences are signals for rapid intracellular proteolysis. *Seminars in Cell Biology*, *1*(6), 433–440.

Redden, J. M., & Dodge-Kafka, K. L. (2011). AKAP Phosphatase Complexes in the Heart. *Journal of Cardiovascular Pharmacology*, *58*(4).

Reinhardt, R. R., Chin, E., Zhou, J., Taira, M., Murata, T., Manganiello, V. C., & Bondy, C. A. (1995). Distinctive anatomical patterns of gene expression for cGMP-inhibited cyclic nucleotide phosphodiesterases. *The Journal of Clinical Investigation*, *95*(4), 1528–1538. https://doi.org/10.1172/JCI117825

Renkema, K. Y., Westermann, J. M., Nievelstein, R. A. J., Lo-A-Njoe, S. M., van der Zwaag, B., Manshande, M. E., & van Haelst, M. M. (2018). PDE3A gene screening improves diagnostics for patients with Bilginturan syndrome (hypertension and brachydactyly syndrome). *Hypertension Research*, *41*(11), 981–988. https://doi.org/10.1038/s41440-018-0094-5

Rhee, D. K., Hockman, S. C., Choi, S., Kim, Y.-E., Park, C., Manganiello, V. C., & Kim, K. K. (2017). SFPQ, a multifunctional nuclear protein, regulates the transcription of *PDE3A*. *Bioscience Reports*, *37*(4), BSR20170975. https://doi.org/10.1042/BSR20170975

Richardson, C. D., Ray, G. J., DeWitt, M. A., Curie, G. L., & Corn, J. E. (2016). Enhancing homology-directed genome editing by catalytically active and inactive CRISPR-Cas9 using asymmetric donor DNA. *Nature Biotechnology*, *34*(3), 339–344. https://doi.org/10.1038/nbt.3481

Richter, W., Xie, M., Scheitrum, C., Krall, J., Movsesian, M. A., & Conti, M. (2011). Conserved expression and functions of PDE4 in rodent and human heart. *Basic Research in Cardiology*, *106*(2), 249–262. https://doi.org/10.1007/s00395-010-0138-8

Roderick, H. L., Higazi, D. R., Smyrnias, I., Fearnley, C., Harzheim, D., & Bootman, M. D. (2007). Calcium in the heart: When it's good, it's very very good, but when it's bad, it's horrid. *Biochemical Society Transactions*, *35*(5), 957–961. https://doi.org/10.1042/BST0350957

Roybal, D., Hennessey, J. A., & Marx, S. O. (2020). The quest to identify the mechanism underlying adrenergic regulation of cardiac $Ca^{2+}$ channels. *Channels*, *14*(1), 123–131. https://doi.org/10.1080/19336950.2020.1740502

Rubattu, S., Forte, M., Marchitti, S., & Volpe, M. (2019). Molecular Implications of Natriuretic Peptides in the Protection from Hypertension and Target Organ Damage Development. *International Journal of Molecular Sciences*, *20*(4), 798. https://doi.org/10.3390/ijms20040798

Rubattu, S., Sciarretta, S., Valenti, V., Stanzione, R., & Volpe, M. (2008). Natriuretic Peptides: An Update on Bioactivity, Potential Therapeutic Use, and Implication in Cardiovascular Diseases. *American Journal of Hypertension*, *21*(7), 733–741. https://doi.org/10.1038/ajh.2008.174

Rubio, M., Campbell, D., Morrice, N., & Mackintosh, C. (2005). Phosphodiesterase 3A binds to 14-3-3 proteins in response to PMA-induced phosphorylation of Ser 428. *The Biochemical Journal*, *392*, 163–172. https://doi.org/10.1042/BJ20051103

Rubio, M. P., Geraghty, K. M., Wong, B. H. C., Wood, N. T., Campbell, D. G., Morrice, N., & Mackintosh, C. (2004). 14-3-3-affinity purification of over 200 human phosphoproteins reveals new links to regulation of cellular metabolism, proliferation and trafficking. *Biochemical Journal*, *379*(2), 395–408. https://doi.org/10.1042/bj20031797

Sabatine, M. S., Morrow, D. A., de Lemos, J. A., Omland, T., Sloan, S., Jarolim, P., Solomon, S. D., Pfeffer, M. A., & Braunwald, E. (2012). Evaluation of Multiple Biomarkers of Cardiovascular Stress for Risk Prediction and Guiding Medical Therapy in Patients With Stable Coronary Disease. *Circulation*, *125*(2), 233–240. https://doi.org/10.1161/CIRCULATIONAHA.111.063842

Schuster, H., Wienker, T. F., Toka, H. R., Bähring, S., Jeschke, E., Toka, O., Busjahn, A., Hempel, A., Tahlhammer, C., Oelkers, W., Kunze, J., Bilginturan, N., Haller, H., & Luft, F. C. (1996). Autosomal Dominant Hypertension and Brachydactyly in a Turkish Kindred Resembles Essential Hypertension. *Hypertension*, *28*(6), 1085–1092. https://doi.org/10.1161/01.HYP.28.6.1085

Seronde, M.-F., Gayat, E., Logeart, D., Lassus, J., Laribi, S., Boukef, R., Sibellas, F., Launay, J.-M., Manivet, P., Sadoune, M., Nouira, S., Solal, A. C., & Mebazaa, A. (2013). Comparison of the diagnostic and prognostic values of B-type and atrial-type natriuretic peptides in acute heart failure. *International Journal of Cardiology*, *168*(4), 3404–3411. https://doi.org/10.1016/j.ijcard.2013.04.164

Shakur, Y., Fong, M., Hensley, J., Cone, J., Movsesian, M. A., & Yoshitake, M. (2002). *Comparison of the Effects of Cilostazol and Milrinone on cAMP-PDE Activity, Intracellular cAMP and Calcium in the Heart*. 11.

Shakur, Y., Takeda, K., Kenan, Y., Yu, Z. X., Rena, G., Brandt, D., Houslay, M. D., Degerman, E., Ferrans, V. J., & Manganiello, V. C. (2000). Membrane localization of cyclic nucleotide phosphodiesterase 3 (PDE3). Two N-terminal domains are required for the efficient targeting to, and association of, PDE3 with endoplasmic reticulum. *The Journal of Biological Chemistry*, *275*(49), 38749–38761. https://doi.org/10.1074/jbc.M001734200

Shimizu, I., & Minamino, T. (2016). Physiological and pathological cardiac hypertrophy. *Journal of Molecular and Cellular Cardiology*, *97*, 245–262. https://doi.org/10.1016/j.yjmcc.2016.06.001

Sin, Y. Y., Edwards, H. V., Li, X., Day, J. P., Christian, F., Dunlop, A. J., Adams, D. R., Zaccolo, M., Houslay, M. D., & Baillie, G. S. (2011). Disruption of the cyclic AMP phosphodiesterase-4 (PDE4)–HSP20 complex attenuates the β-agonist induced hypertrophic response in cardiac myocytes. *Journal of Molecular and Cellular Cardiology*, *50*(5), 872–883. https://doi.org/10.1016/j.yjmcc.2011.02.006

Sinoway, L. S., Maskin, C. S., Chadwick, B., Forman, R., Sonnenblick, E. H., & Le Jemtel, T. H. (1983). Long-term therapy with a new cardiotonic agent, WIN 47203: Drug-dependent improvement in cardiac performance and progression of the underlying disease. *Journal of the American College of Cardiology*, *2*(2), 327–331. https://doi.org/10.1016/S0735-1097(83)80170-3

Skroblin, P., Grossmann, S., Schäfer, G., Rosenthal, W., & Klussmann, E. (2010). Mechanisms of Protein Kinase A Anchoring. *International Review of Cell and Molecular Biology*, *283*(C), 235–330. https://doi.org/10.1016/S1937-6448(10)83005-9

Søberg, K., & Skålhegg, B. S. (2018). The Molecular Basis for Specificity at the Level of the Protein Kinase a Catalytic Subunit. *Frontiers in Endocrinology*, *9*, 538. https://doi.org/10.3389/fendo.2018.00538

Steinhauser, M. L., & Lee, R. T. (2011). Regeneration of the heart. *EMBO Molecular Medicine*, *3*(12), 701–712. https://doi.org/10.1002/emmm.201100175

Surdo, N. C., Berrera, M., Koschinski, A., Brescia, M., Machado, M. R., Carr, C., Wright, P., Gorelik, J., Morotti, S., Grandi, E., Bers, D. M., Pantano, S., & Zaccolo, M. (2017). FRET biosensor uncovers cAMP nano-domains at β-adrenergic targets that dictate precise tuning of cardiac contractility. *Nature Communications*, *8*(1), 15031. https://doi.org/10.1038/ncomms15031

Tajada, S., Cidad, P., Colinas, O., Santana, L. F., López-López, J. R., & Pérez-García, M. T. (2013). Down-regulation of $Ca_V1.2$ channels during hypertension: How fewer $Ca_V1.2$ channels allow more $Ca^{2+}$ into hypertensive arterial smooth muscle: $Ca_v1.2$ channels in essential hypertension. *The Journal of Physiology*, *591*(24), 6175–6191. https://doi.org/10.1113/jphysiol.2013.265751

Takahashi, K., Tanabe, K., Ohnuki, M., Narita, M., Ichisaka, T., Tomoda, K., & Yamanaka, S. (2007). *Induction of Pluripotent Stem Cells from Adult Human Fibroblasts by Defined Factors*. 12.

Takahashi, T., Tang, T., Lai, N. C., Roth, D. M., Rebolledo, B., Saito, M., Lew, W. Y. W., Clopton, P., & Hammond, H. K. (2006). Increased Cardiac Adenylyl Cyclase Expression Is Associated With Increased Survival After Myocardial Infarction. *Circulation*, *114*(5), 388–396. https://doi.org/10.1161/CIRCULATIONAHA.106.632513

Takimoto, E., Soergel, D. G., Janssen, P. M. L., Stull, L. B., Kass, D. A., & Murphy, A. M. (2004). Frequency- and Afterload-Dependent Cardiac Modulation In Vivo by Troponin I With Constitutively Active Protein Kinase A Phosphorylation Sites. *Circulation Research*, *94*(4), 496–504. https://doi.org/10.1161/01.RES.0000117307.57798.F5

Tanaka, A., Yuasa, S., Mearini, G., Egashira, T., Seki, T., Kodaira, M., Kusumoto, D., Kuroda, Y., Okata, S., Suzuki, T., Inohara, T., Arimura, T., Makino, S., Kimura, K., Kimura, A., Furukawa, T., Carrier, L., Node, K., & Fukuda, K. (2014). Endothelin-1 induces myofibrillar disarray and contractile vector variability in hypertrophic cardiomyopathy-induced pluripotent stem cell-derived cardiomyocytes. *Journal of the American Heart Association*, *3*(6), e001263. https://doi.org/10.1161/JAHA.114.001263

Tanaka, T., Tohyama, S., Murata, M., Nomura, F., Kaneko, T., Chen, H., Hattori, F., Egashira, T., Seki, T., Ohno, Y., Koshimizu, U., Yuasa, S., Ogawa, S., Yamanaka, S., Yasuda, K., & Fukuda, K. (2009). In vitro pharmacologic testing using human induced pluripotent stem cell-derived cardiomyocytes. *Biochemical and Biophysical Research Communications*, *385*(4), 497–502.

https://doi.org/10.1016/j.bbrc.2009.05.073

Tani, H., & Tohyama, S. (2022). Human Engineered Heart Tissue Models for Disease Modeling and Drug Discovery. *Frontiers in Cell and Developmental Biology*, *10*, 21.

Tham, Y. K., Bernardo, B. C., Ooi, J. Y. Y., Weeks, K. L., & McMullen, J. R. (2015). Pathophysiology of cardiac hypertrophy and heart failure: Signaling pathways and novel therapeutic targets. *Archives of Toxicology*, *89*(9), 1401–1438. https://doi.org/10.1007/s00204-015-1477-x

Thibault, G., Amiri, F., & Garcia, R. (1999). REGULATION OF NATRIURETIC PEPTIDE SECRETION BY THE HEART. *Annual Review of Physiology*, *61*(1), 193–217. https://doi.org/10.1146/annurev.physiol.61.1.193

Tiburcy, M., Hudson, J. E., Balfanz, P., Schlick, S., Meyer, T., Chang Liao, M.-L., Levent, E., Raad, F., Zeidler, S., Wingender, E., Riegler, J., Wang, M., Gold, J. D., Kehat, I., Wettwer, E., Ravens, U., Dierickx, P., van Laake, L. W., Goumans, M. J., … Zimmermann, W.-H. (2017). Defined Engineered Human Myocardium With Advanced Maturation for Applications in Heart Failure Modeling and Repair. *Circulation*, *135*(19), 1832–1847. https://doi.org/10.1161/CIRCULATIONAHA.116.024145

Toepfer, C. N., Wakimoto, H., Garfinkel, A. C., McDonough, B., Liao, D., Jiang, J., Tai, A. C., Gorham, J. M., Lunde, I. G., Lun, M., Lynch, T. L., McNamara, J. W., Sadayappan, S., Redwood, C. S., Watkins, H. C., Seidman, J. G., & Seidman, C. E. (2019). Hypertrophic cardiomyopathy mutations in *MYBPC3* dysregulate myosin. *Science Translational Medicine*, *11*(476), eaat1199. https://doi.org/10.1126/scitranslmed.aat1199

Toka, O., Tank, J., Schächterle, C., Aydin, A., Maass, P. G., Elitok, S., Bartels-Klein, E., Hollfinger, I., Lindschau, C., Mai, K., Boschmann, M., Rahn, G., Movsesian, M. A., Müller, T., Doescher, A., Gnoth, S., Mühl, A., Toka, H. R., Wefeld-Neuenfeld, Y., … Luft, F. C. (2015). Clinical effects of phosphodiesterase 3A mutations in inherited hypertension with brachydactyly. *Hypertension*, *66*(4), 800–808. https://doi.org/10.1161/HYPERTENSIONAHA.115.06000

Tuluc, P., Yarov-Yarovoy, V., Benedetti, B., & Flucher, B. E. (2016). Molecular Interactions in the Voltage Sensor Controlling Gating Properties of CaV Calcium Channels. *Structure*, *24*(2), 261–271. https://doi.org/10.1016/j.str.2015.11.011

Uretsky, B. F., Jessup, M., Konstam, M. A., Dec, G. W., Leier, C. V, Benotti, J., Murali, S., Herrmann, H. C., & Sandberg, J. A. (1990). Multicenter trial of oral enoximone in patients with moderate to moderately severe congestive heart failure. Lack of benefit compared with placebo. Enoximone Multicenter Trial Group. *Circulation*, *82*(3), 774–780. https://doi.org/10.1161/01.CIR.82.3.774

van den Born, B.-J. H., Oskam, L. C., Zidane, M., Schächterle, C., Klussmann, E., Bähring, S., & Luft, F. C. (2016). The Case| A handful of hypertension. *Kidney International*, *90*(4), 911–913. https://doi.org/10.1016/j.kint.2016.03.037

van der Velden, J. (2011). Diastolic myofilament dysfunction in the failing human heart. *Pflügers Archiv - European Journal of Physiology*, *462*(1), 155–163. https://doi.org/10.1007/s00424-011-0960-3

van Dijk, S. J., Dooijes, D., dos Remedios, C., Michels, M., Lamers, J. M. J., Winegrad, S., Schlossarek, S., Carrier, L., ten Cate, F. J., Stienen, G. J. M., & van der Velden, J. (2009). Cardiac Myosin-Binding Protein C Mutations and Hypertrophic Cardiomyopathy: Haploinsufficiency, Deranged Phosphorylation, and Cardiomyocyte Dysfunction. *Circulation*, *119*(11), 1473–1483. https://doi.org/10.1161/CIRCULATIONAHA.108.838672

van Dijk, S. J., Kooiker, K. B., Napierski, N. C., Touma, K. D., Mazzalupo, S., & Harris, S. P. (2018). Point mutations in the tri-helix bundle of the M-domain of cardiac myosin binding protein-C influence systolic duration and delay cardiac relaxation. *Journal of Molecular and Cellular Cardiology*, *119*, 116–124. https://doi.org/10.1016/j.yjmcc.2018.05.001

van Dijk, S. J., Paalberends, E. R., Najafi, A., Michels, M., Sadayappan, S., Carrier, L., Boontje, N. M., Kuster, D. W. D., van Slegtenhorst, M., Dooijes, D., dos Remedios, C., ten Cate, F. J., Stienen, G. J. M., & van der Velden, J. (2012). Contractile Dysfunction Irrespective of the Mutant Protein in Human Hypertrophic Cardiomyopathy With Normal Systolic Function. *Circulation: Heart Failure*, *5*(1), 36–46. https://doi.org/10.1161/CIRCHEARTFAILURE.111.963702

Vandecasteele, G., Verde, I., Rücker-Martin, C., Donzeau-Gouge, P., & Fischmeister, R. (2001). Cyclic GMP regulation of the L-type $Ca^{2+}$ channel current in human atrial myocytes. *The Journal of Physiology*, *533*(2), 329–340. https://doi.org/10.1111/j.1469-7793.2001.0329a.x

Vandeput, F., Szabo-Fresnais, N., Ahmad, F., Kho, C., Lee, A., Krall, J., Dunlop, A., Hazel, M. W., Wohlschlegel, J. A., Hajjar, R. J., Houslay, M. D., Manganiello, V. C., & Movsesian, M. A. (2013). Selective regulation of cyclic nucleotide phosphodiesterase PDE3A isoforms. *Proceedings of the National Academy of Sciences*, *110*(49), 19778–19783. https://doi.org/10.1073/pnas.1305427110

Vandervelden, J., Papp, Z., Zaremba, R., Boontje, N., Dejong, J., Owen, V., Burton, P., Goldmann, P., Jaquet, K., & Stienen, G. (2003). Increased Ca-sensitivity of the contractile apparatus in end-stage human heart failure results from altered phosphorylation of contractile proteins. *Cardiovascular Research*, *57*(1), 37–47. https://doi.org/10.1016/S0008-6363(02)00606-5

Vinogradova, T. M., Kobrinsky, E., & Lakatta, E. G. (2018). Dual activation of phosphodiesterases 3 and 4 regulates basal spontaneous beating rate of cardiac pacemaker cells: Role of compartmentalization? *Frontiers in Physiology*, *9*(OCT), 1–10. https://doi.org/10.3389/fphys.2018.01301

Vinogradova, T. M., Sirenko, S., Lukyanenko, Y. O., Yang, D., Tarasov, K. V., Lyashkov, A. E., Varghese, N. J., Li, Y., Chakir, K., Ziman, B., & Lakatta, E. G. (2018). Basal Spontaneous Firing of Rabbit Sinoatrial Node Cells Is Regulated by Dual Activation of PDEs (Phosphodiesterases) 3 and 4. *Circulation: Arrhythmia and Electrophysiology*, *11*(6), 1–13. https://doi.org/10.1161/CIRCEP.117.005896

Volpe, M., Rubattu, S., & Burnett, J. (2014). Natriuretic peptides in cardiovascular diseases: Current use and perspectives. *European Heart Journal*, *35*(7), 419–425. https://doi.org/10.1093/eurheartj/eht466

Waithe, D., Ferron, L., Page, K. M., Chaggar, K., & Dolphin, A. C. (2011). β-Subunits Promote the Expression of CaV2.2 Channels by Reducing Their Proteasomal Degradation*. *Journal of Biological Chemistry*, *286*(11), 9598–9611. https://doi.org/10.1074/jbc.M110.195909

Wang, J., Gareri, C., & Rockman, H. A. (2018). G-Protein–Coupled Receptors in Heart Disease. *Circulation Research*, *123*(6), 716–735. https://doi.org/10.1161/CIRCRESAHA.118.311403

Wechsler, J., Choi, Y.-H., Krall, J., Ahmad, F., Manganiello, V. C., & Movsesian, M. A. (2002). Isoforms of Cyclic Nucleotide Phosphodiesterase PDE3A in Cardiac Myocytes*. *Journal of Biological Chemistry*, *277*(41), 38072–38078. https://doi.org/10.1074/jbc.M203647200

Weeks, K. L., & McMullen, J. R. (2011). The Athlete's Heart vs. the Failing Heart: Can Signaling Explain the Two Distinct Outcomes? *Physiology*, *26*(2), 97–105. https://doi.org/10.1152/physiol.00043.2010

Weiss, S., Oz, S., Benmocha, A., & Dascal, N. (2013). Regulation of Cardiac L-Type $Ca^{2+}$ Channel $Ca_V1.2$

Via the β-Adrenergic-cAMP-Protein Kinase A Pathway: Old Dogmas, Advances, and New Uncertainties. *Circulation Research*, *113*(5), 617–631. https://doi.org/10.1161/CIRCRESAHA.113.301781

Wijnker, P. J. M., Boknik, P., Gergs, U., Müller, F. U., Neumann, J., dos Remedios, C., Schmitz, W., Sindermann, J. R., Stienen, G. J. M., van der Velden, J., & Kirchhefer, U. (2011). Protein phosphatase 2A affects myofilament contractility in non-failing but not in failing human myocardium. *Journal of Muscle Research and Cell Motility*, *32*(3), 221–233. https://doi.org/10.1007/s10974-011-9261-x

Wijnker, P. J. M., Murphy, A. M., Stienen, G. J. M., & van der Velden, J. (2014). Troponin I phosphorylation in human myocardium in health and disease. *Netherlands Heart Journal*, *22*(10), 463–469. https://doi.org/10.1007/s12471-014-0590-4

Wong, W., & Scott, J. D. (2004). AKAP signalling complexes: Focal points in space and time. *Nature Reviews Molecular Cell Biology*, *5*(12), 959–970. https://doi.org/10.1038/nrm1527

Yan, B., Ding, Z., Zhang, W., Cai, G., Han, H., Ma, Y., Cao, Y., Wang, J., Chen, S., & Ai, Y. (2022). Multiple PDE3A modulators act as molecular glues promoting PDE3A-SLFN12 interaction and induce SLFN12 dephosphorylation and cell death. *Cell Chemical Biology*, S245194562200006X. https://doi.org/10.1016/j.chembiol.2022.01.006

Yang, L., Katchman, A., Kushner, J., Kushnir, A., Zakharov, S. I., Chen, B. xing, Shuja, Z., Subramanyam, P., Liu, G., Papa, A., Roybal, D., Pitt, G. S., Colecraft, H. M., & Marx, S. O. (2019). Cardiac Ca V 1.2 channels require β subunits for β-adrenergic–mediated modulation but not trafficking. *Journal of Clinical Investigation*, *129*(2), 647–658. https://doi.org/10.1172/JCI123878

Yang, L., Katchman, A., Samad, T., Morrow, J. P., Weinberg, R. L., & Marx, S. O. (2013). \&\#x3b2;-Adrenergic Regulation of the L-type $Ca^{2+}$ Channel Does Not Require Phosphorylation of \&\#x3b1;$_{1C}$ $Ser^{1700}$. *Circulation Research*, *113*(7), 871–880. https://doi.org/10.1161/CIRCRESAHA.113.301926

Yang, T., Puckerin, A., & Colecraft, H. M. (2012). Distinct RGK GTPases Differentially Use α1- and Auxiliary β-Binding-Dependent Mechanisms to Inhibit CaV1.2/CaV2.2 Channels. *PLoS ONE*, *7*(5), e37079. https://doi.org/10.1371/journal.pone.0037079

Yang, X., Lee, W. H., Sobott, F., Papagrigoriou, E., Robinson, C. V., Grossmann, J. G., Sundström, M., Doyle, D. A., & Elkins, J. M. (2006). Structural basis for protein–protein interactions in the 14-3-3 protein family. *Proceedings of the National Academy of Sciences*, *103*(46), 17237–17242. https://doi.org/10.1073/pnas.0605779103

Yang, X., Rodriguez, M. L., Leonard, A., Sun, L., Fischer, K. A., Wang, Y., Ritterhoff, J., Zhao, L., Kolwicz, S. C., Pabon, L., Reinecke, H., Sniadecki, N. J., Tian, R., Ruohola-Baker, H., Xu, H., & Murry, C. E. (2019). Fatty Acids Enhance the Maturation of Cardiomyocytes Derived from Human Pluripotent Stem Cells. *Stem Cell Reports*, *13*(4), 657–668. https://doi.org/10.1016/j.stemcr.2019.08.013

Yokoo, N., Baba, S., Kaichi, S., Niwa, A., Mima, T., Doi, H., Yamanaka, S., Nakahata, T., & Heike, T. (2009). The effects of cardioactive drugs on cardiomyocytes derived from human induced pluripotent stem cells. *Biochemical and Biophysical Research Communications*, *387*(3), 482–488. https://doi.org/10.1016/j.bbrc.2009.07.052

Yu, H., Yuan, C., Westenbroek, R. E., & Catterall, W. A. (2018). The AKAP Cypher/Zasp contributes to β-adrenergic/ PKA stimulation of cardiac CaV1.2 calcium channels. *Journal of General Physiology*, *150*(6), 883–889. https://doi.org/10.1085/jgp.201711818

Yusa, K. (2013). Seamless genome editing in human pluripotent stem cells using custom endonuclease-

based gene targeting and the piggyBac transposon. *Nature Protocols*, *8*(10), 2061–2078. https://doi.org/10.1038/nprot.2013.126

Zaccolo, M., & Pozzan, T. (2002). Discrete Microdomains with High Concentration of cAMP in Stimulated Rat Neonatal Cardiac Myocytes. *Science*, *295*(5560), 1711–1715. https://doi.org/10.1126/science.1069982

Zhang, J., Guy, M. J., Norman, H. S., Chen, Y.-C., Xu, Q., Dong, X., Guner, H., Wang, S., Kohmoto, T., Young, K. H., Moss, R. L., & Ge, Y. (2011). Top-Down Quantitative Proteomics Identified Phosphorylation of Cardiac Troponin I as a Candidate Biomarker for Chronic Heart Failure. *Journal of Proteome Research*, *10*(9), 4054–4065. https://doi.org/10.1021/pr200258m

Zhang, W., Ke, H., & Colman, R. W. (2002). Identification of Interaction Sites of Cyclic Nucleotide Phosphodiesterase Type 3A with Milrinone and Cilostazol Using Molecular Modeling and Site-Directed Mutagenesis. *Molecular Pharmacology*, *62*(3), 514–520. https://doi.org/10.1124/mol.62.3.514

Zhang, X., & Morad, M. (2020). Ca2+ signaling of human pluripotent stem cells-derived cardiomyocytes as compared to adult mammalian cardiomyocytes. *Cell Calcium*, *90*, 102244. https://doi.org/10.1016/j.ceca.2020.102244

Zhang, X., Szeto, C., Gao, E., Tang, M., Jin, J., Fu, Q., Makarewich, C., Ai, X., Li, Y., Tang, A., Wang, J., Gao, H., Wang, F., Ge, X. J., Kunapuli, S. P., Zhou, L., Zeng, C., Xiang, K. Y., & Chen, X. (2013). Cardiotoxic and Cardioprotective Features of Chronic β-Adrenergic Signaling. *Circulation Research*, *112*(3), 498–509. https://doi.org/10.1161/CIRCRESAHA.112.273896

Zhang, X.-H., Haviland, S., Wei, H., Šarić, T., Fatima, A., Hescheler, J., Cleemann, L., & Morad, M. (2013). Ca2+ signaling in human induced pluripotent stem cell-derived cardiomyocytes (iPS-CM) from normal and catecholaminergic polymorphic ventricular tachycardia (CPVT)-afflicted subjects. *Cell Calcium*, *54*(2), 57–70. https://doi.org/10.1016/j.ceca.2013.04.004

Zhang, X.-H., Wei, H., Šarić, T., Hescheler, J., Cleemann, L., & Morad, M. (2015). Regionally diverse mitochondrial calcium signaling regulates spontaneous pacing in developing cardiomyocytes. *Cell Calcium*, *57*(5–6), 321–336. https://doi.org/10.1016/j.ceca.2015.02.003

Zhao, Y., Rafatian, N., Feric, N. T., Cox, B. J., Aschar-Sobbi, R., Wang, E. Y., Aggarwal, P., Zhang, B., Conant, G., Ronaldson-Bouchard, K., Pahnke, A., Protze, S., Lee, J. H., Davenport Huyer, L., Jekic, D., Wickeler, A., Naguib, H. E., Keller, G. M., Vunjak-Novakovic, G., … Radisic, M. (2019). A Platform for Generation of Chamber-Specific Cardiac Tissues and Disease Modeling. *Cell*, *176*(4), 913-927.e18. https://doi.org/10.1016/j.cell.2018.11.042

Zhu, Y. R., Jiang, X. X., Zheng, Y., Xiong, J., Wei, D., & Zhang, D. M. (2019). Cardiac function modulation depends on the A-kinase anchoring protein complex. *Journal of Cellular and Molecular Medicine*, *23*(11), 7170–7179. https://doi.org/10.1111/jcmm.14659

Zimmermann, W.-H., Schneiderbanger, K., Schubert, P., Didié, M., Münzel, F., Heubach, J. F., Kostin, S., Neuhuber, W. L., & Eschenhagen, T. (2002). Tissue Engineering of a Differentiated Cardiac Muscle Construct. *Circulation Research*, *90*(2), 223–230. https://doi.org/10.1161/hh0202.103644

Zwi, L., Caspi, O., Arbel, G., Huber, I., Gepstein, A., Park, I.-H., & Gepstein, L. (2009). Cardiomyocyte Differentiation of Human Induced Pluripotent Stem Cells. *Circulation*, *120*(15), 1513–1523. https://doi.org/10.1161/CIRCULATIONAHA.109.868885

# 8 Publications

## 8.1 Articles

Ercu M*, Mücke MB*, Pallien T*, Marko L*, Sholokh A, Schächterle C, Aydin A, Kidd A, Walter S, Esmati Y, McMurray B, Lato DF, Sunaga-Franze DY, Walker-Gray R, Gong M, Merticariu C, Zühlke K, Russwurm M, Liu T, Bartolomaeus T, Pautz S, Schelenz S, Taube M, Napieczynska H, Heuser A, Eichhorst J, Lehmann M, Miller D, Diecke S, Qadri F, Popova E, Langanki R, Herberg FW, Forslund SK, Müller DN, Borodina T, Bähring S, Maass PG, Hübner N, Luft FC, Bader M, Klussmann E. *Mutant phosphodiesterase 3A protects from hypertension-induced cardiac damage.* Circulation.

Hinrichs GR, Baltzer S, Pallien T, Svenningsen P, Dalgaard EB, Hertz JB, Bistrup C, Jensen BL, Klussmann E. *A Novel AQP2 Sequence Variant Causing Aquaporin-2 Retention in the Cytoplasm and Autosomal Dominant Nephrogenic Diabetes Insipidus*. Kidney International Reports,2022. ISSN 2468-0249. https://doi.org/10.1016/j.ekir.2022.07.001.

Walker-Gray R*, Pallien T*, Miller DC, Oder A, Neuenschwander M, von Kries JP, Diecke S, Klussmann E. *Disruptors of AKAP-Dependent Protein-Protein Interactions*. Methods Mol Biol. 2022; 2483:117-139. doi: 10.1007/978-1-0716-2245-2_8. PMID: 35286673.

Pallien T, Klussmann E. *New aspects in cardiac L-type Ca2+ channel regulation*. Biochem Soc Trans. 2020 Feb 28;48(1):39-49. doi: 10.1042/BST20190229. PMID: 32065210.

Dema A, Faust D, Lazarow K, Wippich M, Neuenschwander M, Zühlke K, Geelhaar A, Pallien T, Hallscheidt E, Eichhorst J, Wiesner B, Černecká H, Popp O, Mertins P, Dittmar G, von Kries JP, Klussmann E. Cyclin-Dependent Kinase 18 Controls Trafficking of Aquaporin-2 and Its Abundance through Ubiquitin Ligase STUB1, Which Functions as an AKAP. Cells. 2020 Mar 10;9(3):673. doi: 10.3390/cells9030673. PMID: 32164329; PMCID: PMC7140648.

*these authors contributed equally.

## 8.2 Oral presentations

Hypertension-causing PDE3A mutations lead to aberrant calcium cycling in cardiomyocytes. *Student Seminar in System Medicine*. Online Meeting. Berlin, Germany, October 7th, 2021.

Identification of novel protein complexes regulating voltage-gated L-type calcium channels. *16th Retreat Schmilka*. Seiffen, Germany, August 25-28, 2019.

## 8.3 Poster presentations

Pallien T, Mücke MB, Ercu M, Bähring S, Diecke S, Bader M, Hübner N, Klussmann E. HTNB-causing PDE3A mutations lead to aberrant calcium cycling in cardiomyocytes. *MDC PostDoc Day 2021*. Berlin, Germany, November 4th, 2021.

Pallien T, Tsemakhovich V, Ashkar M, Katz M, Oz S, Dascal N, Klussmann E. PKA catalytic subunit and $Ca_v1.2$ $\alpha$1c channel interaction enhances kinase activity *in vitro*. *Nanodomains in cyclic nucleotide signaling: from mechanisms to therapeutic approaches*. Conference. London, UK, September 16-18, 2019.

# 9 Appendix

## 9.1 Supplemental Methods

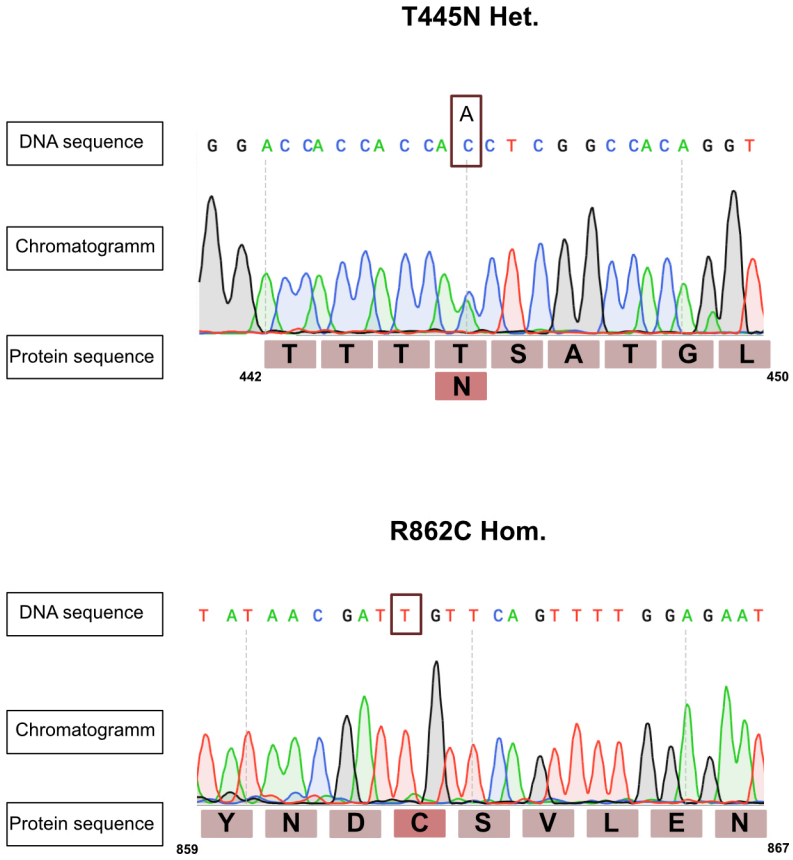


**Figure S 1: DNA and protein sequences of hiPSCs harboring T445N and R862C substitutions.** The chromatograms show the results of the Sanger sequencing for the two different variants. The box highlights the mutation in the DNA sequence. The different colored boxes show the amino acid substitutions. Since the heterozygous mutation does not cause a penetrant phenotype in our animal models and also shows a less severe phenotype in humans, the homozygous mutation was inserted into the hiPSCs.

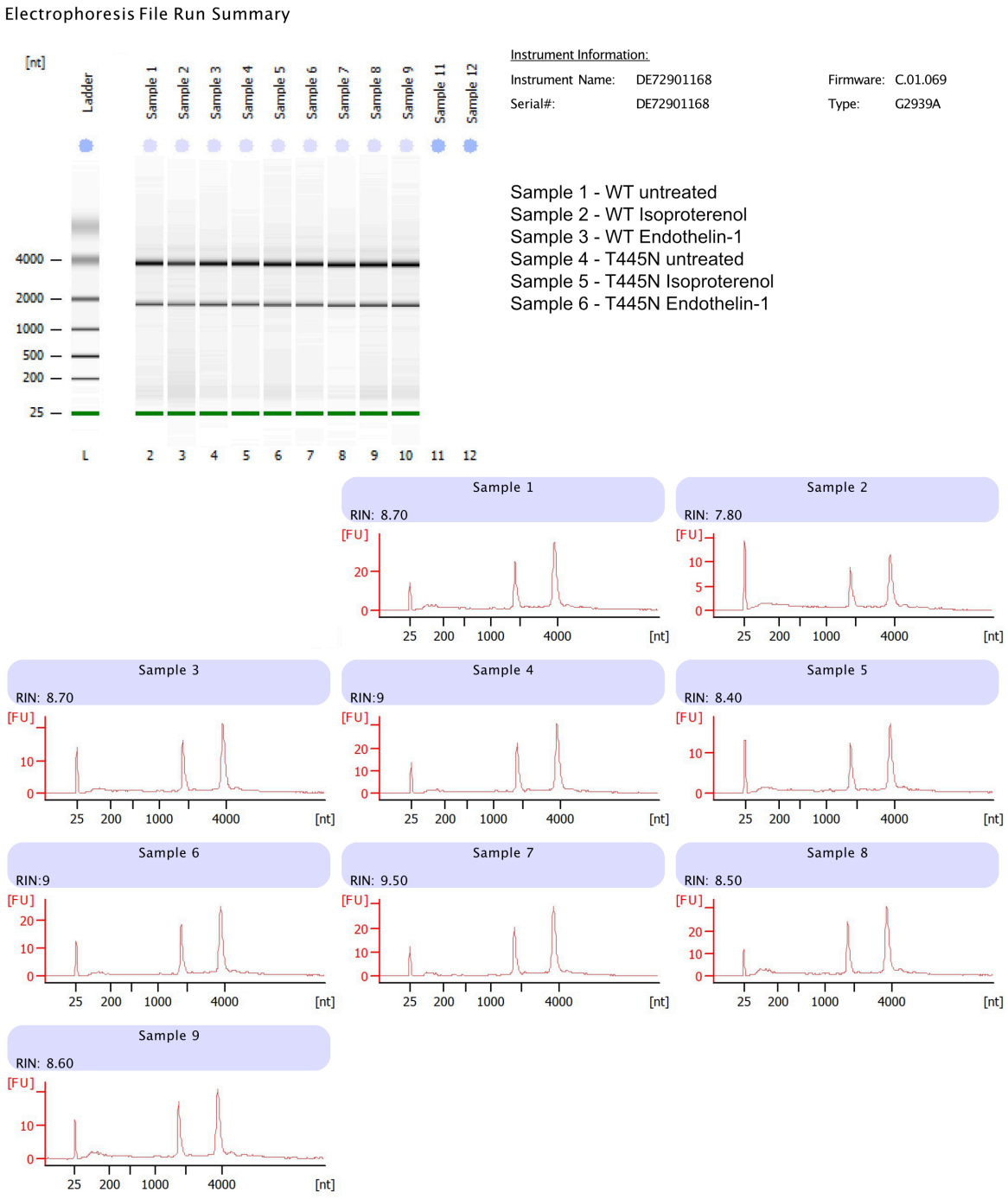


**Figure S 2: BioAnalyzer results of the RNA samples used for qPCR experiments.** Sample 1-6 correspond to samples used to analyze the expression of hypertrophy marker genes (NPPA, NPPB, ACTC, MYH7). The sample identity is indicated in the legend.

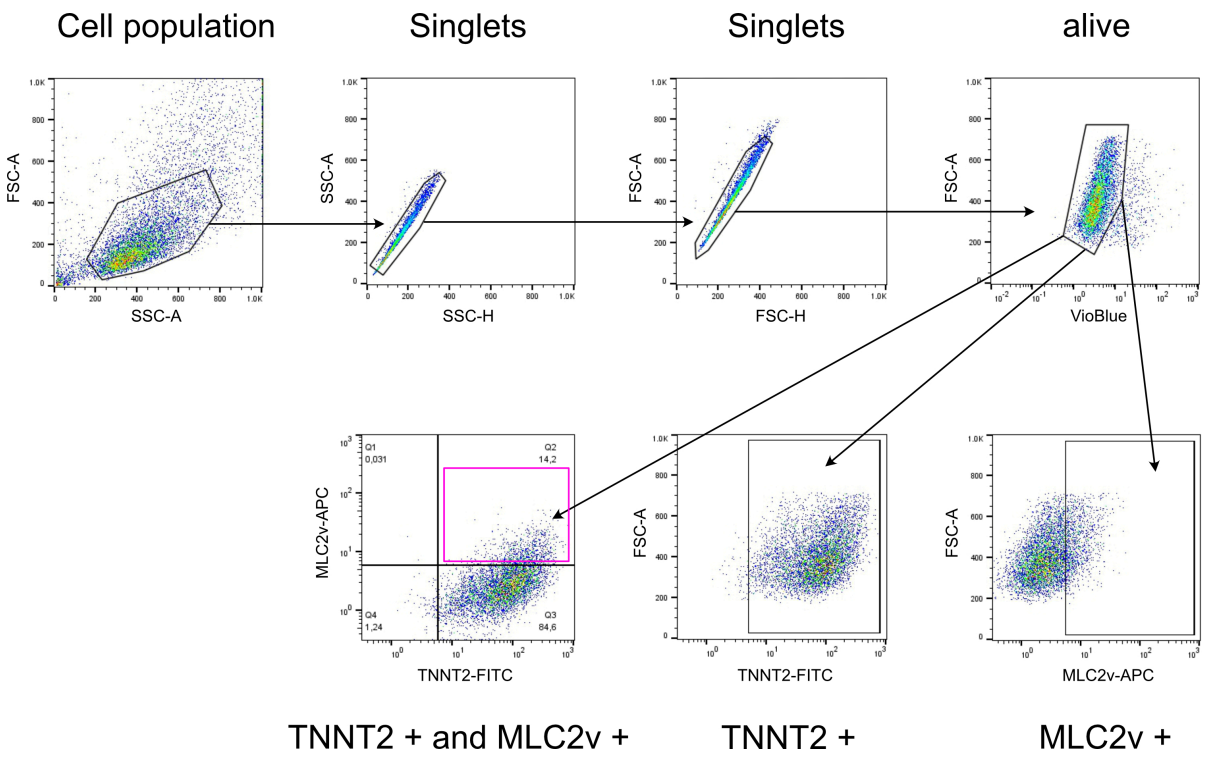


**Figure S 3: Gating strategy to quantify TNNT2 and MLC2v expression in hiPSC-CMs.** The cell population was selected in the cell suspension. This gate was used to select single cells using side scatter (SSC) and forward scatter (FSC) measurements. Living cells were gated using VioBlue dye. From the living cells the TNNT2$^{+}$, MLC2v$^{+}$ and double positive (pink inlet) cells were selected using isotype control sample (not shown).

## 9.2 Supplemental Results

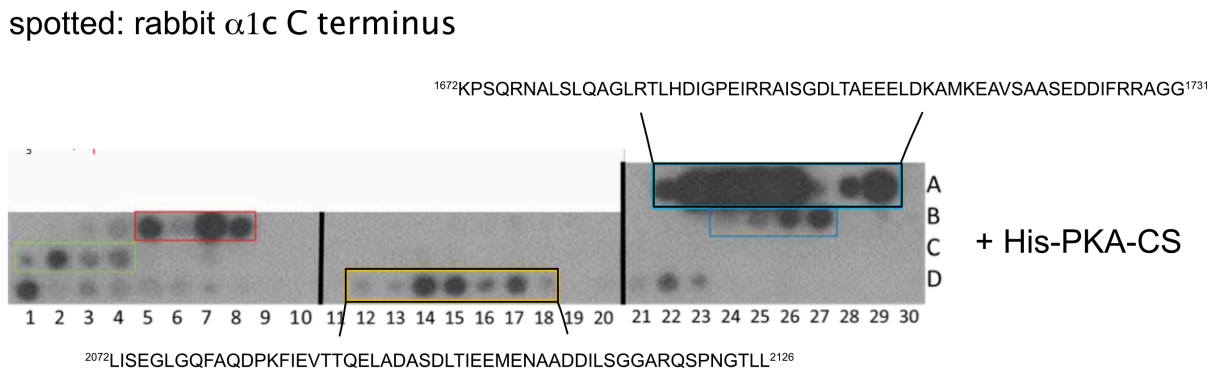


**Figure S 4: PKA-CS binds at DCRD and PCRD in the α1c C terminus**. Peptide array of LTCC α1c C terminus overlaid with His-PKA-CS. The interactions were detected using anti-PKA-CS antibody. Interactions are detected at three sites, with two of them corresponding to proximal C-terminal regulatory domain (PCRD, 1672-1731) and distal C-terminal regulatory domain (DCRD, 2072-2126). This experiment was done by Dr. Shimrit Oz (Dascal lab, Tel Aviv, Israel).

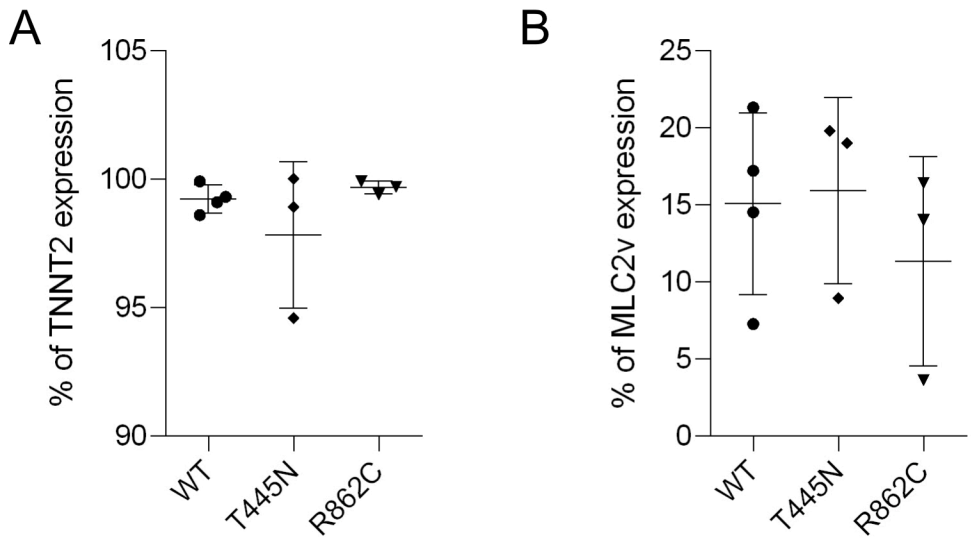


**Figure S 5: Troponin T (TNNT2) and ventricular Myosin light chain 2 (MLC2v) expression in hiPSC-CMs at day 45**. The cells were stained at day 45 of differentiation and the expression of both markers quantified using flow cytometry. The graphs show the percentage ± SD of $TNNT^+$ and $MLC2v^+$ cells from 4 (WT) and three differentiation rounds (T445N, R862C).

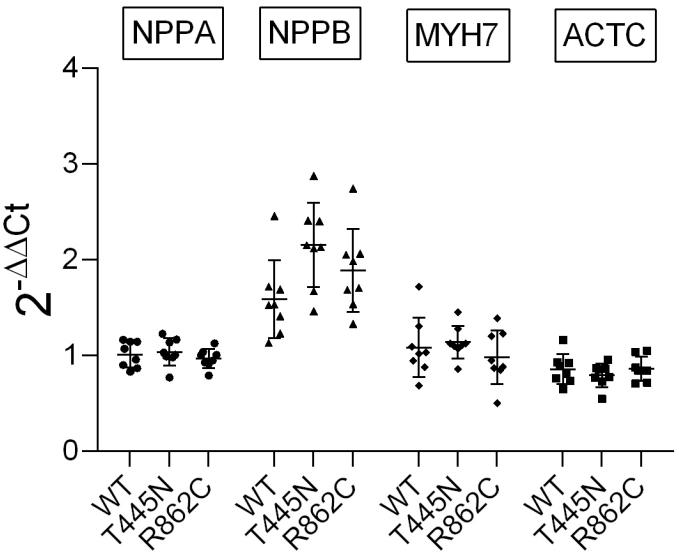


**Figure S 6: Treatment with isoproterenol only induced moderate increase in the expression of hypertrophy marker genes.** Compared to the treatment with endothelin-1 (Figure 14), treatment with 1 µM isoproterenol for 48 h only induced moderate upregulation of *NPPA*, *NPPB*, *MYH7* and *ACTC* genes. The graph shows the fold change for two independent experiments. Mean ± SD is plotted.

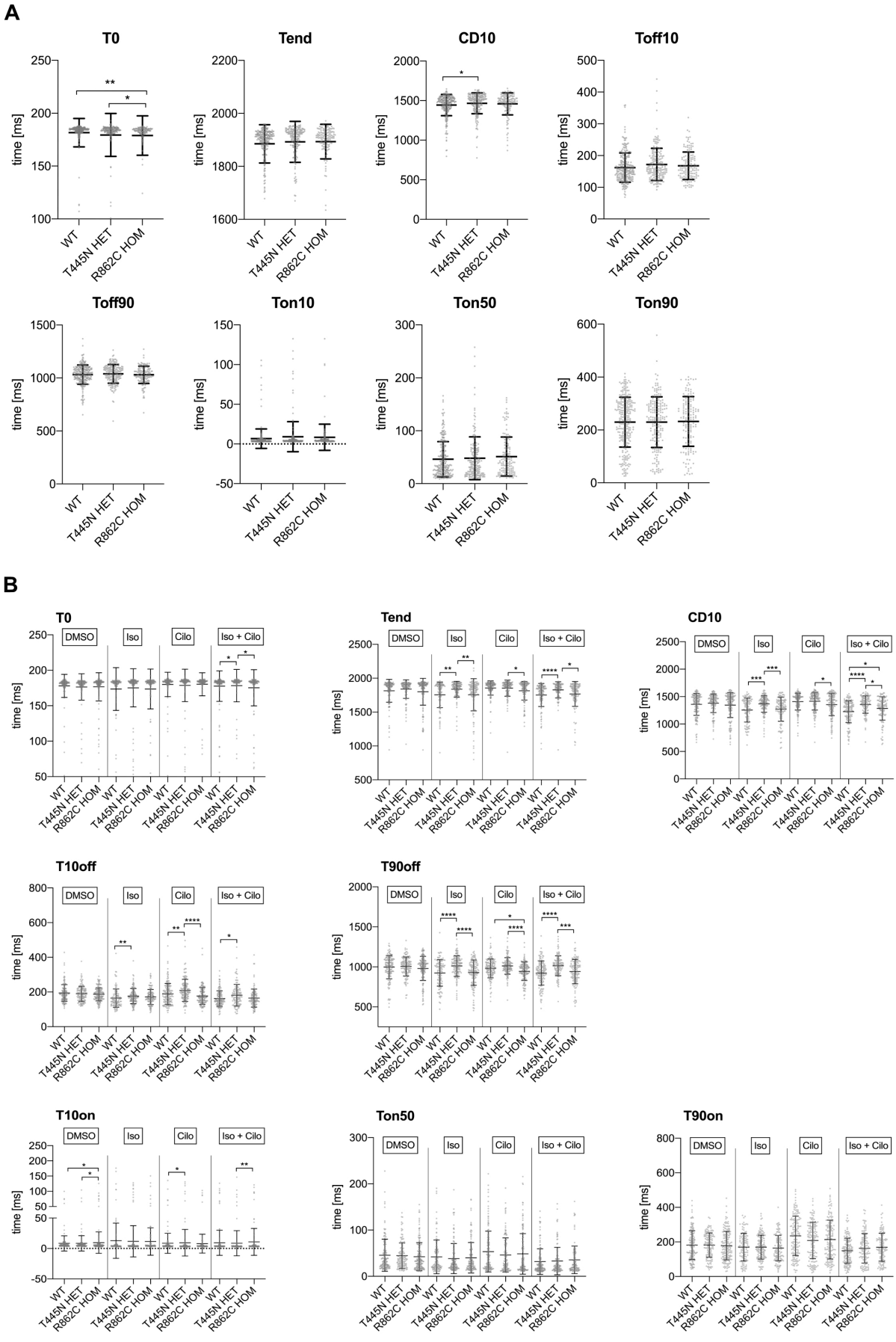


**Figure S 7: Mutant hiPSC-CMs have alterations in $Ca^{2+}$ transient start and end time ($T_0$ and $T_{end}$)**

## 9.3 Plasmid maps

### 9.3.1 DCRD-Cerulean

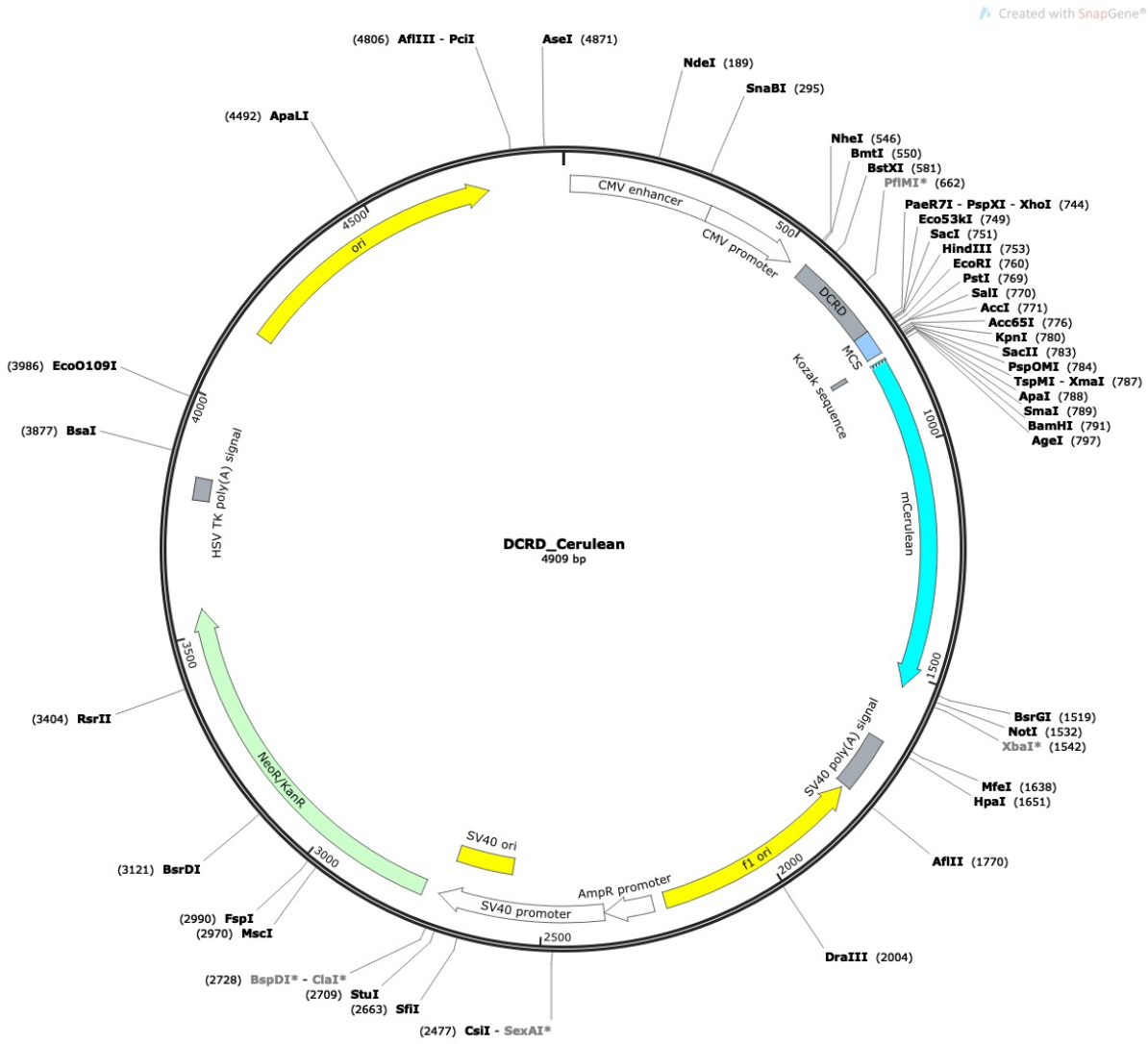


**Figure S 8: Plasmid map for the DCRD-Cerulean construct.** The DCRD sequence (highlighted in gray) was cloned into Cerulean-N1 plasmid (Addgene #54742). The main features and restriction sites are shown.

### 9.3.2 PCRD-Cerulean

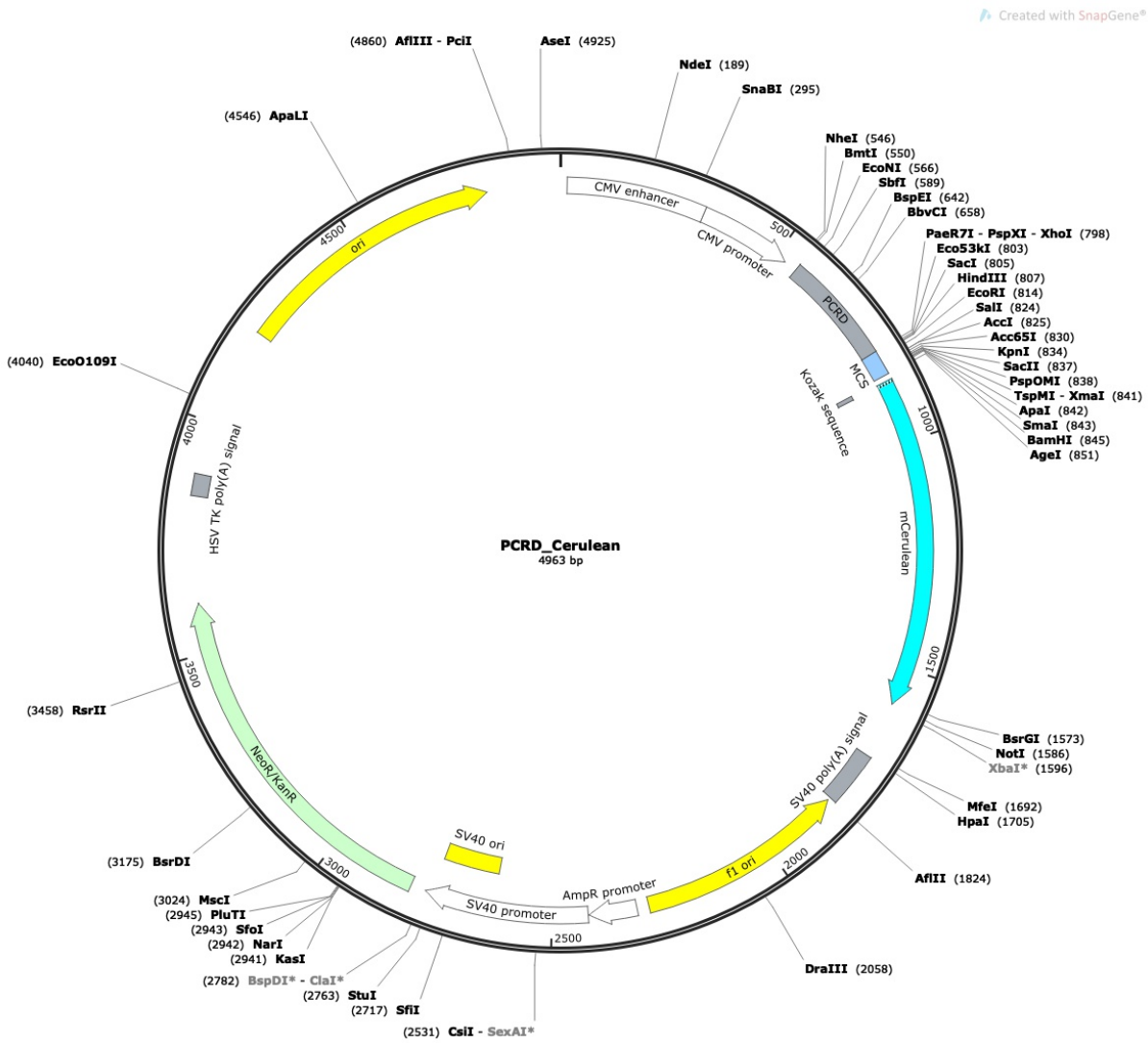


**Figure S 9: Plasmid map for the PCRD-Cerulean construct.** The PCRD sequence (highlighted in gray) was cloned into Cerulean-N1 plasmid (Addgene #54742). The main features and restriction sites are shown.

### 9.3.3 PKA-CS-Venus

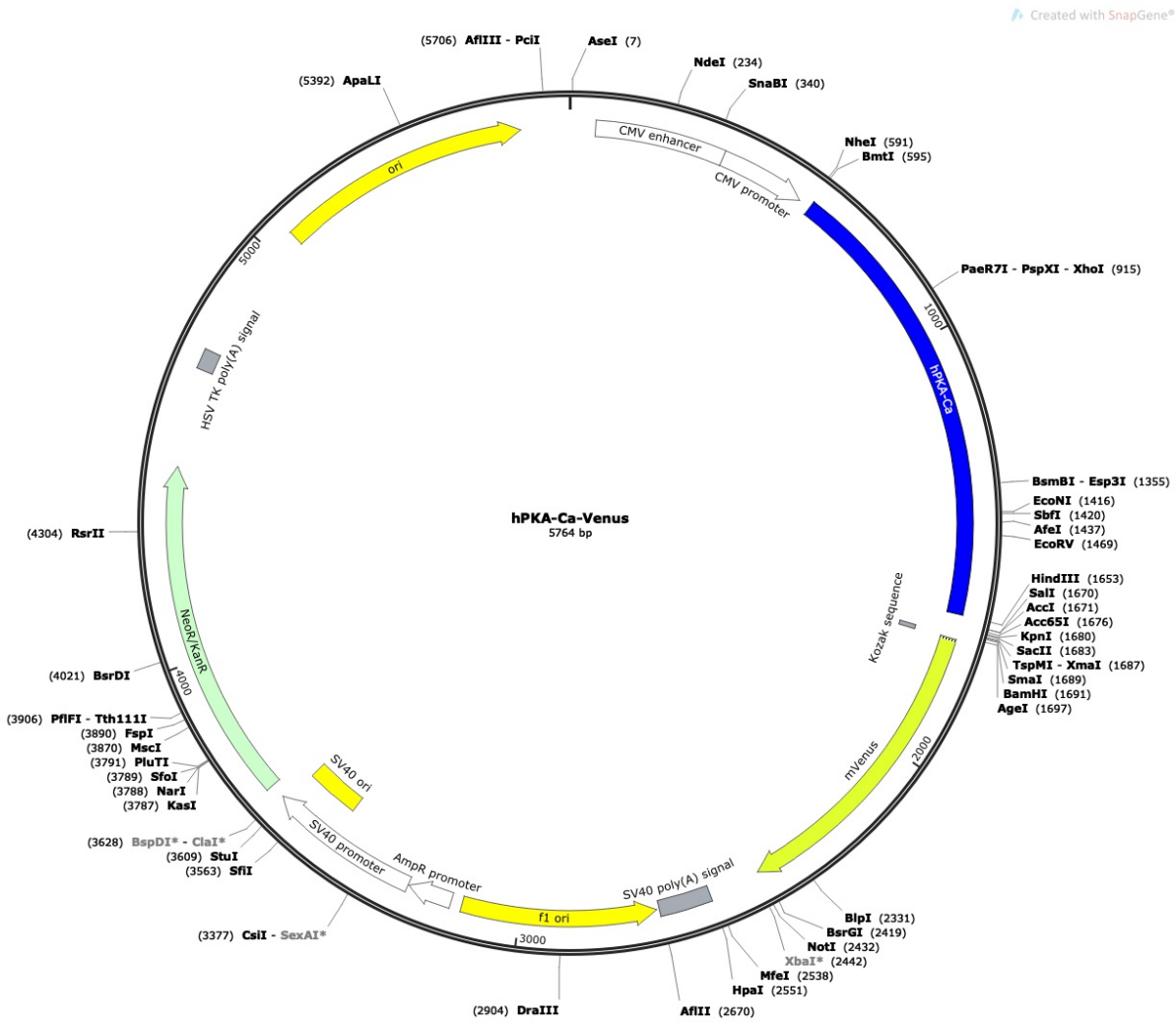


**Figure S 10: Plasmid map for the human PKA-CS-Venus construct.** The human PKA-CS sequence (highlighted in dark blue) was cloned into mVenus-N1 plasmid (Addgene #27793). The main features and restriction sites are shown.

### 9.3.4 CFP-rα1c $Ca_V1.2$

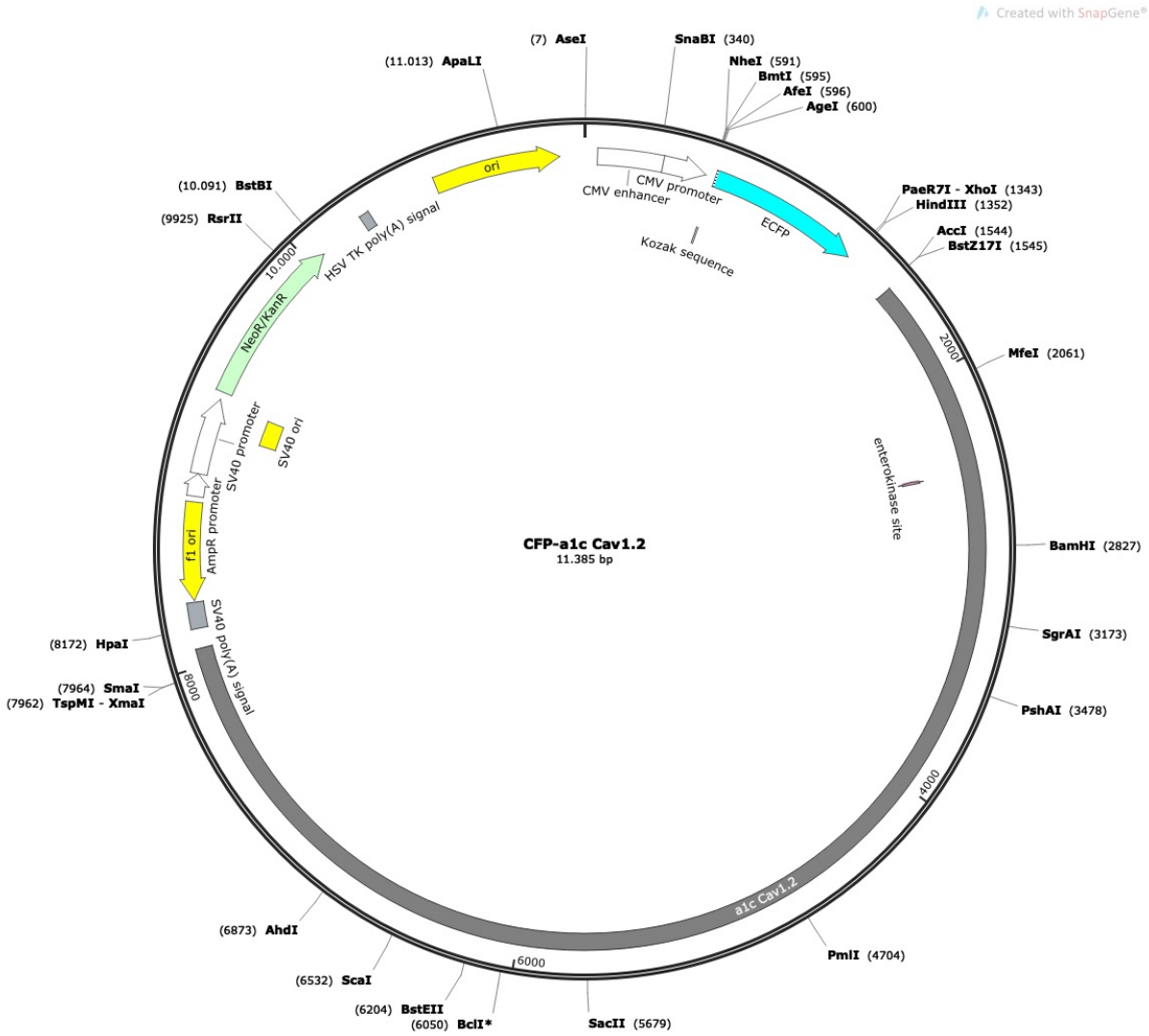


**Figure S 11: Plasmid map for the CFP- rα1c Cav1.2 construct.** The rabbit α1c Cav1.2 sequence (highlighted in dark gray) was cloned into pECFP-C1 plasmid. The main features and restriction sites are shown.